

Cover Page



Universiteit Leiden



The handle <http://hdl.handle.net/1887/60212> holds various files of this Leiden University dissertation.

**Author:** Heijs, B.P.A.M.

**Title:** Lab-on-a-tissue : optimization of on-tissue chemistry for improved mass spectrometry imaging

**Issue Date:** 2018-02-01

**Lab-on-a-tissue:  
Optimization of On-Tissue Chemistry for  
Improved Mass Spectrometry Imaging**

Bram Heijs

ISBN: 978-94-6295-840-1

©2017 Bram Heijs. All rights reserved. No part of this book may be reproduced, stored in a retrieval system or transmitted in any form or by any means without permission of the author or the journals holding the copyrights of the published manuscripts.

The work presented in this thesis was performed at the Center for Proteomics and Metabolomics, Leiden University Medical Center, Leiden, The Netherlands.

This work was supported by: the ZonMW Zenith project Imaging Mass Spectrometry-Based Molecular Histology: Differentiation and Characterization of Clinically Challenging Soft Tissue Sarcomas (No. 93512002)

Cover design: Jasper Kloosterboer at KLOOSTER studio

Printed by ProefschriftMaken || [www.proefschriftmaken.nl](http://www.proefschriftmaken.nl)

# **Lab-on-a-tissue: Optimization of On-Tissue Chemistry for Improved Mass Spectrometry Imaging**

Proefschrift

Ter verkrijging van de graad van Doctor aan de Universiteit Leiden  
op gezag van de Rector Magnificus prof. mr. C.J.J.M. Stolker,  
volgens besluit van het College voor Promoties  
te verdedigen op donderdag 1 februari 2018  
Klokke 13:45 uur

door

**Bram Petrus Antonius Maria Heijs**

Geboren te Tilburg

in 1986

Promotor:

Prof. Dr. J.V.M.G. Bovée

Copromotor:

Dr. L.A. McDonnell, *Leids Universitair Medisch Centrum, Leiden, Nederland; Fondazione Pisana per la Scienza ONLUS, Pisa, Italië*

Leden promotiecommissie:

Prof. Dr. I. Fournier, *University Lille 1, Lille, Frankrijk*

Prof. Dr. R.M.A. Heeren, *Maastricht University, Maastricht, Nederland*

Prof. Dr. F. Koning

"Success consists of going from failure to failure without loss of enthusiasm."

*Winston Churchill*

*Winston Churchill's Great Quotation Book "From Alamein to Zest for Life", 2013*

*To all who have educated me*



# Table of contents

<b>Chapter 1 Introduction .....</b>	<b>9</b>
<b>Chapter 2 Brain region-specific dynamics of on-tissue protein digestion using MALDI-MSI.....</b>	<b>39</b>
<i>Journal of Proteome Research, vol. 14, no. 12, pp. 5348–5354, 2015</i>	
<b>Chapter 3 Comprehensive analysis of the mouse brain proteome sampled in mass spectrometry imaging.....</b>	<b>53</b>
<i>Analytical Chemistry, vol. 87, no. 3, pp. 1867–1875, 2015</i>	
<b>Chapter 4 Histology-guided high resolution MALDI mass spectrometry imaging.....</b>	<b>73</b>
<i>Analytical Chemistry, vol. 87, no. 24, pp. 11978–11983, 2015</i>	
<b>Chapter 5 Multimodal mass spectrometry imaging of N-glycans and proteins from the same tissue section .....</b>	<b>89</b>
<i>Analytical Chemistry, vol. 88, no. 15, pp. 7745–7753, 2016</i>	
<b>Chapter 6 Mass spectrometry imaging of N-glycans identifies biomarkers of tumor progression in myxoid liposarcoma.....</b>	<b>113</b>
<b>Chapter 7 Summary and discussion .....</b>	<b>127</b>
<b>Bibliography.....</b>	<b>137</b>
List of abbreviations.....	154
Nederlandse samenvatting.....	156
List of publications.....	164
Curriculum Vitæ .....	166
Acknowledgements.....	168





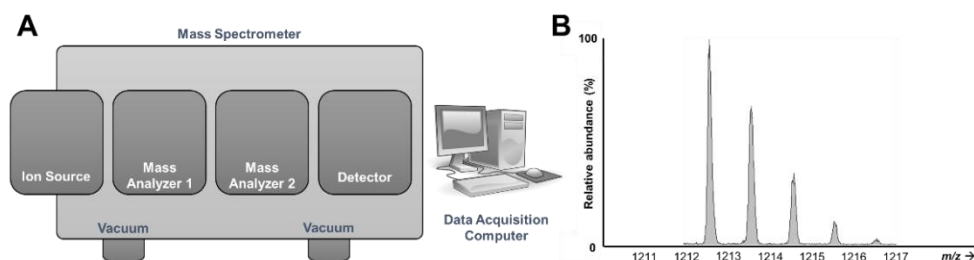
# Chapter **1**

## Introduction



## 1.1 Introduction

In the modern age of personalized medicine and patient stratification, biomolecular markers and accompanying molecular profiling techniques have become deeply embedded in clinical research and molecular pathology (Cristofanilli et al., 2004; Hurvitz et al., 2013; Oviaño et al., 2016; Pecoraro et al., 2016). Specifically analytical chemistry methods are applied to pathological tissues in order to obtain the identity, quantity and localization of disease-specific molecular features. One of these techniques is mass spectrometry imaging (MSI), which is a mass spectrometry-based technique that allows the spatially-correlated analysis of biomolecular ions directly from thin tissue sections (Caprioli et al., 1997). This introduction will cover the basics of the mass spectrometry required for understanding the MSI research described in this thesis and to place it in the context of wider MSI research.



**Figure 1-1:** (A) A schematic overview of the layout of a mass spectrometer with its core components. From left to right, the ion source, one (or more) mass analyzers, a detector, and a data acquisition computer. (B) Example of a mass spectrum, with the horizontal axis representing the mass-to-charge ratio, and the vertical axis representing the (relative) abundance, or signal intensity.

## 1.2 Mass spectrometry

Mass spectrometry (MS) is an analytical chemistry technique that allows the detection, identification and quantification of ionized molecular species. Since the recording of the first mass spectrum in 1912 by Sir J.J. Thomson (Thomson, 1912), numerous technological advances have made MS one of the most sensitive and fast molecular analysis techniques available with a great variety of application areas including petrochemistry, forensic science, pharmaceutical research, food sciences and biomedical research (te Brake et al., 2015; Dekker et al., 2014; Esteve et al., 2015; Frese et al., 2017; Groeneveld et al., 2015; Maleki et al., 2016; Smith et al., 2008).

Mass spectrometers employ a range of different technologies but share the same basic layout (Figure 1-1A); ion source, one or multiple mass analyzers, and a detector and acquisition computer. In the ion source, the molecular analytes are converted from the liquid or solid phase into gas-phase ions. The mass analyzer separates the ions based on their mass-to-charge ( $m/z$ ) ratio. Finally, the separated ions and their relative abundance, are recorded by the detector. The molecular content of the analyzed sample is visualized in a mass spectrum. Consisting of two perpendicular axes, a mass

spectrum is usually displayed with the x-axis representing the  $m/z$  or 'mass' in Daltons (Da) per unit charge, and the y-axis representing intensity of the signal (Figure 1-1B) (Glish and Vachet, 2003).

### 1.2.1 Ion source

A large number of different ionization techniques are available, each with different characteristics that make them more/less suitable to specific application areas. The choice of ionization method can have a large effect on the quantitative and qualitative outcome of the analysis. For example, the analysis of the metabolic content of serum by electrospray (ESI) MS, atmospheric pressure chemical ionization (APCI) MS, and matrix-assisted laser desorption/ionization (MALDI) MS led to the detection of different sets of small molecules (Nordström et al., 2008). Also, the linearity and lower limit of quantification for the same compound were shown to be heavily influenced by the choice of ionization method (Buse et al., 2014). Therefore, a careful understanding of the different ionization methods is essential to determine the application areas most suited to the ionization methods available within any single laboratory. Present day biomolecular MS utilizes soft ionization techniques that are capable of transferring large molecules, such as proteins, from the liquid or solid phase to the gas phase without excessive fragmentation. The two most common ionization techniques in biomolecular MS are ESI, and MALDI (Domon and Aebersold, 2006).

#### 1.2.1.1 Electrospray ionization

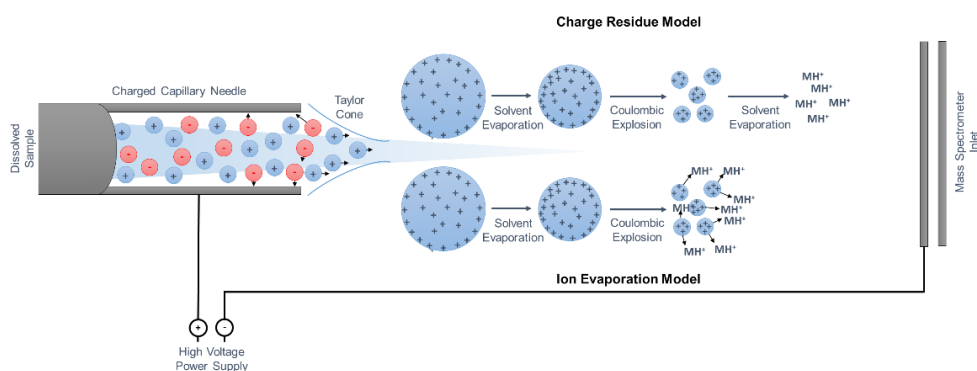
ESI, first reported by Yamashita and Fenn in 1984 (Yamashita and Fenn, 1984) and later demonstrated to enable protein analysis by mass spectrometry (Fenn et al., 1989), is a continuous ionization mechanism, based on the nebulization of a dissolved sample in an atmospheric pressure environment. The analyte molecules are dissolved in an aqueous solution containing an organic solvent (e.g. methanol or acetonitrile) and, in the case of positive ion analysis, a small amount of acid (e.g. formic, or acetic acid). The sample solution is introduced into a needle, which is held at a high electrical potential relative to the mass spectrometer's sampling capillary. Upon leaving the needle, the solution experiences the strong electric field between the needle and the mass spectrometer's sampling capillary, and forms a Taylor cone from which small, highly charged droplets are released. The formation of molecular ions from the charged droplets is depicted in Figure 1-2 (Wilm, 2011).

The strong electric field between the needle and the sampling capillary attracts ions to the solution surface, forming the Taylor cone and a steady stream of charge-enriched droplets. Solvent evaporation then takes place (the ratio of the surface area to volume of the droplets is high and so evaporation takes place quickly). During solvent evaporation charge repulsion between the excess charges on the droplets leads to deformation; when localized repulsion exceeds the local surface tension of the droplet (Rayleigh instability), asymmetric fission occurs in which the smaller droplets carry an excess fraction of the charge. This process of solvent evaporation and

Rayleigh instability continues until only very small droplets remain. In the charge residue model, which is believed to be the dominant mechanism for the formation of multiply charged ions of large molecules, this process continues until a single, solvated, and multiply charged analyte ion is produced. In the ion evaporation model, which is believed to explain the formation of ions of small molecules, the (solvated) ions are desorbed out of the small droplets owing to the very strong electric field in the ion source (Awad et al., 2015; Beaudry et al., 1999; Fenn et al., 1990; Nordström et al., 2008).

Multiple charging and multiple charge states, e.g. lysozyme being detected in charge states +5 to +25, are characteristic of ESI (Krusemark et al., 2009; Valentine et al., 1997). This has two distinct benefits; (i) it brings the  $m/z$  of the protein ions into the  $m/z$  range that can be analyzed by most mass analyzers with higher mass resolution and sensitivity, and (ii) it enables peptide/protein ion fragmentation and the detection of complementary fragments, both of which promote their structural characterization (Wysocki et al., 2005).

The continuity of the ESI method makes it highly suitable for use in a hyphenated system where the mass spectrometer is coupled to a chromatographic separation, such as liquid chromatography (LC), or capillary electrophoresis (CE).



**Figure 1-2:** Schematic overview of the ion formation in electrospray ionization, visualizing both the charge residue model and the ion evaporation model.

### 1.2.1.2 Matrix-assisted laser desorption/ionization

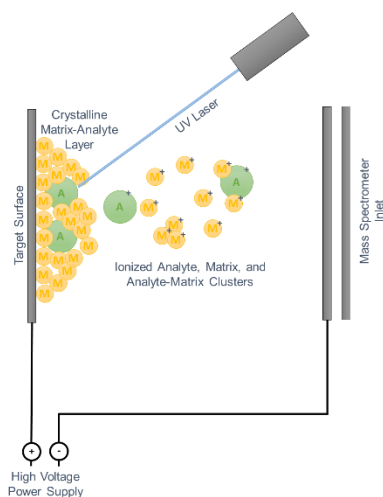
In contrast to the continuity of ESI, MALDI is a pulsed ionization process. Developed by Karas and Hillenkamp (Karas and Hillenkamp, 1988; Karas et al., 1987) the MALDI method requires the analyte molecules to be embedded in an excess amount of a chemical matrix. The matrix is typically a small organic acid and a strong absorber of UV light. In a MALDI experiment a solution of the analyte is mixed with an excess of a matrix solution. During solvent evaporation the matrix crystallizes, incorporating the analyte (proteins) or coming in to close contact with the analyte (small molecules). The matrix crystals have been shown to segregate salts away from the analytes, thereby

effectively helping to de-salt the samples and improve detection sensitivity. Irradiation of the analyte doped matrix crystals with a pulsed UV laser leads to efficient production of molecular ions. MALDI involves the super excitation of the laser-absorbing matrix with the laser (MALDI requires laser fluence thresholds of 30 J/m<sup>2</sup> and pulse lengths <5 ns, so that the laser energy does not have sufficient time to dissipate during irradiation). Above laser fluence threshold the super heating causes an almost explosive phase transition, with rapid collective motion of the matrix substrate into the gas phase. The analyte molecules are brought into the gas phase by being entrained within this collective motion. This process of the explosive phase change leads to the formation of neutral and charged matrix and analyte molecules, as well as clusters. All molecules that form gas-phase ions, anions by deprotonation or cations by available protons (H<sup>+</sup>) or metals (e.g. Na<sup>+</sup>, K<sup>+</sup>, Ag<sup>+</sup>), are accelerated toward the mass analyzer by means of an electric (Figure 1-3) (Dreisewerd, 2014; Hanton et al., 1999; McDonnell and Heeren, 2007).

Careful selection of the matrix is key to the success of a MALDI-MS analysis, as the physicochemical properties of the MALDI matrix will affect its co-crystallization with the analytes, their co-desorption on laser irradiation and the efficiency of the ionization process (Dreisewerd, 2003, 2014; Zenobi and Knochenmuss, 1998). Over the years many compounds have been empirically determined to be suitable MALDI matrices; some for very specific applications, such as 1H-pteridine-2,4-dione (lumazine), 2-aminobenzamide, 2-aminobenzoic acid,  $\beta$ -carboline alkaloids, and graphene (Calvano et al., 2010; Dong et al., 2010; Nonami et al., 1997; Shroff and Svatoš, 2009; Smargiasso et al., 2012), while other matrices are more generally applicable. For example,  $\alpha$ -cyano-4-hydroxycinnamic acid (CHCA), 2,5-dihydroxybenzoic acid (DHB), and sinapinic acid (SA) are matrices that are commonly used for the analysis of peptides, lipids, and proteins in positive ion mode. 9-aminoacridine (9-AA) is commonly used for the negative ion analysis of small molecules.

The experimental conditions of the ion source and the MALDI sample preparation determine the accessible ion yield of the analyte. The ion source instrumentation includes how the laser interacts with the sample. Optimization of the irradiation conditions can affect the ion flux towards the mass analyzer; too low of a laser fluence (energy per illuminated surface) will result in poor MALDI signals, too high of a laser fluence will cause extensive in-source fragmentation of the analyte molecules (Dreisewerd et al., 1995). The focus of the laser is also important, in that it must be tuned along with the laser fluence to ensure that the on-target laser fluence is above threshold but not too high that it leads to extensive fragmentation. Furthermore, the MALDI matrix crystals of the sample preparation can lead to heterogeneity in the sample preparation, mostly observed in dried-droplet sample preparations. In order to effectively average this crystal-derived heterogeneity older MALDI instruments used larger spot sizes (Dreisewerd et al., 1995; McDonnell and Heeren, 2007).

In the last decade, MALDI instruments have moved toward fast, tightly focused laser beams, and even include structured laser spots. Qiao *et al.* demonstrated that with careful control of the laser fluence tightly focused laser beams delivered more signal per unit area (Qiao *et al.*, 2008), and Holle *et al.* demonstrated that increased signal intensity and reduced analyte depletion was observed if a larger laser beam was converted into an array of tightly focused point-illumination beams (Holle *et al.*, 2006). These technologies have now combined to offer high speed, high sensitivity MALDI ionization systems. Part of the driving force for the development of such high speed, high sensitivity, tightly focused laser beam systems has been MALDI-MSI, in which the laser beam focus, sensitivity and throughput helps determine the achievable spatial resolution.



**Figure 1-3:** A schematic overview of the matrix-assisted laser desorption/ionization mechanism.

### 1.2.2 Mass analyzer and ion detection

The mass analyzer separates the ions based on their  $m/z$  ratio, after which the ions are detected at their  $m/z$ . In mass spectrometry two terms are often used to define the quality or the performance characteristics of a mass analyzer: (i) the mass accuracy refers to the error between the measured  $m/z$  and the calculated, true  $m/z$  of a compound, and (ii) the mass resolving power, or resolution, defines the ability of the mass analyzer to distinguish between two peaks with very similar  $m/z$ . A broad range of technologies are available that combine different characteristics in terms of mass accuracy, mass resolving power, sensitivity (ion transmission and detection efficiencies),  $m/z$  range, speed, tandem mass spectrometry, ease of hyphenation with e.g. liquid separations, ease-of-use, cost (purchase & maintenance). Such mass spectrometry systems include: (i) quadrupole mass analyzers, (ii) time-of-flight (TOF) mass analyzers, (iii) magnetic or electrostatic sector mass analyzers, (iv) quadrupole ion trap mass analyzers, (v) Orbitrap mass analyzers, and (vi) Fourier transform (FT)



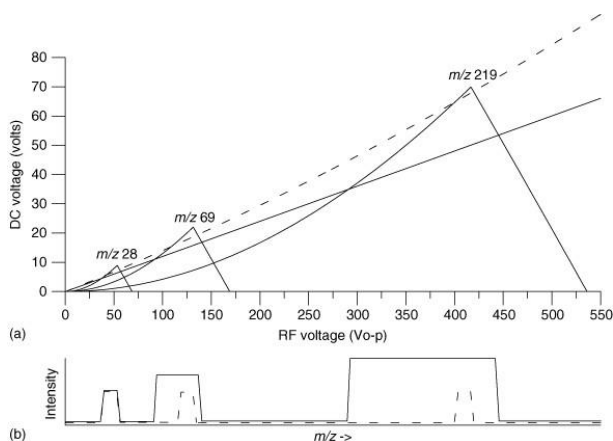
ion cyclotron resonance (ICR) mass analyzers. For a detailed comparison of the systems the interested reader is directed toward the review by Himmelsbach (Himmelsbach, 2012). Here we will focus on the technologies mostly used in MALDI-MSI.

### 1.2.2.1 Quadrupole mass analyzer

The quadrupole mass analyzer consists of a set of four parallel metal rods to which a combination of radio frequency (RF) and direct current (DC) voltages are applied. The stability of ion motion in a quadrupole is governed by the Mathieu parameters

$$a = \frac{8zU}{mr_o^2f^2} \quad q = \frac{4zV}{mr_o^2f^2}$$

where  $U$ ,  $V$  and  $f$  are the DC potential, RF potential and RF frequency, respectively, and  $r_o$  is the quadrupole's field radius (Kero et al., 2005).



**Figure 1-4:** (A) Mathieu stability diagram for ions of  $m/z$  28, 69, and 219. (B) Simulated mass spectra showing these ions as the RF and DC voltages are scanned along the dotted and solid scan lines (in A). Figure recreated from Kero *et al.* (Kero et al., 2005).

The quadrupole is essentially a mass filter, in which the applied RF and DC voltages determine which ions have a stable trajectory through the quadrupole. Figure 1.4 shows the stability diagram for ions of  $m/z$  28, 69 and 219. It can be seen that when the DC voltage (Mathieu parameter  $a$ ) is set to zero, ions of a wide mass range have a stable motion and are passed through the quadrupole. In this mode the quadrupole acts as an ion guide. With increasing DC voltage, the stability region decreases in size, and thus the  $m/z$  range of ions with a stable trajectory decreases. By ramping the RF and DC voltages synchronously it is possible to perform a mass analysis, by sequentially only permitting the transmission of selected ions (and in which the DC voltage determines the mass resolution of the mass analysis). The solid and dashed lines in Figure 1.4 represent two such scan lines, a lower resolution and higher

resolution mass scan. The figure shows idealized mass spectra resulting from these two scans. It can be seen that the values of the RF and DC voltage can be selected to transmit a single ion of interest, which is used extensively in quadrupole-time-of-flight (Q-TOF) type instruments for selection of the precursor ion (Kero et al., 2005).

### 1.2.2.2 Time-of-flight mass spectrometry

A TOF mass analyzer (Figure 1.5A) is a pulsed system and so has been extensively coupled to MALDI ion sources. It is also used with ESI, in which pulsed ion gates are used to introduce packets of ions from the continuous ESI beam. In a MALDI-TOF system the ion source consists of a target plate (containing the MALDI sample) separated by a short distance from a series of counter electrodes. A strong electric field between the target plate and the first counter electrode, 20-30 kV over a distance of a few mm is common, means any ion formed by the MALDI process is immediately accelerated into the mass spectrometer. MALDI generated ions are normally singly charged and so the kinetic energy of the ion (in eV) is simply equal to the accelerating potential of the MALDI-TOF ion source. All ions then enter the time-of-flight region with the same kinetic energy. The time-of-flight ( $T_f$ ) is defined as the time between the MALDI laser pulse and the moment the ion hits the detector. In its most simple form this can be written as:

$$T_f = \frac{L}{v} \quad (1)$$

$$E_k = \frac{mv^2}{2} = zV \quad (2)$$

where  $L$  is the length of the flight tube,  $v$  is velocity,  $E_k$  is the kinetic energy,  $m$  is mass,  $z$  is charge, and  $V$  is the accelerating potential of the ion source. A substitution results in formula (3), which shows that when  $L$  and  $V$  are constant the time-of-flight is proportional to the square root of the  $m/z$  ratio. Higher molecular weight molecules will have longer flight times compared to small molecules (Cotter, 1992; Guilhaus et al., 1997).

$$T_f = L \sqrt{\frac{m}{z}} \sqrt{\frac{1}{2V}} \propto \sqrt{\frac{m}{z}} \quad (3)$$

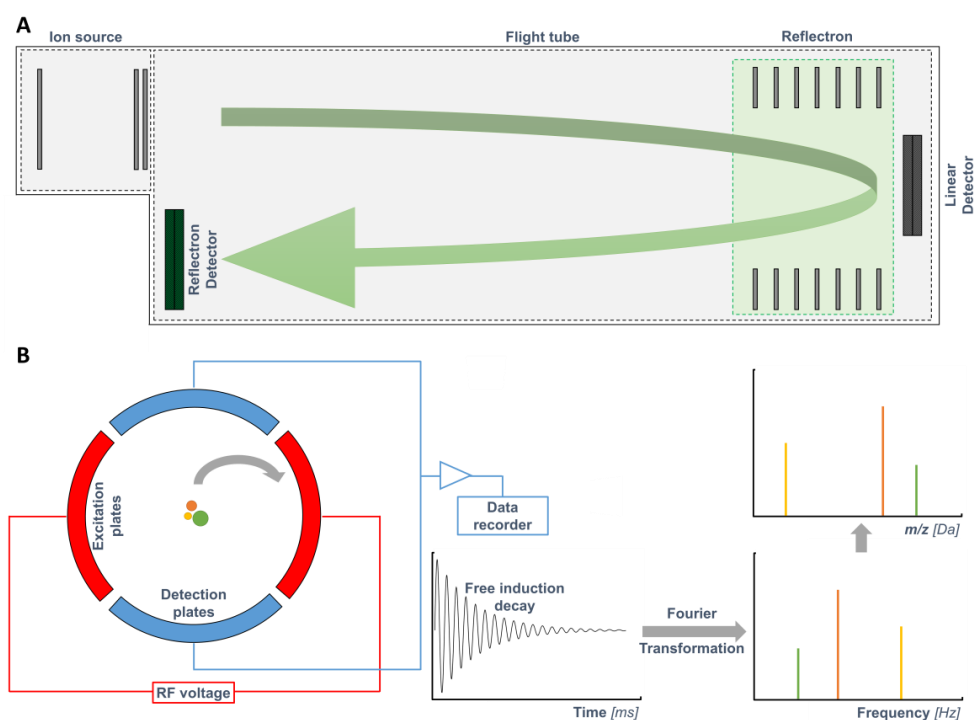
Such a simple TOF mass spectrometer results in a moderate mass resolving power (Radionova et al., 2016). Over the last decades multiple developments have further increased the achievable mass resolution. These include:

(i) pulsed extraction – otherwise known as time-lag focusing or delayed extraction, uses an additional pulsed electric field in the ion source to time focus the ions on to the detector (Brown and Lennon, 1995; Wiley and McLaren, 1955).

(ii) reflectron – effectively an electrostatic mirror that reflects ions onto the detector. Faster ions move deeper into the mirror before being reflected, and thus travel a longer distance. Careful design of the reflectron field enables the ions of different mass to be time-focused onto the detector, thereby improving mass resolution (Mamyrin et al., 1973).

(iii) longer flight tubes – as can be seen in equation (3) a long flight tube theoretically leads to longer flight times, and increased time between ions of different mass (so greater mass resolution). However, this is offset by dispersion of the ions during the time-of-flight. In order to increase the flight path without losing mass resolution, a focusing electrostatic lens was introduced in the flight tube (Vestal and Juhasz, 1998).

(iv) orthogonal acceleration – orthogonal acceleration TOF systems decouple the mass analysis from the ion generation event. In this manner the variability in initial position and energy of ion formation, which compromises the theoretical performance of axial TOF systems, has less effect on the performance of an orthogonal acceleration TOF system (Dawson and Guilhaus, 1989).



**Figure 1-5:** A schematic overview of **(A)** a linear TOF mass analyzer including a reflectron and reflectron detector for ion focusing, and **(B)** the process of FTICR mass analysis and signal conversion.

Modern TOF systems have many characteristics favorable to MSI, including rapid scan speeds, high sensitivity, good mass resolution and mass accuracy (up to several ppm and 50k resolving power for thin layer samples using a highly focused laser beam), wide mass range, and good dynamic range ( $10^2 - 10^3$ ).

### 1.2.2.3 Fourier Transform mass spectrometry

While TOF-MS will provide decent performance, based on mass accuracy and resolving power, for some applications higher performance is required. Fourier Transform MS (FTMS) is capable of providing ultra-high mass resolution and accuracy, as well as a much higher dynamic range. It may not be necessary for every application to analyze samples using ultra-high resolution and accuracy, however, in some applications in which the samples consist of complex analyte mixtures containing many near-isobaric species, FTMS is essential in order to obtain accurate and confident molecular identifications (Scigelova et al., 2011).

In FTMS, the most common mass analyzers are the Fourier Transform Ion Cyclotron Resonance (FTICR) (Comisarow and Marshall, 1974) and the Orbitrap (Makarov, 2000). And, although their appearance is very different, both FTICR and Orbitrap analyzers use an image current detection system and the application of a mathematical Fourier transformation to convert the time domain transients, produced by the image current, into a mass spectrum (Scigelova et al., 2011). FTICR is based on the rotational (cyclotron) motion of an ion in a magnetic field. In FTICR-MS (Figure 1-5B), the ions are guided into a Penning trap placed in the center of a strong magnetic field (usually provided by a superconducting magnet). There, the ions are trapped by an electric field provided by two trapping electrodes at both ends of the trap. The ions trapped in the magnetic field rotate in a plane perpendicular to the magnetic field, at their cyclotron frequency (minus a small frequency due to the trapping field and the presence of other ions in the trap). At room temperature the cyclotron frequency of an ion is very small, e.g. in a 9.4 T field an ion of  $m/z$  1000 has a cyclotron radius of 0.077 mm (Marshall et al., 1998). In order to detect the ions, their cyclotron motion is excited by the application of a radio-frequency (RF) electric field at the ion's cyclotron frequency. All ions of the same  $m/z$  ratio are excited, coherently, within the ICR trap, increasing their cyclotron radius. After the excitation field is switched off, the ICR-motion-excited ions remain at their excited radii. The coherent motion of these ions induces an image charge as they move past a detector plate; using a pair of opposing detector plates leads to the creation of an image current oscillating between the plates, at the ion's cyclotron frequency. This image current is converted to a voltage, amplified and digitized, and forms the free-induction-decay (FID) of the FTICR experiment. A Fourier transform is used to convert the ICR signal from the time domain to the frequency domain. In the absence of an electric field or the presence of other ions (space charge) an ion moving freely in a magnetic field, rotates with a characteristic cyclotron frequency, given by

$$\omega = \frac{q}{m} B \quad (4)$$

in which  $\omega$  is the ICR frequency,  $q$  represents charge,  $m$  is the mass of the ion and  $B$  is the magnetic field strength (Nikolaev et al., 2016). In the presence of space charge the ion moves with two distinct circular motions, the reduced cyclotron motion (at a frequency slightly below that of the free cyclotron frequency) and the magnetron motion (a slow and low frequency secular motion). A number of different equations have been reported for accurate calibration of FTICR datasets (Barry et al., 2013; Marshall, 1998). The two most common calibration equations are those reported by Francl and Ledford (Francl et al., 1983; Ledford et al., 1984).

$$\text{Francl: } \frac{m}{z} = \frac{A}{\omega + B}$$

$$\text{Ledford: } \frac{m}{z} = \frac{A}{\omega} + \frac{B}{\omega^2}$$

The advantage of the Francl equation is that the numerator is dependent only on the magnetic field strength, and  $B$  is essentially a correction factor for the near-constant shift in frequency due to space charge. Accordingly, FTICR mass spectra that have been calibrated using the Francl equation can be recalibrated using a single internal lock mass to correct for differences in space charge from scan to scan (Barry et al., 2013; Easterling et al., 1999).

Ultra-high resolution and mass accuracy of FTICR mass spectrometers are highly dependent on the strength of the magnetic field provided by the superconductive magnets. For this reason, progress in FTICR-MS resolution/mass accuracy has benefited from developments in superconductive magnet technology (Nikolaev et al., 2016).

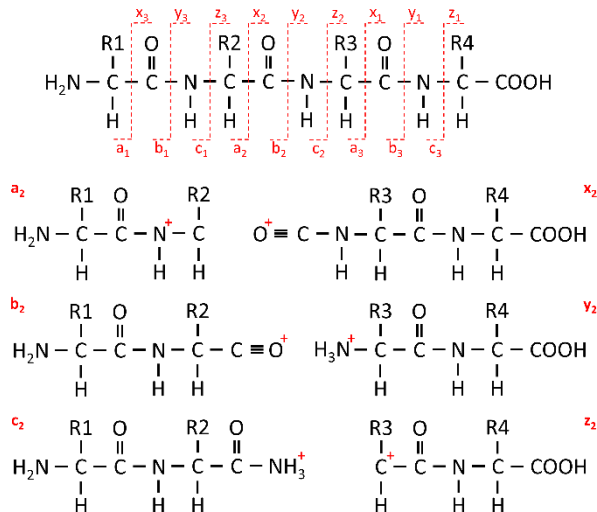
### 1.2.3 Tandem mass spectrometry

The availability of a wide variety of ionization, mass analysis and detection methods has made mass spectrometry a powerful tool for the characterization of biomolecules. In order to assign definitive identities to the detected ions it is necessary to fragment the ions into structurally informative fragments. Structural information is obtained by selecting and isolating single ion species from the sample, cause them to fragment, and analyze the masses of the fragments (de Hoffmann, 1996). This is commonly referred to as tandem mass spectrometry (MS/MS), as it involves at least two stages of mass analysis. The first stage of mass analysis is used to select and isolate the precursor ion. Following the fragmentation event (discussed in more detail below) the fragment ions undergo the second stage of mass analysis where they are separated, based on their

$m/z$ , before reaching the detector. Depending on the instrumental setup MS/MS can be performed either in space by coupling two mass analyzers; in time by performing the two events in the same mass analyzer, utilizing an ion storage device; or in a combination of space and time, in so-called hybrid instruments (de Hoffmann, 1996).

**Table 1-1:** Characteristics of commonly applied fragmentation methods for tandem MS of peptides and proteins.

Fragmentation method	Peptide/protein fragment ions	Satellite ions	Retains labile PTMs	MALDI / ESI	Instruments	References
<b>collision-induced dissociation (CID)</b>	b, y		(-)	Both	TOF, FTMS, IT	Frese et al., 2011; Wells and McLuckey, 2005
<b>higher-energy collisional dissociation (HCD)</b>	a, b, c, x, y, z	d, v, w	(-)	Both	TOF, FTMS, IT	Frese et al., 2011; de Graaf et al., 2011
<b>electron-transfer dissociation (ETD)</b>	c, y, z+1, z+2	w	(+)	ESI	FTMS, IT	Han et al., 2008; Qi and Volmer, 2017
<b>negative electron transfer dissociation (NETD)</b>	a, x		(+)	ESI	FTMS, IT	Coon et al., 2005; Riley et al., 2015
<b>electron-detachment dissociation (EDD)</b>	a, x		(+)	ESI	FTMS, IT	Budnik et al., 2001; Ganisl et al., 2011
<b>infrared multi-photon dissociation (IRMPD)</b>	b, y		(-)	Both	FTMS	Reilly, 2009; Vasicek et al., 2011



**Figure 1-6:** Overview of the different fragment ions produced during peptide fragmentation. The top panel shows the fragmentation of the peptide backbone, the lower panel shows the ions formed during fragmentation.

A common example of MS/MS in space is performed using a Q-TOF type instrument, in which the precursor ion is isolated with a quadrupole mass analyzer. The isolated ions are then accelerated into a collision cell (typically another multipole in a separate vacuum chamber held at higher pressure) where they will collide with an inert gas (e.g. N<sub>2</sub>). The collision converts some of the kinetic energy of the precursor ion into internal energy. If the increase in internal energy is sufficient it will cause the precursor ions to fragment in a process termed collision-induced dissociation (CID), pioneered by Jennings, and McLafferty in the late 1960s (Jennings, 1968; McLafferty et al., 1973). In a Q-TOF setup, the newly formed fragments enter a TOF section for mass analysis and detection. By switching the DC component of the quadrupole off/on, a Q-TOF instrument can be rapidly switched between MS and MS/MS. Such switching is now routinely performed for data dependent MS/MS, in which the most intense ions detected in the MS scan are selected for isolation in the quadrupole, and fragmented by CID before fragment ion analysis.

MS/MS in time is normally employed in trap-based MS platforms (e.g. ion traps and FTICR). The fragmentation step occurs following a chain of events: (i) all ions are guided to the mass analyzer, (ii) all but the selected ions are ejected from the trap, (iii) the ion's flight path is excited by using an auxiliary RF field at the frequency of the ion's secular motion in the trap, (iv) a collision gas is introduced into the trap, collisions between the excited ions and gas molecules cause fragmentation, (v) mass analysis of the fragments (de Hoffmann, 1996).

Many fragmentation methods are currently available, each with its specific set of fragmentation characteristics and application areas, nevertheless the basic principle of fragmenting selected precursor ions in order to obtain structural information remains the same. In the tandem MS analysis of peptides, the choice of fragmentation method will affect the type of fragment ions detected in the MS/MS spectrum. Roepstorff & Fohlman proposed the nomenclature for the different fragment ions which is still used to date, albeit after modifications by Johnson *et al.* (Johnson et al., 1987; Roepstorff & Fohlman, 1984) (Figure 1-6 & Table 1-1).

### 1.3 Mass spectrometry imaging

The mass spectrometric analysis of sample surfaces was made available with the introduction of secondary ion MS (SIMS). However, the introduction of MALDI-MS provided the breakthrough for the analysis of large biomolecules. Both SIMS and MALDI-MS are capable of acquiring mass spectra from discrete locations, which makes them suitable technologies for imaging applications. The first *macromolecular* mass spectrometry imaging (MSI) analysis of biological samples was performed in 1997 by Caprioli *et al.* (Caprioli et al., 1997). This first publication showed the distribution of several proteins and peptides in various biological tissues following analysis by spatially correlated MALDI-MS. While the early work in the Caprioli lab focused on the development of software to automate the spatially correlated tissue analysis by MALDI-

MS, it was quickly recognized that the MSI technology was of great value for biomedical and clinical research (Chaurand et al., 1999; Stoeckli et al., 1999, 2001).

The principle behind every MSI analysis is the acquisition of spatially correlated mass spectra from discrete spots on a sample surface (Figure 1-7). The single mass spectra, acquired following a Cartesian coordinate system, are assembled into a data cube in which the X- and Y-axes represent the X- and Y-coordinates of the image, the Z-axis represents the  $m/z$  ratio, and the values at each voxel the intensities. By selecting a specific  $m/z$ , representing an analyte, one can plot the intensity as a function of position, to display the relative abundance of the analyte throughout the analyzed sample (McDonnell and Heeren, 2007).

### 1.3.1 MSI modalities

Depending on the application and the analytical requirements, a variety of MSI modalities are available (Figure 1-8). Secondary ion mass spectrometry (SIMS, Figure 1-8B) is available for the very high spatial resolution ( $\sim 50$  nm) analysis of atomic ions and small molecules (Slodzian et al., 1992). In SIMS, a focused (primary) ion beam is fired at the sample surface. Upon impact, part of the primary ions' kinetic energy is transferred to the atoms and ions on sample surface. If their resulting kinetic energy exceeds the binding energy of the substrate, the atoms and ions are released (Delcorte and Garrison, 2000). The analysis of larger molecules by SIMS suffers from poor sensitivity, as a result of the decrease in secondary ion emission for higher  $m/z$  species (Touboul et al., 2004). In desorption electrospray ionization (DESI, Figure 1-8C), the first MSI modality capable of analysis under ambient conditions, features of both ESI and desorption ionization methods are combined. An electrospray needle, directed at the sample, is used to create a focused electrospray by applying a high electrical potential to the spray solution. Like in a conventional ESI source, droplet formation, desolvation and acceleration is assisted by a gas flow (Takáts et al., 2004). During the brief interaction of the charged droplets with the target surface, analytes present on the surface are transferred to the mass spectrometer inlet following the droplet pick-up model (Venter et al., 2006). DESI-MSI is very well suited for small molecule and lipid analysis, but similar to SIMS, has a low sensitivity analyzing large biomolecules from tissue samples. One of the major advantages of DESI, and other ambient ionization methods, is that it does not require sample preparation for the analysis of analytes from either solid, frozen, liquid, or gaseous samples (Takáts et al., 2004, 2005). The success of DESI-MSI was followed by the rapid development of many novel ambient ionization methods. A thorough review of a large number of ambient ionization methods is provided by Wu *et al.* (Wu et al., 2013). Here a short description of the more established techniques is provided.

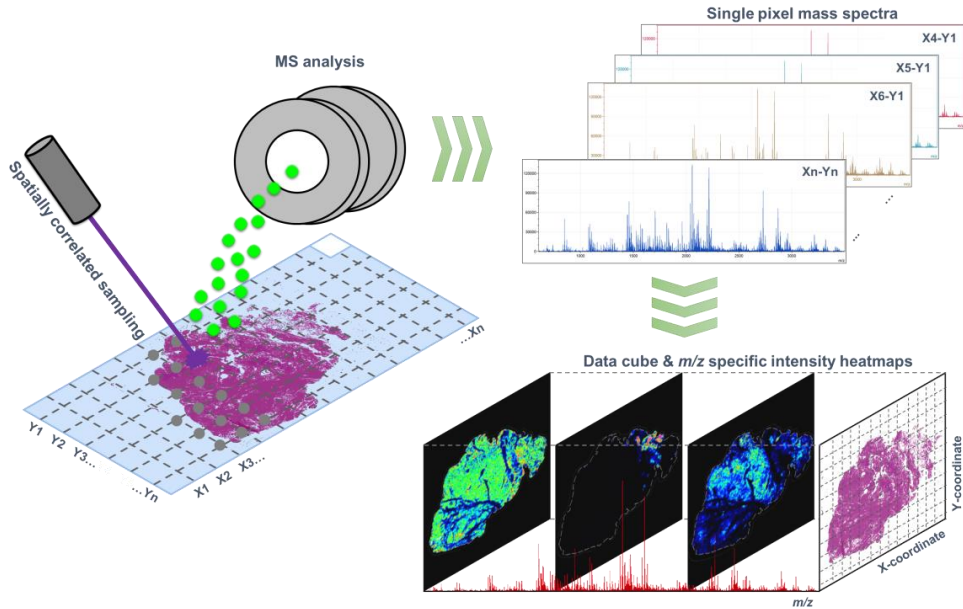
In laser ablation electrospray ionization (LAESI, Figure 1-8D) mass spectrometry, a focused mid-infrared laser irradiates discrete spots on the sample surface exciting OH vibrations of water molecules in the sample, causing desorption of the analyte



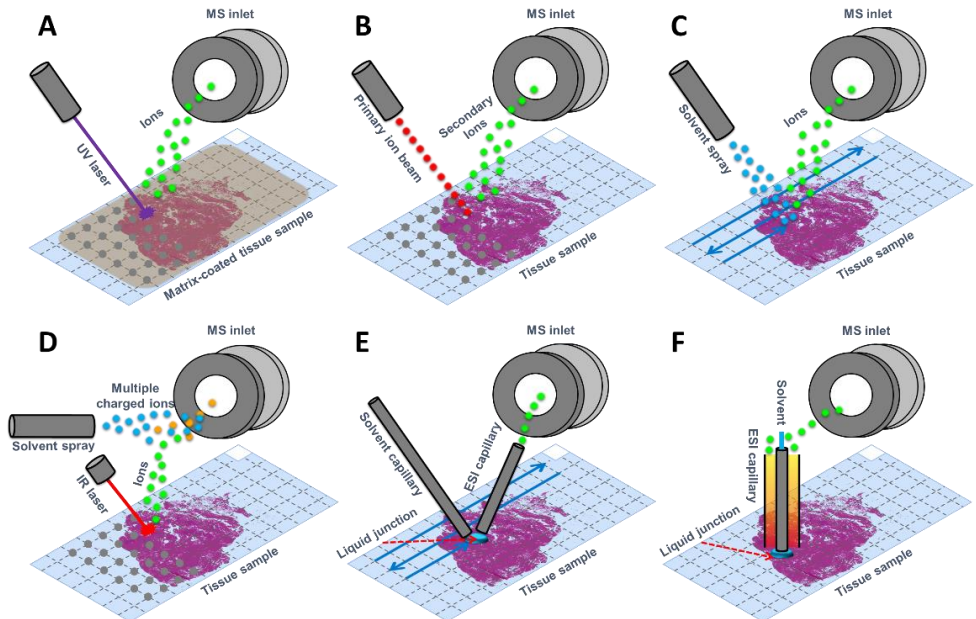
molecules from the sample surface. The desorbed molecules are post-ionized by capturing them in an electrospray jet, positioned 1-3 cm above the sample surface. LAESI is performed under atmospheric pressure in ambient conditions, and does not require extensive sample preparation as it uses water in the sample as the laser-absorption matrix. This MSI modality has been applied for the analysis of a multitude of analyte classes, ranging from small molecules to peptides and proteins (Nemes and Vertes, 2007; Wu et al., 2013).

Nano-DESI (Figure 1-8E) and liquid extraction surface analysis (LESA, Figure 1-8F) are closely related MSI modalities as they both use liquid microjunction surface-sampling (LMJ-SSP) to transfer analytes from the sample surface to the MS. LMJ-SSP is based on a set of capillaries that are in close proximity of each other and to the sample surface. A solvent flow connects the capillaries and sample surface through a liquid microjunction, allowing the localized extraction of analytes from the sample surface (Van Berkel et al., 2002). The configuration of the capillaries is what sets apart nano-DESI and LESA. In a typical LESA setup, a concentric capillary is placed just above the sample surface in a perpendicular fashion. Solvent will flow through the outer capillary, forming a liquid junction with the sample surface, allowing analyte extraction from the sample surface. The inner capillary is used to aspirate the dissolved analytes and guide them to an ESI source where the analytes are ionized and enter the MS, as illustrated in Figure 1-8F (Kertesz and Berkel, 2010). The nano-DESI setup is based on the same principles, but uses two separate capillaries (one solvent supplying capillary, and one aspirating capillary) that move over the sample in conjunction, allowing lower flow rates and smaller liquid bridges (resulting in better lateral resolution) (Lanekoff et al., 2013). Both these MSI modalities operate under atmospheric pressure and ambient conditions and find their applications in the analysis of small molecules, pharmaceuticals, lipids, and (proteolytic) peptides (Van Berkel et al., 2008; Eikel et al., 2011; Rao et al., 2013).

Due to its versatility, the most popular MSI modality is MALDI-MSI (Figure 1-8A); while most ambient MSI modalities are limited to the analysis of small molecules and lipids, MALDI-MSI is routinely used for the analysis of small molecules, lipids, *N*-linked glycans, (proteolytic) peptides, intact proteins, and more recently also proteoforms (Dilillo et al., 2017; Ellis et al., 2016; Kriegsmann et al., 2016; Liu et al., 2013a; Lou et al., 2016a; Powers et al., 2013). Most ambient MSI modalities have in common that, in order to analyze a sample, hardly any sample preparation is required. In MALDI-MSI the class of analytes that is eligible for analysis is determined mostly by the sample preparation method.



**Figure 1-7:** Schematic overview of the principle of mass spectrometry imaging (MSI).



**Figure 1-8:** Schematic representations of various MSI modalities: **(A)** matrix-assisted laser desorption/ionization (MALDI), **(B)** secondary ion mass spectrometry (SIMS), **(C)** desorption electrospray ionization (DESI), **(D)** laser-assisted electrospray ionization (LAESI), **(E)** nano-flow desorption electrospray ionization (nano-DESI), and **(F)** liquid extraction surface analysis (LESA). Adapted from Addie *et al.* (Addie *et al.*, 2015).

## 1.4 Sample preparation for MALDI-MSI

### 1.4.1 Tissue fixation and sampling

MALDI-MSI is commonly used for the analysis of biological tissue samples. While MALDI-MSI analysis of insect and plant tissue have been reported (Grassl et al., 2011; Kaftan et al., 2014; Kaspar et al., 2011; Khalil et al., 2015; Peukert et al., 2012; Sturtevant et al., 2016), MALDI-MSI is more commonly used for biomedical research involving the analysis of human or animal model tissues (Balluff et al., 2010; Carreira et al., 2015; Dekker et al., 2014). MALDI-MSI is usually performed on thin tissue sections of thickness 4-20  $\mu\text{m}$ , obtained from either fresh frozen, heat stabilized, or chemically fixed (most commonly using formalin) tissues (Goodwin, 2012; Thomas and Chaurand, 2014). In order to maintain tissue integrity during the process of tissue sectioning, tissues are often embedded in an embedding material. For different applications, a great variety of embedding materials are available; paraffin, optimal cutting temperature (OCT), aqueous solutions of gelatin, and/or carboxymethyl cellulose (CMC) (Casadonte and Caprioli, 2011; Chen et al., 2009a; Schwartz et al., 2003; Stoeckli et al., 2007). The different tissue fixation and embedding methods each come with their specific set of benefits and limitations (Tables 1-2 & 1-3).

For MALDI analyses, performed in vacuum or intermediate pressure ion sources, the tissue samples are mounted on a conductive surface (the conductive surface is needed for the definition of the electric extraction field, which transfers ions to the mass analyzer). The conductive surface also helps dissipate the charge formed by photoelectrons after illumination with the UV laser. Ineffective dissipation of the charge will result in local distortions of the electric field in the sampled area, and cause mass shifts of the detected ions (Frankevich et al., 2003; Ibáñez et al., 2007; Knochenmuss, 2004). Steel target plates were used in early MALDI-MSI experiments. However, mounting tissues on glass coated with a transparent and conductive material (e.g. indium tin-oxide (ITO)) is now routine as it enables the post-analysis co-registration with histological images (Amstalden van Hove et al., 2010; Chaurand et al., 2004; Chughtai et al., 2012). A common problem in histopathology is the detachment of tissue sections from the glass slides during staining procedures in which the samples are repeatedly submerged in a series of staining solutions. In order to increase the adherence of the tissue sections to the glass slide, the slide is coated using a strong polycationic polymer of L-lysine residues, poly-L-lysine. The cationic sites in the L-lysine polymer interact with the anionic sites in the tissues, strengthening the adherence between the glass and the tissue. This method, first implemented by Zavalin *et al.*, is commonly implemented in the workflow for protein analysis by MALDI-MSI (Zavalin et al., 2012).

### 1.4.2 Tissue washing

The chemical complexity of a tissue section can lead to poor sensitivity in MALDI-MSI analyses. Tissue washes were introduced to reduce the chemical complexity and

improve detection sensitivity by selectively removing interfering compounds from the tissue section, whilst retaining the spatial distribution of the analytes of interest. Tissue washing was first introduced for the MALDI-MSI analysis of intact proteins, and improved measurement sensitivity by removing physiological salts and a large part of the lipid content present in the tissue (Lemaire et al., 2006; Schwartz et al., 2003). Early tissue washing procedures for protein analysis usually contained several steps by

**Table 1-2:** Various tissue fixation methods and relevant characteristics for MSI.

Tissue fixation methods	In situ/ Ex vivo	Ischemia time	Enzymatic activity	Effect on histology	References
<b>Post-mortem freezing</b>	Ex vivo	Minutes	Paused	Freezing artefacts, post-mortem degradation	Hattori et al., 2010
<b>In-situ/funnel freezing</b>	In vivo	None	Paused	Freezing artefacts, post-mortem degradation	Hattori et al., 2010; Mulder et al., 2016
<b>Focussed microwave irradiation</b>	In vivo	None	Terminated	Bubble formation; increased tissue fragility	Sugiura et al., 2014
<b>Heat-induced stabilization</b>	Ex vivo	Minutes	Terminated	Force induced deformation / flattening	Mulder et al., 2016; Sturm et al., 2013; Svensson et al., 2009
<b>Formalin fixation</b>	Ex vivo	Minutes-hours	Terminated	Isotope masking	Thavarajah et al., 2012

**Table 1-3:** Various tissue embedding compounds and relevant characteristics for MSI.

Embedding media	Chemical basis	Dissolves in	Fixation methods	Storage conditions	Potential MSI artefact	References
<b>Optimal Cutting Temperature (OCT)</b>	poly-ethylene polymers	Water	Cryo	Frozen	Signal suppression / Polymer contamination	Cazares et al., 2015; Groseclose and Castellino, 2013
<b>Gelatin</b>	Collagen	Water	Cryo	Frozen	Interference in high mass analysis	Altelaar et al., 2005; Dong et al., 2016
<b>Carboxymethyl cellulose (CMC)</b>	Poly-saccharide	Water	Cryo	Frozen	Polymer contamination in high mass analysis	Kawamoto, 2003
<b>Paraffin</b>	Alkane/ Organic	Aromatic organic solvents	Formalin fixed	Room temp.	Loss of metabolites & lipids	Porter et al., 2017
<b>Poly[N-(2-hydroxy-propyl)-methacryl-amide] (pHPMA)</b>	HPMA polymer	Water	Cryo	Frozen	Polymer contamination in high mass analysis	Strohalm et al., 2011

either rinsing or submersing the samples in a variety of organic solutions (e.g. ethanol, isopropanol, chloroform, acetone, or hexane). Later, also washes with water, or aqueous buffers were added to increase the sensitivity of the analysis of hydrophobic compounds (e.g. membrane proteins, specific classes of lipids), and proteins after on-tissue proteolytic digestion (Angel et al., 2012; Enthaler et al., 2013a; Grey et al., 2009; Groseclose et al., 2007; Nicklay et al., 2013; Thomas et al., 2013). Also, water-based tissue washes were successful in the clean-up of tissue sections by removal of polymers (e.g. polyethylene glycol (PEG), and polyethylene vinyl (PEV)) originating from embedding media, such as OCT (Cazares et al., 2009).

The early tissue washing protocols were developed on (mouse or rat) brain tissue. The brain contains many distinct regions with profound difference in their molecular composition, which simplifies the assessment of molecular delocalization, or lateral diffusion. However, with the introduction of MALDI-MSI in clinical research, studies were set up with tissues of different origin (e.g. other organs, tumors) and methods optimized for brain tissue proved insufficient or incompatible. Several tissue treatment optimization studies exemplify the improvement in analysis quality that can be gained from the tedious effort of method optimization (Enthaler et al., 2013a; Lou et al., 2016b; Martin-Lorenzo et al., 2015).

Tissue washing is usually omitted when it comes to analyzing small molecules, as the tissue washing procedures are commonly used to remove small molecules as interferants in the analysis of other molecular classes. However, Shariatgorji *et al.* have proposed a tissue cleanup procedure based on pH-controlled buffers for the targeted analysis of small molecule drugs by MALDI-MSI. In this particular study, tissues were washed in a pH-controlled, and concentration adjusted buffer in which the target compounds were insoluble and the interfering endogenous compounds were removed, improving the measurement sensitivity for various pharmaceutical compounds (Shariatgorji et al., 2012).

### 1.4.3 On-tissue digestion

In bottom-up proteomics, proteins are identified by analyzing and fragmenting proteolytic fragments, produced by an in-solution digestion with a proteolytic enzyme (Altelaar et al., 2012). Similar to this approach, proteolytic enzymes can be applied directly to tissue sections to digest the proteins *in-situ*. This on-tissue digestion approach was first explored by Shimma *et al.* in 2006, who applied trypsin to a fresh frozen mouse brain section using a chemical inkjet printer and performed on-tissue MALDI-MS/MS to identify proteolytic peptides directly from the tissue (Shimma et al., 2006). In 2007, the on-tissue digestion approach was applied by Groseclose *et al.* to perform MALDI-MSI of proteolytic peptides (Groseclose et al., 2007). In this pioneering work the analysis of proteolytic peptides by MALDI-MS/MS was used to identify the proteolytic peptides in a similar fashion presented by Shimma *et al.* Moreover, the distributions of the proteolytic peptides in the tissue, obtained by MALDI-MSI of the

proteolytic peptides, was used to assign identities to  $m/z$  features detected in an intact protein MALDI-MSI analysis. MALDI-MS/MS directly from tissue sections has, since then, been successfully performed by a number of groups (Groseclose et al., 2007; Schober et al., 2011; Shimma et al., 2008). However, the lack of chromatographic separation and the small amount of tissue present in each pixel make it a very challenging approach. Ion mobility separation (IMS) MALDI-MSI has been performed to compensate for the lack of chromatographic separation, and has proven itself a useful tool for on-tissue feature identification (McLean et al., 2007; Stauber et al., 2010; Trim et al., 2008). However, the greatest number of peptide identity assignments have been achieved through mass matching the MALDI-MSI peak list with peptide identifications obtained through LC-MS/MS analysis of tissue extracts (Casadonte et al., 2014; Schober et al., 2011). High-resolution, accurate mass (HRAM) MS is essential in order to obtain accurate and confident peptide identifications from the LC-MS/MS analysis and to resolve the complex mixture of (near) isobaric proteolytic peptides created by the on-tissue proteolytic digestion (Groseclose et al., 2007; Schober et al., 2012). Despite the challenge that the complexity of the sample imposes on the experiment, the analysis of proteolytic peptides does enhance the proteomic information gained from a single tissue section, by enabling the analysis of larger proteins that are otherwise difficult to analyze by MALDI-MSI (Groseclose et al., 2007). An additional benefit of on-tissue proteolytic digestion is that it allows the analysis of sections originating from FFPE tissues, and as many clinical biobanks consist of FFPE tissues, the ability to obtain spatially correlated proteomic information from these samples is invaluable. A (partial) reversal of the formalin fixation by an antigen retrieval step, followed by a proteolytic digestion 'releases' the peptides and makes them eligible for MALDI-MSI analysis (Djidja et al., 2009b; Groseclose et al., 2008; Lemaire et al., 2007; Ronci et al., 2008).

Trypsin is often the enzyme of choice for bottom-up proteomics and on-tissue digestion MALDI-MSI analyses, nevertheless other proteases, such as pepsin, elastase, Arg-C, Lys-C, and Lys-N, as well as combinations of proteases, such as trypsin/Lys-C, have also been reported and have proven to be beneficial for proteome coverage (Angel et al., 2012; Enthaler et al., 2013a; Grey et al., 2009; Groseclose et al., 2007; Nicklay et al., 2013; Thomas et al., 2013). Although the majority of reports concerning on-tissue digestion MALDI-MSI describes the use of proteolytic enzymes, the pioneering work by Groseclose *et al.* also demonstrated the ability of the endoglycosidase Peptide *N*-glycosidase F (PNGase F) to perform *in-situ* protein deglycosylation (Groseclose et al., 2007). Later, Powers *et al.* demonstrated the ability to perform *N*-linked glycan MALDI-MSI after on-tissue digestion with PNGase F on both fresh frozen and FFPE tissues (Powers et al., 2013, 2014). As *N*-linked glycans are not affected by the chemistry of the formalin fixation, *N*-glycan MALDI-MSI can be performed from FFPE tissues both with and without the prior treatment with an antigen retrieval method (Holst et al., 2016; Briggs et al., 2017; Powers et al., 2013, 2015).

In bottom-up proteomics disulfide bond reduction in conjunction with alkylation is routinely used to help denature the proteins and thereby increase their accessibility to the proteases. Green-Mitchell *et al.* have adapted this approach for direct use on tissue sections, in order to improve and confirm the detection of insulin in pancreatic tissue sections (Green-Mitchell *et al.*, 2011).

#### 1.4.4 On-tissue derivatization

Chemical derivatization, the alteration of the chemical properties of a molecule by adding a (functional) chemical group, is often applied in MS-based research to increase the measurement sensitivity for the analysis of compounds that suffer from poor ionization (Liu and Hop, 2005; Melikian *et al.*, 1999). More recently, this strategy has been translated to enable the *in-situ* analysis of derivatized analytes by MALDI-MSI (Chacon *et al.*, 2011; Franck *et al.*, 2009). Chemical derivatization of small molecules for MALDI-MSI analysis is typically not only used to improve the ionization efficiency, but also to increase the analyte mass to prevent suppression, or masking, by MALDI matrix peaks that are commonly found in the same  $m/z$  range. On-tissue derivatization is commonly used in MALDI-MSI for the analysis of amino acids, neurotransmitters, and amino metabolites, and has been applied in studies on cancer and neurodegenerative disorders (Shariatgorji *et al.*, 2014; Esteve *et al.*, 2016; Toue *et al.*, 2014).

Whilst on-tissue derivatization is mostly used for the analysis of small molecules, an *in situ* derivatization method for protein and peptide N-termini has also been reported. This method was reported to improve the *in-situ* identification of on-tissue digested proteins (Franck *et al.*, 2009). Furthermore, the *in-situ* derivatization of sialylated *N*-glycan species was reported by Holst *et al.*, and resulted in: (i) stabilization of sialic acids during MALDI-MSI analysis, (ii) reduction of the ionization bias induced by the negative charge of the sialic acids in the positive ion analysis, and (iii) differentiation between  $\alpha$ 2,3- and  $\alpha$ 2,6-linked sialic acid, which are implied in tumor progression and resistance to chemotherapy (Holst *et al.*, 2016).

#### 1.4.5 Matrix application

A robust and homogeneous MALDI matrix deposition is key to a high quality MALDI-MSI analysis. The choice of matrix, solvent system, and the deposition method determine which the analyte class may be analyzed, as well as the sensitivity and spatial resolution with which they may be examined (Goodwin, 2012; Thomas and Chaurand, 2014b). In the first MALDI-MSI analyses, described by Caprioli *et al.*, matrix was applied by rinsing the tissues in a saturated matrix solution, resulting in severe lateral diffusion of the analyte molecules. The same publication describes matrix deposition using electrospray resulting in an improvement of the determination of the analyte location (Caprioli *et al.*, 1997). Since these initial experiments many matrix deposition methods have been developed, which can be divided into three groups: (i) spotting methods, (ii) spray-based methods, and (iii) solvent-free methods.

The spotting methods are based on the droplet matrix application approach that is commonly used in sample preparation protocols for regular MALDI-MS. An array of pico-liter-sized droplets is spotted on to the tissue surface using a chemical printer, resulting in matrix spots with a diameter of  $\sim 200 \mu\text{m}$ . The small spotting volumes, e.g.  $\sim 10 \text{ pL}$  per spot per iteration, and the inter-spot spacing decreases the risk of molecular delocalization. Other than the lower risk of molecular delocalization, spot-based methods are known for their superior S/N ratio, and number of detected analytes compared to other matrix deposition methods. One of the major limitations of the spot-based methods is the relatively low spatial resolution, which is limited by the droplet pitch and is defined during the matrix deposition (Aerni et al., 2006; Végvári et al., 2010).

Spray-based matrix application has the advantage that the matrix is deposited in a continuous manner, which enables the definition of the spatial resolution based on the size of the matrix crystals ( $\sim 20 \mu\text{m}$ ). Several automated sprayer systems are available, either based on a pneumatically-assisted spray (TM Sprayer (HTX Technologies, Carrboro, NIC, USA), SunCollect (SunChrom GmbH, Friedrichsdorf, Germany), iMatrix spray (Stoeckli and Staab, 2015)), or vibration-based nebulization (ImagePrep (Bruker Daltonics, Bremen, Germany) of the matrix solution (Thomas and Chaurand, 2014).

More recently, solvent-free matrix deposition by sublimation was introduced for the MALDI-MSI analysis of small molecules and lipids (Hankin et al., 2007; Puolitaival et al., 2008). The absence of solvent results in very small matrix crystal sizes, which allows for extremely high spatial resolution analyses by MALDI-MSI ( $\sim 5 \mu\text{m}$ ) (Chaurand et al., 2011). Initially, sublimation was only used for small molecules and lipids due to the limited molecular extraction capabilities of the method. However, sublimation in combination with a matrix recrystallization step allowed the analysis of intact proteins up to 30 kDa at spatial resolutions as low as  $10 \mu\text{m}$  (Yang and Caprioli, 2011).

## **1.5 Clinical mass spectrometry imaging**

In the two decades since its introduction, MSI has established itself as an invaluable tool in many scientific areas, including pharmaceutical research, forensic science, and clinical research (Aichler and Walch, 2015; Atkinson et al., 2007; Balluff et al., 2010; Groeneveld et al., 2015; Reyzer et al., 2003; Wolstenholme et al., 2009). One of the key characteristics of MALDI-MSI, resulting in its widespread application in clinical research is the non-destructive nature of the method, allowing post-MSI histological staining and co-registration of the histological image with the MSI data. This multimodal MSI-histological imaging approach allows a direct investigation of how the underlying molecular composition varies with the tissue's histology.

### **1.5.1 Biomarker discovery**

The discovery of disease- or phenotype-specific biomolecular markers or profiles is a research area in which the capabilities of MSI are commonly exploited. Especially in



cancer, the histological landscape is extremely complex and heterogeneous and often contains a multitude of different cell types, including tumor cells with variable levels of differentiation, surrounding normal tissue such as adipose or connective tissue, tumor vasculature, and infiltrating immune cells. Moreover, when comparing tissue specimens from multiple patients the inter-patient variation will add to the complexity, as the cellular composition of the tumor microenvironment and the differentiation state of the tumor cells will vary with each patient. The multimodal MSI-histological imaging data enables a retrospective, digital extraction of molecular profiles from specific regions of interest, a process called virtual microdissection. By carefully selecting the regions of interest by expert pathologists, based on the clinical question, the virtual microdissection reduces the histological heterogeneity, and thereby enables a meaningful comparison of the molecular profiles from histologically homogeneous regions within and between patients. Once specific molecular features have been identified for the relevant areas they can be compared with clinical patient data (e.g. disease prognosis, treatment response, metastasis) in specialized statistical tests (Addie et al., 2015; Aichler and Walch, 2015; Lou et al., 2016b). The described methodology has been used to identify that the absence of the functional mitochondrial polypeptide cytochrome C oxidase 7A2 (COX7A2) serves as a prognostic marker for poor survival in cohort of esophageal adenocarcinoma (fresh frozen, n = 39). A result that was confirmed through a validation study applying immunohistochemical (IHC) stainings of the identified protein biomarkers to an independent tissue set (FFPE, n = 102) (Elsner et al., 2012). Moreover, an MSI-based follow-up study revealed a positive correlation between the absence of functional COX7A2 and response to neo-adjuvant chemotherapy with cisplatin. This finding was later confirmed in work on esophageal cell lines treated with a COX7A2-specific siRNA, which resulted in defective mitochondria causing an increased sensitivity to the cisplatin therapy (Aichler et al., 2013). These studies are excellent examples of the capabilities of MALDI-MSI in clinical research, although it must be noted that these studies were based on the analysis of intact proteins from fresh frozen tissue sections. The analysis of fresh frozen tissue samples often hampers the size of the analyzed cohorts as most tissue archives consist of FFPE tissues.

A tissue microarray (TMA) consists of an assembly of needle core biopsies, in which the selection of relevant and comparable regions from different patients is performed during TMA construction, and thus prior to MSI data acquisition. The advantages of TMA analysis by MALDI-MSI include the increased throughput and a reduced experimental variance. Several examples of large scale clinical studies including TMA analyses by MALDI-MSI are available. These include an early study by Djidja *et al.*, in which peptide classifiers for various tumor grades of pancreatic adenocarcinoma were constructed, based on the on-tissue digestion MALDI-MSI of a TMA of FFPE biopsies from 30 patients (Djidja et al., 2010). More recently, Kriegsmann *et al.* were successful in subtyping patients diagnosed with non-small cell lung cancer (NSCLC) into

adenocarcinoma (ADC) and squamous cell carcinoma (SqCC), an important classification for treatment stratification. The classifier was built using the data from a training TMA that contained needle core biopsies of 110 ADC and 98 SqCC patients, and utilized 339 distinct  $m/z$  features. The application of the classifier to the MALDI-MSI data from a validation TMA containing 58 ADC and 60 SqCC samples resulted in the correct classification of 117 cases (accuracy 99.1%). Several differentially expressed proteins, including known proteins used in current IHC classification (CK5, CK7), as well as novel markers (CK15, HSP27), were identified and validated by MS/MS and IHC (Kriegsmann et al., 2016).

### 1.5.2 Molecular histology

It is well established that the progression of some cancers can be described as a process of clonal evolution that starts with a single aberrant cell that, driven by (epi)genetic and/or metabolic changes, ultimately evolves into a heterogeneous tumor containing various subclones of the initial tumor clone (Dalerba et al., 2011; Gerlinger et al., 2012; Greaves and Maley, 2012). Typically, most biomarker discovery studies are based on the molecular characterization of homogenized tissue samples, ideally after microdissection of tumor cell-rich regions. While some of the tumor subpopulations may have distinct morphological features, others cannot be discerned on the basis of histology alone due to similar or overlapping morphologies. As these subpopulations are thought to drive tumor progression and influence the patient's prognosis, their elucidation is of high importance to increase our knowledge on the evolution of cancer (Greaves and Maley, 2012; Wu et al., 2010). MSI has been shown to be able to uncover the molecular intratumor heterogeneity, otherwise obscured by the lack of characterizing morphological features. In this case tissue annotation is not performed by visual inspection of the tissue's histology, but by a statistical segmentation based on the similarity of the tissue's biomolecular content (Deininger et al., 2008; Jones et al., 2011). A more recent publication by Balluff *et al.* displays the capability of MALDI-MSI to unravel the biomolecular intra-tumor heterogeneity and define distinct tumor subpopulations purely on the basis of molecular information obtained in the MSI experiment. Correlation to clinical patient information resulted in the identification of clinically relevant tumor subpopulations (Balluff et al., 2015).

## 1.6 Sarcoma

Soft tissue sarcoma (STS) is a class of uncommon tumors that arise in mesenchymal tissues, such as bone, cartilage, and connective tissues (e.g. muscle and fat). While STS can occur anywhere in the human body, approximately 75% occurs in the extremities (commonly in the thigh), 10% in the trunk wall, and another 10% in the retroperitoneum. The combination of their limited occurrence, 1% of all malignant tumors, and a large number of histological subtypes (> 50) often with overlapping morphology, results in challenges regarding diagnosis and treatment (Fletcher et al., 2013; Taylor et al., 2011). Firstly, their rarity results in a very low probability for a

general pathologist to encounter many of the STS subtypes. Secondly, the overlapping morphology, demonstrated intra-tumor heterogeneity and the only sparse availability of discriminating diagnostic markers complicate tumor subtyping (Willems et al., 2010a).

Previously, different sarcoma subtypes have been studied using MALDI-MSI. Caldwell *et al.* were the first to publish the potential of MSI in sarcoma research. MALDI-MSI of proteins was performed on a variety of STS tissues, including “fibrosarcoma”, leiomyosarcoma, liposarcoma, undifferentiated pleomorphic sarcoma, malignant peripheral nerve sheath tumor and synovial sarcoma, in order to establish biomolecular differences between low-grade STS, high-grade STS and skeletal muscle control tissue. Several proteins, including previously characterized markers for other tumor types (calgizzarin, calyculin, macrophage inhibitory factor, and calgranulin) as well as multiple histones, were found to differentiate high- and low-grade STS. Other proteins, including several myosin light-chains, appeared completely absent in tumor tissues, while vimentin was exclusively detected in the STS tissues. Five of the markers established by MSI, were successfully validated by IHC on FFPE tissues and showed similar expression patterns compared to MSI results (Caldwell et al., 2005). Additionally, Caldwell *et al.* studied the capability of MSI to establish tumor margins of an undifferentiated pleomorphic sarcoma. Using MALDI-MSI of intact proteins they were able to extend the tumor margin beyond the capabilities of histological examination through the detection of differential, disease-like, molecular signatures in regions that were considered non-diseased after histological examination. IHC validation of the MSI markers revealed a mixture of non-diseased cells and transforming tumor cells, morphologically indistinguishable from the non-diseased cells, stretching beyond the histologically determined tumor margins (Caldwell et al., 2006). Willems *et al.* studied the lipid and protein content of myxofibrosarcoma (MFS) and myxoid liposarcoma (MLS) using MALDI-MSI. Lipid MSI analysis revealed that the presence of various triglycerides (TG) was associated with low grade MLS, and the presence of different phosphatidylcholines (PC) was indicative of high grade MLS. These findings confirmed previous NMR-based findings that demonstrated the ability of histology-specific lipid analysis to classify different liposarcoma subtypes (Willems et al., 2010a). Additionally, biomolecular intratumor heterogeneity of intermediate-grade MFS was demonstrated and confirmed the multinodular tumor pattern, based on clonal selection previously observed on the genetic level in low-grade MFS (Jones et al., 2011; Willems et al., 2010a). These methods for the investigation of molecular intratumor heterogeneity were applied in a biomarker discovery study on chondrosarcoma, and demonstrated that different histological variants of central and peripheral chondrosarcoma were distinguishable by specific sets of proteins, including Vimentin, a well-established generic marker of sarcomas (Jones et al., 2013). Lou *et al.* published a study in which the ability of MALDI-MSI to distinguish between four types of high-grade sarcoma (osteosarcoma (OS), undifferentiated pleomorphic sarcoma (UPS), myxofibrosarcoma (MFS), and leiomyosarcoma (LMS)) was demonstrated. A total of

twenty proteins were found as diagnostic markers for the different tumor types, an additional nine proteins showed prognostic value as they were associated with overall patient survival (Lou et al., 2016a). A similar study was performed investigating a metabolic marker for STS. Inositol cyclic phosphate and carnitine were established as potential generic prognostic markers for STS patients (Lou et al., 2017).

### 1.6.1 Myxoid liposarcoma

MLS is a malignant myxoid STS, which accounts for 5% of all adult cases of STS. Representing a third of the cases, it is the second most common type of liposarcoma (LPS) (Fletcher, 2014). MLS is often found in the extremities of young adults, and is treated by surgical resection (Antonescu et al., 2001; Fletcher, 2014). The histology of MLS consists of a mixture of cells, including uniform round mesenchymal cells, oval shaped primitive, nonlipogenic mesenchymal cells and small signet-ring lipoblasts in a myxoid ECM with a characteristic capillary vasculature (Fletcher et al., 2013). Specific, highly dense regions containing undifferentiated round cells with little cytoplasm and no ECM, termed 'round cell' regions are associated with high metastatic potential and a general poor prognosis. Other indicators for poor prognosis are the presence of necrotic tissue, the male gender, high age, and multifocal disease (Antonescu et al., 2001; Nishida et al., 2010; de Vreeze et al., 2010; Hoffman, et al., 2012; Fletcher et al., 2013). The myxoid ECM, clearly visible in conventional light microscopy, consists of a variety of secreted proteins and polysaccharides, and determines the physical properties of the tissue (Graadt van Roggen et al., 1999). The myxoid ECM is characteristic for various types of epithelial and mesenchymal tumors. In epithelial tumors a myxoid ECM is often a secondary phenomenon, while in mesenchymal tumors it is often considered an intrinsic part of the tumor (Willems et al., 2010a). Albeit that the myxoid ECM is an intrinsic part of the tumor entity it is not considered directional in diagnosis. Myxoid STSs contains a variety of morphologically similar tumors with varying clinical behavior, ranging from truly benign to highly malignant (Graadt van Roggen et al., 1999; Willems et al., 2010b).

The chimeric transcription factor oncogene, *FUS-DDIT3* is characteristic to MLS (>95% of all cases), and is the result of a reciprocal translocation  $t(12;16)(q13;p11)$ . In this translocation, the 5' half of the *FUS* gene is fused with the complete reading frame of the *DDIT3* gene. The remaining 5% of the cases harbor a similar translocation,  $t(12;22)(q13;p12)$ , which fuses the *EWSR1* gene to the *DDIT3* gene. The exact mechanism of oncogenesis remains unknown, although it is hypothesized that the chimeric fusion gene acts as an aberrant transcriptional factor, stimulating cell proliferation whilst inhibiting adipogenic differentiation (de Graaff et al., 2016; Powers et al., 2010).

## 1.7 Aims of the thesis

MSI is a useful tool for the investigation of pathologies in which established histopathological methods may not always be conclusive. In this thesis, the aim was to develop novel enzyme-based on-tissue chemistry methods for an improved characterization of the biomolecular landscape of tissues. These methods were developed to further implement MSI in clinical research in general, and were applied to aid the biomolecular characterization of tumor progression in MLS.

While MSI has been proven to be a valuable tool in clinical research, questions remain about the technical reproducibility and applicability of this technology in *routine* clinical research. Furthermore, the use of proteolytic enzymes has raised questions in the field of in-solution bottom-up proteomics, regarding the influence of the enzyme incubation time on the repeatability of the analysis. However, enzyme incubation time and repeatability had not been addressed for on-tissue digestion MALDI-MSI. **Chapter 2** of this thesis addresses the question: What is the influence of the enzyme incubation time on the repeatability and spatiotemporal dynamics of on-tissue digestion?

The use of on-tissue proteolytic digestion can improve proteome coverage in a MALDI-MSI analysis, compared to the analysis of intact proteins. Nevertheless, the information obtained from a single tissue section is still limited. **Chapters 3 and 5** of this thesis address the question whether the use of multiple enzymes can increase the molecular information obtained using on-tissue digestion MALDI-MSI on both fresh frozen and FFPE tissues.

The field of MSI is currently moving toward high-resolution analyses, both in mass resolution and image resolution. The application of high resolution MSI in clinical research is compromised by the long data acquisition times and the large data load which characterize the high-resolution measurements. The virtual microdissection normally performed to focus the data analysis on specific/comparable cell types means that, in many instances, only a fraction of the MSI data is used in the subsequent statistical evaluation. Thus, throughput may be increased, measurement time decreased, and dataload reduced, if the MSI data acquisition could be focused on these histological regions of interest. **Chapter 4** of this thesis describes an automated histology-guided MSI platform, to facilitate high-resolution MSI analysis in clinical research. The functionality and performance of the histology-guided MSI platform are described using a histologically well-characterized selection of FFPE MLS tissues.

**Chapter 6** describes a clinical biomarker discovery study to establish a molecular marker for MLS tumor progression based on the application of the multimodal MSI approach described in **Chapter 5** on a previously constructed TMA containing FFPE tissue material from 32 MLS patients.





## Chapter 2

# Brain region-specific dynamics of on-tissue protein digestion using MALDI-MSI

**Bram Heijs**; Else A. Tolner; Judith V.M.G. Bovée; Arn M.J.M. van den Maagdenberg; Liam A. McDonnell, "Brain region-specific dynamics of on-tissue protein digestion using MALDI-MSI," *Journal of Proteome Research* 14(12), pp. 5348-5354, 2015.





*In MSI, on-tissue proteolytic digestion is performed to access larger protein species and to assign protein identities through matching the detected peaks with those obtained by LC-MS/MS analyses of tissue extracts. The on-tissue proteolytic digestion also allows the analysis of proteins from FFPE tissues. For these reasons on-tissue digestion-based MSI is frequently used in clinical investigations, e.g. to determine changes in protein content and distribution associated with disease. In this work we sought to investigate the completeness and uniformity of the digestion in on-tissue digestion MSI. Based on an extensive experiment investigating three groups with varying incubation times: (i) 1.5 hours, (ii) 3 hours, and (iii) 18 hours, we have found that longer incubation times improve the repeatability of the analyses. Furthermore, we discovered morphology-associated differences in the completeness of the proteolysis for short incubation times. These results support the notion that a more complete proteolysis allows better quantitation.*

## 2.1 Introduction

Since its introduction in 1997 by Caprioli *et al.* (Caprioli *et al.*, 1997) matrix-assisted laser desorption/ionization (MALDI) mass spectrometry imaging (MSI) has become a valuable tool in clinical research. MALDI-MSI has the ability of simultaneously recording hundreds of untargeted biomolecular analytes in a spatially correlated manner to provide the analyst with cell type-specific molecular signatures. Different sample preparation strategies can be applied to investigate the abundance and spatial distribution of various molecular classes, ranging from endogenous small molecules and pharmaceuticals, to lipids, peptides, and proteins, directly from a tissue section (McDonnell and Heeren, 2007). The aforementioned characteristics make MALDI-MSI a well-suited tool for biomarker discovery or for the investigation of the molecular mechanisms underlying disease (Balluff *et al.*, 2011; Carreira *et al.*, 2015; Cole *et al.*, 2011; Djidja *et al.*, 2010; Poté *et al.*, 2013).

In order to identify proteins, increase proteome coverage and enable the analysis of proteins from formalin-fixed paraffin embedded tissue sections, the enzymatic digestion performed in classic bottom-up proteomics has been adapted to MALDI-MSI and is also mostly performed using the endopeptidase trypsin (Groseclose *et al.*, 2008; Heijs *et al.*, 2015; Lemaire *et al.*, 2006; Shimma *et al.*, 2006).

As discussed by Brownridge *et al.* (Brownridge and Beynon, 2011), for *in solution* bottom-up proteomics, the digestion of a protein to its 'limit peptides' can follow many pathways, resulting in a large number of intermediate digestion products. In this context, 'limit peptides' are proteolytic peptides that lack missed proteolytic cleavage sites, meaning that all peptide bonds that *could* be cleaved *were* cleaved. It can be argued that the repeatability of an enzymatic digestion is solely achieved and only guaranteed if all proteins are converted to their limit peptides. In the same study it was shown that not all amino acid sequences have the same digestion efficiency, and it was

concluded that enzyme incubation time is key to achieving repeatable digestion results (Brownridge and Beynon, 2011).

A tissue section can be very heterogeneous and constitutes a chemically complex environment. Accordingly, there are questions pertaining to the efficiency of the proteolysis and whether there may be region-specific differences in reaction rate, both of which would affect the repeatability of on-tissue proteolytic digestion MSI experiments. Surprisingly, in literature there is little consensus on the incubation times that have to be used for such digestions (Casadonte and Caprioli, 2011; Groseclose et al., 2007; Heijs et al., 2015; Sio et al., 2015). A workshop organized by the large European MSI network COST Action BM1104 that focused on comparing on-tissue digestion methods and data found little consensus and significant variation.

For example, in brain tissue white and grey matter are known to have distinct molecular compositions with different chemical characteristics, e.g. white matter is richer in lipid content making it more hydrophobic (Kaufman and Bard, 1999; Watson, 2012). However, it is unknown whether these differences have an effect on the on-tissue enzymatic digestion. Here we have investigated the brain region-specific efficiency of on-tissue digestion using MALDI-MSI. Using three groups of mouse brain tissue sections ( $N = 9$ ) we varied the length of the incubation time: (i) 1.5 hours, (ii) 3 hours, and (iii) 18 hours. To get more quantitative insight into the success of the digestion, three previously identified proteolytic fragments originating from myelin basic protein (MBP, MBP\_MOUSE, UniProt: P04370), were synthesized as isotopically-labeled reference standards (ILRS). Following the digestion incubation, the ILRS peptides were homogeneously sprayed on the tissue sections to enable intensity normalization of the endogenous MBP fragments. In this manner ionization bias could be traced throughout the tissue (Hamm et al., 2012; Källback et al., 2012; Porta et al., 2015) and throughout the evolution of the on-tissue digestion experiment.

Although the on-tissue digestion method is very effective and its application more commonly used, little has been reported about the repeatability, dynamics and spatial uniformity of on-tissue digestion in histologically heterogeneous tissue sections. One of the most comprehensive studies regarding on-tissue digestion, recently reported by Diehl *et al.* (Diehl et al., 2015), compared many parameters such as incubation time, type of MALDI matrix, and protease, but the main focus was to improve spatial resolution and image quality. The dynamics of the digestion, its repeatability and region-specific differences were not addressed. To the best of the author's knowledge, this is the first in depth investigation into the dynamics and mechanics of on-tissue digestion MALDI-MSI in a region-specific manner.

## 2.2 Methodology

### 2.2.1 Chemicals and reagents

All chemicals were purchased from Sigma-Aldrich (Steinheim, Germany) except ethanol

(Merck, Darmstadt, Germany). Trypsin was purchased from Promega (Madison, USA). The isotopically-labeled peptide standards were produced by the Peptide Synthesis facility at Leiden University Medical Center (Leiden, Netherlands).

### 2.2.2 Isotopically labelled peptide standards

Isotopically labeled variants containing L-Threonine- $^{13}\text{C}_4$ ,  $^{15}\text{N}$ , (+5 Da, designated T\*) of the following, previously identified (Heijs et al., 2015), tryptic peptides of myelin basic protein (MBP\_MOUSE, UniProt P04370) were synthesized: (i) T\*THYGSLPQK –  $m/z$  1,136.5 Da, (ii) T\*QDENPFFHFFK –  $m/z$  1,465.71 Da, and (iii) T\*QDENPFFHFFK $^{\wedge}$ NIVTPR –  $m/z$  2146.1 Da (missed cleavage,  $^{\wedge}$ ). The isotopically labeled peptides were dissolved in 0.1% trifluoroacetic acid (TFA) and mixed to get an equal response for each peptide from the mass spectrometer: (i)  $m/z$  1,136.5 Da – 500 nM, (ii)  $m/z$  1,465.71 Da – 100 nM, and (iii)  $m/z$  2,146.1 Da – 75 nM.

### 2.2.3 Sample collection

A three-month-old, male, C57BL/6J mouse was sacrificed by cervical dislocation. The brain was excised, flash-frozen on dry ice and stored at  $-80^{\circ}\text{C}$  until analysis. Twelve- $\mu\text{m}$  thick coronal tissue sections ( $-1.06$  –  $0.74$  mm bregma) were obtained using a cryostat microtome (Leica Microsystems, Wetzlar, Germany) at  $-12^{\circ}\text{C}$ . Three adjacent sections were thaw-mounted per poly-L-lysine coated indium-tin-oxide (ITO) glass slide (Bruker Daltonics, Bremen, Germany) and stored at  $-80^{\circ}\text{C}$ . For every incubation time a group of three slides was prepared, resulting in 9 replicates for each incubation time (Figure 2-1A). All experiments were approved by the Animal Experiment Ethics Committee of Leiden University Medical Center.

### 2.2.4 Sample preparation

Tissue sections were brought to room temperature in a freeze-drier for 30 minutes. The tissue sections were then washed for 30 s in 70% ethanol, 30 s in 96% ethanol, 10 dips in deionized water, 30 s in 70% ethanol, and 30 s in 96% ethanol. Trypsin (20 ng/ $\mu\text{L}$  in deionized water) was then applied using a SunCollect automatic sprayer (SunChrom, Friedrichsdorf, Germany) as previously described (Heijs et al., 2015). In order to investigate the digestion dynamics different incubation times (1.5 h, 3 h & 18 h) were used. The digestion was incubated at  $37^{\circ}\text{C}$  in an airtight saturated chamber (50% methanol in deionized water). Proteolysis was terminated by covering the tissue sections with the mixture of isotopically labeled peptides (in 0.1% trifluoroacetic acid (TFA)) using the SunChrom SunCollect sprayer. A total of 2 layers was sprayed at 5  $\mu\text{L}/\text{min}$  using the same sprayer settings as the trypsin application (Heijs et al., 2015). Finally, MALDI matrix (25 mg/mL 2,5-dihydroxybenzoic acid (DHB) in 50% acetonitrile (ACN) and 0.1% TFA) was applied using the SunCollect sprayer as described (Heijs et al., 2015).

### 2.2.5 MALDI-FTICR imaging

MALDI-FTICR-MSI was performed using a 9.4 T Solarix XR mass spectrometer (Bruker

Daltonics) in positive-ion mode, using 150 laser shots per spot and 100 x 100  $\mu\text{m}$  pixel size. Data was acquired for each tissue section and additional areas adjacent to the tissues to function as a matrix control. Spectra were recorded in the  $m/z$  range 600–3,500 Da with a 512k data point transient (1.1 s duration), corresponding to an estimated resolution of 200,000 at  $m/z$  400 Da. The average detected mass resolution over the analyzed mass range was 54,000, and the mass resolution in the center of the mass range, at  $m/z$  1,500, was 65,000. Data acquisition was performed using *ftmsControl* (Bruker Daltonics) and peptides visualized with *flexImaging 4.0* (Bruker Daltonics). After MSI data acquisition the MALDI matrix was removed by washing the glass slides in 70% ethanol (2x 2 min), then Nissl stained and digitally scanned using a digital slide scanner (*IntelliSite Pathology Ultra-Fast Scanner*, Philips, Eindhoven, The Netherlands). The scanned histology images were co-registered to the MSI datasets in *flexImaging*.

## 2.2.6 Data analysis

The digestion dynamics were determined globally for the full tissue sections, and locally for specific histological features present in the mouse brain sections.

### 2.2.6.1 Global analysis – total average spectra

For the global analysis, the average spectra for each of the analyzed sections and their respective matrix controls, obtained from *flexImaging*, were exported as comma-separated values (CSV) and read into the freely available software tool *mMass* (<http://www.mmass.org>) (Strohalm et al., 2008). Mass spectral processing was performed using the following settings: (i) baseline subtraction – precision 15, relative offset 25, (ii) smoothing – Savitzky-Golay, width 0.05  $m/z$ , 1 cycle, (iii) peak picking –  $S/N \geq 5$ , relative intensity  $\geq 0.6\%$ , (iv) deisotoping – max. charge 2+, isotope mass tolerance 0.02  $m/z$ , isotope intensity tolerance 50%, remove isotopes and unknowns, and (v) recalibration to a reference list containing the masses of the isotopically labeled peptide standards. Using *mMass'* peak list comparison tool, the peaks present in the matrix control were removed from the tissue peak list leaving only tissue specific peaks. The tissues specific peaks were exported to Excel 2010 (Microsoft). In Excel the total number of tissue specific peaks were grouped per digestion time point, and statistical comparison of the time-associated changes performed. A Kolmogorov-Smirnov test was applied to test the groups for normal distributions. Differences in distribution between the three groups were investigated using a Kruskal-Wallis test. If it was found that a group was distributed differently with statistical significance ( $p \leq 0.05$ ), a Mann-Whitney test was used instead.

### 2.2.6.2 Global analysis – myelin basic protein

To investigate the digestion of MBP, the intensities of the three selected MBP peptides and their isotopically labeled variants were extracted from the average spectra of the tissues. In Excel, the intensities of the endogenous peptides were normalized using the intensities of the ILRS using (1).

$$I_{norm} = \frac{I_{endogenous}}{I_{ILRS}} \quad (1)$$

Statistical comparisons of the time-associated changes were performed similar to the analysis of the full spectra (detailed description above).

### 2.2.6.3 Local analysis – MBP digestion in white and grey matter

The alignment of the histology images to the MSI datasets facilitated the extraction of mass spectral data from specific histological regions. Two specific regions, equal in size (i.e. number of pixels) were selected from each tissue section: (i) white matter, a part of the lateral forebrain bundle system and, (ii) grey matter, a part of the cerebral cortex. The resulting XML files listed all spectra contained within these regions of interest (ROIs).

The MALDI-MSI datasets and corresponding XMLs were read into Data Analysis 4.2 (Bruker Daltonics), average spectra were calculated for all ROIs and peak picking was performed using the FTMS peak picking algorithm ( $S/N \geq 5$ , Rel. Int.  $\geq 0.6\%$ ). The intensities of the three MBP fragments and their respective isotopically labeled standards were exported to Excel 2010. In Excel the intensities of the endogenous proteolytic peptides were normalized to their respective ILRS, using (1). Statistical analysis of the histology-associated differences was performed as described above for the full average mass spectra.

## 2.3 Results and discussion

The on-tissue enzymatic digestion of proteins is used in MALDI-MSI to increase proteome coverage and assign protein identities to the peaks detected by MALDI-MSI. It is known from efforts to perform absolute protein quantification using LC-MS/MS that enzyme incubation time determines the completeness of the protein digestion and also the repeatability of the analysis (Brownridge and Beynon, 2011). Accordingly, we investigated the completeness of the digestion and the repeatability of on-tissue digestion by varying the incubation time and analyzing the resulting peptides using MALDI-MSI. A series of mouse brain tissue sections was analyzed: three groups of 9 tissue sections were digested for (i) 1.5 hours, (ii) 3 hours, or (iii) 18 hours and analyzed using a 9.4 T MALDI-FTICR instrument (Figure 2-1A).

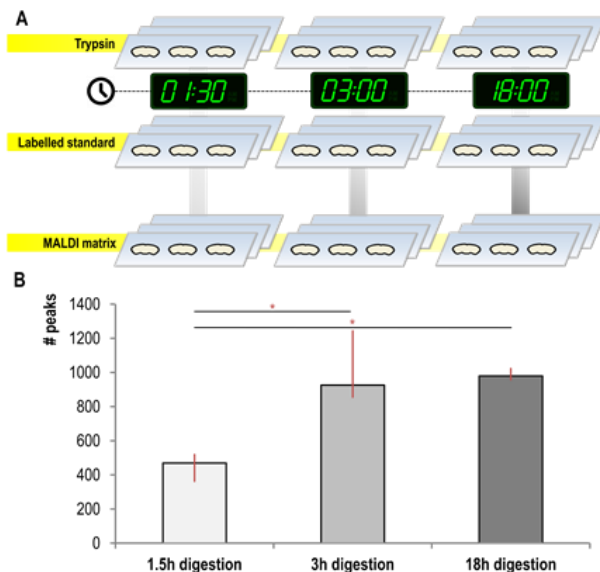
### 2.3.1 Global analysis – total average spectra

The average mass spectrum from each complete tissue section was extracted, processed (background subtraction, smoothing), peak-picked and then recalibrated using the ILRS peptides as internal calibrants (Figure S2-1, Supplementary information). To obtain the number of tissue specific ions per tissue section, each tissue section's peak list was corrected by subtracting all peaks detected in the matrix control area adjacent to the tissue section. This correction removed all  $m/z$  features originating from the MALDI matrix, protease, and isotopically labeled reference

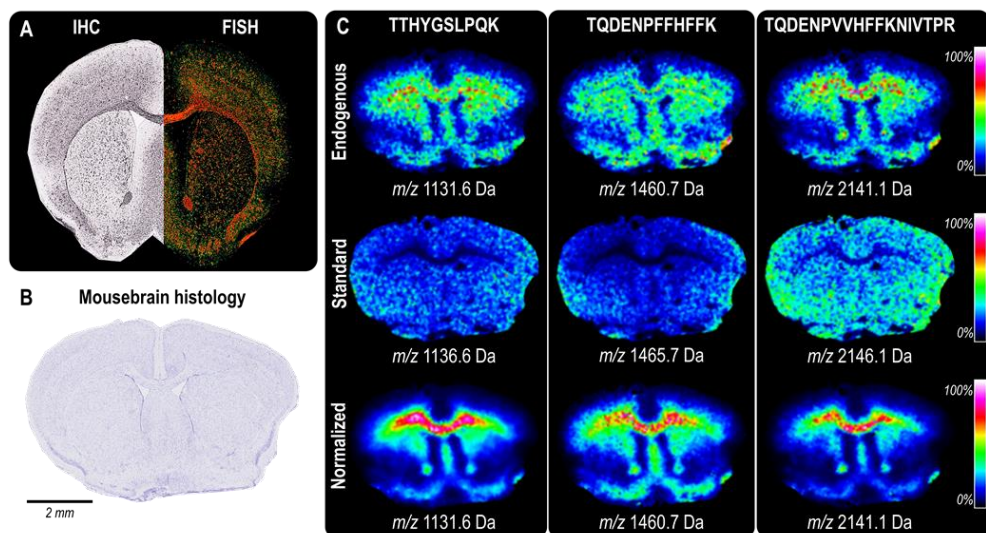
standard, leaving only tissue-specific  $m/z$  features. The resulting peak lists were deisotoped, grouped according to incubation time and then averaged (Figure 2-1B). A Mann-Whitney test was performed to calculate the statistical significance of the differences observed between the number of tissue-specific peptide ions per incubation time. It was found that after a 1.5-hour incubation the number of peptide ions was significantly lower, compared to the 3-hour and 18-hour incubations. No significant difference was observed between the number of tissue specific peptide ions from the 3-hour and 18-hour incubations. Although the number of peaks did not differ significantly between the 3-hour and 18-hour incubations, the variability was considerably larger in the 3-hour group compared to the 18-hour group. Great care should be employed when interpreting such peak lists of MSI data because the continuous production of new proteolytic fragments results in an increasingly complex chemical environment, which is known to cause ion suppression in MALDI mass spectrometry (Stauber et al., 2010).

### 2.3.2 Global analysis – myelin basic protein

To acquire more clarity into the dynamics of on-tissue digestion, a single protein was selected and isotopically labeled variants of the tryptic peptides were synthesized for use as internal reference standards. In this manner the ion suppression could be traced throughout the tissue and during the evolution of the digestion. Myelin basic protein (MBP, MBP\_MOUSE, UniProt: P04370) was selected owing to its ready detection by MALDI-MSI (Clemis et al., 2012; Diehl et al., 2015; Heijs et al., 2015) and its distinct localization in the brain. MBP is an abundant protein in the central nervous system and has a crucial role in maintaining the multi-layered myelin membrane that builds up the myelin sheaths covering the nerve cells axons (Siegel et al., 1999). MBP is known to interact with the lipids in the myelin membrane and has a strong expression in regions consisting largely of white matter (Figure 2-2A-B) (Min et al., 2009; Siegel et al., 1999). Three of the MBP proteolytic fragments frequently reported by on-tissue digestion MALDI-MSI were selected: (i) TTHYGSLPQK (196-205, 1,131.5793 Da), (ii) TQDENPFFHFFK (211-222, 1,460.7168 Da), and (iii) TQDENPVVHFFKNIVTPR (211-228, 2,141.1138 Da). Fragment 211-228 is a missed-cleavage peptide that indicates incomplete digestion. Fragment 211-222 is the 'limit peptide' produced by the complete digestion of fragment 211-228, so any differences in their relative intensities may be interpreted as differences in the relative completion of the digestion. The isotopically labeled reference standards for the three MBP peptides were synthesized using a  $N^{15}$  and  $C^{13}$  labeled threonine residue ( $\Delta[M+H^+] = +5$  Da) incorporated on the N-terminal side of the three MBP fragments. A mixture of these peptides was prepared such that their intensities were similar to those of endogenous MBP fragments. From the respective concentrations for each of the three isotopically-labeled MBP peptides in the ILRS peptides mixture ((i)  $m/z$  1,136.5 Da – 500 nM, (ii)  $m/z$  1,465.71 Da – 100 nM, (iii)  $m/z$  2,146,1 Da – 75 nM) it appears that the analysis of missed-cleavage peptides by MALDI mass spectrometry does not exhibit a similar bias in analysis sensitivity as

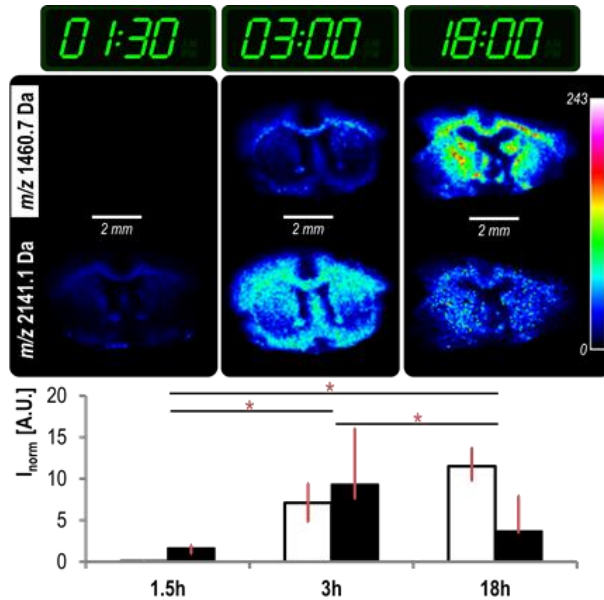


**Figure 2-1: (A)** Overview of the experiments. For each of the incubation times nine tissue sections were analysed. Three sections were mounted on one glass slide, the three slides were analysed on different days. **(B)** The number of tissue specific peaks (median) for each of the incubation times. The error bars represent the first and third quartile values. The asterisks represent  $p \leq 0.05$ .

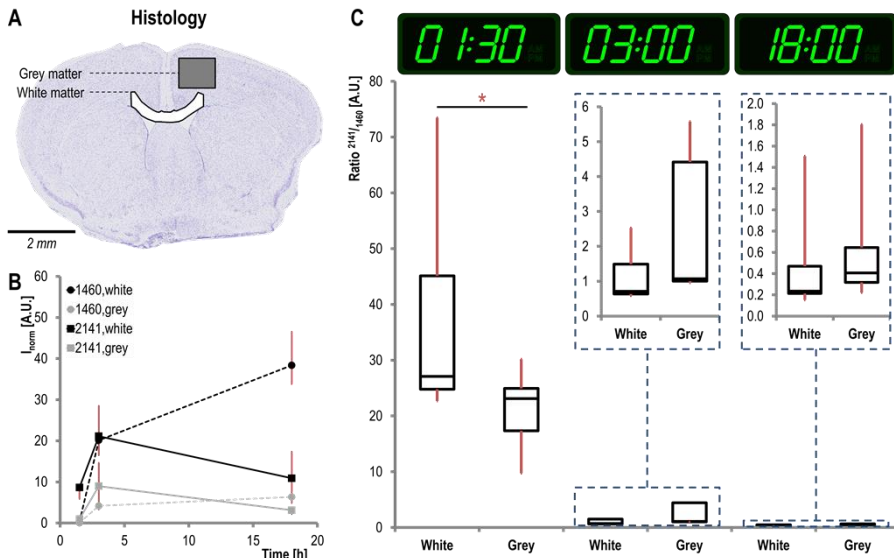


**Figure 2-2: (A)** Immunohistochemistry (IHC) and fluorescent in situ hybridization (FISH) data for myelin basic protein from the Allen Mouse Brain Atlas (©2015 Allen Institute for Brain Science. Available from: <http://mouse.brain-map.org>). **(B)** A scanned image of the histology (Nissl staining) of the MSI analyzed tissue section. **(C)** The effect of normalization to ILRS peptides on the distributions of MBP determined by on-tissue digestion MALDI-MSI. The top row contains the non-normalized images of the proteolytic fragments. The middle row shows the intensity distribution of the ILRS peptides, and the lower row shows the normalized images.





**Figure 2-3:** ILRS normalized visualizations of the MBP 'limit peptide' at  $m/z$  1,460.7 Da (TQDENPFFHFFK) and missed-cleavage peptide  $m/z$  2,141.1 Da (TQDENPFFHFFKNIVTPR) for each of the three incubation times. The bar plot shows the normalized intensities (median) for both the 'limit peptide' (white) and the missed-missed cleavage peptide (black) for each of the incubation times. The error bars represent the first and third quartile values and the asterisks  $p \leq 0.05$ .



**Figure 2-4:** Comparison of MBP on-tissue digestion in mouse brain white and grey matter. **(A)** Selection of regions consisting largely of white and of grey matter that contain identical numbers of pixels. **(B)** The normalized intensities of 'limit peptide'  $m/z$  1,460.5 Da and missed-cleavage peptide  $m/z$  2,141.1 Da in regions with white and grey matter plotted versus incubation time. The error bars represent the 1st and 3rd quartile values. **(C)** Box plots showing the ratio of the intensity of the missed-cleavage peptide to the 'limit peptide' in white and grey matter over time. The insets show magnifications of the boxplots for 3 h and 18 h. The asterisks represent  $p \leq 0.05$ .

during the analysis by electrospray ionization (ESI)-based mass spectrometry (Brownridge and Beynon, 2011). The equal sensitivity for the analysis of both 'limit peptides' and missed-cleavage peptides in MALDI-MSI emphasizes the need to drive the on-tissue digestion to completion, as the detection of missed-cleavage peptides will affect the reproducibility of the analysis.

Following the MALDI-MSI analysis the intensities of the endogenous peptides were normalized to the intensity of their ILRS peptides. Figure 2-2C shows the effect ILRS normalization has on the visualization of the peptide distributions. Visualization of the homogeneously applied ILRS peptides on the mouse brain tissue sections clearly shows that there is more suppression within the lateral forebrain bundle system, which is a part of the brain's white matter, as compared to the rest of the tissue section. The impact of ILRS normalization has been previously described for small molecules, such as pharmaceuticals and endogenous metabolites, and for proteolytic peptides in MALDI-TOF-MSI and MALDI-MRM-TOF-MSI (Clemis et al., 2012; Hamm et al., 2012; Prideaux and Stoeckli, 2012; Shariatgorji et al., 2014).

Following the normalization of the endogenous MBP peptides to their ILRS analogues the experiments with different incubation times, and the different regions could be quantitatively compared. The average (normalized) intensity was calculated for each incubation time and for each ROI to find whether the incubation time had a significant effect on the on-tissue digestion of MBP (Figure 2-3, Figure S2-2, Supplementary information). The presented data indicates significant differences between the intensity distributions of all three MBP fragments between 1.5 h and 3 h incubations. Additionally, the 211-222 ( $m/z$  1,460.7 Da) and 211-228 ( $m/z$  2,141.1 Da) fragments also show significant differences between the 3 h and 18 h incubations. As expected, the intensity distributions of both 'limit peptide' and missed-cleavage peptide have an inverse correlation, indicating that between the 3 h and 18 h time points MBP digestion is still ongoing.

### 2.3.2 Local analysis – MBP digestion in white and grey matter

It is known that the varying chemical composition of different organs/regions-of-tissue can have different mass spectral responses, leading to biased MSI representations of the true peptide distribution (Hamm et al., 2012; McDonnell and Heeren, 2007). Figure 2-2C shows such difference in ionization response for all three MBP peptides between regions in the mouse brain that contain white or grey matter. In this study we have investigated whether the different physical-chemical properties of the different morphological regions also affect the proteolytic digestion. Two regions, equal in size, from both grey and white matter were selected in each of the analyzed tissue sections and the spectra were extracted (Figure 2-4A). The ILRS normalized intensities of the MBP fragments 211-222 ( $m/z$  1,460.7 Da) and 211-228 ( $m/z$  2,141.1 Da) were determined for the two regions, and plotted versus time (Figure 2-4B). These results indicate a greater abundance of MBP in the region with white matter as compared to

the region with grey matter, which is in line with mRNA expression and immunohistochemistry results obtained from the Allen Brain Atlas (Figure 2-2A). Furthermore, it appears that MBP digestion is performed faster in white matter compared to grey matter as the equilibrium intensity between the 'limit peptide' and the missed-cleavage peptide lies close to 1.5 h in white matter and close to 12 h in grey matter. Furthermore, statistical analysis of the ratio between the missed-cleavage peptide and the 'limit peptide' (ratio =  $I_{2141}/I_{1460}$ ) showed a significant difference between white and grey matter after only 1.5 h of incubation (Figure 2-4C). However, the results also indicated that these morphology-induced differences did not persist after 3-h and 18-h incubations, providing further evidence that a longer incubation provides more repeatable and reliable data.

In the current work we have demonstrated that in order to improve on-tissue digestion MALDI-MSI data longer incubation times are required. By performing an 18-h incubation, we were able to decrease the variability of the data sets regarding the number of tissue specific peaks. Furthermore, we were able to show differences in the digestion of MBP: (i) the missed-cleavage fragment 211-228 ( $m/z$  2,141.1 Da) was significantly less abundant after 18 h compared to 3 h incubation time, (ii) the 'limit peptide' (fragment 211-222,  $m/z$  1,460.5 Da) resulting from the digestion of the missed-cleavage peptide significantly increased after 18 h compared to 3 h. More importantly, for short digestions we were able to show differences in MBP digestion induced by the tissue morphology. These results urge caution owing to the numerous sources of technical bias in the MALDI-MSI data after short on-tissue digestion incubation times; as repeatability was improved, digestion more complete and morphology associated bias absent at longer incubation times, longer incubation times are advised.

## 2.4 Conclusions

Here we present the first in-depth investigation into the mechanics and spatio-temporal dynamics of on-tissue enzymatic digestion. To improve the repeatability and comparability of the MALDI-MSI data, normalization of targeted proteolytic fragments of MBP using isotopically-labeled reference standards was applied. The results indicate that a longer incubation of the enzymatic proteolysis reaction improves the quality of on-tissue digestion MALDI-MSI datasets by making the datasets more repeatable and remove morphology-induced measurement bias. This work is another step towards more trustworthy data obtained from on-tissue digestion MALDI-MSI analyses and towards the further implementation of the technique to clinical research.

## 2.5 Acknowledgements

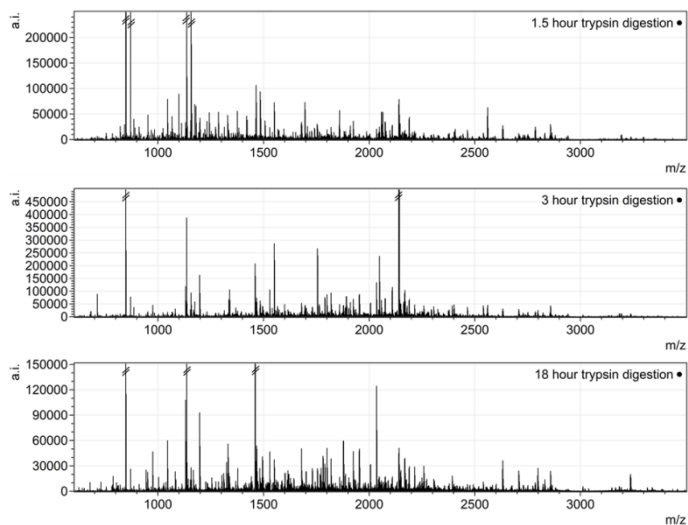
This work was supported by the ZonMW Zenith project Imaging Mass Spectrometry-Based Molecular Histology: Differentiation and Characterization of Clinically Challenging

Soft Tissue Sarcomas (No. 93512002; BH) and Marie Curie IAPP Program BRAINPATH (No. 612360; AvdM & EAT).

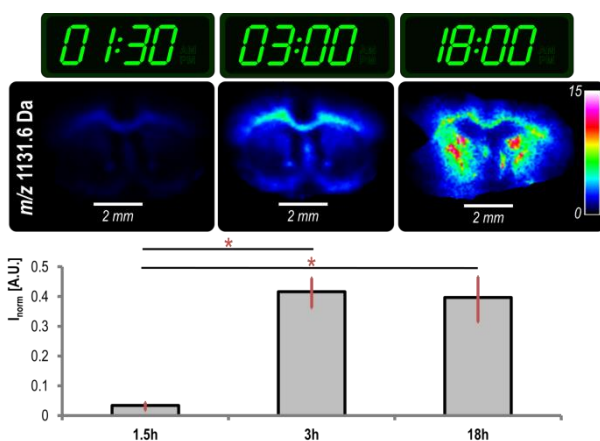
## 2.6 Supplementary information

The full supplementary information are available on the internet via <http://pubs.acs.org/doi/abs/10.1021/acs.jproteome.5b00849>.

### 2.6.1 Supplementary figures



**Figure S2-1:** Examples of pre-processed average spectra for (top) 1.5 hour digestion, (middle) 3 hour digestion, and (bottom) 18 hour digestion.



**Figure S2-2:** Visualizations of ILRS normalized 'limit peptide' at  $m/z$  1,131.5 Da (TTHYGLPQK) for each of the three incubation times. The plot shows the normalized intensities (median) for the 'limit peptide'. The error bars represent the first and third quartile values and the asterisks represents  $p \leq 0.05$ .



## Chapter 3

# Comprehensive analysis of the mouse brain proteome sampled in mass spectrometry imaging

**Bram Heijs**; Ricardo J. Carreira; Else A. Tolner; Arnoud H. de Ru; Arn M.J.M. van den Maagdenberg; Peter A. van Veelen; Liam A. McDonnell, "Comprehensive analysis of the mouse brain proteome sampled in mass spectrometry imaging," *Analytical Chemistry* 87(3), pp. 1867-1875, 2015.



*On-tissue enzymatic digestion is performed in MSI experiments to access larger proteins and to assign protein identities. Most on-tissue digestion MSI studies have focused on method development rather than identifying the molecular features observed. Herein, we report a comprehensive study of the mouse brain proteome sampled by MSI. Using complementary proteases, we were able to identify 5,337 peptides in the MALDI matrix, corresponding to 1,198 proteins. 630 of these peptides, corresponding to 280 proteins, could be assigned to peaks in MSI data sets. Gene ontology and pathway analyses revealed that many of the proteins are involved in neurodegenerative disorders, such as Alzheimer's, Parkinson's and Huntington's disease.*

### **3.1 Introduction**

Matrix-assisted laser desorption/ionization (MALDI) mass spectrometry imaging (MSI) is an analytical technique in which the distributions of hundreds of biomolecular ions can be recorded directly from tissue sections (Caprioli et al., 1997). It allows the simultaneous and untargeted investigation of many molecular classes, including pharmaceuticals, metabolites, lipids, peptides, and proteins (McDonnell and Heeren, 2007). One of the principal application areas of MALDI-MSI is the investigation of the molecular content of pathological tissue samples in order to find biomarkers or provide insights into the molecular mechanisms underlying a disorder. The discovery of putative biomarkers has often focused on proteins since the results can then be independently validated using immunohistochemistry (Balluff et al., 2010; Cazares et al., 2011; Meding et al., 2012).

To increase proteome coverage, aid protein identification, and enable the analysis of formalin-fixed paraffin embedded (FFPE) tissues, the enzymatic protein digestion performed in classic bottom-up proteomics has been adapted for MALDI-MSI (Groseclose et al., 2008; Lemaire et al., 2006; Shimma et al., 2006). Protein identification directly from the tissue section can be performed by MS/MS analysis of the proteolytic peptides but remains challenging due to the very high complexity of the peptide mixture generated after digestion (Houel et al., 2010). Instead the peptide identities are commonly assigned to those previously identified via extraction of proteolytic peptides followed by LC-MS/MS analysis (Maier et al., 2013; Schober et al., 2011).

As in bottom-up LC-MS/MS based proteomics, on-tissue digestion is most often performed using trypsin; its cleavage specificity, C-terminal of arginine and lysine, results in proteolytic peptides that have an intrinsic positive charge on the C-terminus, thus enhancing their detection by positive-ion MS (Brownridge and Beynon, 2011; Vandermarliere et al., 2013). A crucial difference is that MALDI-MS is biased towards the detection of Arg-terminated peptides (Krause et al., 1999). The suppression of Lys C-terminated tryptic peptides in MALDI-MS results in an undesired loss of sequence



information and proteome coverage. This is likely to be exacerbated in MALDI-MSI because of the absence of any explicit peptide separation.

The use of multiple proteases has been shown to have a beneficial effect on proteome and sequence coverage in both LC-ESI-MS and LC-MALDI-MS based studies (Choudhary et al., 2003; Gatlin et al., 2000; Hohmann et al., 2009; Wa et al., 2006). A recent study indicated that similar complementarities might be obtained in on-tissue digestion MALDI-MSI experiments: a combination of trypsin, pepsin and elastase was shown to have a positive effect on protein sequence coverage (Enthaler et al., 2013b). However since pepsin and elastase do not cleave basic amino acids many of the proteolytic peptides will not be detected with high sensitivity. To maintain high detection sensitivity it is essential that the proteases cleave the most basic amino acids, i.e. Lys and Arg. While these are the same residues cleaved by trypsin, previous LC-MS/MS results have already demonstrated that the different sequence and conformation specificities of Lys-C, Arg-C and Lys-N can improve proteome and sequence coverage by reducing the number of missed cleavages (Brownridge and Beynon, 2011).

Here we have investigated the degree of increased proteome coverage that may be obtained in MALDI-MSI by using a similar complementary cohort of enzymes, specifically (i) trypsin, (ii) Lys-C, (iii) recombinant Lys-N (r-Lys-N), (iv) Arg-C, and (v) a mixture of trypsin and Lys-C (trypsin/Lys-C).

## 3.2 Methodology

### 3.2.1 Chemicals and reagents

All chemicals were purchased from Sigma-Aldrich (Steinheim, Germany) except ethanol (Merck, Darmstadt, Germany). All proteases were purchased from Promega (Madison, USA) except r-Lys-N (U-Protein Express BV, Utrecht, The Netherlands).

### 3.2.2 Sample collection

Three-month-old, male, C57BL/6J mice were sacrificed by cervical dislocation. The brains were excised, flash-frozen on dry-ice and stored at  $-80^{\circ}\text{C}$  until analysis. Twelve- $\mu\text{m}$  thick coronal tissue sections were obtained using a cryostat microtome (Leica Microsystems, Wetzlar, Germany) at  $-12^{\circ}\text{C}$ . The sections were thaw-mounted onto poly-L-lysine coated indium-tin-oxide (ITO) glass slides (Bruker Daltonics, Bremen, Germany) and stored at  $-80^{\circ}\text{C}$ . All experiments were approved by the Animal Experiment Ethics Committee of Leiden University Medical Center.

### 3.2.3 Tissue preparation

The tissue sections mounted on indium tin oxide (ITO) coated slides were collected from  $-80^{\circ}\text{C}$  storage and equilibrated to room temperature in a freeze dryer for 30 minutes. Thereafter, all tissues were washed as follows: (i) submerge in 70% ethanol for 30 s; (ii) submerge in 96% ethanol for 30 s; (iii) 10 short dips in deionized water;

(iv) submerge in 70% ethanol for 30 s; (v) submerge in 96% ethanol for 30 s (Enthaler et al., 2013a). Finally, the sections were dried in a vacuum desiccator for 15 min.

### 3.2.4 On-tissue disulphide bond reduction

Tissue sections were covered with 4 layers of 2 mM tris(2-carboxyethyl)phosphine (TCEP) (in deionized water) using the SunCollect automatic sprayer (SunChrom, Friedrichsdorf, Germany). The flow rate for the TCEP application was set to 10  $\mu\text{L}/\text{min}$ , which resulted in the application of 360 nmol TCEP/ $\text{cm}^2$ . Detailed information on the SunCollect settings can be found in Table S3-1 (Supplementary information). The total incubation time at 23°C (room temperature) was 30 min (including ca. 10 min spraying time).

### 3.2.5 On-tissue enzymatic digestion

All proteases were dissolved in deionized water to a final concentration of 0.02  $\mu\text{g}/\mu\text{L}$ . 4-(2-Hydroxyethyl)-1-piperazineethanesulfonic acid (HEPES) containing enzyme buffers for Lys-C and r-Lys-N were exchanged with deionized water using a 10 kDa molecular weight cut off (MWCO) spin filter (Merck Millipore, Billerica, MA, USA). Arg-C was dissolved in 2 mM dithiothreitol (DTT) to activate the enzyme. Five layers of proteolytic enzymes were applied using the SunCollect automatic sprayer at a flow rate of 5  $\mu\text{L}/\text{min}$ . This resulted in the application of 7.5  $\mu\text{g}$  enzyme/ $\text{cm}^2$  (Table S3-1, Supplementary information). The tissues were incubated for 18 hours at 37°C in a saturated air chamber (50% methanol in deionized water). Finally, MALDI matrix was applied using the SunCollect sprayer. For the MALDI-TOF-MSI analyses 5 mg/mL  $\alpha$ -cyano-4-hydroxycinnamic acid (CHCA) in 50% acetonitrile (ACN) and 0.3% trifluoroacetic acid (TFA) was applied. For MALDI-MSI experiments performed with the MALDI-FTICR mass spectrometer it was found that the CHCA matrix produced excessive matrix clusters. Accordingly for MALDI-FTICR-MSI analyses, 50 mg/mL 2,5-dihydroxybenzoic acid (DHB) in 50% ACN and 0.1% TFA was used as matrix.

### 3.2.6 MALDI-TOF imaging

MALDI-TOF-MSI was performed on an UltrafleXtreme MALDI-TOF/TOF (Bruker Daltonics) in positive-ion reflectron mode, using 500 laser shots per spot and 100 x 100  $\mu\text{m}$  pixel size. Data was acquired in a  $m/z$  range from 800-3,000 Da. Data acquisition, pre-processing and visualization were performed using the flex software package by Bruker Daltonics (flexControl 3.4; flexAnalysis 3.4; flexImaging 3.0).

### 3.2.7 MALDI-FTICR imaging

MALDI-FTICR-MSI was performed on a 9.4 T SolariX XR mass spectrometer (Bruker Daltonics) in positive-ion mode, using 250 laser shots per spot and 150 x 150  $\mu\text{m}$  pixel size. Data was acquired in a  $m/z$  range from 600-3,500 Da with a 512k datapoint transient (1.1 s duration) and an estimated resolution of 200,000 at  $m/z$  400 Da. Data acquisition was performed using ftmsControl (Bruker Daltonics) and visualizations were obtained from flexImaging 4.0 (Bruker Daltonics).

### 3.2.8 Data analysis MALDI-TOF-MSI

Regions of interest (ROIs) containing the full area of the coronal section were selected in flexImaging and 500 random spectra from within each ROI extracted into ClinProTools 3.0 (build 22, Bruker Daltonics). The spectra underwent smoothing and baseline subtraction (Top Hat algorithm), total-ion-count normalization, and peak picking at different signal-to-noise ratios. The peak lists were exported to Excel 2010 for further calculations.

### 3.2.9 Peptide extraction

Consecutive tissue sections were prepared for MALDI-MSI using the same sample preparation protocol. Instead of MALDI-MSI analysis, the proteolytic peptides were extracted from the matrix coating using a series of solvents with increasing organic content: (i) 10  $\mu$ L of 0.1% TFA (repeat 4 times); (ii) 10  $\mu$ L of 50% ACN / 0.1%TFA (repeat 4 times); (iii) 90% ACN / 0.1% TFA (repeat 4 times) (Enthaler et al., 2013a). Extracts were combined, dried and resuspended in 0.1% TFA, and then cleaned with Omix C18 tips (Agilent). The purified extracts were dried and stored at -20°C until LC-MS/MS analysis.

### 3.2.10 LC-MS/MS analysis

Peptide extracts were analyzed using an Easy nLC1000 (Thermo, Bremen, Germany) coupled to a Q-Exactive mass spectrometer (Thermo). Fractions were injected onto a homemade pre-column (100  $\mu$ m  $\times$  15 mm; Reprosil-Pur C18-AQ 3  $\mu$ m, Dr. Maisch, Ammerbuch, Germany) and eluted via a homemade analytical column (15 cm  $\times$  50  $\mu$ m; Reprosil-Pur C18-AQ 3  $\mu$ m). The gradient was 0% to 30% solvent B (90% ACN / 0.1% formic acid (FA)) in 120 min. The analytical column was drawn to a tip of  $\sim$ 5  $\mu$ m and acted as the electrospray needle of the MS source. The Q-Exactive mass spectrometer was operated in top10-mode. Parameters were: Full scan - resolution 17,500; AGC target 3,000,000; max fill time 20 ms; MS/MS - resolution 35,000; AGC target 1,000,000; max fill time 60 ms; intensity threshold 17,400; Apex trigger was set to 1-5 seconds, and allowed charges were 1-5.

### 3.2.11 LC-ESI-MS/MS database search

Peptide and protein identifications were extracted from the SwissProt database using the Mascot server. Up to two missed cleavages were allowed and methionine oxidation was set as a variable modification. Peptide assignments were made with a tolerance of 10 ppm. MS/MS fragment tolerance was 20 mmu. Protein identifications were assigned based on a minimum of one confident peptide at 1% false discovery rate (FDR). Only peptides and proteins with red bold notification were included in the final lists of non-redundant peptides. For trypsin and trypsin/Lys-C, peptides and proteins with a Mascot significance score  $\geq$  30 were included, for Lys-C, r-Lys-N and Arg-C the threshold score was  $\geq$  25.

### 3.2.12 Gene ontology and pathway analysis

A list containing the Uniprot accession numbers of the identified proteins was uploaded into the STRAP software tool (v1.1.0.0, Boston University School of Medicine) (Bhatia et al., 2009). The KEGG pathway analysis (PA) was performed by uploading the list in the online STRING 9.1 tool (Jensen et al., 2009). As p-value correction, the "FDR correction" option was applied.

### 3.2.13 Data analysis MALDI-FTICR-MSI

Average spectra from the MALDI-FTICR-MSI datasets were exported into CSV format and loaded into mMass (<http://www.mmass.org>) (Strohalm et al., 2008). Peak picking was performed on peaks with  $S/N \geq 5$  and intensity  $\geq 1,500$  A.U.. The peak lists were then deisotoped with a maximum charge of 3+ and an isotope mass tolerance of 0.05 Da.

### 3.2.14 MALDI-FTICR-MSI peptide identity assignment

MALDI-FTICR-MSI peak lists and Mascot database search results from the LC-MS/MS analyses were exported to Excel 2010. The MSI peaks were assigned to identified peptides based on a mass tolerance of 20 ppm.

## 3.3 Results

On-tissue digestion is used to increase proteome coverage and to assign identities to the peaks detected by MALDI-MSI. In this study we investigated whether additional arginine and lysine proteolytic enzymes, with different cleavage specificities, could further improve on-tissue digestion MALDI-MSI by increasing sequence and proteome coverage. MALDI-MSI was combined with LC-MS/MS of on-tissue digestion matrix extracts to compare the accessible proteolytic peptides produced by the enzymes trypsin, Lys-C, trypsin/Lys-C, r-Lys-N and Arg-C, and to determine which proteolytic peptides were detected by MALDI-MSI.

### 3.3.1 MALDI-TOF-MSI: image comparison

To assess the effects of sample preparation (online Supplementary information) for the different enzymes, ion distributions for proteolytic peptides from the same protein were compared with both each other and the gene expression data from the Allen Mouse Brain Atlas (<http://www.brain-map.org>). Figure 3-1 shows example mass spectra and MSI images obtained from coronal sections of a C57BL/6J mouse brain subject to on-tissue digestion with the different proteases. The images are of proteolytic peptides originating from myelin basic protein (MBP), assigned to confidently identified peptides from the LC-MS/MS analysis of matrix extracts. The mass resolution of the UltrafleXtreme MALDI-TOF/TOF platform used for these MSI experiments is insufficient to resolve the isobaric ions produced by on-tissue digestion, and so the images may include contributions from unresolved isobaric ions. The distributions of the MBP

proteolytic peptides were consistent with the MBP gene expression images contained in the Allen Brain Atlas, Figure 3-1F, indicating that any isobaric ions were minor contributors and that no artifacts resulted from the on-tissue digestion procedure.

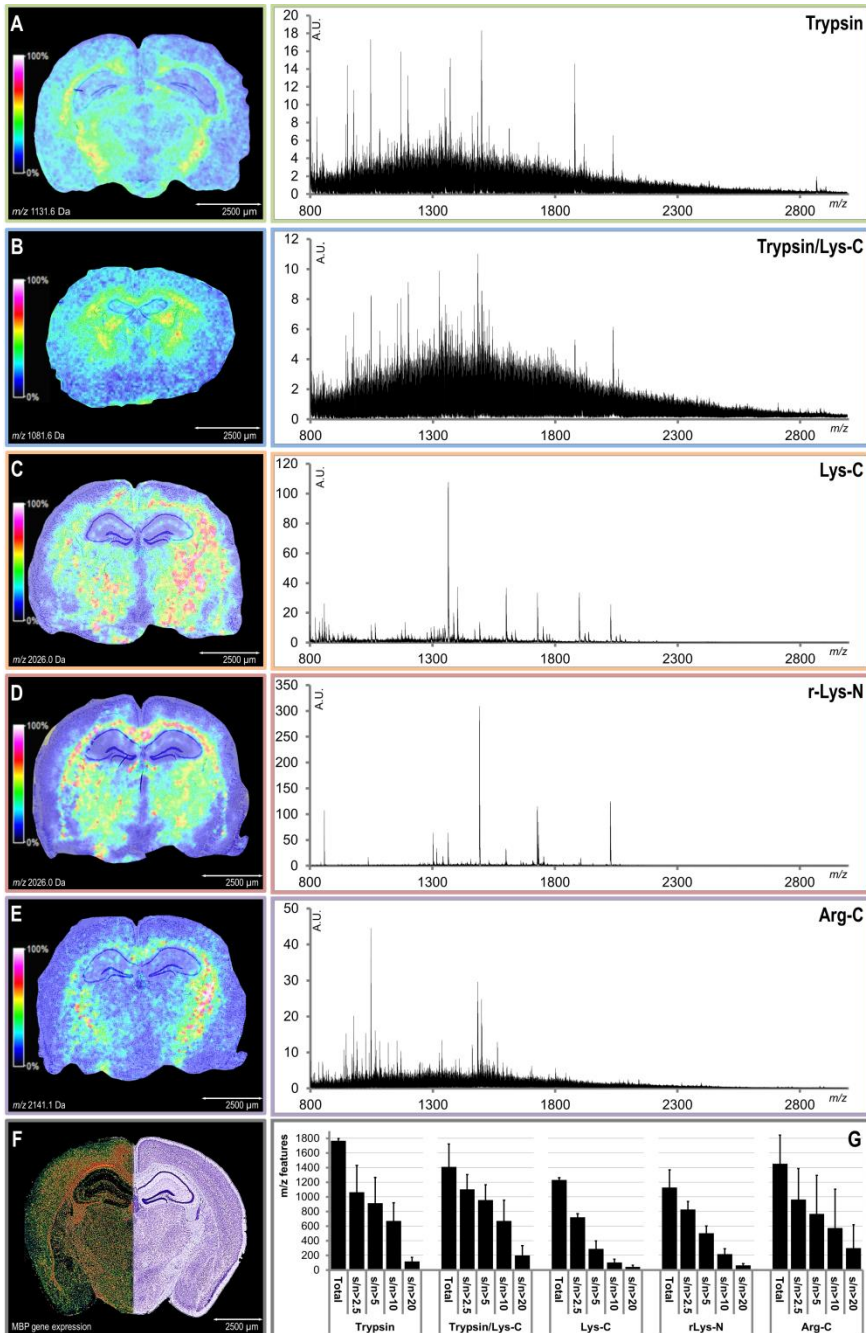
It is important to note that the quality of the MSI images was poor when the enzymes were applied using the buffer system recommended by the manufacturers (e.g. ammonium bicarbonate; HEPES; Tris-HCl), with no visualization of clear anatomical structures for different  $m/z$  values (Figure S3-1, Supplementary information). For this reason, all enzymes, except Arg-C, were dissolved in milliQ water (pH 6.5 – 7).

### 3.3.2 MALDI-TOF-MSI: comparison of average spectra

The average mass spectra obtained by MALDI-MSI analysis for both trypsin (Figure 3-1A) and trypsin/Lys-C (Figure 3-1B) digestions presented a curved mass spectral profile that has already been described in several publications (Groseclose et al., 2008; Lemaire et al., 2006; Shimma et al., 2006). The profile reflects the very high complexity of the resulting proteolytic peptide mixtures as well as the inability of the reflectron-TOF mass analyzer to fully resolve all peaks. Proteolytic digestions using proteases with cleavage specificity for single amino acids, such as Lys-C, r-Lys-N or Arg-C, yielded a smaller number of peptides. As can be seen in Figure 3-1C-E, when Lys-C, r-Lys-N or Arg-C were used, the spectra exhibited a flatter baseline and peaks with higher absolute intensity. Figure 3-1G shows that digestion with trypsin yielded a higher total number of  $m/z$  features than digestions using proteases with single-site cleavage specificity. However, on-tissue digestion with Arg-C presented the largest number of high intensity  $m/z$  features,  $S/N > 20$ , consistent with the previously reported bias of MALDI towards Arg-terminated tryptic peptides. Note: the number of  $m/z$  features reported in Figure 3-1G should be considered a low estimate because of the inability of the reflectron-TOF mass analyzer to resolve isobaric ions (Schober et al., 2012).

### 3.3.3 Peptide and protein identification

To further investigate the dependence of the on-tissue digestion MALDI-MSI experiment on the protease, the proteolytic peptides extracted from the tissue section, following deposition and crystallization of the matrix, were analyzed by LC-MS/MS (using consecutive tissue sections that had undergone identical sample preparation). The analysis of the matrix extracts of the five protease preparations resulted in a total of 5,050 non-redundant peptides (online Supplementary information), over 2.8 times the number obtained from the matrix extract of the trypsin digested tissue. When including redundant peptides, the total number increased to 5,339 (online Supplementary information), which was also 2.8 times the number of peptides identified with trypsin alone (Figure 3-2A). The relatively low number of peptides identified after digestion with Lys-C and r-Lys-N was unexpected, but confirmed by repeat experiments. This observation is due to the enzyme buffer exchange performed



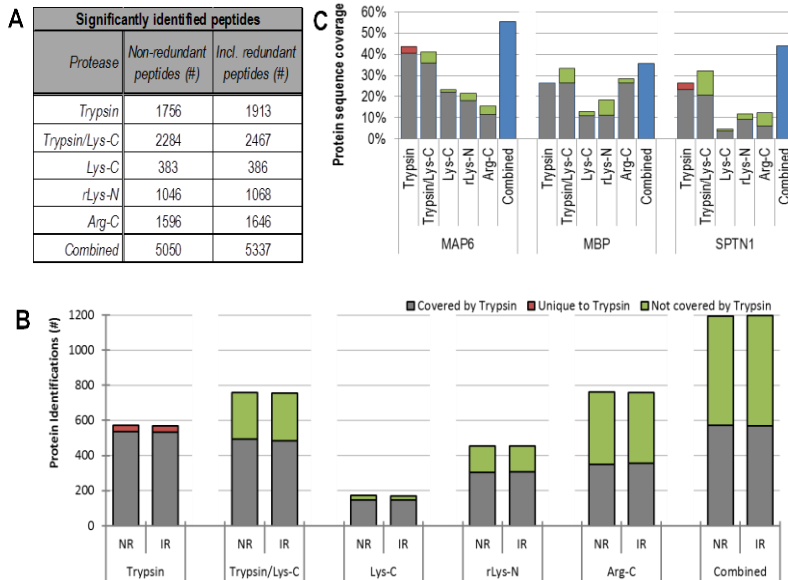
**Figure 3-1:** Overview of the on-tissue-digestion MALDI-MSI data. Myelin basic protein peptide ion distributions and average mass spectra for the digested tissue sections; **(A)**  $m/z = 1,131.6$  (TTHYGSLPQK); **(B)**  $m/z = 1,081.6$  (FFSGDRGAPK); **(C)**  $m/z = 2,026.0$  (SQHGRTQDENPVVHFFK); **(D)**  $m/z = 2,026.0$  (KSQHGRTQDENPVVHFF); **(E)**  $m/z = 2,141.1$  (TQDENPVVHFFKNIVTPR); **(F)** mouse brain Nissl histologic staining and MBP gene expression data from the Allen Brain Atlas; **(G)** average number ( $n = 4$ ) of extracted  $m/z$  features with different signal to noise ratios.

for both enzymes. To achieve optimal digestion conditions proteases are usually dissolved in specific buffer systems containing additives, such as chelating agents, salts and sugars. The buffers for both Lys-C and r-Lys-N contained HEPES, a compound known to cause signal suppression in MALDI-MS above a certain concentration threshold (Amini et al., 2000; Signor and Erba, 2013). This effect is demonstrated in Figure S3-1 (Supplementary information), which compares the average spectra obtained after on-tissue digestion MALDI-MSI with Lys-C dissolved in the manufacturer's recommended buffer (50 mM HEPES (pH 8.0), 10 mM ethylenediaminetetraacetic acid (EDTA) and 5 mg/mL raffinose), and the average spectra obtained after digestion with the same enzyme dissolved in MQ-water after buffer exchange. The latter spectrum shows an increase of more than 2-fold in absolute intensity but the number of peptides is significantly less than would be expected on the basis of previous LC-MS/MS experiments.

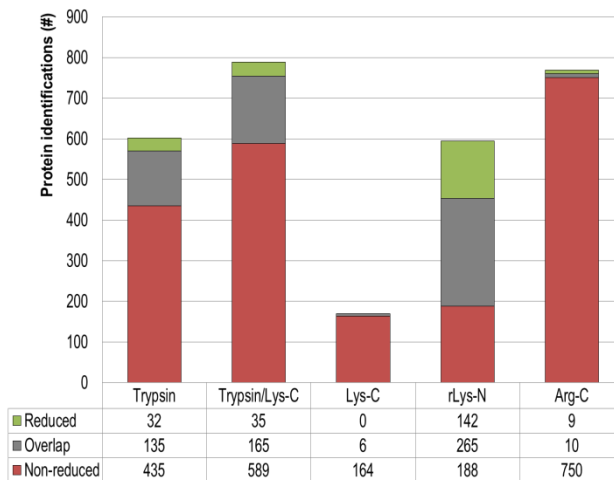
Similar results were achieved at the protein level (Figure 3-2B). The combined data of all on-tissue digestion experiments resulted in a total of 1,194 confidently identified non-redundant proteins. When redundant proteins were included, a total of 1,198 proteins was identified of which 52.2% had not been previously identified in the matrix extract of the trypsin-digested tissue section. Thirty-seven proteins, including redundant proteins, were identified exclusively in the tryptic digests, corresponding to 3.1% of the total number of identified proteins. The largest gain in proteome coverage was achieved using Arg-C: 22.7% of the total number of identified proteins originated exclusively from this extract. A subset of only 96 proteins was identified in all matrix extracts, which corresponds to 8.0% of the total number of identified proteins.

Besides the increase in proteome coverage, individual protein sequence coverage also gained from combining the data obtained with multiple proteases (Figure 3-2C). For instance, analysis of spectrin-1 (SPTN1; 2,472 amino acid residues; MW = 284 kDa; Uniprot entry: P16546), a highly abundant protein in mouse brain that is involved cytoskeletal structure (Zagon et al., 1986), resulted in a sequence coverage of 26.3% from the matrix extract of the trypsin digested tissue section. By combining the data from all enzymes the sequence coverage for SPTN1 increased to 44%. Similar trends were observed for other proteins as shown in Figure 3-2C.

To test whether the proteome coverage could be improved by reducing protein disulfide bonds before enzymatic digestion, a series of experiments were performed in which on-tissue enzymatic digestion was preceded by on-tissue disulfide bond reduction using 2 mM TCEP (in milliQ water), a compound that was previously shown to be compatible with MALDI-MS (Fischer et al., 1993; Kulak et al., 2014). The ion distributions from the reduced tissues were of similar quality as the ones obtained from non-reduced tissues, indicating that the TCEP reduction did not affect the localization of the peptides in the tissue (data not shown). The gain in proteome coverage for each



**Figure 3-2:** Analysis of the on-tissue digested matrix proteome. **(A)** Number of peptides identified for each protease above the significant threshold. Confident non-redundant peptides required a red bold notation in Mascot and a 1% FDR. Mascot score thresholds were  $\geq 30$  for trypsin and trypsin/Lys-C, and  $\geq 25$  for Lys-C, r-Lys-N and Arg-C. Addition of redundant peptides was achieved by removing the red bold requirement. **(B)** Number of proteins identified for each protease. Confident non-redundant (NR) protein identifications were assigned based on 1 or more significant peptides, a red bold notation in Mascot and 1% FDR. Mascot score thresholds were  $\geq 30$  for trypsin and trypsin/Lys-C, and  $\geq 25$  for Lys-C, r-Lys-N and Arg-C. Addition of redundant proteins (IR) was achieved by removing the red bold requirement. **(C)** A comparison of sequence coverage for microtubule associated protein 6 (MAP6), myelin basic protein (MBP) and spectrin-1 (SPTN1). The blue bars represent the total sequence coverage after combining the separate measurements.



**Figure 3-3:** Comparison of confident unique protein identifications obtained from matrix extracts taken from tissue sections treated with on-tissue digestion (red) and tissue sections treated with on-tissue disulfide bond reduction followed by on-tissue digestion (green). Proteins occurring in both experiments were designated as overlap (grey).



protease was determined by comparing protein identifications from both non-reduced and reduced datasets (Figure 3-3). For r-Lys-N the TCEP-reduced protein extract resulted in the identification of an additional 142 proteins, which were not previously identified in the non-reduced sample. A small gain in proteome coverage was also observed in the extract of trypsin (32 additional identified proteins) and trypsin/Lys-C (35 additional identified proteins).

### 3.3.4 Gene ontology analysis of the matrix proteome

The combined data from the digested matrix proteomes was submitted to a gene ontology analysis. The results show that the matrix proteome contained mostly cytoplasmic proteins (48.7%), followed by nuclear proteins (14.9%) and membrane proteins (16.3%) (online Supplementary information). These results are in accordance with previous data by Maier *et al.* (Maier et al., 2013), which focused on the intact proteins sampled by MALDI-MSI.

A KEGG pathway analysis (online Supplementary information), revealed that many of the proteins in the digested matrix proteome play a role in metabolism: amongst the most significant pathways are oxidative phosphorylation, the Krebs cycle, glycolysis and pyruvate metabolism. Protein pathways involved in neurodegenerative disorders (e.g. Alzheimer's disease, Parkinson's disease and Huntington's disease) as well as in long-term depression were identified amongst the most significant hits.

### 3.3.5 MALDI-FTICR-MSI: linking MSI to LC-MS/MS

To resolve isobaric peptide ions and assign identities the on-tissue digestion experiments were repeated with a 9.4T MALDI-FTICR-MS. For trypsin digestion 156 peptides, corresponding to 100 proteins (Table 3.1) and 8.2% of the peptides identified by LC-MS/MS, could be assigned to peaks in the MSI dataset. For the other proteases the numbers were: (i) trypsin/Lys-C 9.8%; (ii) Lys-C 17.4%; (iii) r-Lys-N 12.6%; (iv) Arg-C 9.2%. The combined list of assigned peptides for the five proteases corresponded to 280 proteins (an increase of 180 proteins if compared to just trypsin alone).

**Table 3.1:** Results of the peptide identity assignment on the MALDI-FTICR-MSI data.

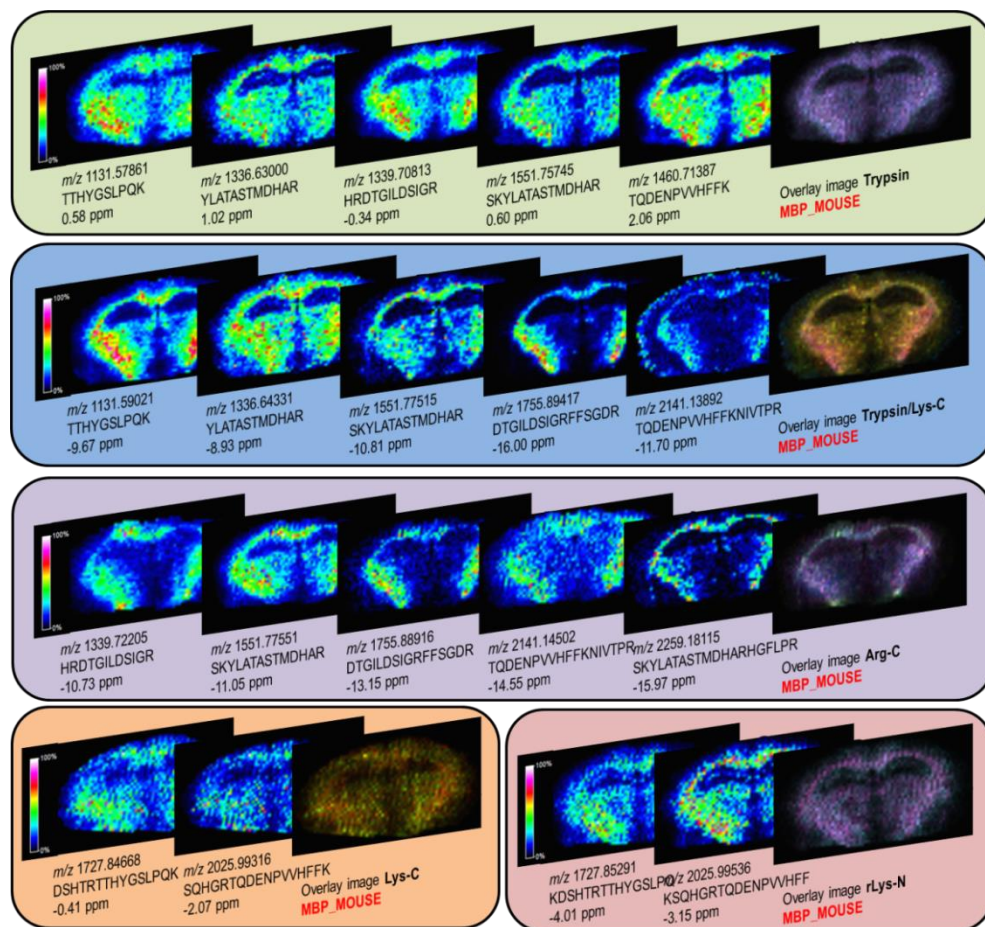
Protease	Assigned peptides incl. redundant peptides total (#)	Corresponding proteins total (#)
<b>Trypsin</b>	156	100
<b>Trypsin/Lys-C</b>	242	133
<b>Lys-C</b>	67	40
<b>r-Lys-N</b>	135	86
<b>Arg-C</b>	152	115

For several proteins, more than one peptide was assigned, which allowed for comparison of the peptide distribution within one tissue section or between tissue sections that were digested with different proteases. Figure 3-4 shows several examples of MBP proteolytic fragments that were assigned based on the described methodology. The peptide distributions were verified using the gene expression profile for the *Mbp* gene obtained from the Allen Brain Atlas (Figure 3-1F). More examples are presented in the online Supplementary information.

### 3.4 Discussion

One of the most comprehensive studies regarding the proteome sampled by MALDI-MSI identified 1,400 proteins from diverse human tissues (Maier et al., 2013). It was based on the extraction of intact proteins from tissues coated with MALDI matrix, the matrix proteome, followed by separation by gel electrophoresis and in-gel trypsin digestion. Despite the valuable information collected, in terms of the proteins ultimately accessible by MSI, the published data does not allow a direct comparison with MALDI-MSI because most identified proteins are substantially larger than those usually detected by MALDI-MSI (McDonnell et al., 2014; Schober et al., 2012). Instead, the identification of the proteins analyzed by MALDI-MSI is often performed using on-tissue enzymatic digestion, in which the MALDI-MSI data is assigned, on the basis of accurate mass, to LC-MS/MS data from tissue extracts (Maier et al., 2013; Groseclose et al., 2007; Gustafsson et al., 2013). Digestion with different enzymes has been shown to increase proteome coverage in bottom-up proteomics (Choudhary et al., 2003; Gatlin et al., 2000; Hohmann et al., 2009; Wa et al., 2006). Similarly, Enthaler *et al.* (Enthaler et al., 2013b) demonstrated that the combination of trypsin, pepsin and elastase increased protein sequence coverage in MALDI-MSI. The increased sequence coverage follows from the high number of cleavage sites – elastase cleaves at the C-terminus of small hydrophobic amino acids, G, S, I, L, A, V (Rietschel et al., 2008) and pepsin at the C-terminus of amino acids, P, Y, W, L (Mótyán et al., 2013) – but at the expense of very complex MSI datasets containing many isobaric ions.

Instead we investigated whether the different activities of additional enzymes that cleave at the basic amino acids (to maintain MS detection sensitivity) can also aid MALDI-MSI. The enzymes trypsin, Lys-C, trypsin/Lys-C, Lys-N and Arg-C were investigated. A standard digestion protocol was first established using trypsin. Once similar results were reproducibly obtained, including from different animals, the method was adapted for the other proteases by changing the solution conditions (minimal changes to the spraying and incubation conditions). The success of the different proteases further demonstrates the robustness of the method (see Table S3-1 (Supplementary information) for spray method). In this paper we have focused on the improvement in proteome coverage that may be obtained in on-tissue digestion MALDI-MSI by combining the results from different proteases; to ensure comparability the data presented are obtained from a single animal.



**Figure 3-4:** Ion distributions representing MBP peptides obtained from MALDI-FT-ICR-MSI were assigned to peptides identified by LC-ESI-MS/MS. The images were obtained from the MALDI-FT-ICR-MSI datasets of (i) trypsin (green box), (ii) trypsin/Lys-C (blue box), (iii) Arg-C (purple box), (iv) Lys-C (orange box), (v) r-Lys-N (red box). For each of the single ion images (represented by the jet intensity scale) the corresponding sequence and measurement error are presented

All enzymes were diluted to the same concentration and sprayed over the tissue with the same method. The presence of salts and buffers in the protease solutions of Lys-C and r-Lys-N led to poor matrix crystallization, low signal intensity and noisy MSI images (Figure S3-1, Supplementary information). A buffer exchange with milliQ water (pH 6.5 – 7) improved the quality of the MS images but the low number of peptide and protein identifications indicated that the lack of salts and buffers adversely affected enzymatic activity (Figure 3-2). Still, the combination of proteases greatly increased the number of detected peptides and proteins; the 5,337 peptides and 1,198 proteins represent an increase of 179% and 110%, respectively, as compared to trypsin alone (1,913 peptides; 570 proteins).

Unlike LC-MS/MS based protein identification, MSI of proteolytic peptides does not differentiate unique peptides from non-unique peptides and all peptides are detected in the same mass spectrum. Consequently, the datasets will contain non-unique peptides as well as many isobaric ions. Both of these characteristics frustrate efforts to identify proteolytic peptides directly from tissue using MS/MS (Houel et al., 2010). The use of multiple enzymes for on-tissue digestion has the advantage of producing different peptides from the same protein that can be used to confirm its distribution in the tissue sample (Figures 3-1 and 3-4).

To connect the confidently identified peptides and proteins from the matrix extracts to the on-tissue digestion MALDI-MSI experiments high mass resolution MALDI-MSI data was acquired on a 9.4T MALDI-FTICR instrument. Between 8.2 - 17.4% of the peptides identified by LC-MS/MS could be assigned to peaks in the high mass resolution MALDI-MSI datasets (Table 3.1). The combined total number of 633 peptides originated from 280 proteins (online Supplementary information). A previous publication by Schober *et al.* (Schober et al., 2012) reports a similar approach where over 1,100 peptides were first identified from a mouse brain tissue homogenate, of which 13% were assigned to  $m/z$  features in a high mass resolution MALDI-MSI dataset, and corresponded to 101 proteins. The Schober paper used extensive peptide fractionation to increase protein identification rates and analyzed the entire tissue's proteome. In contrast the results reported here utilized no fractionation and only analyzed the matrix proteome. Without the fractionation step 140 peptides were identified in the LC-MS/MS analysis of which 60 could be assigned to  $m/z$  features in the MALDI-MSI dataset, corresponding to 38 proteins (Schober et al., 2012). Here, using complementary enzymes for on-tissue digestion and LC-MS/MS of the matrix peptides (without any fractionation step) we could assign more than 600 peptides, corresponding to 280 proteins.

The peptide assignments were based on a mass error tolerance of  $\pm 20$  ppm. The cyclotron frequency of an ion inside an ICR cell, and therefore the accurate calibration of an FTICR instrument, is dependent on the magnetic field strength as well as the local electric field. Accordingly, the calibration is dependent on the number of ions in the cell, which in MALDI-MS varies from shot-to-shot, and in MALDI-MSI from pixel to pixel. Consequently, there are slight mass deviations in all pixels, resulting in broader peaks in the average mass spectrum. Peak picking and peptide identity assignment were based on the average, non-aligned mass spectrum and therefore a higher mass tolerance was applied. However, the consensus between the images obtained for different peptides, utilizing different proteases provides additional corroboration.

The LC-MS/MS data reported here of MALDI matrix extracts also acts as a guide to the proteins/peptides that may be analyzed via MALDI-MSI. It has previously been shown that MSI detected only a fraction of those detected by LC-MS/MS analysis of tissue extracts (Schober et al., 2011). A single 100 x 100  $\mu\text{m}$  pixel analyses the

equivalent of  $\approx 12$  cells (assuming average cell size of 20  $\mu\text{m}$  and tissue thickness of 10  $\mu\text{m}$ ), and which is analyzed without any explicit purification and separation step. To be detected by MALDI-MSI the peptides are required to be present in the MALDI matrix and present at sufficiently high levels. While we have demonstrated an increase in proteome coverage the number remains a fraction of the tissue's total proteome, because of the sample-volume-limited nature of the analysis and the need for matrix incorporation of the peptides. The FTICR-MS used here, and the Orbitrap used previously (Schober et al., 2012), are characteristically very high dynamic range mass analyzers. To significantly increase the number of peptides detected by MSI will require significant increases in the charge capacity of these ion trap mass analyzers (while maintaining performance) in order for the lower level peptides to be above the detection threshold.

Amongst the 280 assigned proteins detected here were several histones. Histones are highly implicated in cancer progression through their role in determining chromatin structure and gene accessibility. Proteolytic fragments of histones have been previously reported in cancerous tissues analyzed by on-tissue-digestion MALDI-MSI (Djidja et al., 2009a, 2009b). Several peptides were assigned to subunits of mitochondrial ATPases (AT1A1, -2, -3, AT2B1, -2, ATPA, ATP5H & ATP5J). These trans-membrane proteins are known to be involved in a multitude of neurological disorders, e.g. familial hemiplegic migraine (Morth et al., 2009; Poulsen et al., 2010) and Alzheimer's disease (Markesbery, 1997; Zlokovic, 2011). These results were confirmed by the GO analysis and KEGG pathway analysis which show that proteins involved in several metabolic pathways and neurological disorders are well represented in the digested matrix proteome (online Supplementary information).

### 3.5 Conclusions

This work reports the peptides identified from the on-tissue-digestion matrix proteome as well as the peptides detected by ultra-high mass resolution MALDI-MSI, for multiple enzymes; both valuable sources of information for researchers applying on-tissue digestion MSI. The results demonstrate the ability to increase proteome coverage by using different enzymes and indicate that on-tissue digestion MALDI-MSI analysis of the mouse brain can be applied in a wide range of disease related, biomarker discovery or other neuro-scientific research applications.

It should be noted that we have been deliberately conservative with the thresholds used in the assignments ( $>0.6\%$  base peak). It is known that FTICR and Orbitrap mass spectrometry can span a very wide dynamic range, and more peptides could have been assigned if a lower threshold was used. However, at lower thresholds many peaks were associated with noisy images and the greatly increased number of peaks is accompanied by an increased risk of mis-assignment. It is expected that with additional improvements in dynamic range, sensitivity and on-tissue MS/MS based verification of

peptide identities that even more peptides will be assignable and the application potential of MALDI-MSI increased further.

### 3.6 Acknowledgements

This work was supported by the ZonMW Zenith project Imaging Mass Spectrometry-Based Molecular Histology: Differentiation and Characterization of Clinically Challenging Soft Tissue Sarcomas (No. 93512002; BH), Centre for Medical Systems Biology (CMSB) in the framework of the Netherlands Genomics Initiative (NGI) (AvdM), EU-funded Marie Curie Action ENIGMAS FP7-PEOPLE-2011-IEF (No. 303344; RC), Marie Curie Career Integration Grant (No. 294233; EAT), FP7 EUROHEADPAIN (No. 602633;AvdM) and Marie Curie IAPP Program BRAINPATH (No. 612360; AvdM & EAT). The authors thank Nathalie Rieff for technical assistance.

### 3.7 Supplementary information

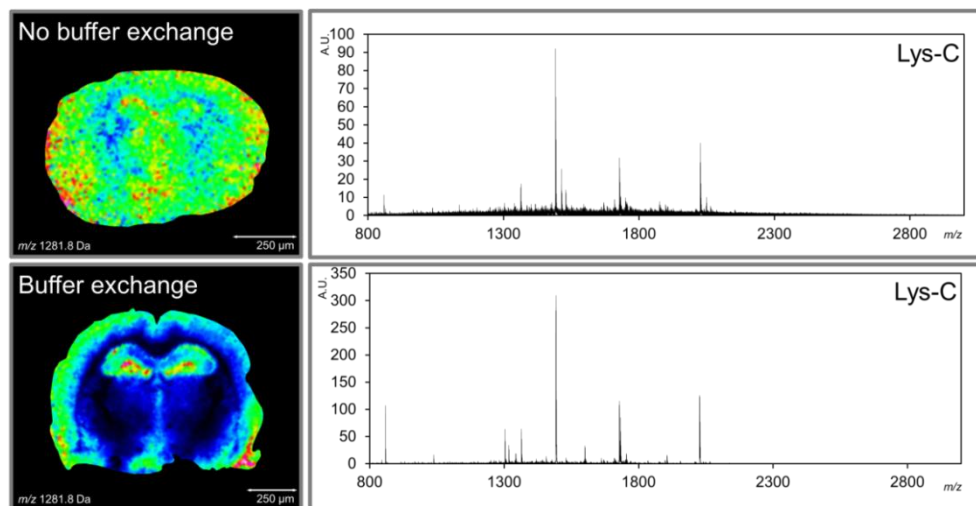
The full supplementary information, files and tables are available on the internet via <http://pubs.acs.org/doi/suppl/10.1021/ac503952q>.

#### 3.7.1 Supplementary tables

**Table S3-1:** Overview of the settings used on the SunChrom SunCollect sprayer during TCEP-, protease and matrix application.

Setting	TCEP	Protease	Matrix
Vial X ( <i>mm</i> )	0.5	0.3	0.5
Vial Y ( <i>mm</i> )	2.0	0.3	2.0
Z ( <i>mm</i> )	25.0	45.5	25.0
Z-offset ( <i>mm</i> )	0.0	0.0	0.0
Layers (#)	4	5	3
Flowrate Layer 1 ( $\mu\text{L}/\text{min}$ )	10	5	10
Flowrate Layer 2 ( $\mu\text{L}/\text{min}$ )	10	5	35
Flowrate Layer 3 ( $\mu\text{L}/\text{min}$ )	10	5	35
Flowrate Layer 4> ( $\mu\text{L}/\text{min}$ )	10	5	-
Speed X	Low (3)	Low (4)	Low (3)
Speed Y	Medium (1)	Medium (1)	Medium (1)

### 3.7.2 Supplementary figures



**Figure S3-1:** The effect of the enzyme buffer exchange procedure required to remove ion suppressing compounds (e.g. HEPES) from the enzyme buffer. The **top** panel contain an image and an average spectrum taken from a lys-C on-tissue digestion MALDI-MSI analysis, without performing enzyme buffer exchange. The **bottom** image and spectrum were taken from a lys-C on-tissue digestion MALDI-MSI analysis, subsequent to the enzyme buffer exchange procedure. Ion intensities in the MALDI-MSI data are represented by the jet intensity color scale.







## Chapter 4

# Histology-guided high resolution MALDI mass spectrometry imaging

**Bram Heijs**†; Walid M. Abdelmoula†; Sha Lou; Inge H. Briaire-de Bruijn; Jouke Dijkstra; Judith V.M.G. Bovée; Liam A. McDonnell, "Histology-guided high resolution MALDI mass spectrometry imaging," *Analytical Chemistry* 87(24), pp. 11978-11983, 2015.



*Mass spectrometry imaging (MSI) is widely used for clinical research because when combined with histopathological analysis the molecular signatures of specific cells/regions can be extracted from the often-complex histologies of pathological tissues. The ability of MSI to stratify patients according to disease, prognosis and response is directly attributable to this cellular specificity. MSI developments are increasingly focused on further improving specificity, through higher spatial resolution to better localize the signals or higher mass resolution to better resolve molecular ions. Higher spatial/mass resolution leads to increased data size and longer data acquisition times. For clinical applications, which analyze large series of patient tissues, this poses a challenge to keep data load and, acquisition time manageable. Here we report a new tool to perform histology guided MSI; instead of analyzing large parts of each tissue section the histology from adjacent tissue sections is used to focus the analysis on the areas of interest, e.g. comparable cell types in different patient tissues, thereby minimizing data acquisition time and data load. The histology tissue section is annotated and then automatically registered to the MSI-prepared tissue section; the registration transformation is then applied to the annotations, enabling them to be used to define the MSI measurement regions. Using series of formalin-fixed, paraffin-embedded human myxoid liposarcoma tissues we demonstrate an 80% reduction of data load and acquisition time, thereby enabling high resolution (mass or spatial) to be more readily applied to clinical research. The software is freely available for download.*

## **4.1 Introduction**

Histological analysis is arguably the most common tool in diagnostic pathology and clinical research. The use of molecular assays further aids in understanding, determining, and differentiating diseases (Aichler and Walch, 2015; Altelaar et al., 2012; Bovée and Hogendoorn, 2010). A technique that recently emerged is matrix-assisted laser desorption/ionization (MALDI) mass spectrometry imaging (MSI), which is an analytical technique that combines conventional microscopy with spatially resolved and label-free detection of hundreds of biomolecules directly from a tissue section (Caprioli et al., 1997). MALDI-MSI has proven itself a valuable tool in molecular pathology as it is capable of revealing the molecular histology of a tissue section and finding distinct molecular profiles that can predict the nature of the underlying tissue (Willems et al., 2010b; Balluff et al., 2015; Casadonte et al., 2014; Gustafsson et al., 2011; Meding et al., 2012).

The impact of MSI in clinical research is directly attributable to the cellular specificity of the analysis; signatures of specific cells/regions can be extracted from the often-complex histologies of pathological tissues. MSI developments are increasingly focused on further improving specificity, through higher spatial resolution to better localize the signals or higher mass resolution to better resolve ions with identical nominal masses.

MSI analysis of proteins via on-tissue enzymatic digestion, metabolites, lipids and recently even intact proteins, all benefit from higher mass resolution by better resolving the many molecular species with the same nominal mass, so-called isobaric ions (Buck et al., 2015; Heijs et al., 2015; Muller et al., 2015; Spraggins et al., 2015). When analyzing large tissue series, a compromise must be sought between resolution and throughput, to keep the data load, acquisition time and computational challenges manageable. This is primarily because the established approach is to first record MSI data, and then use histopathological analysis of the same tissue section to define via a virtual microdissection which MSI data will be used in the statistical analysis. However only a fraction of the MSI data is typically used in the statistical analysis, as the cellular content of the compared regions must be well matched within the same tissue as well as within tissues from different patients. Accordingly, the data acquisition throughput and data load could be better optimized by adapting the histology-defined protein-profiling approach (Cornett et al., 2006) to high resolution MSI, namely limiting MSI data acquisition to those regions whose data will be used in the statistical analysis.

In the current work we have developed an automated image registration pipeline to register an annotated, histological image of an adjacent tissue section to a lower resolution image of the MSI-prepared tissue section. Subsequently, the annotation borders are propagated to the low resolution image, enabling the exclusive analysis of the annotated regions by MSI. This histology-guided MSI approach ensures that the MSI data is acquired solely from tissue regions with similar morphological makeup. Using series of formalin-fixed, paraffin-embedded human myxoid liposarcoma tissue we demonstrate an 80% reduction of data load and acquisition time, thereby enabling high resolution (mass or spatial) to be more readily applied in clinical research.

## 4.2 Methodology

### 4.2.1 Chemicals and reagents

All chemicals were purchased from Sigma-Aldrich (Steinheim, Germany) except ethanol and xylene (Merck, Darmstadt, Germany). Trypsin was purchased from Promega (Madison, USA).

### 4.2.2 Tissues & sample collection

Myxoid liposarcoma (MLS) tissues were fixed in formalin and embedded in paraffin following standard histopathological procedures. All tissue samples were handled in a coded fashion according to Dutch national ethical guidelines (Code for proper secondary use of human tissue, Dutch Federation of Medical Scientific Societies). Adjacent tissue sections, 6  $\mu\text{m}$ , were cut from the formalin-fixed, paraffin-embedded (FFPE) tissue blocks using a microtome. Tissue sections designated for MALDI-MSI analyses were mounted on poly-L-lysine coated indium-tin-oxide (ITO) glass slides (Bruker Daltonics, Bremen, Germany), dried overnight at 37°C and stored at 4°C until the analysis. Tissues designated for histological analysis were mounted on Starfrost

adhesive microscope slides (Light Labs, Dallas (TX), USA), stained with haematoxylin & eosin (H&E) and scanned using a digital slide scanner (IntelliSite Pathology Ultra-Fast Scanner, Philips, Eindhoven, The Netherlands). This tissue section is referred to as the histological-tissue-section in the subsequent text.

### 4.2.3 On-tissue digestion MALDI-MSI

FFPE tissue sections designated for MSI analysis were first put on a 60°C heating block to improve adherence of the tissue section to the slide. Deparaffination was performed by washing the slides twice in 100% xylene (I - 5 min, II - 10 min). Prior to heat-induced antigen retrieval (HIAR) in 10 mM citric acid pH6, the slides were washed twice in 100% ethanol (2 min each) and twice in milliQ water (5 min each). After HIAR two more washes in milliQ water (1 min each) were performed. The tissues were dried in a vacuum desiccator for 15 minutes. Fiducial markers were placed using water-based Tipp-Ex and a lower resolution (2400 dpi) optical image recorded using a flatbed scanner. This image is referred to as the *pre-MSI-optical-image*. Immediately thereafter trypsin (20 ng/μL in deionized water) was sprayed on the tissue using the SunCollect automatic sprayer (SunChrom, Friedrichsdorf, Germany) (5 layers at 5 μL/min). Following an 18 h incubation in a saturated (50% methanol) environment at 37°C, three layers (at 10, 35, and 35 μL/min) of MALDI matrix (20 mg/mL 2,5-dihydroxybenzoic acid in 50% acetonitrile and 0.1% trifluoroacetic acid) were sprayed on the tissue using the SunCollect automatic sprayer (Heijs et al., 2015).

MALDI-FTICR-MSI was performed on a 9.4 T Solarix XR mass spectrometer (Bruker Daltonics) in positive-ion mode, using 150 laser shots per spot and 100 x 100 μm pixel size, calibrated using Peptide Calibration Standard (Bruker Daltonics). Spectra were recorded in the  $m/z$  range 600–3,500 Da with a 512k data point transient (1.1 s duration), corresponding to an estimated resolution of 200,000 at  $m/z$  400 Da. The average detected mass resolution over the analyzed mass range was 54,000, and the mass resolution in the center of the mass range, at  $m/z$  1,500, was 65,000. Data acquisition was performed using ftmsControl (Bruker Daltonics), and visualizations were obtained from flexImaging 4.0 (Bruker Daltonics). Following the MALDI-MSI data acquisition, excess matrix was removed by washing in 70% ethanol (2x 2 min) and this MSI-analyzed-tissue-section also stained with H&E. The stained tissues were scanned using a digital slide scanner and used to assess the accuracy of the registration between this MSI-analyzed-tissue section and the histological tissue section. This image is referred to as the *post-MSI-histological-image*.

### 4.2.4 Image registration software tool

#### 4.2.4.1 Pre-processing

Background noise was first removed from both the *histological-tissue-section* image and *pre-MSI-optical-image*. The pre-processing retains the tissue foreground information while setting the background pixels to zero. The intensity distribution of the

optical image follows a bimodal histogram that represent background and foreground pixel distribution, hence their separation is readily achieved by setting a global threshold using Otsu's method<sup>16</sup>. Morphological operations then followed to fill-in any gaps introduced by setting the image intensity threshold. The region with the maximum area of connected components was selected to form a mask that separates the tissue from the background. The high-resolution histology images were pre-processed using the pre-processing-pipeline presented by Abdelmoula *et al.* (Abdelmoula et al., 2014).

#### 4.2.4.2 Image Registration

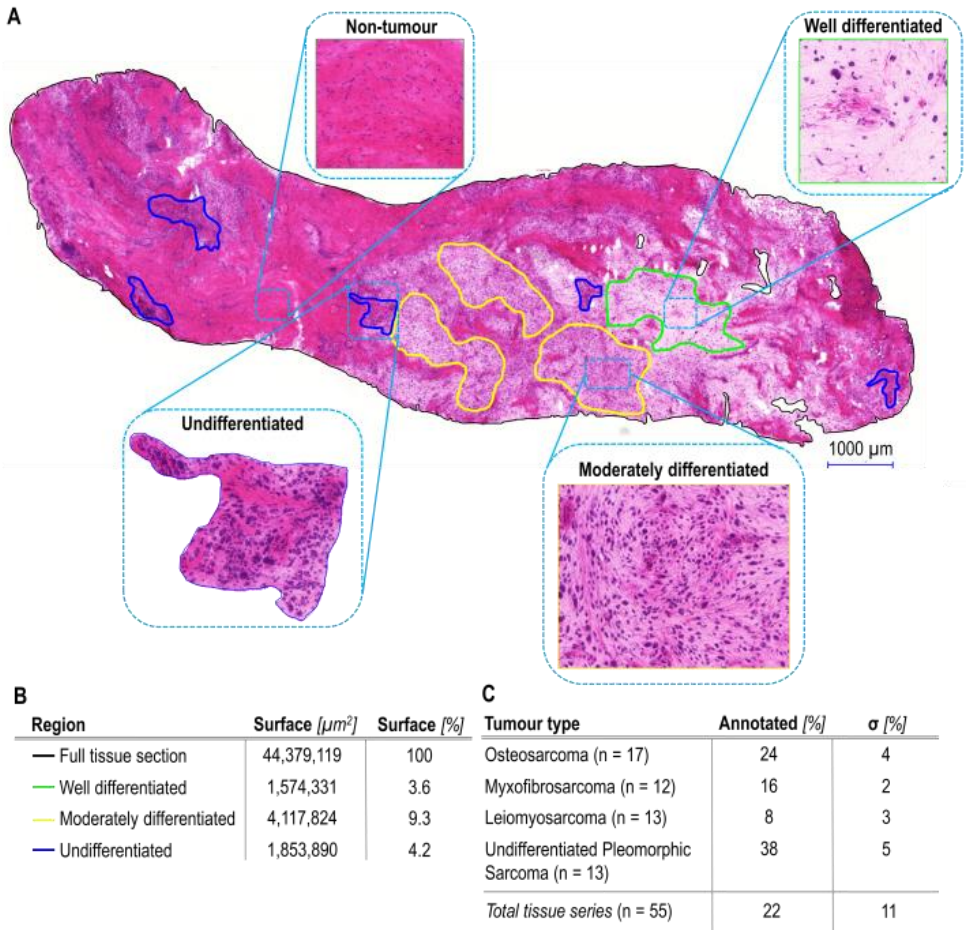
The registration process is performed between a fixed image ( $I_f$ ), in this case the *pre-MSI-optical-image*, and a moving image ( $I_m$ ), the *histological-tissue-section* image. The moving image is warped to be spatially aligned with the fixed image according to the standard registration optimization problem given in equation (1).

$$\hat{\mu} = \arg \min_{\mu} C[I_f, T(I_m)] \quad (1)$$

The optimized transformation parameters are captured in the vector  $\mu$  in such a way the cost function  $C$  is minimized with respect to the transformation model  $T$  using the adaptive stochastic gradient descent optimizer (Klein et al., 2011). First,  $I_m$  was linearly transformed, using affine transformation, to capture the global deformation parameters (i.e. translation, rotation, scaling, and shearing), followed by a non-linear transformation model of B-Spline to correct for local deformations. The registration was performed in a multi-resolution scheme (4 levels) using a Gaussian pyramid model and the mutual information was used as a cost function to assess the registration quality. The multi-resolution registration has proven faster and more robust than single-scale techniques with a convergence that is less likely to be trapped in a local optimum (Unser et al., 1993). The mutual information has been introduced for multi-modality image registration, as it measures the statistical dependence between two images with the same geometrical information but different intensity distributions and maximizing their statistical measure implies they are geometrically aligned (Maes et al., 1997; Pluim et al., 2003). The Elastix software package was used to implement the reported registration algorithms (Klein et al., 2010).

#### 4.2.4.3 Evaluation

The accuracy of the image registration was assessed by comparing expert pathological annotations of the *post-MSI-histological-image* (JVMGB) with those provided by registering the annotations of the *histological-tissue-section* to the *pre-MSI-histological-image*. The accuracy was quantified by using the Dice similarity coefficient (DSC), which is a measure for the similarity between two samples (Dice, 1945).



**Figure 4-1:** (A) Scanned image of an H&E stained myxofibrosarcoma tissue with annotated regions of clinical interest. Pixels present in the ROIs were selected for data analysis. Various tumour grades were selected based on their cellular differentiation, green, yellow and blue annotations represent well differentiated, moderately differentiated and undifferentiated tissue regions respectively. (B) The (relative) surface of the differently diagnosed tissue regions compared to the total surface of the full tissue section. (C) The average percentage of pixels used for data analysis per tumour subtype for a total of 55 soft tissue sarcoma samples.

### 4.3 Results and discussion

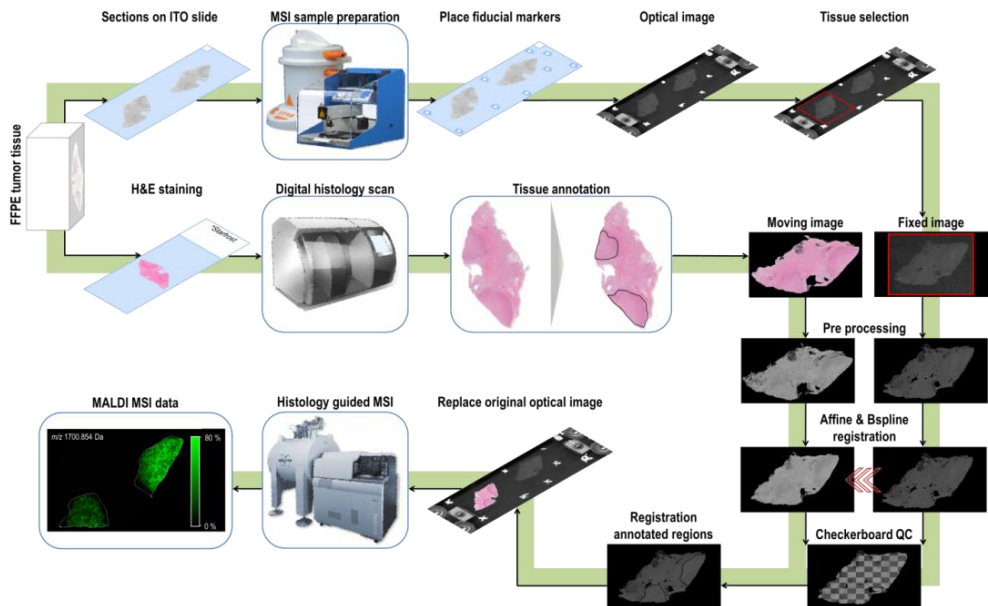
An established approach in clinical MALDI-MSI is to analyze large areas of a series of tissue sections at a predefined spatial resolution. Subsequently, excess matrix is removed and a histological staining of the analyzed section allows to perform virtual microdissection, and to export the pixels from regions with similar cellular makeup for further data analysis (Figure 4-1A).

A previous analysis to study intact proteins from a patient series of high grade sarcomas (n = 55) revealed that, after virtual microdissection, an average of just 22% ( $\pm 11\%$ ) of the MALDI-MSI data was used in the subsequent data analysis (Figure 4-1B-C). This dataset was acquired at a 100  $\mu\text{m}$  spatial resolution on a relatively low



mass resolution MALDI-TOF/TOF platform (UltrafleXtreme, Bruker Daltonics) but already resulted in a total dataset size of 232 GB for the 55 analyzed tissue sections. This post-MSI virtual microdissection approach is sub optimal for high resolution studies, because of the greatly increased data load and data acquisition times associated with higher mass/spatial resolution.

We recognized that we could increase the measurement throughput and, decrease data load if MSI data acquisition was limited to histologically comparable regions, in an MSI analogue of the histology defined protein profiling approach (Cornett et al., 2006). Therefore, we have developed histology-guided MSI (HG-MSI) software that makes use of automated image registration to limit data acquisition to specific histologically pre-defined regions (Figure 4-2).

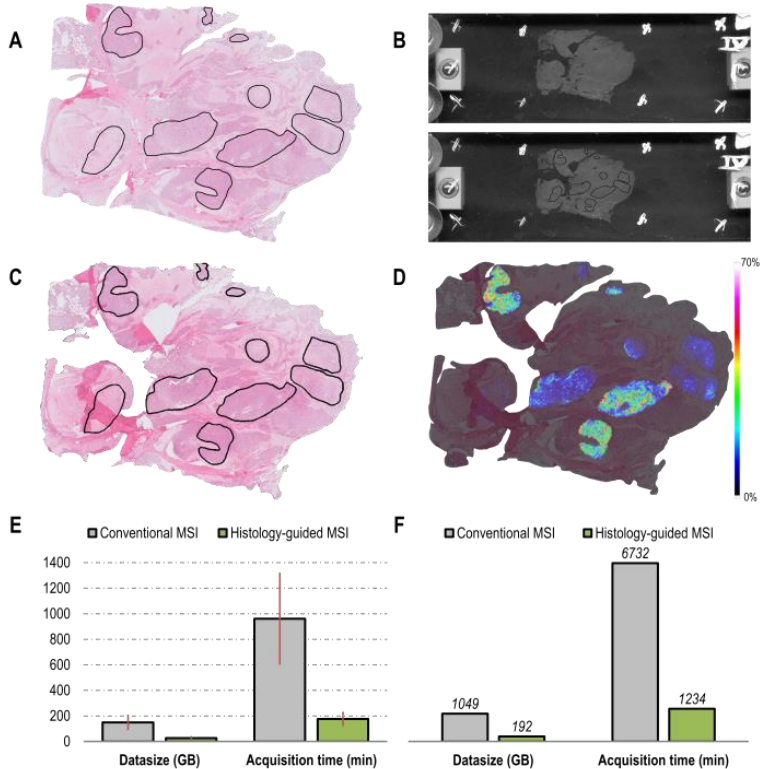


**Figure 4-2:** A schematic overview of the most important steps in the HG-MSI workflow. The workflow enables the selection of MALDI-MSI measurement regions to be guided by the tissue’s histology.

The *Histology\_Guided\_MS* software performs an automatic registration of images of adjacent tissue sections: (i) the moving image ( $I_m$ ), which is represented by an annotated high resolution image of an H&E stained tissue section, here referred to as the *histological-tissue section* (Figure 4-3A), and (ii) the fixed image ( $I_f$ ), a lower resolution optical image required for the MALDI-MSI analysis, here referred to as the *pre-MSI-optical-image* (Figure 4-3B-top). In this manner the histological annotations are mapped onto the *pre-MSI-optical-image* and can be used to define the measurement regions (Figure 4-3B-bottom).

The adjacent tissue sections were manually mounted onto different glass slides and scanned at different resolutions; and so the registration encompasses a linear, affine

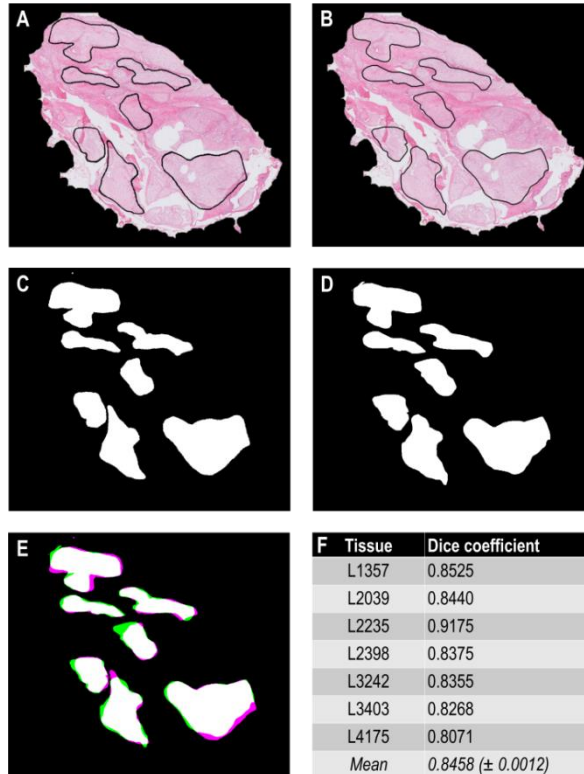
registration to correct for global deformations (e.g. translation, scaling, rotation, and shearing) as well as a non-linear, B-spline transform to compensate for local deformations (e.g. differences in sizes of regions, stretches introduced during mounting) (Abdelmoula et al., 2014).



**Figure 4-3:** (A) *Histological-tissue-section* image of a myxoid liposarcoma tissue, including annotations marking the clinically relevant regions. (B-top) *Pre-MSI-optical-image* of the tissue prior to the MALDI-MSI analysis. The section was adjacent to the section shown in (A). (B-bottom) The output image of the *Histology\_guided\_MS* registration algorithm. The image shows the aligned, annotated regions from (A) propagated to the *pre-MSI-optical-image* (B-top). (C) *Post-MSI-optical-image*; the H&E stained tissue after MALDI-MSI data acquisition (B), including the aligned annotated regions from (A). (D) Example MSI image of  $m/z$  944,51 Da corresponding to Histone H2A peptide AGLQFPVGR represented by the Jet intensity scale. (E-F) Comparison between conventional MSI and histology-guided MSI. Shown are the average (E) and total (F) data size and acquisition times for the MLS tissue series ( $n = 7$ ).

As the MSI measurement regions are determined by the histological annotations from an adjacent section, an investigation of the image registration accuracy is necessary. After MSI data acquisition excess MALDI matrix was removed and the tissue sections were H&E stained and, digitally scanned, this is the *post-MSI-optical-image*. The automatically registered annotations from the *histological-tissue-section* were mapped on to this image (Figure 4-3C & 4-4A), and then compared with the results of an expert manual histopathological annotation of the *post-MSI-optical-image* (Figure 4-4B). Visually it can be seen that there is a good agreement between the annotations.

The HG-MSI software was tested by analyzing the proteolytic peptides from an on-tissue digestion investigation of a patient series of FFPE MLS tissues (n = 7) using a 9.4 T MALDI-FTICR instrument (Figure S4-1, Supplementary information). MLS was chosen as these tumors have a very heterogeneous histology (Willems et al., 2010b) that allowed the selection of ROIs with different tumour grades and/or additional histological features (e.g. fat differentiation, and mucine pools).



**Figure 4-4:** An evaluation of the image registration through the measure of annotation overlap using the Dice coefficient. **(A)** Automatically aligned annotations propagated to the post-MSI-optical-image. **(B)** Manually annotated post-MSI-optical-image. **(C)** + **(D)** Binary masks of the annotated regions in **(A)** and **(B)**. **(E)** Fusion of the two binary mask showing the degree of overlap. In white, truly overlapping regions. In green and pink the non-overlapping regions. **(F)** An overview of the Dice coefficients for the analyzed tissues.

Analyzing the tissue series, utilizing the HG-MSI software, resulted in a total data load of 192 GB, which was just 18% of the 1,049 GB that would be generated by analyzing each tissue section of the series completely (Figure S4-2, Supplementary information). Similarly, the data acquisition time was also reduced by 82% from 112 hours to 20 hours (Figure 4-3E-F). Ultimately, throughput and data load are determined by the total area of the selected ROIs. For these tissues only regions with clear histologic grades (e.g. low, moderate and high grade) based on distinct histological features were selected, resulting in annotated areas varying between 12 - 29% of the total tissue surface.

The effectiveness of the HG-MSI software to focus on specific histological regions was then quantified using the Dice similarity coefficient (DSC) (Figure 4-4A-E), to provide a metric for the spatial overlap of the annotated regions in the automatically and manually annotated *post-MSI-optical image*. No overlap would result in a DSC of 0, perfect overlap in DSC of 1. For this tissue series the average DSC was 0.8458 ( $\pm$  0.0012), confirming that the HG-MSI approach does indeed allow the analyst to target the specific regions (Figure 4-4F).

There are several causes that may contribute to the 15% reduction of the DSC. The first is that adjacent sections are not identical and so small differences are expected. Second, it was found that some of the histological regions were harder to define in the *post-MSI-optical-image*, and which may have led to slight differences in the annotation areas. Third, artifacts from the tissue sectioning and mounting such as stretches, tears and folds can cause large differences even between adjacent sections. For example, tissue L2235 and L4175 (Figure S4-1, Supplementary information) represent the experiments with the highest and lowest DSCs respectively (Figure 4-4F). Whereas the images of L2235 exhibit no clear sectioning/mounting artifacts and very distinct histological features, the *histological-tissue-section* of L4175 was folded and the histological features less distinct. To limit the impact of sectioning/mounting artifacts on the registration a manual, free-hand cropping function was added to the registration tool to exclude such regions from the registration process.

We have demonstrated this HG-MSI software for the analysis of proteolytic peptides from specific histopathological regions in tumor tissues using a Bruker Daltonics MALDI-FTICR-MSI. However, the tool is vendor neutral and is applicable to all MSI methodologies (e.g. DESI, SIMS, etc.), the only requirement is that an optical image of the tissue section is used to define the measurement regions. Similarly, the HG-MSI software may be used to better focus high spatial resolution as well as high mass resolution analysis, for all analyte classes and, all tissue types. The software is freely available for download ([http://www.maldi-msi.org/download/SW\\_HG\\_MSI.rar](http://www.maldi-msi.org/download/SW_HG_MSI.rar)). A detailed overview of the histology-guided MSI workflow and software manual is available as online Supplementary information. The only prerequisite to run the *Histology\_guided\_MS* executable is the installation of the Matlab Compiler Runtime (R2012a (7.17)) which is free to download from the Mathworks website ([www.mathworks.com/product/compiler/mcr](http://www.mathworks.com/product/compiler/mcr)).

The compromise associated with specifying data acquisition from distinct histological regions is that retrospective data analysis possibilities are more limited than if each tissue section was analyzed in its entirety. For example, for the myxofibrosarcoma sample shown in Figure 4-1 if only the well-differentiated tumor regions (3.6% of the example tissue section) were selected for MSI data acquisition then it would no longer be possible to compare its mass spectral signature with those from the moderately differentiated tumor (9.3%) and undifferentiated tumor regions

(4.2%), or the tumor stroma and healthy tissue. It is thus crucial to specify, at the outset, which histological comparisons will/may be made. Accordingly, the tool is better suited to those analyses in which the slow scan speed (high mass resolution) or large number of pixels (high spatial resolution) makes it impractical to apply to a large patient series of complete tissue sections.

## 4.4 Conclusions

In this work we report a new freely available tool for histology-guided MALDI-MSI and provide the software required to perform automated image registration so that the annotations from an adjacent histological image can be transferred to the tissue section that will be analyzed by MSI. The results demonstrate the strength of the approach, particularly for high resolution MSI, in which the high resolution leads to longer acquisition times. The ease of use and general applicability of the tool in any MSI workflow will ultimately result in a higher throughput, a smaller data load, and more comparable data.

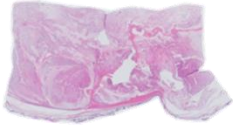
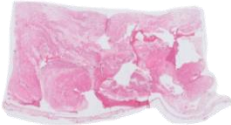
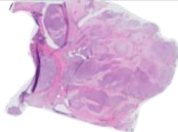
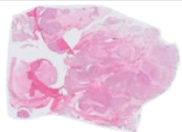
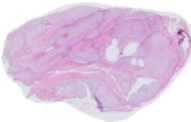
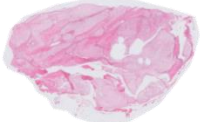
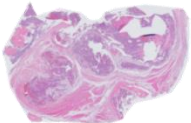
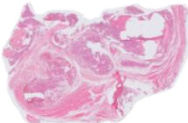


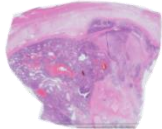
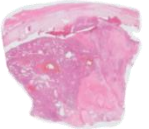

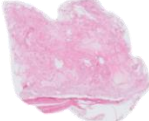
## 4.5 Acknowledgements

This work was supported by the ZonMW Zenith project "Imaging Mass Spectrometry-Based Molecular Histology: Differentiation and Characterization of Clinically Challenging Soft Tissue Sarcomas" (No. 93512002; B.H.), the ICT consortium COMMIT project "e-biobanking with Imaging" and the Cyttron II project "Imaging Mass Spectrometry".

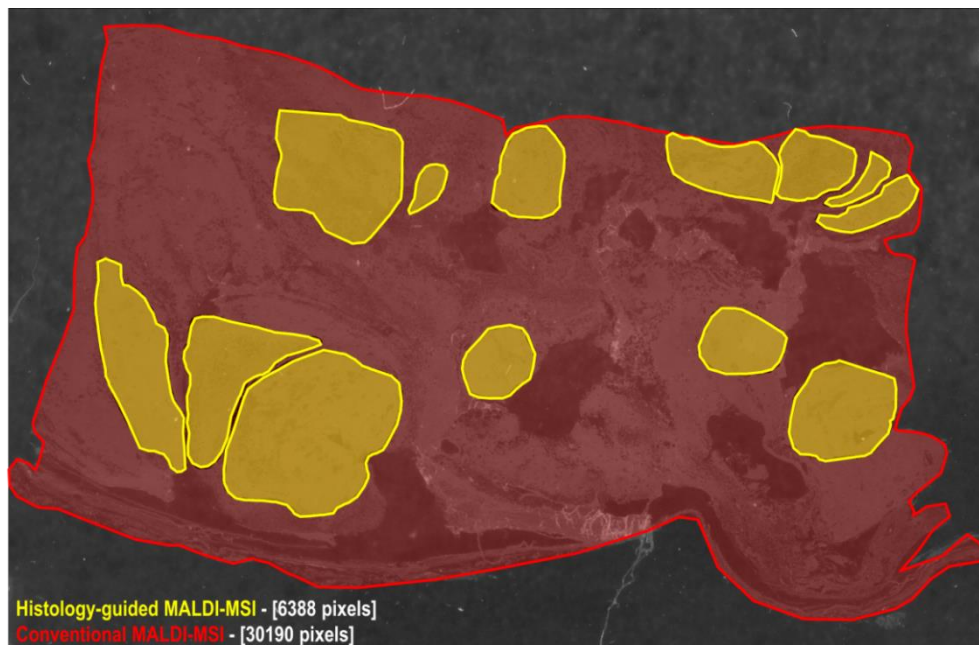
## 4.6 Supplementary information

The full supplementary information, files and tables are available on the internet via <http://pubs.acs.org/doi/abs/10.1021/acs.analchem.5b03610>.

### 4.6.1 Supplementary figures

Tissue No.	Histology	MSI / Quality Control
L1357		
L2039		
L2235		
L2398		
L3242		
L3403		
L4175		

**Figure S4-1:** An overview of the H&E stained MLS tissues. **(left)** Tissue numbers; **(middle)** histology image prior to annotation; **(right)** MSI tissue after quality control staining.



**Figure S4-2:** An example showing the differences in analysis surface between the HG-MSI platform and conventional MSI analysis. In yellow, the histology-guided analysis regions, and in red, the full surface area of the tissue analyzed in a conventional MSI experiment. The number of pixels is based on a spatial resolution of 100  $\mu\text{m}$ . The datasize of the conventional MALDI-MSI dataset was calculated using (1).

$$Size_{Normal} = Pixels_{Normal} \left( \frac{Size_{HG}}{Pixels_{HG}} \right) \quad (1)$$







## Chapter 5

# Multimodal mass spectrometry imaging of *N*-glycans and proteins from the same tissue section

**Bram Heijst**†; Stephanie Holst†; Inge H. Briaire-de Bruijn; Gabi W. van Pelt; Arnoud H. de Ru; Peter A. van Veelen; Richard R. Drake; Anand S. Mehta; Wilma E. Mesker; Rob A. Tollenaar; Judith V.M.G. Bovée; Manfred Wuhrer; Liam A. McDonnell, "Multimodal mass spectrometry imaging of *N*-glycans and proteins from the same tissue section," *Analytical Chemistry* 88(15), pp. 7745-7753, 2015.



*On-tissue digestion matrix-assisted laser desorption/ionization mass spectrometry imaging (MALDI-MSI) is able to record spatially correlated molecular information from formalin-fixed, paraffin-embedded (FFPE) tissue sections. In this work we present the in-situ multimodal analysis of N-linked glycans and proteins from the same FFPE tissue section. The robustness and applicability of the method are demonstrated for several tumors, including epithelial and mesenchymal tumor types. Major analytical aspects, such as lateral diffusion of the analyte molecules and differences in measurement sensitivity due to the additional sample preparation methods have been investigated for both N-glycans and proteolytic peptides. By combining the MSI approach with extract analysis we were also able to assess which mass spectral peaks generated by MALDI-MSI could be assigned to unique N-glycan and peptide identities.*

## 5.1 Introduction

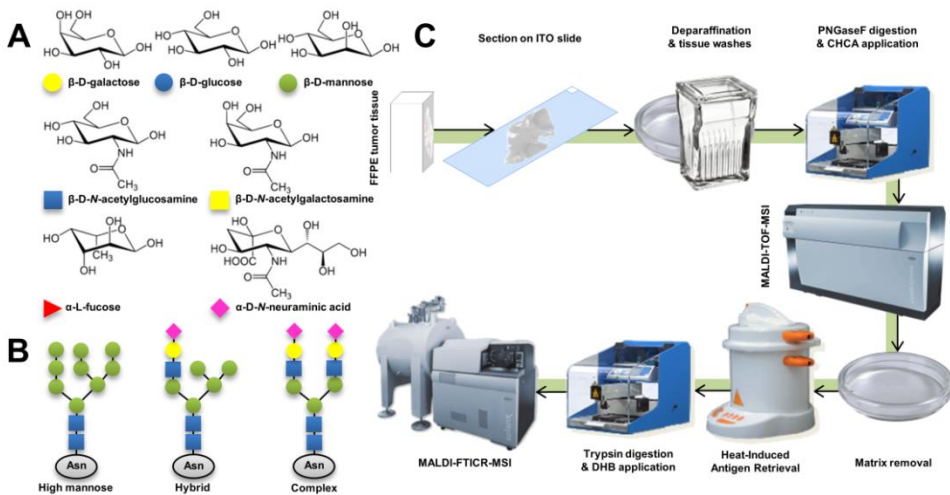
Matrix-assisted laser desorption/ionization mass spectrometry imaging (MALDI-MSI) is an analytical technique for the spatially resolved biomolecular investigation of tissue sections (Caprioli et al., 1997; McDonnell and Heeren, 2007). A major advantage of MSI is that it can be combined with histology so that cell-type specific mass spectral profiles can be extracted from the MSI datasets. Such cell-type specific molecular signatures have been used to identify diagnostic and prognostic biomarkers (Balluff et al., 2011, 2015; Dekker et al., 2014; Meding et al., 2012).

MALDI-MSI is also able to analyze different molecular classes, using essentially the same technology but different sample preparation strategies. MALDI-MSI has been used to assess how protein, lipid, metabolite, and glycan profiles change in cancerous tissues. To readily exploit the potential insights and improved diagnostic performance that may be obtained by combining the molecular information from different molecular classes, the multimodal molecular profiles from identical histological features can be compared. Multimodal MSI is a widely-used term and covers different strategies. For example, one could combine MSI with a complementary imaging modality, or apply repeated MSI analyses to the same tissue: (i) utilizing different ionization modalities (Eberlin et al., 2011; Amstalden van Hove et al., 2010), (ii) analyzing multiple polarities using the same ionization source (Ellis et al., 2016), or (iii) analyze multiple analyte classes using the same ionization source. Previous work by Steven et al., in which the separate analysis of lipids and proteins from the same fresh frozen mouse brain section was presented, shows the potential of the latter multimodal MSI approach (Steven and Bunch, 2013). However, to better exploit the tissue banks available in most clinical centers, as well as the improved histological clarity, the multimodal analysis should be applicable to formalin-fixed, paraffin-embedded (FFPE) tissues.

FFPE tissue sections can be analyzed using on-tissue digestion, in which enzymes are directly applied to the tissue and MALDI-MSI used to analyze the released species (Shimma et al., 2006). On-tissue digestion MALDI-MSI of proteins has been performed using a variety of different proteolytic enzymes, including trypsin, pepsin, elastase, Arg-

C, Lys-C, and recombinant Lys-N (Enthaler et al., 2013b; Heijs et al., 2015). A recent extension to the on-tissue digestion approach is the use of peptide *N*-glycosidase F (PNGase F), which releases *N*-linked glycans, or *N*-glycans, from glycoproteins (Powers et al., 2013).

*N*-glycans are one of the most common post-translational modifications (Figure 5-1A+B), play a fundamental role in many molecular and cellular processes, and are established biomarkers in clinical research (Adamczyk et al., 2012; Pinho and Reis, 2015; Varki et al., 2015). Serum biomarkers, such as the glycoproteins CA19-9 and carcinoembryonic antigen are currently used for the prediction of pancreatic cancer and follow-up in colorectal cancer (CRC) (Drake et al., 2010; Thirunavukarasu et al., 2011). In MALDI-MSI, despite only being recently introduced, PNGase F-based on-tissue digestion has been successfully applied for the analysis of *N*-glycans in normal tissues (Miyoshi and Nakano, 2008; Muinelo-Romay et al., 2008; Pinho and Reis, 2015), in human hepatocellular carcinomas (Powers et al., 2015), and in tissue microarrays (Powers et al., 2014).



**Figure 5-1:** (A) An overview showing the structural formulas of the most prevalent monosaccharide building blocks of *N*-linked glycans, and their symbol in the schematic representation. (B) Schematic representations of the three *N*-glycan classes with common core structure. The asparagine (Asn) residue represents the first amino acid of the consensus sequence “Asn-X-Thr/Ser”. (C) An overview of the sequential on-tissue digestion MALDI-MSI workflow, showing the order of the various sample preparation steps.

Combining the information on the protein and glycan levels in a given tissue has been demonstrated to increase their potential utility as diagnostic biomarkers:  $\alpha$ -1,6-core-fucosylated haptoglobin is explored as a biomarker in various malignancies such as pancreatic and colorectal cancer, and the U.S. Food and Drug Administration (FDA) approved  $\alpha$ -1,6-core-fucosylated alpha-fetoprotein was demonstrated as biomarker for

hepatocellular carcinomas. (Miyoshi and Nakano, 2008; Muinelo-Romay et al., 2008; Park et al., 2011)

Here, we report a multimodal MALDI-MSI analysis of both *N*-linked glycans and proteolytic peptides from a single tissue section using sequential on-tissue digestion MALDI-MSI. Importantly, the tissue section remains almost un-damaged by the analysis and so can be histologically stained, annotated and registered to the MSI datasets. In this manner, *N*-glycans and proteins from exactly the same cells or histological features can be extracted, and used for further analysis.

## 5.2 Methodology

### 5.2.1 Chemicals and reagents

All chemicals were purchased from Sigma-Aldrich (Steinheim, Germany) except ethanol and xylene (Merck, Darmstadt, Germany). Trypsin was purchased from Promega (Madison, USA). Recombinant Peptide *N*-Glycosidase F (PNGase F) from *Flavobacterium meningosepticum* was expressed and purified as previously described (Powers et al., 2013).

### 5.2.2 Tissues & sample collection

Leiomyosarcoma (LMS, L1091-3), myxoid liposarcoma (MLS, L2039), and colorectal carcinoma (CRC, C67) tissues were formalin-fixed and paraffin-embedded following established histopathological methods (Figure S5-1, Supplementary information). Following Dutch national ethical guidelines (Code for proper secondary use of human tissue, Dutch Federation of Medical Scientific Societies), all tissue samples were handled in a coded fashion. Using a microtome, 6  $\mu\text{m}$  thick sections were cut from the FFPE tissue blocks. The tissue sections were mounted on poly-L-lysine coated indium-tin-oxide (ITO) glass slides (Bruker Daltonics, Bremen, Germany), dried overnight at 37°C and stored at 4°C protected from light until further treatment. Slides dedicated for MALDI-MSI analysis contained two consecutive tissue sections, one used for the enzymatic digestions, the other used for a negative, no-enzyme control. Single sections for histology staining and molecular extractions were placed on Starfrost adhesive microscope slides (Light Laboratories, Dallas, TX).

### 5.2.3 Sequential on-tissue digestion MALDI-MSI

A buffer exchange, using a 10 kDa molecular weight cut-off (MWCO) spin filter (Merck Millipore, Billerica, MA), was performed on the recombinant PNGase F enzyme to ensure uniform purity and enzyme concentration over all performed experiments. The buffer exchange was performed according to the manufacturers' protocol. Prior to the sample preparation, the ITO slides containing FFPE tissue sections were placed on a hot plate (60°C) for 60 minutes to increase the adherence of the tissues to the ITO slides. Paraffin was removed by submerging the slides in xylene (wash 1 - 5 min; wash 2 - 10 min). The tissues were washed with ethanol (100%, 2x 2 min) and deionized

water (2x 5 min), dried in a vacuum desiccator (~10 min) before homogeneously applying PNGase F (100 ng/ $\mu$ L in deionized water) using a SunCollect pneumatic sprayer (SunChrom, Friedrichsdorf, Germany; 15 layers at 10  $\mu$ L/min). Following overnight incubation, MALDI matrix (5 mg/mL  $\alpha$ -2,4-hydroxycinnamic acid in 50% ACN and 0.1% TFA) was homogeneously deposited on the tissue sections using the SunCollect sprayer (6 layers: (1) 10  $\mu$ L/min, (2) 20  $\mu$ L/min, (3) 30  $\mu$ L/min, and (4+) 40  $\mu$ L/min). MSI analysis of the *N*-linked glycan species was performed on a Bruker UltrafleXtreme MALDI-TOF/TOF instrument (Bruker Daltonics). Data was recorded in reflectron positive ion mode covering the mass range between  $m/z$  900 to  $m/z$  4,000, using 500 laser shots per spot and a 100 x 100  $\mu$ m pixel size. More in-depth information on the MALDI-TOF-MS method is provided in Table S5-1A (Supplementary information).

Following the *N*-glycan data acquisition, excess MALDI matrix was removed from the tissues using ethanol washes (70%, 2x 1 min) and the tissue was conditioned for heat-induced antigen retrieval (HIAR) by washing with deionized water (2x 5 min). HIAR was performed in a 10 mM citric acid buffer adjusted to pH6 with 1 M NaOH. After HIAR, the tissues were carefully washed with deionized water (2x 2 min) and trypsin (20 ng/ $\mu$ L in deionized water) was deposited homogeneously using a SunCollect pneumatic sprayer (15 layers at 10  $\mu$ L/min). Following overnight incubation at 37°C, in a saturated environment (50% methanol in deionized water), MALDI matrix was applied using the SunCollect system and a solution of 20 mg/mL 2,5-dihydroxybenzoic acid (DHB) in 50% ACN and 0.1% TFA. MSI analysis of the proteolytic peptides was performed on a 9.4 T Bruker Solarix XR MALDI-FTICR instrument equipped with a dynamically harmonized ParaCell™. Data was acquired in positive ion mode in the mass range  $m/z$  600 to  $m/z$  3,500 with an average resolving power of 54,000 over the analyzed mass range, using 150 laser shots per spot and a 100 x 100  $\mu$ m pixel size. More in-depth information on the MALDI-FTICR-MS method is provided in Table S5-1B (Supplementary information).

For both *N*-glycan, and proteolytic peptide analysis, control experiments were performed on consecutive tissue sections on the same glass slides. The control samples were treated following the same protocols described above but without application of enzymes, and MALDI-MSI data acquisition was performed at a 250 x 250  $\mu$ m pixel size. Also, to show repeatability of the method on the same tissue, the sequential on-tissue digestion MALDI-MSI analysis of the LMS (L1091-3) was performed in duplicate. The two analyses are indicated as LMS-1 and LMS-2.

### 5.2.4 *N*-glycan extraction and identification

For MS/MS identification of the *N*-glycans present in the tissue sections, separate tissue sections on Starfrost adhesive microscope slides were treated following the protocols described in the previous section, although matrix application was omitted. Released *N*-glycans were extracted by carefully distributing 100  $\mu$ L deionized water on top of the

tissue, 15 min incubation at 37°C, and collected by micropipette. Extracts were dried in a vacuum centrifuge and resuspended in 20 µL deionized water. For purification, 10 µL of the sample was brought to 85% ACN, followed by cotton hydrophilic interaction liquid chromatography (HILIC) micro-solid phase extraction (SPE) using 200 µL pipette tips (Selman et al., 2011). *N*-glycans were eluted in 15 µL deionized water from which 5 µL were spotted in duplicate onto a Bruker AnchorChip plate. Dried samples were co-crystallized with 0.5 µL super DHB matrix (5 mg/mL in 50% ACN) supplemented with 1 mM NaOH. MS1 and MS2 spectra were recorded using an UltrafleXtreme MALDI-TOF/TOF-MS for the identification of the *N*-glycans. Furthermore, overall average spectra from the MALDI-MSI analyses were exported from flexImaging 4.1 (Bruker Daltonics) to CSV format. The CSV-formatted spectra were imported in mMass (v5.5.0, <http://www.mmass.org>) (Strohalm et al., 2008), where baseline correction, smoothing, peak picking ( $S/N \geq 6$ ), de-isotoping and internal re-calibration was performed. The mMass peak lists were exported to both Excel 2010 (Microsoft) and the GlycoPeakfinder tool (<http://www.eurocarbdb.org/ms-tools/>) in GlycoWorkbench (2.1 stable build 146, <http://www.eurocarbdb.org/>), which was used for generating a preliminary glycan composition list. The suggested compositions were then compared to the results of the MS/MS analyses for confirmation.

### 5.2.5 Proteolytic peptide extraction and identification

Consecutive tissue sections were prepared for extracts using the same sample preparation protocol as for MALDI-MSI. The matrix application and MALDI-MSI analysis were omitted, and instead, the proteolytic peptides were extracted from the matrix using a series of solvents: (i) 50 µL of 0.1% TFA, and (ii) 50 µL of 50% ACN in 0.1% TFA. The extracts were combined, dried, resuspended in 0.1% TFA, and cleaned using Omix C18 tips (Agilent, Santa Clara, California). Peptide extracts were analyzed using an Easy nLC1000 (Thermo, Bremen, Germany) coupled to a Q-Exactive mass spectrometer (Thermo). Fractions were injected onto an in-house prepared pre-column (100 µm × 15 mm; Reprosil-Pur C18-AQ 3 µm, Dr. Maisch, Ammerbuch, Germany) and eluted via a homemade analytical column (15 cm × 50 µm; Reprosil-Pur C18-AQ 3 µm). The gradient was 0% to 30% solvent B (90% ACN / 0.1% FA) in 120 min. The analytical column was drawn to a tip of ~5 µm and acted as the electrospray needle of the MS source. The Q-Exactive mass spectrometer was operated in top10-mode. Parameters were as follows: full scan, resolution 17,500, AGC target 3,000,000, max fill time 20 ms; MS/MS, resolution 35,000, AGC target 1,000,000, max fill time 60 ms, intensity threshold 17,400. Apex trigger was set to 1–5 s, and allowed charges were 1–5. The Thermo.RAW files were converted to MGF files using the MSconvert software (64-bit for Windows, <http://proteowizard.sourceforge.net>). Peptide and protein identifications were extracted from the SwissProt database using the Mascot server. A maximum of two missed cleavages was allowed and methionine oxidation, deamidation (NQ), and N-terminal acetylation were set as variable modifications. Peptide assignments were made with a tolerance of 10 ppm. MS/MS fragment tolerance was



set to 20 mmu. Results were searched against a decoy database. Protein identifications were assigned based on a minimum of one confident peptide at 1% false discovery rate (FDR). Only peptides and proteins with red bold notification and a Mascot significance score  $\geq 38$  were included in the final lists of unique peptides.

### 5.2.6 Peptide identity assignment

Average spectra from the MALDI-FTICR-MSI datasets were exported into CSV format and loaded in mMass. Peak picking was performed on peaks with  $S/N \geq 5$  and a relative intensity  $\geq 2.5\%$ . The peak lists were treated with a deisotoping algorithm set to remove isotope peaks with a maximum charge of 2+ and an isotope mass tolerance of 0.02 Da. MALDI-FTICR-MSI peak lists and Mascot database search results from the LC-ESI-MS/MS analyses were exported to Excel 2010 (Microsoft). The  $m/z$  features originating from the MSI data were aligned to the  $m/z$  values of the identified peptides from the Mascot search results. Peptide identity assignments were based on a mass tolerance of  $\pm 10$  ppm.

### 5.2.7 Fold change calculations

Regions of interest (ROIs) for (non-)tumor regions were selected in both N-glycan and peptide MSI datasets. The MSI data was loaded in Data Analysis 4.2 (Bruker Daltonics) to obtain average spectra and extract intensities for N-glycans and peptides from the ROIs. Intensities from (non-)tumor ROIs were averaged in Excel 2010 to obtain a single intensity value for the (non-)tumor areas. The fold change was calculated as the ratio  $I_{tumor} / I_{non-tumor}$ .

## 5.3 Results and discussion

On-tissue digestion MALDI-MSI, utilizing proteases and endoglycosidases, enables the analysis of proteins and glycans from FFPE tissues (Casadonte and Caprioli, 2011; Gustafsson et al., 2013; Heijs et al., 2015; Powers et al., 2013, 2014). In this work we have merged both on-tissue digestion protocols to create a new multimodal method that enables the analysis of both N-glycans and proteolytic peptides from the same FFPE tissue section (Figure 5-1C). By combining the workflows, we increased the comparability between the MSI datasets of two intimately related analyte classes.

### 5.3.1 Antigen retrieval

When analyzing proteins in FFPE tissues an antigen retrieval step is necessary to remove the cross-links between the proteins established by formalin fixation (Shi et al., 2013, 1991). However, it was found that heat-induced antigen retrieval (HIAR) prior to PNGase F digestion (and subsequently followed by proteolytic digestion) caused desialylation of the N-glycans and severe delocalization of the proteins (data not shown). These artefacts were circumvented by performing the HIAR-based antigen retrieval after analysis of the N-glycans and removal of the excess MALDI-matrix (Figure 5-1C). For N-glycan MSI analysis, protocols both including (Gustafsson et al., 2015; Powers et

al., 2014) and excluding (Powers et al., 2013) HIAR have been described. The chemical reactions involved in formalin fixation (Tanca et al., 2012) and the chemical composition of the *N*-linked glycans (Figure 5-1A+B) make it unlikely that the *N*-glycans will become part of the formalin-cross-linked network and so remain accessible to PNGase F. This was confirmed by our *N*-glycan MALDI-MSI analyses prior to HIAR, as a large number of *N*-glycan species were detected (Table 5-1 & Figure 5-2A). The *N*-glycan MSI analyses of the different tumor tissues yielded a total of 59 unique *N*-glycan species, of which we were able to confirm 25 by MALDI-MS/MS on glycan extracts (Table 5-1 & online Supplementary information).

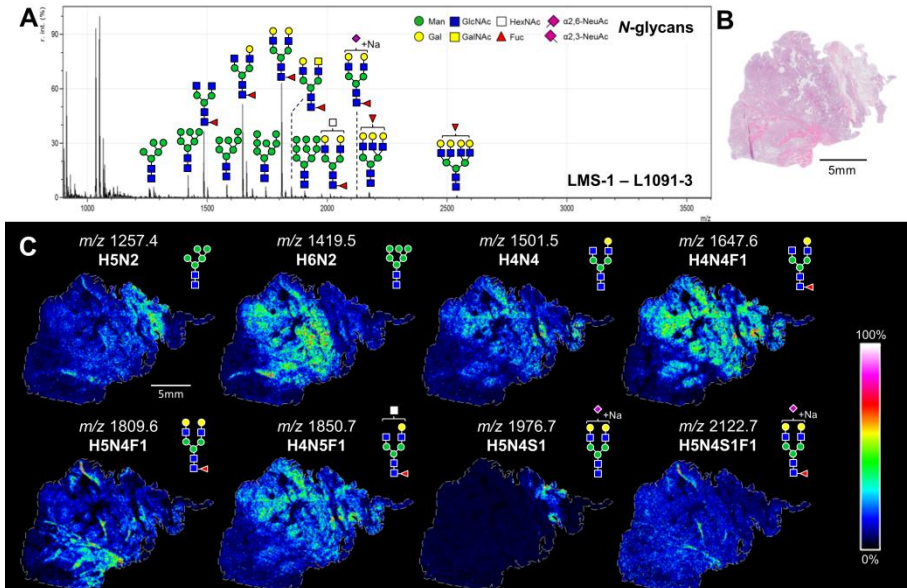
### 5.3.2 *N*-glycan MALDI-TOF-MSI

Visualizing the distributions of several specific *N*-glycan species revealed that their abundance in the CRC, LMS, and MLS tissues was restricted to specific morphological structures in the tissue (Figure 5-2 & Figures S5-2 and S5-3, Supplementary information). For example, the complex-type *N*-glycan Hex5HexNAc4dHex1 (Hexose = Hex, N-acetylhexosamine = HexNAc, fucose = dHex) detected at  $m/z$  1,809.6 [M+Na]<sup>+</sup> co-localized exclusively with healthy striated muscle cells and collagen-rich areas in both analyses of the LMS tissue, while other *N*-glycans, such as Hex4HexNAc4dHex1 at  $m/z$  1,647.6 [M+Na]<sup>+</sup>, and Hex4HexNAc4 at  $m/z$  1,501.5 [M+Na]<sup>+</sup> were almost exclusively localized in the tumor area of the same LMS tissues (Figure 5-2B+C & Figure S5-1A and S5-2, Supplementary information). In the CRC and MLS tissues similar patterns were observed, e.g. the high-mannose type *N*-glycans (Hex6HexNAc2 at  $m/z$  1,419.5 [M+Na]<sup>+</sup>, Hex7HexNAc2 at  $m/z$  1,581.5 [M+Na]<sup>+</sup>, and Hex9HexNAc2 at  $m/z$  1,905.6 [M+Na]<sup>+</sup>) were detected in the tumor areas. These *N*-glycans have previously been associated with tumor cells in pancreatic, prostate, and hepatocellular carcinoma tissues (Powers et al., 2014, 2015). Hex5HexNAc2 at  $m/z$  1,257.4 [M+Na]<sup>+</sup>, was highly abundant in several non-calcified necrotic regions present within the tumor area of the CRC tissue (Figure S5-3B+C, Supplementary information). The high mannose-type glycans are the precursors of the intracellular *N*-glycan biosynthesis pathway (Freeze, 2006; Varki et al., 2015). The high abundance of this specific glycan in the necrotic regions is likely the result of increased cell lysis, a common phenomenon in necrotic tissue, causing an uncontrolled release of intercellular molecules (Proskuryakov et al., 2003).

**Table 5-1:** Overview of the *N*-glycans detected in the MALDI-MSI and MS/MS datasets. Structural confirmation by MS/MS is within  $\pm 1$  monosaccharide.

<i>m/z</i>	Composition	Neutral Exchange	LMS		CRC		MLS
[M+Na] <sup>+</sup>			MSI	MS/MS	MSI	MS/MS	MSI
933.32	H3N2		X		X		X
1079.37	H3N2F1		X	X	X	X	X
1095.37	H4N2		X		X		X
1136.40	H3N3		X		X		X
1257.42	H5N2		X	X	X	X	X
1282.45	H3N3F1		X	X	X		X

1298.45	H4N3		X	X	X	X	X
1339.48	H3N4		X		X		X
1419.48	H6N2		X	X	X		X
1444.51	H4N3F1		X	X	X	X	X
1460.50	H5N3		X		X		X
1485.53	H3N4F1		X	X	X	X	X
1501.53	H4N4		X		X	X	X
1542.56	H3N5		X	X	X		X
1581.53	H7N2		X	X	X		X
1590.57	H4N3F2		X				X
1606.56	H5N3F1						X
1622.55	H6N3		X		X	X	X
1647.59	H4N4F1		X	X	X	X	X
1663.58	H5N4		X	X	X	X	X
1688.61	H3N5F1		X	X	X	X	X
1704.61	H4N5		X		X		X
1743.58	H8N2		X		X	X	X
1793.64	H4N4F2		X	X			X
1809.64	H5N4F1		X	X	X	X	X
1825.63	H6N4		X		X	X	X
1850.67	H4N5F1		X	X	X	X	X
1866.66	H5N5		X		X		X
1891.69	H3N6F1		X	X	X		X
1905.63	H9N2		X		X	X	
1955.70	H5N4F2		X				
1976.66	H5N4S1	Na-H	X		X	X	
1996.72	H4N5F2		X				
2012.72	H5N5F1		X		X	X	
2028.71	H6N5		X		X		
2053.75	H4N6F1		X				
2100.73	H5N4S1F1		X		X		
2122.72	H5N4S1F1	Na-H	X	X	X	X	
2158.78	H5N5F2		X				
2174.77	H6N5F1		X		X		
2199.80	H4N6F2		X				
2215.80	H5N6F1		X		X		
2267.75	H5N4S2	Na-H	X		X		
2289.74	H5N4S2	2Na-2H	X	X	X	X	
2304.83	H5N5F3		X				
2320.83	H6N5F2		X				
2325.80	H5N5S1F1	Na-H	X		X		
2341.79	H6N5S1	Na-H			X		
2361.86	H5N6F2		X				
2377.85	H6N6F1		X		X		
2393.85	H7N6				X		
2435.79	H5N4S2F1	2Na-2H			X		
2466.89	H6N5F3		X				
2487.85	H6N5S1F1	Na-H	X		X		
2507.91	H5N6F3		X		X		
2523.91	H6N6F2		X				
2539.90	H7N6F1		X		X		
2580.93	H6N7F1		X				
2669.97	H6N6F3		X				



**Figure 5-2:** (A) The overall average mass spectrum after the *N*-glycan MALDI-MSI analysis of the LMS-1 tissue (L1091-3). The annotated glycan compositions were either confirmed by MS/MS identification or were known from literature. (B) Scanned image of the H&E stained LMS-1 (L1091-3) tissue. (C) Visualizations of the distribution of various *N*-glycans throughout the tissue. The shown glycan species were confirmed by MS/MS or confirmed by literature. The images were obtained from a TIC normalized dataset.

### 5.3.3 MALDI-FTICR-MSI of proteolytic peptides

The performance of the trypsin digestion after *N*-glycan release, referred to as sequential digestion, was compared to a regular on-tissue trypsin digestion experiment, referred to as the control digestion. The MALDI-FTICR-MSI data obtained from sequential digestions and control digestions were very similar for all analyzed tumor types (Figure 5-4A & Figures S5-4 and S5-5A+D, Supplementary information). On average, the spectra from the sequential digestions yielded 806( $\pm$ 148) isotope clusters and the spectra from the control digestions contained 844( $\pm$ 207) isotope clusters, with a peak overlap of 79( $\pm$ 14)%. The MSI images of specific peptide ions were also highly comparable between both control and sequential digestions and duplicate analyses (Figure 5-4B & Figures S5-4 and S5-5C+F, Supplementary information). For example, for sequential and control digestions of the LMS and CRC tissues the Histone H2A type 1 peptide AGLQFPVGR ( $m/z$  944.5312 [M+H]<sup>+</sup>) was highly specific to the tumor areas; the proteolytic fragment NSLESYAFNMK ( $m/z$  1,303.5986 [M+H]<sup>+</sup>) originating from heat shock cognate 71 kDa protein (HSP7C\_HUMAN) was found to be very abundant in the tumor regions in both control and sequential digestion of the MLS tissue. Heat shock cognate 71 kDa protein is an established marker to distinguish myxoid liposarcoma from myxofibrosarcoma (Wang et al., 2014).

It was then investigated whether the additional sample preparation procedures for the multimodal on-tissue digestion MALDI-MSI, based on sequential analysis of glycans

and proteins, induced lateral diffusion of proteins. Figures 5-3 and 5-4 provide examples of proteolytic peptides highly localized to specific morphological features, indicating that any lateral diffusion was insignificant on the length-scale of the experiments.

### 5.3.4 Multimodal accessible proteins and glycoproteins

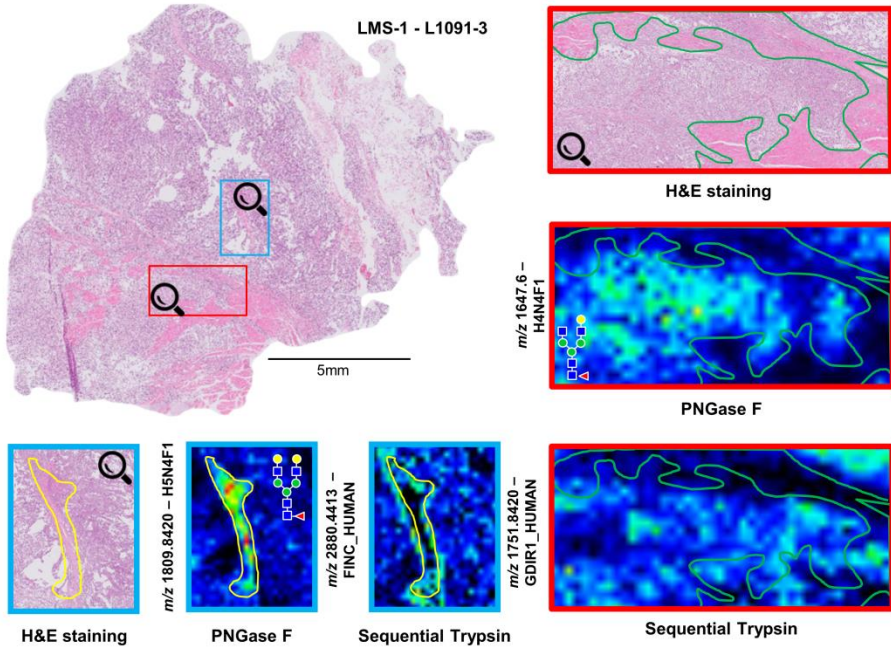
To determine if multimodal on-tissue digestion influenced which proteins are accessible by on-tissue digestion, and to determine if it included glycosylated peptides the matrix proteomes of both control digestion and sequential digestion of the LMS and CRC tissue sections were investigated by LC-MS/MS (Table 5-2 & online Supplementary information). The results show that the number of unique peptides identified from LMS increased from 795 (corresponding to 325 proteins) for the control digestion to 940 (corresponding to 351 proteins) for the sequential digestion. Similarly, for CRC the number of unique peptides were 948 (corresponding to 236 proteins) for the control digestion and 1,334 (corresponding to 509 proteins) for the sequential digestion. The number of proteins unique to the sequential digestion was notably greater compared to the control digestion (Figure S5-6A, Supplementary information). These numbers indicate increased proteome coverage as a result of the sequential digestion. Furthermore, the sequential digestion also increased protein sequence coverage, as the number of identified peptides per protein systematically increased (Figure S5-6B, Supplementary information).

*N*-glycans are attached via Asn residues present in the consensus sequence "Asn-X-Ser/Thr" ("X" can be any amino acid except proline). *N*-glycan release by PNGase F induces a deamidation of the Asn, but Asn deamidation is also a common protein modification. To identify which peptides may have been deglycosylated by PNGase F digestion the deamidated peptides, with the consensus sequence, obtained after PNGase F treatment were determined. The number of candidate deamidated peptides identified from LMS increased from 2 for the control digestion to 8 for the sequential digestion; for CRC no deamidated peptides were detected from the control digestion and 20 from the sequential digestion (Table 5-2).

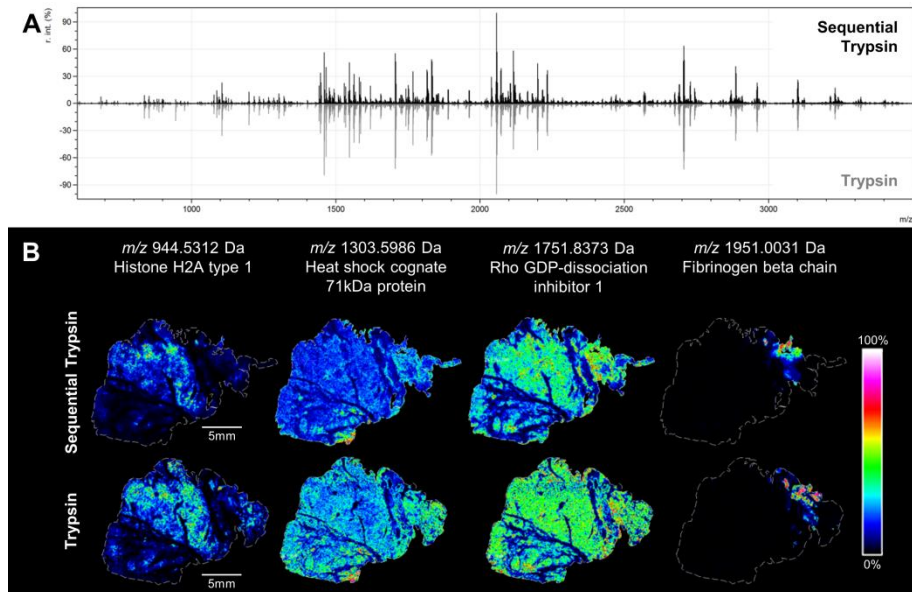
**Table 5-2:** Overview of the peptide identifications obtained after LC-MS/MS analysis of tissue extracts.

Tumor	Control Trypsin			Sequential Trypsin		
	Unique peptides	Deglycosylated*	Assigned to MSI	Unique peptides	Deglycosylated*	Assigned to MSI
LMS	795	2	94	940	8	88
CRC	948	0	132	1334	20	134

\* Deamidation of asparagine occurred in glycosylation consensus sequence (N-x-T/S)



**Figure 5-3:** Visualizations of the distributions of several *N*-glycan structures and proteolytic peptides corresponding to specific morphological features (red box): healthy striated muscle tissue and connective tissue (green), blue box: collagen fibrotic connective tissue (yellow) in the LMS-1 tissue (L1091-3).



**Figure 5-4:** (A) A comparison of the profiles of MALDI-FTICR-MSI overall average spectra obtained after both sequential trypsin digestion (top, black) and control trypsin digestion (bottom, grey) of the LMS-1 tissue (L1091-3). (B) Comparison of the visualizations of specific peptide distributions. The peptides were confirmed to be present in the MALDI-matrix by LC-MS/MS of extracts and were assigned to the MALDI-FTICR-MSI datasets with an error < 10 ppm. The images were obtained from RMS normalized datasets.

### 5.3.5 On-tissue deglycosylation increases accessibility of proteins to proteolysis

The increase in the number of peptides identified after *N*-glycan release was significantly greater than the number of deamidated peptides. It was found that the sequential digestion affected the protein sequence coverage of both glycoproteins, and proteins without *N*-linked glycan modification. Three additional tryptic peptides of the glycoprotein galectin-3 binding protein (LG3BH\_HUMAN) were detected in the sequential digestion of CRC tissue (online Supplementary information), and all three peptides were deamidated, indicating that the trypsin cleavage sites were hindered by the *N*-glycans in the control digestion. Five additional tryptic peptides of vimentin (VIME\_HUMAN) were detected in the sequential digestion of the LMS tissue (online Supplementary information). Vimentin does not contain *N*-glycans (only *O*-glycans, which are not released by PNGase F), but is known to interact with other glycoproteins (Keuschnigg et al., 2009; Wang et al., 2010). This indicates that, within the tissue environment, deglycosylation of the proteome can reduce the steric hindrance caused by the *N*-glycans, making proteins more accessible to proteolytic digestion. The increased detection of non-glycosylated peptides has been previously observed in LC-MS/MS, and is even exploited as a biomarker assay (Lee et al., 2011).

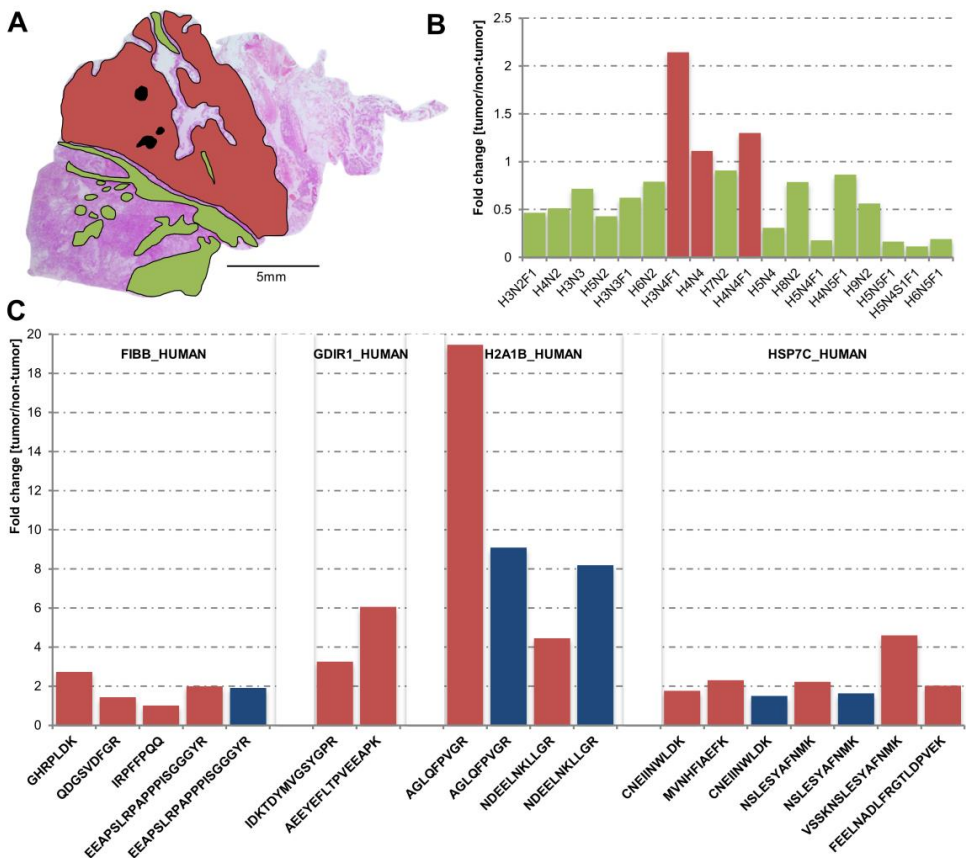
The peptides detected by MALDI-FTICR-MSI were assigned to the peptide identifications obtained from LC-MS/MS extract analysis (Table 5-2 & online Supplementary information). The number of assigned peptides (matching criteria < 10 ppm, S/N > 5, intensity > 2.5% of basepeak) in the LMS control digestion experiment was 69 (66 unique peptides, corresponding to 49 proteins), and was similar in the sequential digestion (65 peptides, 54 of which were unique, corresponding to 47 proteins). Similarly, the number of assigned peptides in the CRC control digestion experiment was 110 (101 unique peptides, corresponding to 72 proteins), and was similar in the sequential digestion (112 peptides, 96 of which were unique, corresponding to 74 proteins). These numbers are greater than those reported in recent MALDI-MSI investigations of FFPE tissues (Casadonte et al., 2014; Meding et al., 2013), and included a deamidated peptide, which was detected only in the sequential digestion of both LMS and CRC and contains a known glycosylation site. The deamidated peptide detected at  $m/z$  1,669.8431, could be assigned to TVIRPFYLTN\*SSGVD ([M+H]<sup>+</sup>), and is the C-terminal end of the glycoprotein Galectin-3 binding protein (LG3BP\_HUMAN), whose hyperglycosylated form is associated with tumor cell aggregation (Chen et al., 2009b; Lin et al., 2015).

### 5.3.6 Differentially expressed glycans and proteins

The results described above indicate that multimodal on-tissue digestion MALDI-MSI is robust and able to deliver high quality MALDI-MSI data for *N*-glycans and (an increased number of) proteolytic peptides from the same FFPE tissue section. By way of example Figure 5-5A shows the LMS tissue section reported in Figures 5-2, 5-3, and 5-4, with

annotations for tumor and non-tumor regions. Figure 5-5B shows the detected (area normalized) fold changes of 18 *N*-glycans, confirming the previous observation from visual inspection of the images that most glycans were detected at lower levels in the tumor. Figure 5-5C shows the fold changes from all peptides from the proteins reported in Figure 5-4. It can be seen that there is a good agreement between peptides from the same proteins, and even from the same peptide if it is detected as both protonated (red bars) and sodiated (blue bars) pseudomolecular ions.

These results, together with the results from other tumors presented in the Supporting Information, indicate how such multimodal imaging could prove valuable in future clinical studies, as many of the assigned peptides originate from proteins



**Figure 5-5:** (A) Histology image of LMS-1 (L1091-3) with annotated non-tumor (green) and tumor (red) regions. Spectra acquired from holes in the tissue (black) were excluded from data analysis. (B) Area normalized fold changes of 18 *N*-glycans detected by MALDI-MSI. The green bars represent higher abundance in non-tumor regions. The red bars indicate a higher abundance in tumor regions. (C) Area normalized fold changes of protonated (red) and sodiated (blue) peptide ions originating from FIBB\_HUMAN, GDIR1\_HUMAN, H2A1B\_HUMAN and HSP7C\_HUMAN as detected by MALDI-MSI.



previously associated with disease. For example, multiple peptides from different histone variants (H1.2, H2A, and H4) were detected and it is well established that histones are heavily involved in tumor biology (online Supplementary information) (Singh et al., 2015; Wang et al., 2015a). Amongst the assigned peptides were fragments originating from vimentin, and glucose regulated protein 78kDa, proteins that have been associated with ovarian cancer and pancreatic adenocarcinoma in previous MALDI-MSI based studies (online Supplementary information) (Djidja et al., 2009b; El Ayed et al., 2010). In the CRC tissue we were able to detect proteolytic fragments from Carcinoembryonic antigen-related cell adhesion molecule 5 (CEAM5\_HUMAN), a member of the carcinoembryonic antigen (CEA) family of proteins. The CEA proteins have been in use as diagnostic markers for CRC (online Supplementary information) (Zhang et al., 2015).

## 5.4 Conclusions

In this work we have presented multimodal analysis of both *N*-glycans and proteolytic peptides from the same tissue section. We have been able to: (i) image 59 unique *N*-glycan species from the *N*-glycan MALDI-TOF-MSI datasets, and (ii) assign a total of 89 unique peptide identifications to high-mass resolution MALDI-FTICR-MSI datasets from LMS tissue sections and 154 from CRC tissue sections, including a deglycosylated (*N*-linked glycan) peptide. Considering these results, the sequential on-tissue digestion MALDI-MSI method shows great promise for application to any FFPE tissues of clinical relevance.

## 5.5 Acknowledgements

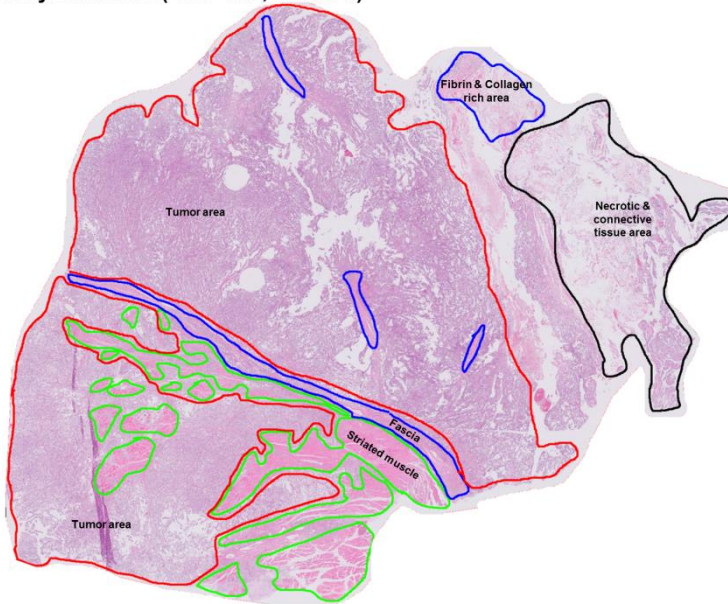
This work was supported by the ZonMW Zenith project "Imaging Mass Spectrometry-Based Molecular Histology: Differentiation and Characterization of Clinically Challenging Soft Tissue Sarcomas" (No. 93512002; B.H.), the European Union Seventh Framework Programmes HighGlycan project (No. 278535; S.H.), the National Institutes of Health/National Cancer Institute (No. R21CA186799; R.R.D.), the state of South Carolina SmartState Endowed Research program to R.R.D, and by grants R01 CA120206 and U01 CA168856 from the National Cancer Institute (NCI), the Hepatitis B Foundation, and an appropriation from The Commonwealth of Pennsylvania to A.M. (R.R.D.). The authors thank Dr. P. Angel for her valuable input.

## 5.6 Supplementary information

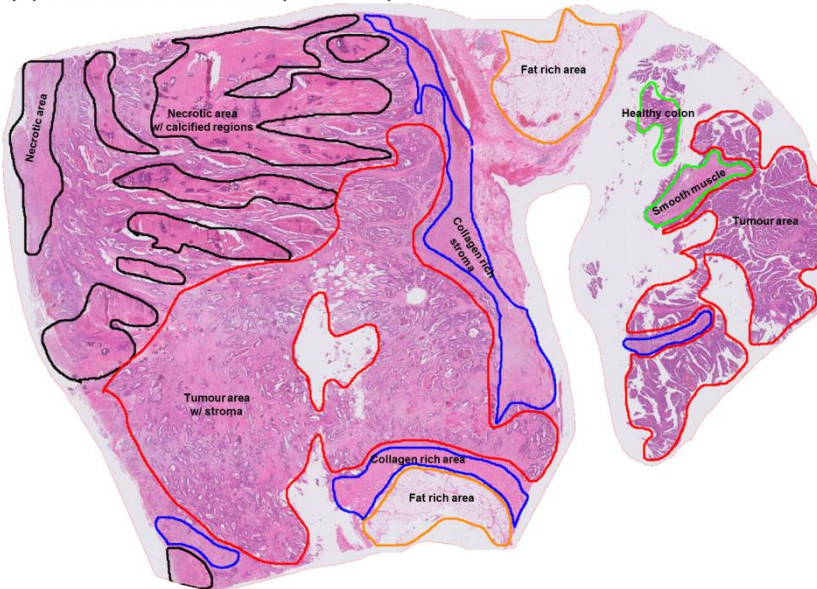
The full supplementary information, files and tables are available on the internet via <http://pubs.acs.org/doi/abs/10.1021/acs.analchem.6b01739>.

### 5.6.1 Supplementary figures

(A) Leiomyosarcoma (LMS-1&2, L1091-3)



(B) Colorectal Carcinoma (CRC, C67)



(C) Myxoid Liposarcoma (MLS, L2039)

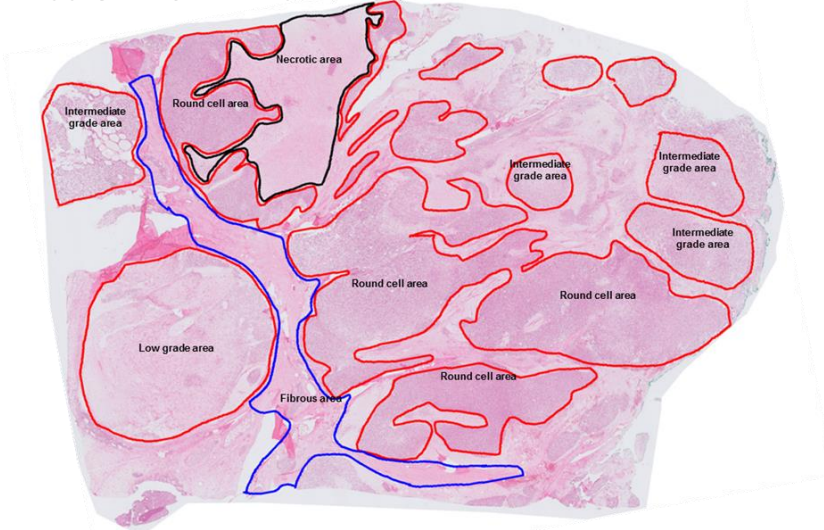


Figure S5-1: Annotated histology images of (A) Leiomyosarcoma (LMS-1&2, L1091-3), (B) Colorectal carcinoma (CRC, C67), (C) Myxoid liposarcoma (MLS, L2039).

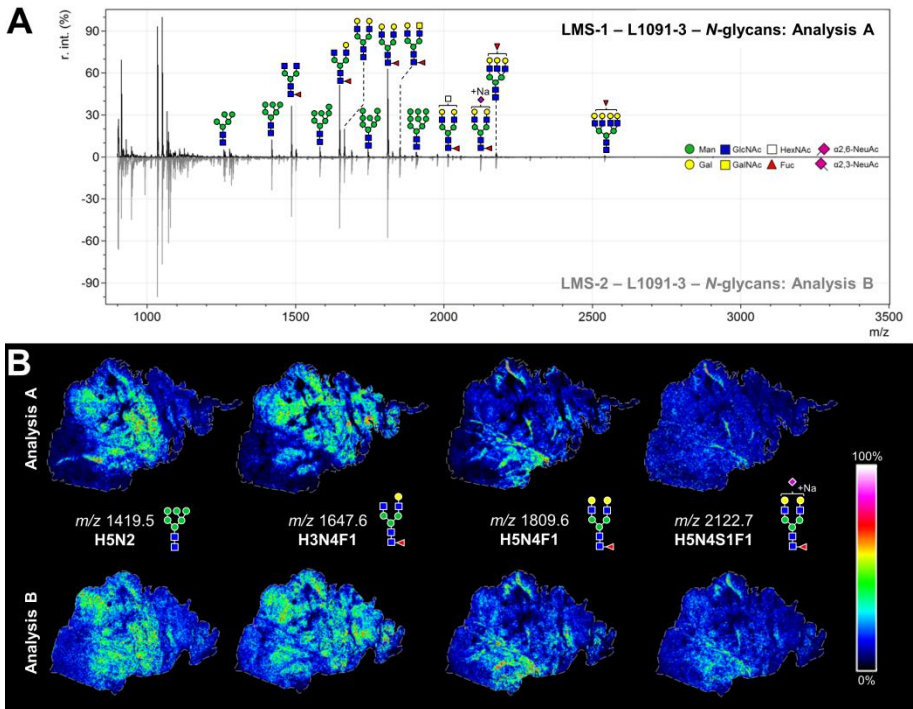
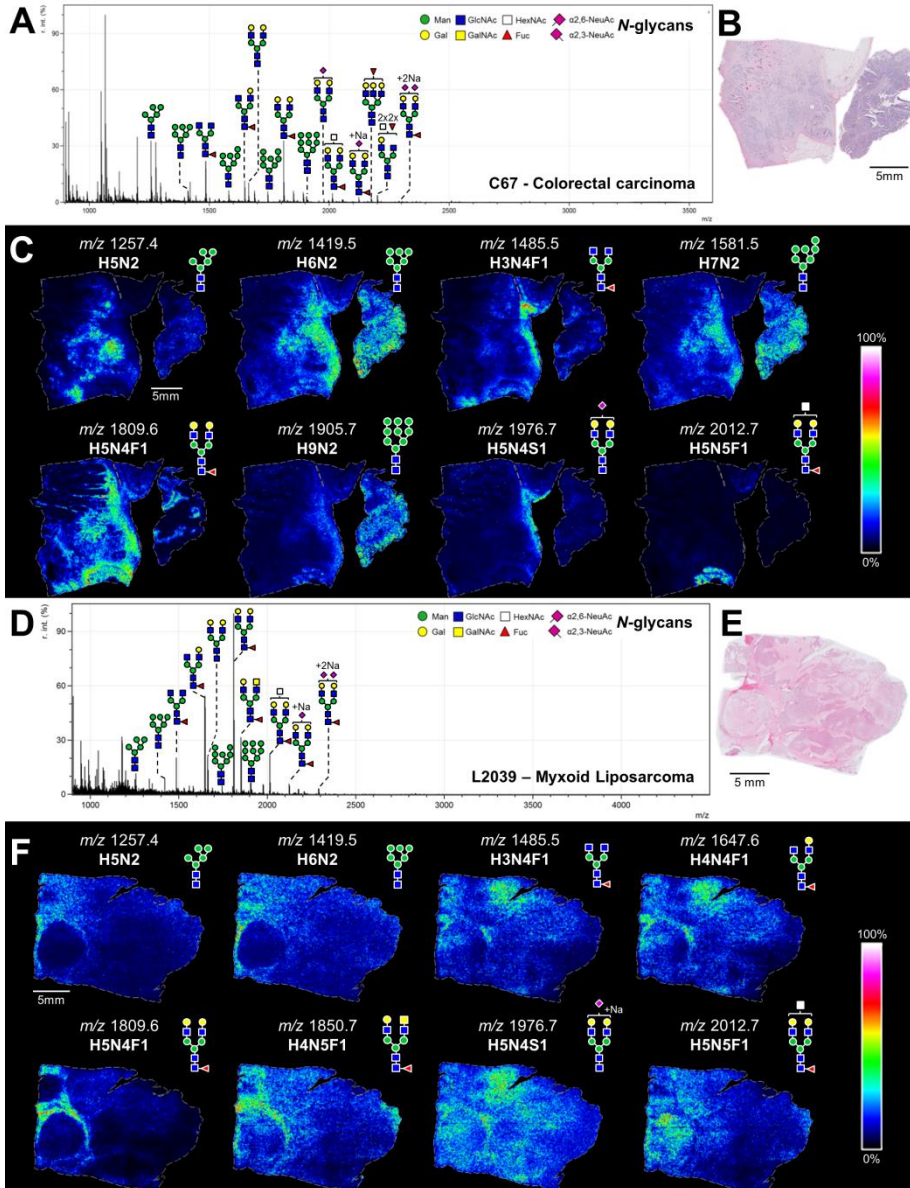
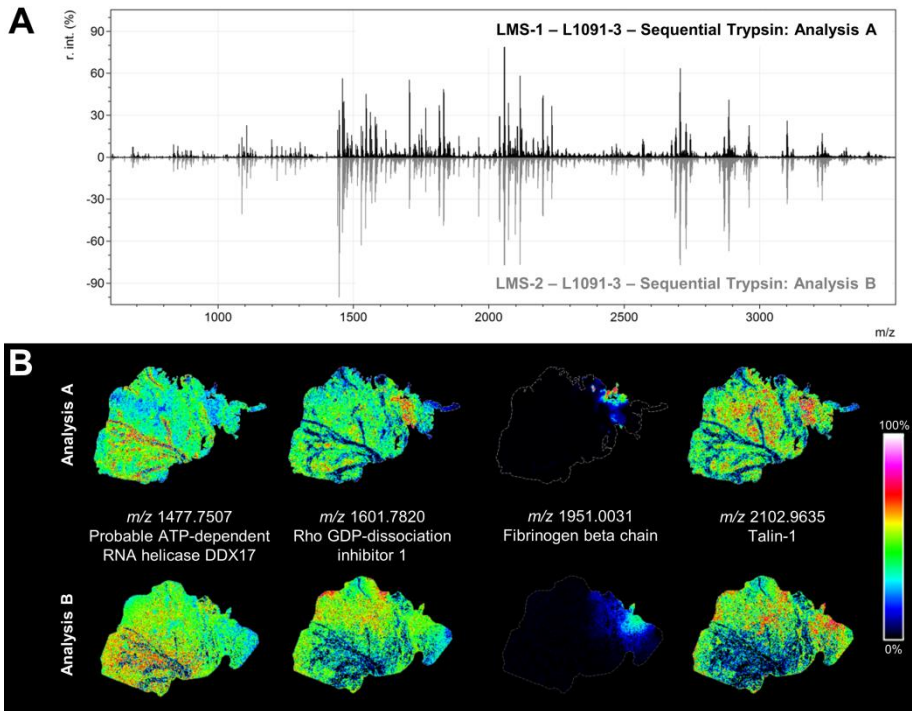


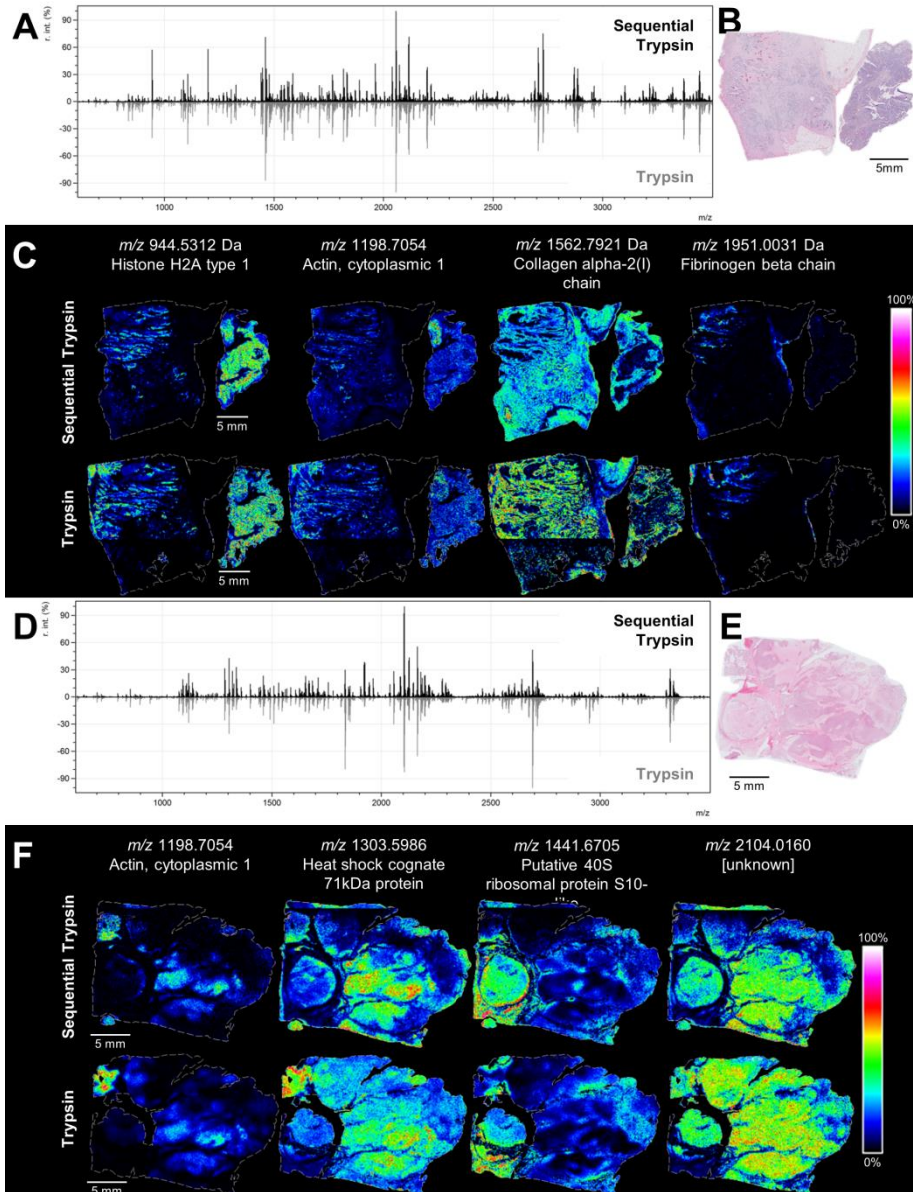
Figure S5-2: (A) A comparison of the overall average spectra obtained from the LMS-1 (L1091-3, black) and the duplicate, LMS-2 (L1091-3, grey) tissue sections during N-glycan MALDI-MSI. (B) Visualizations of the distribution of various N-glycans throughout the LMS-1 and LMS-2 tissues. The annotated glycan structures represent compositions which were either confirmed by MS/MS identification or were known from literature, but structural isomers cannot be excluded. The images were obtained from TIC normalized datasets.



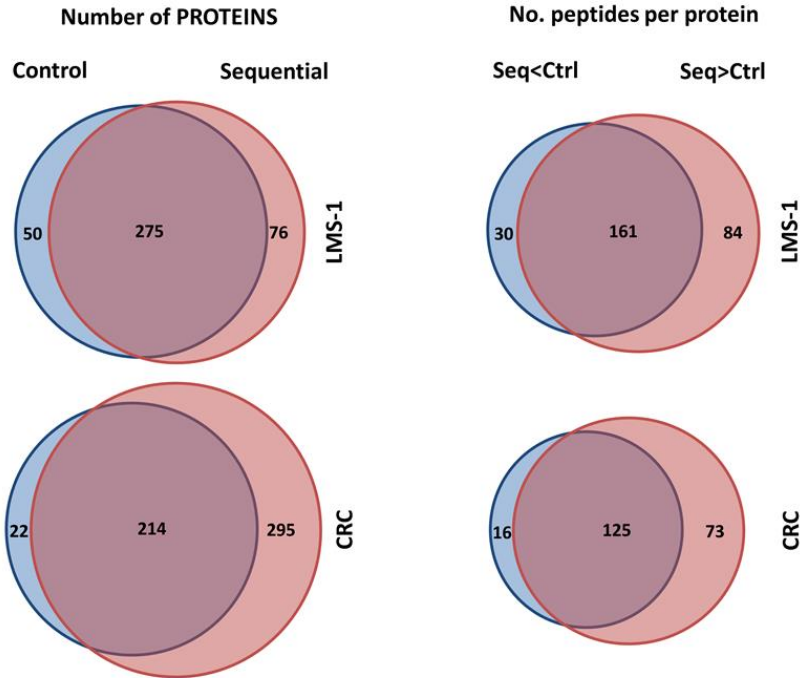
**Figure S5-3:** (A) The overall average mass spectrum after the *N*-glycan MALDI-MSI analysis of the CRC (C67) tissue. (B) Scanned image of the H&E stained CRC (C67) tissue. (C) Visualizations of the distribution of various *N*-glycans throughout the tissue. The images were obtained from a TIC normalized dataset. (D) The overall average mass spectrum after the *N*-glycan MALDI-MSI analysis of the MLS tissue (L2039). (E) Scanned image of the H&E stained MLS (L2039) tissue. (F) Visualizations of the distribution of various *N*-glycans throughout the tissue. The annotated glycan structures represent compositions which were either confirmed by MS/MS identification or were known from literature, but structural isomers cannot be excluded. The images were obtained from a TIC normalized dataset.



**Figure S5-4:** (A) A comparison of the overall average spectra obtained from the LMS-1 (L1091-3, black) and, the duplicate, LMS-2 (L1091-3, grey) tissue sections during MALDI-MSI analysis of proteolytic peptides. (B) Comparison of the visualizations of specific peptide distributions in both duplicate LMS analyses. The peptides were confirmed to be present in the MALDI-matrix by LC-MS/MS of extracts and were assigned to the MALDI-FTICR-MSI datasets with an error < 10 ppm. The images were obtained from a RMS normalized datasets.



**Figure S5-5:** (A) A comparison of the profiles of MALDI-FTICR-MSI overall average spectra obtained after both sequential trypsin digestion (top, black) and control trypsin digestion (bottom, grey) of the CRC (C67) tissue. (B) Scanned image of the H&E stained CRC (C67) tissue. (C) Comparison of the visualizations of specific peptide distributions. (D) A comparison of the profiles of MALDI-FTICR-MSI overall average spectra obtained after both sequential trypsin digestion (top, black) and control trypsin digestion (bottom, grey) of the MLS (L2039) tissue. (E) Scanned image of the H&E stained MLS (L2039) tissue. (F) Comparison of the visualizations of specific peptide distributions. Unless indicated otherwise, the peptides were confirmed to be present in the MALDI-matrix by LC-MS/MS of extracts and were assigned to the MALDI-FTICR-MSI datasets with an error < 10 ppm. The images were obtained from a RMS normalized datasets.



**Figure S5-6:** Venn diagrams showing the differences and overlap between **(A)** the number of protein identifications in both control and sequential digestions, and **(B)** the differences in the number of identified peptides per protein. The numbers in (B) represent the number of proteins. In blue, the number of proteins for which the number of peptides in the control digestion was larger than in the sequential digestion. In red, the number of proteins for which the number of peptides was higher in the sequential digestion than in the control digestion. The overlapping part represents the proteins where the number of peptides was equal between control and sequential digestions.

## 5.6.2 Supplementary tables

**Table S5-1: (A)** An overview of important parameters in the MALDI-TOF-MS method used to obtain *N*-glycan MALDI-MSI data. **(B)** An overview of important parameters in the MALDI-FTICR-MS method used to obtain MALDI-MSI data on proteolytic peptides.

<b>A - Bruker UltrafleXtreme</b>	
<b>Parameter</b>	<b>Value</b>
Laser power	70%
Laser shots per pixel	500
Laser focus setting	3_medium
Laser frequency	2000 Hz
Ion Source 1 voltage	25.0 kV
Ion Source 2 voltage	22.5 kV
Lens voltage	8.5 kV
Reflector 1 voltage	26.46 kV
Reflector 2 voltage	13.45 kV (50.8% refl)
Matrix suppression	Deflection up to 890 Da

<b>B - Bruker Solarix XR (9.4T)</b>	
<b>Parameter</b>	<b>Value</b>
Laser power	35%
Laser shots per pixel	150
Laser focus setting	Minimum
Laser frequency	2000 Hz
Source optics – plate offset voltage	100.0 V
Source optics – deflector plate voltage	200.0 V
Source optics – capillary exit voltage	150.0 V
Source optics – funnel 1 voltage	150.0 V
Source optics – skimmer 1 voltage	18.0 V
Source optics – funnel RF amplitude	150.0 Vpp
Octopole – frequency	5 MHz
Octopole – RF amplitude	350.0 Vpp
Quadrupole – Q1 mass	1000 <i>m/z</i>
Collision cell – collision voltage	-2.0 V
Collision cell – DC Extract bias	0.5 V
Collision cell – RF frequency	2 MHz
Collision cell – collision RF amplitude	1500.0 Vpp
Transfer optics – time of flight	1.7 ms
Transfer optics – frequency	2 MHz
Transfer optics – RF amplitude	300.0 Vpp
Para Cell – transfer exit lens voltage	-20.0 V
Para Cell – analyzer entrance voltage	-10.0 V
Para Cell – side kick voltage	0.0 V
Para Cell – side kick offset voltage	0.0 V
Para Cell – front trap plate voltage	1.5 V
Para Cell – back trap plate voltage	1.5 V
Para Cell – back trap plate quench voltage	-30.0 V
Para Cell – sweep excitation power percentage	45.0%





## Chapter 6

# Mass spectrometry imaging of *N*-glycans identifies biomarkers of tumor progression in myxoid liposarcoma

**Bram Heijs;** Stephanie Holst; Inge H. Briaire-de Bruijn; Manfred Wuhrer; Judith V.M.G. Bovée; Liam A. McDonnell, *in preparation*, 2017



*Myxoid liposarcoma (MLS) is the second most common subtype of liposarcoma, accounting for approximately 6% of all sarcoma cases. MLS is characterized by a myxoid extracellular matrix and, in 95% of the cases, by the chromosomal translocation t(12;16)(q13;p11), which results in the FUS-DDIT3 chimeric gene. The presence of >5% round cells in MLS is associated with a poorer prognosis for the patient, along with other risk factors like the presence of necrosis, increased tumor size, increased age, and the male gender. While activation of PI3K/Akt signaling and overexpression of microRNA miR-135b have been associated with tumor progression in MLS, the molecular mechanisms underlying the disease progression are largely unknown. Here we have applied matrix-assisted laser desorption/ionization mass spectrometry imaging (MALDI-MSI), an analytical technique capable of simultaneously recording the spatial distributions of hundreds of biomolecules directly from a tissue section, to analyze N-linked glycans from a MLS tissue microarray in order to identify molecular markers for MLS tumor progression. Comparison of the N-glycan profiles revealed that several high-mannose type glycans, and a monofucosylated, triantennary complex-type glycan were associated with tumor progression, and which mirror recent observations in colorectal cancer, breast cancer, and ovarian cancer.*

## 6.1 Introduction

Liposarcomas (LPS) are mesenchymal neoplasms displaying variable levels of adipogenic differentiation. Liposarcoma has a yearly incidence of approximately 30 cases per million, and represents 17-25% of all sarcoma cases (Fletcher et al., 2013; Lemeur et al., 2015). The World Health Organization (WHO) classification describes four different LPS subtypes: (i) well-differentiated, (ii) dedifferentiated, (iii) pleomorphic, and (iv) myxoid (Fletcher et al., 2013). Myxoid liposarcoma (MLS) is the second most common subtype of LPS, accounting for approximately 30% of all LPS cases and 6% of all sarcoma cases (Nishida et al., 2010). MLS is characterized by a myxoid extracellular matrix (ECM) and, in over 95% of cases, by the chromosomal translocation t(12;16)(q13;p11), which results in the chimeric FUS-DDIT3 gene. MLS commonly occurs in the extremities of patients that are typically of a younger age compared to other LPS subtypes (Fletcher et al., 2013). The presence of >5% round cells in MLS is associated with a poorer prognosis, as are the presence of necrosis, increased tumor size (>10 cm), increased age (> 45 years), and the male gender. The treatment of MLS is fairly effective; nonetheless 35-50% will develop either recurrence or metastasis. Treatment includes surgical excision, or a combination of chemo- and/or radiotherapy with surgical excision. Grading of MLS is done by histological examination of the MLS tissue, and depends on the extent of the round cell component in the tissue: <5% round cell component equals a low grade MLS, and ≥5% round cell component defines high grade MLS cases (previously designated as round cell liposarcoma) (Fletcher et al., 2013; de Graaff et al., 2016; Lemeur et al., 2015; Nishida et al., 2010). High intra-tumor heterogeneity may complicate the determination of histological grade, especially when the tumor mass is poorly represented by a small

biopsy (Fritchie et al., 2012). While it is widely accepted that the presence of the round cells is associated with a poor prognosis and higher risk of metastasis, the underlying molecular mechanisms of tumor progression are largely unknown. In a previous immunohistochemistry (IHC) –based study by Demicco *et al.* the progression of MLS was shown to be accompanied by activation of the PI3K/Akt pathway caused by overexpression of insulin-like growth factor 1 receptor (IGF1R), a loss of phosphatase and tensin homolog (PTEN), and activating mutations in phosphatidylinositol 4,5-bisphosphate 3-kinase catalytic subunit alpha isoform (PIK3CA) (Demicco et al., 2011). A more recent report by Nezu *et al.* shows that the overexpression of microRNA miR-135b in MLS results in down regulation of the THBS2 gene, coding for the glycoprotein thrombospondin-2 (TSP2), which in its turn increases expression of matrix metalloproteinase 2 (MMP2), responsible for enhanced degradation of the ECM and ultimately results in increased MLS aggressiveness (Nezu et al., 2016).

Conventional omics-analyses (e.g. genomics, transcriptomics, proteomics) have had limited success in MLS due to its high degree of intra-tumor heterogeneity. Nezu *et al.* used laser-capture microdissection to separate the contributions from the different cell-types present in MLS (Nezu et al., 2016). This result strongly indicates the need for histopathological specification for any investigation of the molecular changes associated with MLS.

Matrix-assisted laser desorption/ionization mass spectrometry imaging (MALDI-MSI) is an analytical technique that allows the spatially-correlated molecular analysis of various molecular classes directly from tissue (Caprioli et al., 1997; McDonnell and Heeren, 2007). By combining the molecular analysis of modern biomolecular mass spectrometry with the imaging capabilities of microscopy MALDI-MSI enables the spatial distributions of 100's to 1000's of biomolecules to be simultaneously recorded without labeling and is untargeted in nature. Furthermore, MALDI-MSI does not adversely affect the tissue's underlying histology; consequently, the tissue may be histologically stained after the MSI experiment and the histological image aligned with the MSI dataset. This multimodal data, MSI and histology, allows the tissue's molecular content to be examined in its correct histopathological context, and thus, for instance, to compare low and high grade areas within a single tissue section. In a process termed virtual microdissection cell-type specific molecular signatures can be extracted, and then used to identify biomarkers (Balluff et al., 2015; Elsner et al., 2012; Lou et al., 2016; Meding et al., 2012).

MALDI-MSI can be used to analyze different molecular classes, using essentially the same technology but different tissue preparation procedures. On-tissue digestion MALDI-MSI using proteolytic enzymes is used to increase the range of proteins amenable to MALDI-MSI analysis, aid their identification and allows the analysis of formalin-fixed, paraffin-embedded (FFPE) tissues (Gustafsson et al., 2013; Heijs et al., 2015; Kriegsmann et al., 2016; Schober et al., 2011). On-tissue digestion MALDI-MSI

using the endoglycosidase PNGase F enables the analysis of *N*-linked glycans, also from both fresh frozen and FFPE tissue sections (Powers et al., 2013, 2015). Proteins, previously associated with MLS tumor progression, such as TSP2, IGF1R, and other receptor tyrosine kinases, involved in the activation of the PIK3/Akt pathway, are known glycoproteins (Carlson et al., 2005; Itkonen and Mills, 2015; Negri et al., 2010). While these proteins have a known role in MLS progression, the role of the *N*-glycans is unknown. Therefore, we have analyzed the *N*-glycans by on-tissue digestion MALDI-MSI, to investigate the molecular alterations underlying tumor progression, and aid the accurate diagnosis and grading of MLS tumors.

## 6.2 Methodology

### 6.2.1 Chemicals and reagents

All chemicals were purchased from Sigma-Aldrich (Steinheim, Germany) except ethanol and xylene (Merck, Darmstadt, Germany). Recombinant Peptide *N*-Glycosidase F (PNGase F) from *Flavobacterium meningosepticum* was expressed and purified as previously described (Powers et al., 2013).

**Table 6-1:** Overview of tissue specimens present on the MLS TMA.

TMA		Total	MYX	INT	RC
<b>No. samples</b>		37	23	20	9
<b>No. of patients</b>		32	23	20	9
<b>Gender</b>	<i>Male vs. Female</i>	18 vs. 14	14 vs. 9	11 vs. 9	5 vs. 4
<b>Age</b>	<i>Median [years]</i>	43	42	43	46
<b>Recurrence</b>		5	3	3	0
<b>Metastasis</b>		4	0	1	1

### 6.2.2 Tissues, TMA construction and patient grouping

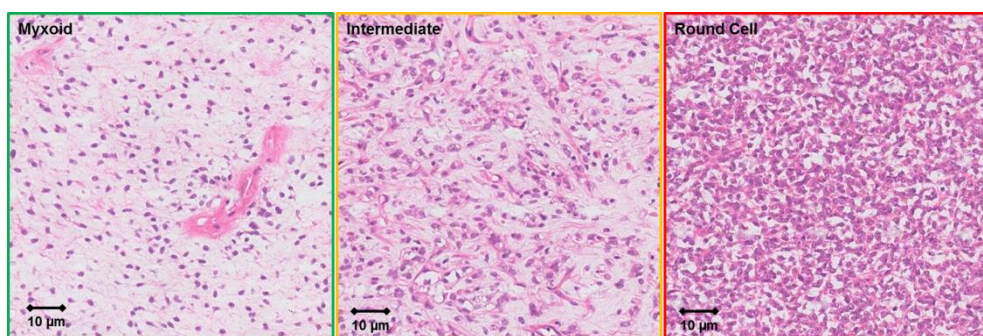
A tissue microarray (TMA) was previously constructed from formalin-fixed, paraffin-embedded (FFPE) MLS tissues from 32 patients diagnosed in the Leiden University Medical Center (Endo et al., 2015; de Graaff et al., 2017). The array consists of 141 needle core biopsies with a 1.5 mm diameter, divided in two paraffin blocks, here referred to as MLS-1 and MLS-2. Both blocks contain an additional six control cores, originating from human placenta, colon, spleen, neuronal, lung, and tonsil tissues. Cores were obtained from three distinct morphological regions in the tumor, myxoid (MYX) areas, intermediate (INT) areas, and round cell (RC) areas. If a patient presented only a single morphology three needle cores were included in the TMA; if more than one morphology was present (MYX+INT, MYX+RC, or INT+RC) two cores per morphology were included. An overview of the TMA is reported in Table 6-1. All samples were handled following the ethical guidelines described in the "Code for Proper Secondary Use of Human Tissue in the Netherlands" of the Dutch Federation of Medical Scientific Societies.

### 6.2.3 *N*-glycan MALDI-MSI

Both TMA blocks were sectioned using a microtome. 6  $\mu\text{m}$  thick sections were mounted on indium tin-oxide (ITO) coated glass slides (Bruker Daltonics, Bremen, Germany), additionally coated with poly-L-lysine for better adhesion of the needle cores. Importantly, TMA sections were not transferred to the glass slide using a tape transfer system due to the risk of polymer contamination. Slides were dried overnight at 37°C, and stored at 4°C in the dark until further processing. Sample preparation for the on-tissue digestion with PNGase F was performed as previously described (Heijs et al., 2016). *N*-glycan MALDI-MSI analysis was performed using a Bruker Rapiflex MALDI-TOF/TOF instrument (Bruker Daltonics). Data was recorded in reflectron, positive-ion mode covering the mass range between  $m/z$  900-3,200, using 500 laser shots per spot and a 50 x 50  $\mu\text{m}$  pixel size.

### 6.2.4 Histology staining and annotation

Following MALDI-MSI analysis, excess MALDI matrix was removed with two ethanol washes (70%, 2x 1min), and the TMA's stained with haematoxylin and eosin (H&E) following routine pathology procedures. The H&E stained TMA's were then scanned using a digital slide scanner (IntelliSite Pathology Ultra-Fast Scanner, Philips, Eindhoven, The Netherlands). The scanned histology images were co-registered to the MALDI-MSI data in flexImaging 5.0 (Bruker Daltonics). In order to obtain a more accurate cellular specificity, the individual TMA cores were annotated by an expert pathologist (JVMGB). The annotations account for intra-core heterogeneity and differentiate between myxoid (MYX), intermediate (INT), and round cell (RC) areas (Figure 6-1). Intermediate areas were more cellular than low grade myxoid areas, but contained too much myxoid matrix to be considered as round cell areas (JVMGB). A total of 157 regions of interest (ROIs) were annotated from the 141 MLS cores.



**Figure 6-1:** Example H&E images of the myxoid, intermediate and round cell areas.

### 6.2.5 Data pre-processing – *N*-glycans

A TIC normalized average spectrum for each of the 157 annotated ROIs was exported in CSV file format using flexImaging 5.0. Spectral processing, analyte extraction and analyte curation was performed using MassyTools (version 0.1.8.1) (Jansen et al.,

2015). In MassyTools a recalibration of all ROI spectra was performed on the basis of a predefined list of calibrants. Spectra with at least four calibrants (Table S6-1, Supplementary information) with a signal-to-noise (S/N) ratio over nine were considered for further analysis, this resulted in the exclusion of one spectrum. Feature extraction of 115 previously identified *N*-glycans (Heijs et al., 2016; Holst et al., 2016) was performed through integration of the areas of 95% of the theoretical isotopic envelope. A feature specific baseline correction was performed by subtracting the baseline detected within a window of 20 *m/z*. MassyTools additionally included information on the fraction of the analyte area above S/N 9, highest isotope S/N, the mass error per analyte in ppm (averaged for all spectra), as well as a value representing the similarities between the analyzed and theoretical isotope patterns for each analyte (QC, averaged for all spectra). Two spectra were excluded as the "fraction of the analyte area above S/N 9" was below three standard deviations of the mean. The relative areas of a total of 34 *N*-glycans with an average mass error below 30 ppm, and a QC value below 0.4 were rescaled to 100% and considered for the subsequent statistical analysis.

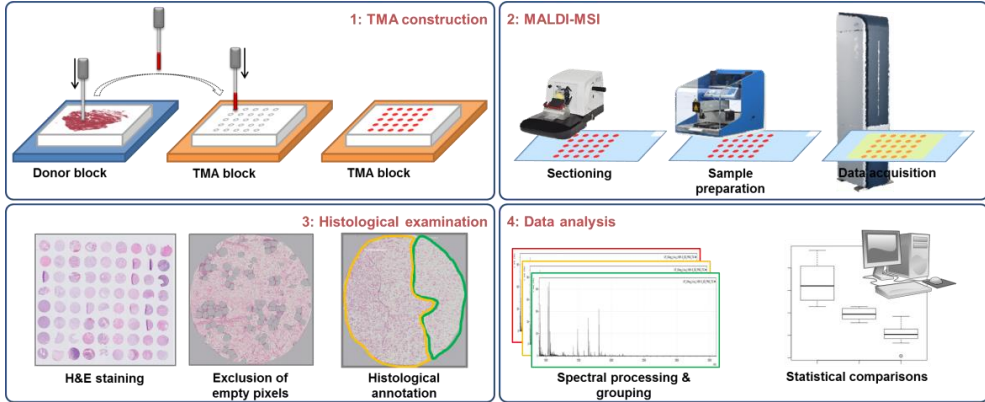
### 6.2.6 Data analysis

A statistical comparison of the different morphological MLS subtypes (MYX, INT, RC) was performed in MatLab (R2017a, Mathworks, Natick, MA, USA), to find molecular features correlated with tumor progression. The average baseline corrected, relative area for each of the 34 *N*-glycans was calculated for each subtype and for all patients. An Anderson-Darling normality test (adtest) was performed to test the distribution for each of the 34 variables. Variables that did not follow a normal distribution were log-transformed (LOG10) in Microsoft Excel 2010, and retested for normality. A one-way ANOVA analysis (anova1) was used to compare the means of each morphological subtype (p-value < 0.05) for the normally distributed variables. The remaining, non-normally distributed variables were tested using a non-parametric ANOVA (Kruskal-Wallis, *kruskalwallis*) (p-value < 0.05). Paired tests (Wilcoxon signed rank, *signrank*) were applied for the comparisons between individual morphological classes (Myx vs. Int, Myx vs. RC, and Int vs. RC). All reported p-values were corrected for multiple testing using the Benjamini-Hochberg test for multiple testing (q-value < 0.05).

## 6.3 Results & discussion

Grading of MLS patients involves the determination of the round cell component of the tumor. If the round cell component is larger than 5% the patient is considered high grade, as an increased round cell component is associated with poor prognosis (Fletcher et al., 2013; de Graaff et al., 2016; Lemeur et al., 2015; Nishida et al., 2010). In this study we investigated whether MALDI-MSI of *N*-glycans could elucidate diagnostic molecular markers associated with the progression of MLS.

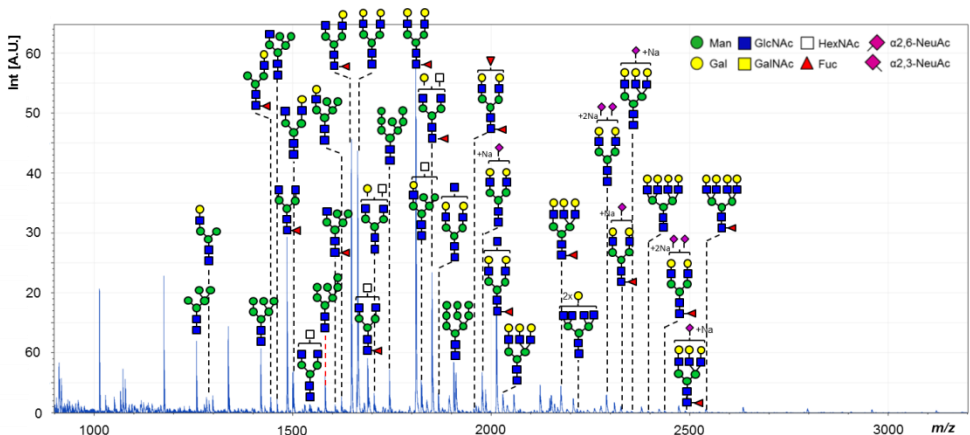




**Figure 6-2:** Schematic overview of the applied workflow. (1) TMA construction was performed as described in the methodology section, (2) MALDI-MSI of *N*-glycans, (3) histological examination and annotation, and (4) data analysis consisted of processing, grouping of average ROI spectra, and statistical testing.

### 6.3.1 *N*-glycan MALDI-MSI

The TMA was analyzed by on-tissue digestion MALDI-MSI to characterize the *N*-glycan composition of MLS. 34 *N*-glycans were detected and identified from the MALDI-TOF-MSI dataset. Their respective relative areas were submitted to an ANOVA test to find morphology-associated differences (Figure 6-2&3), Table 6-2). After applying a multiple testing correction five *N*-glycans were significantly associated with morphological changes in MLS (Table 6-2, Figure 6-4), four of which were high-mannose type (H6N2,  $m/z$  1419.48 [M+Na]<sup>+</sup>; H7N2,  $m/z$  1581.53 [M+Na]<sup>+</sup>; H8N2,  $m/z$  1743.58 [M+Na]<sup>+</sup>; H9N2,  $m/z$  1905.63 [M+Na]<sup>+</sup>, where H = Hexose, and N = *N*-acetylhexosamine). Although the sample numbers are small (Table 6-1, MYX vs. INT,  $n = 14$ ; MYX vs. RC,  $n = 4$ ; and INT vs. RC,  $n = 5$ ) hampering paired statistical comparisons and linear regression analysis, there is a clear trend showing elevated levels of high-mannose



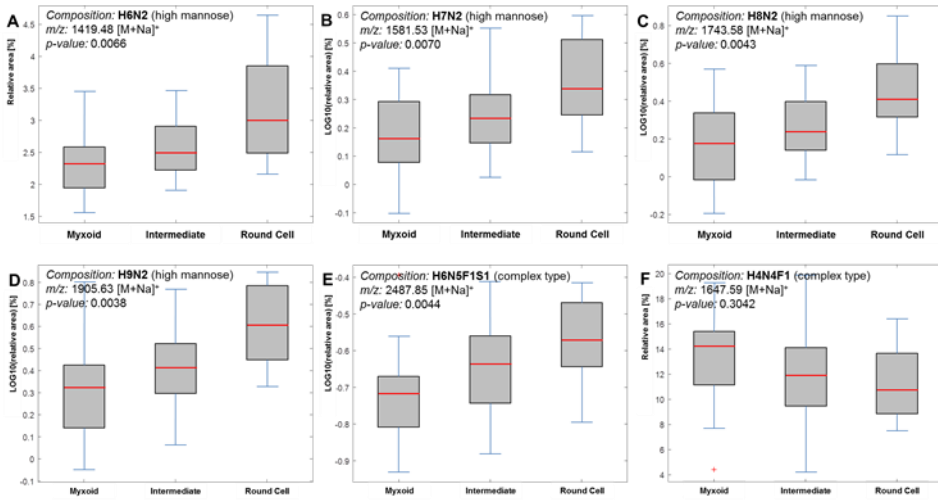
**Figure 6-3:** Visual representation of the MLS TMA *N*-glycan MSI basepeak spectrum compiled from all MLS cores present on the TMA. The spectrum represents the TMA’s total *N*-glycan content and includes the 34 annotated *N*-glycans and their assigned compositions.

glycans with MLS tumor progression (Table 6-2 & S6-2, Supplementary information) (Figure 6-4A,B,C,D). Similarly, the association between high-mannose type glycans and tumor progression was previously described for breast cancer, ovarian cancer, and colorectal cancers (Anugraham et al., 2014; Kaprio et al., 2015; Leoz et al., 2011; Liu et al., 2013). The exact role of high-mannose glycans in cancer is still unknown. However, their higher abundance has been hypothesized to be an effect of reduced or incomplete maturation during the protein glycosylation pathway (Holst et al., 2015; Zhao et al., 2008). High-mannose type glycans can occur both intracellular and on the cell surface. During *N*-glycan biosynthesis on the surface of the cytoplasmic side of the endoplasmic reticulum (ER), lipid-linked oligosaccharide precursors (LLO) are produced, containing up to five mannose residues. Once the LLO contains five mannose residues it moves to the ER lumen where an additional 4 mannose and 3 glucose residues are added. Upon completion, the glycan is transferred to its protein carrier and the glucose and mannose residues are trimmed resulting in the production of protein-bound high-mannose type glycans. The high-mannose glycosylated proteins will either be transferred to the cell- surface or to the Golgi apparatus for further processing in to complex- or hybrid-type *N*-glycans (Freeze, 2006). In normal cells, high-mannose type glycans play a crucial role in both protein folding and the protection of proteins against degradation during intracellular relocalization. The hypothesis of an increased abundance of high-mannose glycans caused by a disruption of the biosynthesis pathway or through reduced expression of mannosidases is very plausible. The MALDI-MSI experiments were not performed with the spatial resolution needed to distinguish between intra- or extracellular *N*-glycans; microscopic analysis of tissues immuno-stained with high-mannose-binding antibodies, like Concanavalin A, could be performed to provide additional information on the subcellular location of the high-mannose glycans, although it is not solely specific for high-mannose type glycans and was beyond the scope of this study.

The other *N*-glycan that displayed significant differences between the three morphological groups was a monofucosylated, monosialylated tri-antennary complex-type glycan (H6N5F1S1,  $m/z$  2487.85 [M+Na]<sup>+</sup>, where F = fucose, and S = *N*-acetylneuraminic acid) (Figure 6-4E). It should be noted that the *N*-glycans, and more specifically the sialic acids, were not derivatized prior to the MALDI-MSI analysis. Sialic acids are highly labile groups, frequently lost during the MALDI-MS analysis, and so represents a detection bias against sialylated *N*-glycan species (Holst et al., 2016). Like the high-mannose type glycans, the abundance of the triantennary complex type glycan shows a positive correlation with tumor progression. The increased  $\beta$ 1,3- and  $\beta$ 1,6-linked GlcNAc branching of *N*-glycans, caused by an overexpression of the MGAT4 and MGAT5 genes which are coding for *N*-acetylglucosaminyltransferase IV (GnT-IV) and *N*-acetylglucosaminyltransferase V (GnT-V), has been previously associated with invasion and metastasis in breast and colorectal cancer (D'Arrigo et al., 2005; Dennis et al., 1987, 1999; Fernandes et al., 1991). Overexpression of GnT-V and the resulting

**Table 6-2:** Kruskal-Wallis results for the morphological comparison. Compositions legend: H = Glc/Gal/HexNAc, N = Man/Gal, F = Fucose, S = NeuAc. Sialic acids (S) were detected in their sodium salt form. P-values and q-values < 0.05 are highlighted in green.

Composition	m/z	QC value	Error	Relative areas			INT			RC			Statistics Kruskal- Wallis p-value	ANOVA p-value	Benjamini- Hochberg q-value
				MYX	Median	Q1	Q2	Median	Q1	Q2	Median	Q1			
H5I2	1257.42	0.03	3.43	0.2269	0.0810	0.3798	0.2316	0.1360	0.3877	0.4252	0.1964	0.5181	0.4252	0.2203	0.6247
H4N3	1298.45	0.29	17.87	-0.1321	-0.1714	-0.0864	-0.1090	-0.1690	-0.0790	-0.1628	-0.2390	-0.0141	0.5694	0.5694	0.6940
H6N2	1419.48	0.04	2.28	2.3224	1.9771	2.5792	2.4980	2.2434	2.8684	3.0039	2.5097	3.8470	0.0066	0.0066	0.0170
H4N3F1	1444.51	0.11	11.73	0.6509	0.5904	0.7310	0.6659	0.5742	0.7493	0.6228	0.5346	0.7151	0.7465	0.7465	0.9380
H5N3	1460.50	0.09	13.58	0.4876	0.3822	0.6478	0.5019	0.4472	0.6437	0.5782	0.4651	0.7713	0.5941	0.5941	0.9380
H5M4F1	1465.53	0.03	2.37	0.8305	0.6438	0.9138	0.7425	0.5883	0.9240	0.8273	0.6503	0.8987	0.6721	0.6721	0.9380
H4H4	1501.53	0.12	8.91	2.0870	1.8289	2.3192	1.9762	1.7407	2.1993	1.8632	1.6050	2.1815	0.7798	0.7798	0.9380
H3N5	1542.56	0.29	14.69	-0.2449	-0.3801	-0.1456	-0.2963	-0.3663	-0.1789	-0.2742	-0.3184	-0.2168	0.4896	0.4896	0.9499
H7N2	1581.53	0.06	5.13	0.1651	0.0798	0.2870	0.2358	0.1525	0.3064	0.3385	0.2707	0.4969	0.0070	0.0070	0.0476
H5N3F1	1606.56	0.22	26.79	0.5038	0.3228	0.6572	0.5610	0.3785	0.7181	0.5646	0.4894	0.6965	0.4651	0.4651	0.9380
H6N3	1622.55	0.14	13.76	0.7664	0.5456	1.0289	0.7609	0.5347	0.9910	0.8253	0.5731	1.0335	0.6733	0.6733	0.9380
H4H4F1	1647.59	0.02	2.62	14.2666	11.5159	15.3986	11.8450	9.6574	13.8976	10.7546	8.9886	13.0586	0.2182	0.2182	0.7388
H5N4	1663.58	0.11	7.10	13.6345	10.2220	17.4224	14.2730	10.7191	15.7761	12.7201	11.0405	15.1622	0.9534	0.9534	0.9499
H5M5F1	1688.61	0.22	3.43	0.4430	0.3860	0.5719	0.4828	0.3735	0.5312	0.4910	0.4325	0.5528	0.9348	0.9348	0.9499
H4H5	1704.61	0.19	7.39	-0.0025	-0.0514	0.1585	0.0168	-0.0666	0.1263	0.0571	-0.0322	0.0852	0.6879	0.6879	0.9380
H6N2	1743.58	0.03	6.36	0.1782	-0.0111	0.3598	0.2399	0.1421	0.3811	0.4138	0.3992	0.5948	0.0043	0.0043	0.0374
H5N4F1	1809.64	0.05	2.40	17.2096	15.7826	20.8344	17.6100	16.0625	19.5415	15.4246	12.9683	17.4112	0.1403	0.1403	0.5963
H6N4	1825.63	0.13	16.04	1.1434	1.0673	1.2882	1.3642	1.1535	1.7781	1.2466	1.2039	1.3582	0.9135	0.9135	0.9499
H4N5F1	1850.67	0.04	2.77	5.5834	4.9093	10.2248	6.0127	4.8494	10.0062	5.3689	5.0601	7.9270	0.7860	0.7860	0.9499
H5N5	1866.66	0.07	5.01	-0.0215	-0.0619	0.0599	0.0145	-0.1136	0.1307	-0.0219	-0.1170	0.0205	0.7860	0.7860	0.9499
H6N2	1905.63	0.03	4.24	0.3102	0.1368	0.4059	0.4010	0.2838	0.5001	0.5935	0.4693	0.7681	0.0038	0.0038	0.0374
H5M4F2	1955.70	0.17	8.49	-0.6903	-0.8110	-0.6225	-0.7385	-0.8154	-0.5830	-0.7611	-0.8803	-0.5459	0.4803	0.4803	0.9380
H5N4S1	1976.66	0.10	5.24	2.8883	1.8839	3.4559	2.7699	1.9896	3.7392	2.2893	2.2435	2.9301	0.8917	0.8917	0.9499
H5N9F1	2012.72	0.05	2.36	6.8598	4.9867	9.0870	8.0536	4.4895	10.9335	5.7821	4.7750	7.9416	0.8236	0.8236	0.9499
H6N5	2028.71	0.18	7.47	0.2195	0.0567	0.2508	0.1970	0.0650	0.2777	0.1614	0.0877	0.2667	0.8837	0.8837	0.9499
H6M5F1	2174.77	0.14	5.81	0.2463	0.1811	0.3292	0.3065	0.2350	0.4063	0.3842	0.2689	0.4538	0.0664	0.0664	0.3225
H5N6F1	2215.80	0.15	9.89	1.1548	0.0840	0.3669	0.3886	0.1223	0.4872	0.2675	0.2048	0.5149	0.1808	0.1808	0.6147
H5M4S2	2289.74	0.16	9.12	1.6829	0.9493	2.1357	1.6612	1.2861	1.8581	1.4698	1.1300	1.9194	0.9921	0.9921	0.9499
H5N5F1S1	2325.80	0.17	18.10	-0.2408	-0.2924	-0.1567	-0.1773	-0.2460	-0.1450	-0.1636	-0.1767	-0.124	0.2590	0.2590	0.7315
H6N5S1	2341.79	0.25	15.16	0.2063	0.1455	0.2498	0.2051	0.1720	0.2779	0.2111	0.1586	0.2734	0.6251	0.6251	0.9380
H7N6	2383.65	0.31	15.99	-0.7508	-0.8184	-0.6098	-0.6531	-0.7307	-0.5391	-0.6932	-0.7169	-0.5632	0.2797	0.2797	0.7315
H6N5F1S2	2435.79	0.28	16.89	0.2190	0.1567	0.2851	0.2244	0.1857	0.2638	0.2727	0.2239	0.3027	0.3157	0.3157	0.8183
H6M5F1S1	2487.85	0.27	24.40	-0.7168	-0.8005	-0.6704	-0.6365	-0.7398	-0.5638	-0.5717	-0.6219	-0.4783	0.0044	0.0044	0.0374
H7M6F1	2539.90	0.19	20.69	-0.5305	-0.6061	-0.4418	-0.3653	-0.5547	-0.3034	-0.3946	-0.4403	-0.3188	0.0234	0.0234	0.1326



**Figure 6-4:** (A-E) Boxplots displaying the relative area distributions of the five *N*-glycans with significant variance between the three morphological classes. (F) Boxplot displaying the relative area distributions of a monofucosylated bi-antennary complex type *N*-glycan.

increase in *N*-glycans with extended  $\beta$ 1,6-linked GlcNAc branching, resulted in an increased cell motility, a loss of contact inhibition, and caused morphological transformation of normal human epithelial cells (Demetriou et al., 1995; Holst et al., 2015). Additionally, mice with a MGAT5 deficiency showed a suppression of mammary tumor cell growth and metastasis (Granovsky et al., 2000; Holst et al., 2015). The increased activity of GnT-V is also believed to result in a complementary decrease in biantennary complex type *N*-glycans (Dennis et al., 1987). Although not statistically significant, the presented results show a similar trend (Figure 6-4F, Table 6-2). While little is known about glycosylation changes in MLS, these previous findings would support a role for *N*-glycans in tumor progression in MLS. The biosynthesis of complex-type *N*-glycans is dependent on the activity of a large number of different glycosyltransferases, changes in the expression of these enzymes result in changed glycosylation profiles. The increased abundance of complex-type glycans indicates that the maturation of glycans is not completely disrupted, as this would primarily result in an increased abundance of high-mannose-type glycans and truncated glycans. Expression analysis of the genes coding for the various glycosyltransferases, or a quantitative (micro)proteomics approach, could help identify which enzymes cause the altered glycosylation profiles in the different MLS grades. While the presented results clearly display a positive correlation between the abundance of several *N*-glycans and the progression of MLS (Figure 6-4A-E), a potential complicating factor is that MLS tumor progression is associated with an increase in cellularity (Fletcher et al., 2013). The majority of the glycoproteins are either secreted or membrane-bound. The *N*-glycans analyzed by MALDI-MSI are no longer attached to their carrier proteins, which makes it impossible to establish whether a glycan was bound to a membrane protein or

a secreted, extracellular protein. Correcting for cell density may correct for contribution from membrane-bound proteins, but would introduce a bias for secreted proteins. Importantly the changed glycan profile reported here for MLS shows a clear correlation with previously published work performed on cell lines in which the number of cells were monitored and the results normalized (Demetriou et al., 1995) indicating that the changed glycan profile represents a biological effect, such as the overexpression of GnT-V causing the increase in  $\beta$ 1,6-linked GlcNAc branching, or the reduced expression of mannosidases causing the increase in high-mannose-type glycans, rather than an artifact due to differences in cell density.

## 6.4 Conclusions

The presented results indicate an association between the increase of high-mannose-type *N*-glycans and a triantennary complex-type glycan with progression of MLS. Additional protein and lipid MSI studies, as well as an in-depth analysis of the proteome should shed light on the nature of these molecular alterations.

## 6.5 Acknowledgements

This work was supported by the ZonMW Zenith project "Imaging Mass Spectrometry-Based Molecular Histology: Differentiation and Characterization of Clinically Challenging Soft Tissue Sarcomas" (No. 93512002; B.H.), and the Liddy Shriver Sarcoma Initiative. The authors would like to thank Dr. Sarantos Kostidis for his valuable input and Prof. dr. Richard Drake and dr. Anand Mehta for kindly producing and providing the PNGase F required for this study.

## 6.6 Supplementary information

### 6.6.1 Supplementary tables

**Table S6-1:** Glycan compositions used as calibrants. Compositions legend: H = Glc/Gal/HexNAc, N = Man/Gal, F = Fucose.

Composition	<i>m/z</i> [M+Na] <sup>+</sup>
<b>H5N2</b>	1257.42
<b>H3N4F1</b>	1485.53
<b>H4N4F1</b>	1647.58
<b>H5N4F1</b>	1809.64
<b>H5N5F1</b>	2012.72

**Table S6-2:** Wilcoxon signed rank test results for the morphological comparison. Compositions legend: H = Glc/Gal/HexNAc, N = Man/Gal, F = Fucose, S = NeuAc (as sodiated species). P-values and q-values < 0.05 are highlighted in green.

Composition	<i>m/z</i> [M+Na] <sup>+</sup>	Myx vs Int (n = 11)		Myx vs RC (n = 4)		Int vs RC (n = 5)	
		<i>p-value</i>	<i>q-value</i>	<i>p-value</i>	<i>q-value</i>	<i>p-value</i>	<i>q-value</i>
<b>H6N2</b>	1419.48	0.5830	0.7212	0.2500	0.4688	0.6250	0.7212
<b>H7N2</b>	1581.53	0.3575	0.5959	0.2500	0.4688	0.1875	0.4688
<b>H8N2</b>	1743.58	0.5416	0.7212	0.1250	0.4688	0.1250	0.4688
<b>H9N2</b>	1905.63	0.7609	0.8152	0.2500	0.4688	0.1875	0.4688
<b>H6N5F1S1</b>	2487.85	0.0017	0.0256	1.0000	1.0000	0.4375	0.6563



## Chapter **7**

# Summary and discussion





*The work presented in this thesis describes the improvement and application of on-tissue chemistry for in-situ biomolecular analysis using matrix assisted-laser desorption/ionization mass spectrometry imaging (MALDI-MSI). We have proposed new methodologies, applying on-tissue (enzymatic) chemistry, to increase the molecular information obtained in a MALDI-MSI analysis. We have also developed an automated histology-guided MSI platform, based on state-of-the-art image processing tools, to facilitate high mass and spatial resolution MALDI-MSI while maintaining reasonable data loads and acquisition times. We have shown the importance of these methods in a clinical biomarker discovery study on myxoid liposarcoma tissues. The following section will summarize, discuss, and provide future perspectives on the reported developments.*

## **7.1 Technical developments**

### **7.1.1 Improving and innovating on-tissue chemistry for MALDI-MSI analysis of proteins and post-translational protein modifications**

Since its introduction in 2006 by Shimma *et al.* (Shimma *et al.*, 2006) on-tissue digestion has become increasingly popular in the MSI community, owing to its ability to increase proteome coverage and aid the (*in-situ*) identification of peptides/proteins. Moreover, it enables the proteomic analysis of formalin-fixed, paraffin-embedded (FFPE) tissues by MALDI-MSI, thereby greatly increasing the number of patient samples available for clinical MSI studies.

The use of proteolytic enzymes in bottom-up proteomics has been frequently investigated, especially with regard to the repeatability and quantification of the analysis (Brownridge and Beynon, 2011). Only a small number of studies have been conducted into the fundamentals and reproducibility of on-tissue enzymatic digestion, even though a workshop organized by the European MSI network COST Action BM1104 specifically focusing on comparing different on-tissue digestion methods found very little consensus. Diehl *et al.* have previously published a study on the effect of different parameters during on-tissue digestion, including the protease, the incubation time, and the MALDI matrix. However, this study was mostly focused on improving the spatial resolution, and the quality and repeatability of the MSI images (Diehl *et al.*, 2015). Two more recent studies by Erich *et al.* and De Sio *et al.* have compared multiple previously published on-tissue digestion sample preparation methods and tested the relative repeatability of those methods (Erich *et al.*, 2016; Sio *et al.*, 2015). Erich *et al.* proposed an automated, user-independent, computational approach to provide a more objective evaluation of the repeatability of MALDI-MSI (Erich *et al.*, 2016). In **Chapter 2**, we investigated the spatiotemporal dynamics of on-tissue enzymatic digestion. The investigation was based on the analysis of three sample groups with varying incubation times (1,5 h, 3 h, and 18 h), resulted in the finding that longer digestion times improved the repeatability of the on-tissue digestion. Additionally, it was found that differences in the chemical background of distinct morphological regions, specifically

the white and grey matter in mouse brain, resulted in differences in digestion efficiency. These sample preparation artifacts disappeared with the use of longer incubation times, supporting the hypothesis that longer incubation times improve the repeatability of on-tissue digestion experiments by ensuring a more complete digestion for all morphological regions.

The on-tissue digestion dynamics study focused on the global differences between the three incubation times by comparing the number of peaks in the total average spectra. Additional insight into the digestion dynamics was obtained by tracing the digestion of Myelin Basic Protein (MBP, MBP\_MOUSE) throughout the tissue and the duration of the digestion. In order to reduce ionization bias and increase the comparability of the different datasets ( $n = 27$ , nine replicates per incubation time), three proteolytic fragments of MBP were selected and isotopically-labeled reference standard (ILRS) peptides were synthesized and sprayed homogeneously onto the tissue. The MBP fragments included two 'limit peptides' (end product of the proteolytic digestion), and one 'missed-cleavage peptide'. The fragments were chosen in such a manner that the full digestion of the missed-cleavage peptide resulted in one of the limit peptides, so that relative intensity differences between the two peptides could be used to represent the efficiency of the digestion (with the proviso that other proteins might have different digestion efficiencies and other tissue types might affect the digestion dynamics). Also, it should be taken into account that the results were obtained for analysis from fresh frozen tissues; the dynamics of on-tissue digestion for FFPE tissues may well differ. While this study provides useful insight into the dynamics of on-tissue digestion, additional investigations spanning more proteins, more tissue types and tissue formats would be needed for a complete understanding of the factors affecting the dynamics of on-tissue digestion. Nevertheless the methodology reported here, to obtain quantitative data of digestion rate (for one cleavage site) from different tissue regions, presents the methodology that should be expanded for all future investigations.

The extensive work performed in the field of proteomics over the last two decades is an invaluable resource for the improvement and adaptation of MALDI-MSI methods. As described above, adaptation of the bottom-up proteomics approach led to the introduction of on-tissue digestion MALDI-MSI. As is the case in LC-MS/MS-based bottom-up proteomics, on-tissue proteolytic digestion is predominantly performed using trypsin. Due to its cleavage specificity, C-terminal of the basic amino acid residues arginine and lysine, trypsin produces proteolytic peptides with intrinsically positively charged C-termini that are detected with high sensitivity by mass spectrometry (Brownridge and Beynon, 2011; Vandermarliere et al., 2013). However, previous work in the proteomics field has also concluded that the use of different enzymes (even with a shared cleavage specificity) can lead to increased proteome coverage (Choudhary et al., 2003; Hohmann et al., 2009). In **Chapter 3** and **Chapter 5** we describe two different multi-enzyme approaches; **Chapter 3** describes the combination of several

proteolytic enzymes with lysine and arginine cleavage specificity, and how the use of different enzymes could increase proteome coverage as well as protein sequence coverage; **Chapter 5** describes a multimodal MSI approach, in which sequential on-digestions were performed with the glycosidase PNGase F and trypsin in order to analyze both *N*-linked glycans and proteolytic peptides in two sequential MALDI-MSI analyses, but from the same FFPE tissue section. While the methodology proposed in **Chapter 3** is dependent on the analysis of multiple tissue sections (although the analysis with the combination of trypsin/Lys-C is based on the same principle), the methodology in **Chapter 5** requires only a single tissue section for the acquisition of two datasets on two closely related molecular classes. The benefit is that the information obtained in both datasets originates from exactly the same morphological and histological features. It should be noted that the MALDI-MS analysis of *N*-glycans can be improved further by performing a linkage-specific sialic acid derivatization. This derivatization stabilizes the otherwise labile sialic acid residues, enables the differentiation between the isobaric  $\alpha$ 2,3- and  $\alpha$ 2,6-linked sialic acids, and reduces the adverse effects on positive-mode ionization of the negative charge of native sialic acids (Holst et al., 2016). A potential complication is the dimethylamidation derivatization reaction modifies all free carboxylic acid (COOH) groups, and therefore also affects protein C-termini and acidic amino acid residues. The exact derivatization-induced changes of the proteins were not characterized in detail, but which could complicate the identification of proteolytic fragments from the same FFPE tissue section. Nevertheless, the sequential on-tissue digestion approach has proven itself a useful tool for *N*-glycan MALDI-MSI as is described in **Chapter 5**.

### 7.1.2 Histology-guided MALDI-MSI

Recent technological advances, mainly the development of an ultrafast MALDI-TOF-MS platform, and resolution for MALDI-FTICR-MS analysis, have made high spatial resolution and high mass resolution analysis readily available for MSI. However, the increased cellular and chemical specificity achieved by the high-resolution analysis come at the cost of data acquisition time and data load. Especially in the field of clinical MSI where large patient tissue series need to be analyzed, this imposes challenges on both the MSI infrastructure and data management systems. To overcome these challenges, we have developed a histology-guided MSI (HG-MSI) platform based on an automated image registration pipeline in **Chapter 4**. The image registration pipeline registers a high-resolution annotated histological image of a tissue section to a lower resolution image of an adjacent tissue section, prepared for MALDI-MSI analysis. Following the image registration, the annotation borders are reproduced on the low-resolution image, enabling the exclusive MSI analysis of the *a priori* selected regions of interest. In a study on a small tissue cohort the HG-MSI approach resulted in a reduction of data acquisition time and data load of 80%, and thereby improving the applicability of high spatial and mass resolution MSI for clinical research.

The prior histological specification of the HG-MSI approach is well suited for applications in which an *a priori* histological specification is possible, meaningful, and needed, e.g. the analysis of tumor progression based on cellular dedifferentiation or other specific morphological hallmarks. The tool is especially useful for those applications where high spatial resolution, or high mass resolution is required, but at the same time impractical or limited by extremely large pixel counts and/or slow data acquisition speeds. **Chapter 4** describes the application of the HG-MSI platform for the analysis of proteolytic peptides from FFPE tissues using an ultrahigh mass resolution MALDI-FTICR-MS instrument manufactured by Bruker Daltonics. To ensure this tool can become a valuable asset for the MSI community it is vendor neutral, applicable to all MSI modalities (e.g. SIMS, DESI, LESA, etc.), and freely available online.

The analysis of tissue microarrays (TMA), as described in **Chapter 6**, offers a solution for the analysis of a large patient series. A TMA is an assembly of needle core biopsies (diameter 0.5 – 2 mm), obtained from histologically predefined tissue regions from many patients. The major advantages of analyzing TMAs are that a large number of patient samples can be rapidly compared; the experimental variance is reduced substantially as all needle cores are prepared during the same sample preparation and analyzed together; and a substantial histological pre-selection of tissue regions has already taken place.

## 7.2 Clinical application

### 7.2.1 The molecular background of tumor progression in myxoid liposarcoma

The methods described in this thesis, and especially those in **Chapters 4** and **5**, were ultimately designed for their application in clinical research. **Chapter 6** describes the application of the multimodal MSI method described in **Chapter 5** in a study focusing on the molecular characterization of tumor progression in myxoid liposarcoma (MLS). We have demonstrated an association between a higher abundance of high-mannose type glycans, and highly branched complex-type glycans with MLS tumor progression. While this phenomenon was not previously described for MLS or any other mesenchymal tumor, it was described for several other tumor types, including colorectal cancer, breast cancer, and ovarian cancer. High-mannose type glycans are found both intra- and extracellular. However, the MALDI-MSI experiments in **Chapter 6** were not performed at a spatial resolution needed to discriminate between intra- or extracellular molecules. Therefore, the results presented in **Chapter 6** should be validated with independent techniques such as immunohistochemistry to provide additional information on the exact location of the *N*-glycans in the cellular environment. Further insights into the changes associated with MLS progression could be garnered by also including protein and lipid MSI data as well as an in-depth analysis of the proteome, to further unravel the relevant pathways and molecular alterations leading to the advanced stages of MLS.

### 7.3 Future work

This thesis describes the optimization and application of on-tissue digestion MALDI-MSI to improve its applicability in clinical research. Since the introduction of MSI, the identification of detected molecules has been one of the major challenges. Especially in clinical studies and/or biomarker discovery studies, the identity of the detected molecules is paramount to obtain valuable biological insights about the nature of the potential MSI-based biomarkers. One of the advantages of applying the on-tissue digestion method to *in situ* protein analysis is that it aids protein identification. The work described in the thesis shows that the number of protein identities that could be assigned to  $m/z$  features increased substantially with high mass resolution MSI. However, it should be noted that approximately only 10-15% of all peaks in the MSI average spectra were assigned with a peptide identity, and which did not include many of the high intensity peaks. The solution to improve the peptide identification rate in MSI is multifaceted.

First, in FFPE tissues, formalin is used to cross-link proteins and does so by connecting the basic amino acids lysine, arginine & histidine within and between proteins. For the analysis of proteins in FFPE tissue, formalin-fixation is reversed by a process called antigen retrieval. However, the reversal of the formalin fixation is often not complete and results in irregular, and predominantly uncharacterized remnants of the formalin fixation attached to the peptides/proteins. This results in both a large number of unmatched MS/MS spectra during the database search following LC-MS/MS analysis, and a large number of unassigned peaks in the MSI average spectrum. In order to utilize the full potential of proteomic MSI from FFPE tissue a thorough characterization of the formalin-induced modifications should be performed. However, previous attempts, and the fact that the majority of the bottom-up proteomics field remains distant from FFPE tissue, indicate the enormous challenges it encompasses. Alternatively, targeted offline LC-MS/MS approaches, based on MSI peak lists, could aid in additional identity assignments.

Second, the digested proteome with its large number of (near-)isobaric proteolytic fragments, is an extremely complex sample and results in a very complex mass spectrum containing many overlapping isotope envelopes. The spectra are further complicated by the presence of adducts. Tissues are a salt-rich environment, and although the tissues are washed during sample preparation, various salt-adducts ( $\text{Na}^+$ ,  $2\text{Na-H}^+$ ,  $\text{K}^+$ ,  $2\text{K-H}^+$ ) are commonly detected in MSI analyses, as is described in **Chapter 5**. While the removal of adduct peaks from the mass spectra is a possible solution to simplify the spectra, the preferred strategy would be to reduce adduct formation during the analysis by applying additional washes, or using a more salt resistant MALDI matrix that reduces the adduct formation. Wang *et al.* recently reported that the matrix (E)-propyl  $\alpha$ -cyano-4-hydroxyl cinnamylate, formed by the reaction of the regular peptide MALDI matrix  $\alpha$ -cyano-4-hydroxycinnamic acid with

propyl alcohol, displayed high salt tolerance for intact protein analysis (Wang et al., 2015b). We synthesized this matrix but preliminary MALDI-MSI experiments using on-tissue digestion revealed the matrix exhibited an increased propensity to form salt adducts.

Third, the peptide identity assignments described in **Chapter 3** and **Chapter 5** of this thesis were all performed on the basis of accurate mass. While the use of this method provides a lot of valuable information on the potential identities of the detected molecules, the preferred method would involve the acquisition of their tandem MS spectra directly from the tissue section. While this approach is commonly described in literature using low mass resolution MALDI-TOF-MS platforms, its availability for high mass resolution MS systems is very limited. To improve the true peptide identification in MSI, mass spectrometers should be equipped with improved quadrupole technology, allowing a more specific selection of  $m/z$  features for fragmentation, leading to a more accurate identification directly from tissue.

The additional work described above would improve our basic understanding of the samples we work with, which will ultimately result in more specific and more efficient methods better suited for the MSI analysis of FFPE tissues. Nevertheless, the impact of MSI on clinical research rapidly increased over the last years, improved methodology and technology will ascertain further establishment of MSI in clinical research, and might result in an implementation of MSI in molecular diagnostics in the future.







# Bibliography



- Abdelmoula, W.M., Carreira, R.J., Shyti, R., Balluff, B., van Zeijl, R.J.J., Tolner, E.A., Lelieveldt, B.F., van den Maagdenberg, A.M.J.M., McDonnell, L.A., and Dijkstra, J. (2014). Automatic registration of mass spectrometry imaging data sets to the Allen brain atlas. *Anal Chem* 86, 3947–3954.
- Adamczyk, B., Tharmalingam, T., and Rudd, P.M. (2012). Glycans as cancer biomarkers. *Biochim Biophys Acta* 1820, 1347–1353.
- Addie, R.D., Balluff, B., Bovée, J.V., Morreau, H., and McDonnell, L.A. (2015). Current state and future challenges of mass spectrometry imaging for clinical research. *Anal Chem* 87, 6426–6433.
- Aerni, H.R., Cornett, D.S., and Caprioli, R.M. (2006). Automated acoustic matrix deposition for MALDI sample preparation. *Anal Chem* 78, 827–834.
- Aichler, M., and Walch, A. (2015). MALDI Imaging mass spectrometry: current frontiers and perspectives in pathology research and practice. *Lab Invest* 95, 422–431.
- Aichler, M., Elsner, M., Ludyga, N., Feuchtinger, A., Zangen, V., Maier, S., Balluff, B., Schöne, C., Hierber, L., Braselmann, H., et al. (2013). Clinical response to chemotherapy in oesophageal adenocarcinoma patients is linked to defects in mitochondria. *J Pathol* 230, 410–419.
- Alteelaar, M., van Minnen, J., Jiménez, C., Heeren, R., and Piersma, S. (2005). Direct molecular imaging of Lymnaea stagnalis nervous tissue at subcellular spatial resolution by mass spectrometry. *Anal Chem* 77, 735–741.
- Alteelaar, M., Munoz, J., and Heck, A. (2012). Next-generation proteomics: towards an integrative view of proteome dynamics. *Nat Rev Genet* 14, 35–48.
- Amini, A., Dormady, S.J., Riggs, L., and Regnier, F.E. (2000). The impact of buffers and surfactants from micellar electrokinetic chromatography on matrix-assisted laser desorption/ionization (MALDI) mass spectrometry of peptides. Effect of buffer type and concentration on mass determination by MALDI-time-of-flight mass spectrometry. *J Chromatogr A* 894, 345–355.
- Amstalden van Hove, E.R., Blackwell, T.R., Klinkert, I., Eijkel, G.B., Heeren, R.M., and Glunde, K. (2010). Multimodal mass spectrometric imaging of small molecules reveals distinct spatio-molecular signatures in differentially metastatic breast tumor models. *Cancer Res* 70, 9012–9021.
- Angel, P.M., Spraggins, J.M., Baldwin, H.S., and Caprioli, R.M. (2012). Enhanced sensitivity for high spatial resolution lipid analysis by negative ion mode matrix assisted laser desorption/ionization imaging mass spectrometry. *Anal Chem* 84, 1557–1564.
- Antonescu, C.R., Tschernyavsky, S.J., Decuseara, R., Leung, D.H., Woodruff, J.M., Brennan, M.F., Bridge, J.A., Neff, J.R., Goldblum, J.R., and Ladanyi, M. (2001). Prognostic impact of P53 status, TLS-CHOP fusion transcript structure, and histological grade in myxoid liposarcoma: a molecular and clinicopathologic study of 82 cases. *Clin Cancer Res* 7, 3977–3987.
- Anugraham, M., Jacob, F., Nixdorf, S., Everest-Dass, A.V., Heinzmann-Schwarz, V., and Packer, N.H. (2014). Specific glycosylation of membrane proteins in epithelial ovarian cancer cell lines: glycan structures reflect gene expression and DNA methylation status. *Mol Cell Proteomics* 13, 2213–2232.
- Atkinson, S.J., Loadman, P.M., Sutton, C., Patterson, L.H., and Clench, M.R. (2007). Examination of the distribution of the bioreductive drug AQ4N and its active metabolite AQ4 in solid tumours by imaging matrix-assisted laser desorption/ionisation mass spectrometry. *Rapid Commun Mass Spectrom* 21, 1271–1276.
- Awad, H., Khamis, M.M., and El-Aneel, A. (2015). Mass spectrometry, review of the basics: ionization. *Appl Spectrosc Rev* 50, 158–175.
- Balluff, B., Elsner, M., Kowarsch, A., Rauser, S., Meding, S., Schuhmacher, C., Feith, M., Herrmann, K., Röcken, C., Schmid, R., et al. (2010). Classification of HER2/neu status in gastric cancer using a breast-cancer derived proteome classifier. *J Proteome Res* 9, 6317–6322.
- Balluff, B., Rauser, S., Meding, S., Elsner, M., Schöne, C., Feuchtinger, A., Schuhmacher, C., Novotny, A., Jütting, U., Maccarrone, G., et al. (2011). MALDI imaging identifies prognostic seven-protein signature of novel tissue markers in intestinal-type gastric cancer. *Am J Pathol* 179, 2720–2729.
- Balluff, B., Frese, C.K., Maier, S.K., Schöne, C., Kuster, B., Schmitt, M., Aubele, M., Höfler, H., Deelder, A.M.M., Heck, A., et al. (2015). De novo discovery of phenotypic intratumour heterogeneity using imaging mass spectrometry. *J Pathol* 235, 3–13.
- Barry, J., Robichaud, G., and Muddiman, D. (2013). Mass recalibration of FT-ICR mass spectrometry imaging data using the average frequency shift of ambient ions. *J Am Soc Mass Spectrom* 24, 1137–1145.
- Beaudry, F., Le Blanc, Y., Coutu, Ramier, I., Moreau, J.P., and Brown, N.K. (1999). Metabolite profiling study of propranolol in rat using LC/MS/MS analysis. *Biomed Chromatogr* 13, 363–369.
- Bhatia, V.N., Perlman, D.H., Costello, C.E., and McComb, M.E. (2009). Software tool for researching annotations of proteins: open-source protein annotation software with data visualization. *Anal Chem* 81, 9819–9823.
- Bovée, J.V.M.G., and Hogendoorn, P.C. (2010). Molecular pathology of sarcomas: concepts and clinical implications. *Virchows Arch* 456, 193–199.
- Briggs, M.T., Ho, Y.Y., Kaur, G., Oehler, M.K., Everest-Dass, A.V., Packer, N.H., and Hoffmann, P. (2017). N-glycan matrix-assisted laser desorption/ionization mass spectrometry imaging protocol for formalin-fixed paraffin-embedded tissues. *Rapid Commun Mass Spectrom* epub ahead of print.
- Brown, R.S., and Lennon, J.J. (1995). Mass resolution improvement by incorporation of pulsed ion extraction in a matrix-assisted laser desorption/ionization linear time-of-flight mass spectrometer. *Anal Chem* 67, 1998–2003.
- Brownridge, P., and Beynon, R.J. (2011). The importance of the digest: proteolysis and absolute quantification in proteomics. *Methods* 54, 351–360.

- Buck, A., Ly, A., Balluff, B., Sun, N., Gorzalka, K., Feuchtinger, A., Janssen, K.-P.P., Kuppen, P.J., van de Velde, C.J., Weirich, G., et al. (2015). High-resolution MALDI-FT-ICR MS imaging for the analysis of metabolites from formalin-fixed, paraffin-embedded clinical tissue samples. *J Pathol* 237, 123–132.
- Budnik, B., Haselmann, K., and Zubarev, R. (2001). Electron detachment dissociation of peptide di-anions: an electron-hole recombination phenomenon. *Chem Phys Lett* 342, 299–302.
- Buse, J., Purves, R.W., Verrall, R.E., Badea, I., Zhang, H., Mulligan, C.C., Bailey, J., Headley, J.V., and El-Aneid, A. (2014). The development and assessment of high-throughput mass spectrometry-based methods for the quantification of a nanoparticle drug delivery agent in cellular lysate. *J Mass Spectrom* 49, 1171–1180.
- Caldwell, R.L., Holt, G.E., and Caprioli, R.M. (2005). Tissue Profiling by MALDI Mass Spectrometry Distinguishes Clinical Grades of Soft Tissue Sarcomas. *Cancer Genom Proteom* 2, 333–345.
- Caldwell, R.L., Gonzalez, A., Oppenheimer, S.R., Schwartz, H.S., and Caprioli, R.M. (2006). Molecular Assessment of the Tumor Protein Microenvironment Using Imaging Mass Spectrometry. *Cancer Genome Proteom* 3, 279–287.
- Calvano, C.D., Carulli, S., and Palmisano, F. (2010). 1H-Pteridine-2,4-dione (lumazine) a new MALDI matrix for complex (phospho) lipid mixtures analysis. *Anal Bioanal Chem* 398, 499–507.
- Caprioli, R.M., Farmer, T.B., and Gile, J. (1997). Molecular imaging of biological samples: localization of peptides and proteins using MALDI-TOF MS. *Anal Chem* 69, 4751–4760.
- Carlson, B., Bernstein, D., Annis, D., Misenheimer, T., Hannah, B., Mosher, D., and Keck, J. (2005). Structure of the calcium-rich signature domain of human thrombospondin-2. *Nat Struct Mol Biology* 12, 910–914.
- Carreira, R.J., Shyti, R., Balluff, B., Abdelmoula, W.M., van Heiningen, S.H., van Zeijl, R.J., Dijkstra, J., Ferrari, M.D., Tolner, E.A., McDonnell, L.A., et al. (2015). Large-scale mass spectrometry imaging investigation of consequences of cortical spreading depression in a transgenic mouse model of migraine. *J Am Soc Mass Spectrom* 26, 853–861.
- Casadonte, R., and Caprioli, R.M. (2011). Proteomic analysis of formalin-fixed paraffin-embedded tissue by MALDI imaging mass spectrometry. *Nat Protoc* 6, 1695–1709.
- Casadonte, R., Kriegsmann, M., Zweynert, F., Friedrich, K., Baretton, G., Bretton, G., Otto, M., Deininger, S.-O., Paape, R., Belau, E., et al. (2014). Imaging mass spectrometry to discriminate breast from pancreatic cancer metastasis in formalin-fixed paraffin-embedded tissues. *Proteomics* 14, 956–964.
- Cazares, L.H., Troyer, D.A., Mendrinos, S., Lance, R.A., Nyalwidhe, J.O., Beydoun, H.A., Clements, M.A., Drake, R.R., and Semmes, O.J. (2009). Imaging mass spectrometry of a specific fragment of mitogen-activated protein kinase/extracellular signal-regulated kinase kinase 2 discriminates cancer from uninvolved prostate tissue. *Clin Cancer Res* 15, 5541–5551.
- Cazares, L.H., Troyer, D.A., Wang, B., Drake, R.R., and Semmes, O.J. (2011). MALDI tissue imaging: from biomarker discovery to clinical applications. *Anal Bioanal Chem* 401, 17–27.
- Cazares, L.H., Van Tongeren, S.A., Costantino, J., Kenny, T., Garza, N.L., Donnelly, G., Lane, D., Panchal, R.G., and Bavari, S. (2015). Heat fixation inactivates viral and bacterial pathogens and is compatible with downstream MALDI mass spectrometry tissue imaging. *BMC Microbiol* 15, 1–11.
- Chacon, A., Zagol-Ikapitte, I., Amarnath, V., Reyzer, M.L., Oates, J.A., Caprioli, R.M., and Boutaud, O. (2011). On-tissue chemical derivatization of 3-methoxysalicylamine for MALDI-imaging mass spectrometry. *J Mass Spectrom* 46, 840–846.
- Chaurand, P., Schwartz, S.A., Billheimer, D., Xu, B.J., Crecelius, A., and Caprioli, R.M. (2004). Integrating histology and imaging mass spectrometry. *Anal Chem* 76, 1145–1155.
- Chaurand, P., Cornett, D.S., Angel, P.M., and Caprioli, R.M. (2011). From whole-body sections down to cellular level, multiscale imaging of phospholipids by MALDI mass spectrometry. *Mol Cell Proteomics* 10, O110.004259.
- Chaurand, P., Stoekli, M., Caprioli, R.M. (1999). Direct profiling of proteins in biological tissue sections by MALDI mass spectrometry. *Anal Chem* 71, 5263–5270.
- Chen, R., Hui, L., Sturm, R.M., and Li, L. (2009a). Three dimensional mapping of neuropeptides and lipids in crustacean brain by mass spectral imaging. *J Am Soc Mass Spectrom* 20, 1068–1077.
- Chen, R., Jiang, X., Sun, D., Han, G., Wang, F., Ye, M., Wang, L., and Zou, H. (2009b). Glycoproteomics analysis of human liver tissue by combination of multiple enzyme digestion and hydrazide chemistry. *J Proteome Res* 8, 651–661.
- Choudhary, G., Wu, S.-L., Shieh, P., and Hancock, W.S. (2003). Multiple enzymatic digestion for enhanced sequence coverage of proteins in complex proteomic mixtures using capillary LC with ion trap MS/MS. *J Proteome Res* 2, 59–67.
- Chughtai, K., Jiang, L., Greenwood, T.R., Klinkert, I., Amstalden van Hove, E.R., Heeren, R.M.A., and Glunde, K. (2012). Fiducial markers for combined 3-dimensional mass spectrometric and optical tissue imaging. *Anal Chem* 84, 1817–1823.
- Clemis, E.J., Smith, D.S., Camenzind, A., Danell, R.M., Parker, C.E., and Borchers, C.H. (2012). Quantitation of spatially-localized proteins in tissue samples using MALDI-MRM imaging. *Anal Chem* 84, 3514–3522.
- Cole, L.M., Djidja, M.-C., Bluff, J., Claude, E., Carolan, V.A., Paley, M., Tozer, G.M., and Clench, M.R. (2011). Investigation of protein induction in tumour vascular targeted strategies by MALDI MSI. *Methods* 54, 442–453.
- Comisarow, M.B., and Marshall, A.G. (1974). Fourier transform ion cyclotron resonance spectroscopy. *Chem Phys Lett* 25, 282–283.
- Coon, J.J., Shabanowitz, J., Hunt, D.F., and Syka, J.E.P. (2005). Electron transfer dissociation of peptide anions. *J Am Soc Mass Spectrom* 16, 880–882.
- Cornett, D.S., Mobley, J.A., Dias, E.C., Andersson, M., Arteaga, C.L., Sanders, M.E., and Caprioli, R.M. (2006). A novel histology-directed strategy for MALDI-MS tissue profiling that improves throughput and cellular specificity in human breast cancer. *Mol Cell Proteomics* 5, 1975–1983.

- Cotter, R.J. (1992). Time-of-flight mass spectrometry for the structural analysis of biological molecules. *Anal Chem* 64, 1027A–1039A.
- Cristofanilli, M., Budd, G.T., Ellis, M.J., Stopeck, A., Matera, J., Miller, M.C., Reuben, J.M., Doyle, G.V., Allard, J., Terstappen, L.W.M.M., et al. (2004). Circulating tumor cells, disease progression, and survival in metastatic breast cancer. *N Engl J Med* 351, 781–791.
- Dalerba, P., Kalisky, T., Sahoo, D., Rajendran, P.S., Rothenberg, M.E., Leyrat, A.A., Sim, S., Okamoto, J., Johnston, D.M., Qian, D., et al. (2011) Single-cell dissection of transcriptional heterogeneity in human colon tumors. *Nat Biotechnol* 29, 1120–1127.
- D'Arrigo, A., Belluco, C., Ambrosi, A., Digito, M., Esposito, G., Bertola, A., Fabris, M., Nofrate, V., Mammano, E., Leon, A., et al. (2005). Metastatic transcriptional pattern revealed by gene expression profiling in primary colorectal carcinoma. *Int J Cancer* 115, 256–262.
- Dawson, J.H.J., and Guilhaus, M. (1989). Orthogonal acceleration time of flight mass spectrometer. *Rapid Commun Mass Spectrom* 3, 155–159.
- de Graaf, E.L., Alteleaar, A.F.M., van Breukelen, B., Mohammed, S., and Heck, A.J.R. (2011). Improving SRM assay development: a global comparison between triple quadrupole, ion trap, and higher energy CID peptide fragmentation spectra. *J Proteome Res* 10, 4334–4341.
- de Graaff, M.A., Yu, J.S., Beird, H.C., Ingram, D.R., Nguyen, T., Juehui Liu, J., Bolshakov, S., Suzhai, K., Åman, P., Torres, K., et al. (2016). Establishment and characterization of a new human myxoid liposarcoma cell line (DL-221) with the FUS-DDIT3 translocation. *Lab Invest* 96, 885–894.
- de Graaff, M., Malu, S., Guardiola, I., Kruijselbrink, A., de Jong, Y., Corver, W., Gelderblom, H., Hwu, P., Nielsen, T., Lazar, J., et al. (2017). High-throughput screening of myxoid liposarcoma cell lines reveals survivin as a potential novel druggable target. Leiden University.
- de Hoffmann, E. (1996). Tandem mass spectrometry: a primer. *J Mass Spectrom* 31, 129–137.
- de Leoz, M.L., Young, L.J., An, H.J., Kronewitter, S.R., Kim, J., Miyamoto, S., Borowsky, A.D., Chew, H.K., and Lebrilla, C.B. (2011). High-mannose glycans are elevated during breast cancer progression. *Mol Cell Proteomics* 10, M110.002717.
- de Vreeze, R., de Jong, D., Nederlof, P., Ruijter, H.J., Boerrigter, L., Haas, R., van Coevorden, F. (2010) Multifocal myxoid liposarcoma - Metastasis or second primary tumor? A molecular biological analysis. *J Mol Diagn* 12, 238–243
- Deiningner, S.-O., Ebert, M.P., Fütterer, A., Gerhard, M., and Röcken, C. (2008). MALDI imaging combined with hierarchical clustering as a new tool for the interpretation of complex human cancers. *J Proteome Res* 7, 5230–5236.
- Dekker, T.J., Balluff, B.D., Jones, E.A., Schöne, C.D., Schmitt, M., Aubele, M., Kroep, J.R., Smit, V.T., Tollenaar, R.A., Mesker, W.E., et al. (2014). Multicenter matrix-assisted laser desorption/ionization mass spectrometry imaging (MALDI MSI) identifies proteomic differences in breast-cancer-associated stroma. *J Proteome Res* 13, 4730–4738.
- Delcorte, A., and Garrison, B.J. (2000). High yield events of molecular emission induced by kiloelectronvolt particle bombardment. *J Phys Chem* 104, 6785–6800.
- Demetriou, M., Nabi, I., Coppolino, M., Dedhar, S., and Dennis, J. (1995). Reduced contact-inhibition and substratum adhesion in epithelial cells expressing GlcNAc-transferase V. *J Cell Biol* 130, 383–392.
- Demiccio, E., Torres, K., Ghadimi, M., Colombo, C., Bolshakov, S., Hoffman, A., Peng, T., Bovée, J., Wang, W.-L., Lev, D., et al. (2011). Involvement of the PI3K/Akt pathway in myxoid/round cell liposarcoma. *Modern Pathology* 25, 212–221.
- Dennis, J.W., Laferte, S., Waghorne, C., Breitman, M.L., and Kerbel, R.S. (1987). Beta 1-6 branching of Asn-linked oligosaccharides is directly associated with metastasis. *Science* 236, 582–585.
- Dennis, J.W., Granovsky, M., and Warren, C.E. (1999). Glycoprotein glycosylation and cancer progression. *Biochim Biophys Acta* 1473, 21–34.
- Dice, L.R. (1945). Measures of the amount of ecologic association between species. *Ecology* 26, 297–302.
- Diehl, H.C., Beine, B., Elm, J., Trede, D., Ahrens, M., Eisenacher, M., Marcus, K., Meyer, H.E., and Henkel, C. (2015). The challenge of on-tissue digestion for MALDI MSI— a comparison of different protocols to improve imaging experiments. *Anal Bioanal Chem* 407, 2223–2243.
- Dilillo, M., Ait-Belkacem, R., Esteve, E., Pellegrini, D., Nicolardi, S., Costa, M., Vannini, E., de Graaf, E.L., Caleo, M., McDonnell, L.A. (2017) Ultra-high mass resolution MALDI imaging mass spectrometry of proteins and metabolites in a mouse model of glioblastoma. *Sci Rep* 7, 603
- Djidja, M.-C., Francese, S., Loadman, P.M., Sutton, C.W., Scriven, P., Claude, E., Snel, M.F., Franck, J., Salzet, M., and Clench, M.R. (2009a). Detergent addition to tryptic digests and ion mobility separation prior to MS/MS improves peptide yield and protein identification for in situ proteomic investigation of frozen and formalin-fixed paraffin-embedded adenocarcinoma tissue sections. *Proteomics* 9, 2750–2763.
- Djidja, M.-C., Claude, E., Snel, M.F., Scriven, P., Francese, S., Carolan, V., and Clench, M.R. (2009b). MALDI-ion mobility separation-mass spectrometry imaging of glucose-regulated protein 78 kDa (Grp78) in human formalin-fixed, paraffin-embedded pancreatic adenocarcinoma tissue sections. *J Proteome Res* 8, 4876–4884.
- Djidja, M.-C., Claude, E., Snel, M.F., Francese, S., Scriven, P., Carolan, V., and Clench, M.R. (2010). Novel molecular tumour classification using MALDI-mass spectrometry imaging of tissue micro-array. *Anal Bioanal Chem* 397, 587–601.
- Domon B., and Aebersold, R. (2006). Mass spectrometry and protein analysis. *Science* 312, 212–217.
- Dong, X., Cheng, J., Li, J., and Wang, Y. (2010). Graphene as a novel matrix for the analysis of small molecules by MALDI-TOF MS. *Anal Chem* 82, 6208–6214.

- Dong, Y., Li, B., Malitsky, S., Rogachev, I., Aharoni, A., Kaftan, F., Svatoš, A., and Franceschi, P. (2016). Sample preparation for mass spectrometry imaging of plant tissues: a review. *Front Plant Sci* 7, 60.
- Drake, P.M., Cho, W., Li, B., Prakobphol, A., Johansen, E., Anderson, N.L., Regnier, F.E., Gibson, B.W., and Fisher, S.J. (2010). Sweetening the pot: adding glycosylation to the biomarker discovery equation. *Clin Chem* 56, 223–236.
- Dreisewerd, K., Schürenberg, M., and Karas, M., Hillenkamp, F. (1995). Influence of the laser intensity and spot size on the desorption of molecules and ions in matrix-assisted laser desorption/ionization with a uniform beam profile. *Int J Mass Spectrom Ion Process* 141, 127–148.
- Dreisewerd, K. (2003). The desorption process in MALDI. *Chem Rev* 103, 395–426.
- Dreisewerd, K. (2014). Recent methodological advances in MALDI mass spectrometry. *Anal Bioanal Chem* 406, 2261–2278.
- Easterling, M.L., Mize, T.H., and Amster, J. (1999). Routine part-per-million mass accuracy for high-mass ions: space-charge effects in MALDI FT-ICR. *Anal Chem* 71, 624–632.
- Eberlin, L.S., Liu, X., Ferreira, C.R., Santagata, S., Agar, N.Y.R., and Cooks, R.G. (2011). Desorption electrospray ionization then MALDI mass spectrometry imaging of lipid and protein distributions in single tissue sections. *Anal Chem* 83, 8366–8371.
- Eikel, D., Vavrek, M., Smith, S., Bason, C., Yeh, S., Korfmacher, W.A., and Henion, J.D. (2011). Liquid extraction surface analysis mass spectrometry (LESA-MS) as a novel profiling tool for drug distribution and metabolism analysis: the terfenadine example. *Rapid Commun Mass Spectrom* 25, 3587–3596.
- El Ayed, M., Bonnel, D., Longuespée, R., Castelier, C., Franck, J., Vergara, D., Desmons, A., Tasiemski, A., Kenani, A., Vinatier, D., et al. (2010). MALDI imaging mass spectrometry in ovarian cancer for tracking, identifying, and validating biomarkers. *Med Sci Monit* 16, BR233–45.
- Ellis, S.R., Cappell, J., Potočník, N.O., Balluff, B., Hamaide, J., der Linden, A., and Heeren, R.M. (2016). More from less: high-throughput dual polarity lipid imaging of biological tissues. *Analyst* 141, 3832–3841.
- Elsner, M., Rauser, S., Maier, S., Schöne, C., Balluff, B., Meding, S., Jung, G., Nipp, M., Sarioglu, H., Maccarrone, G., et al. (2012). MALDI imaging mass spectrometry reveals COX7A2, TAGLN2 and S100-A10 as novel prognostic markers in Barrett's adenocarcinoma. *J Proteomics* 75, 4693–4704.
- Endo, M., Graaff, M., Ingram, D., Lim, S., Lev, D., Bruijn, I., Somaiah, N., Bovée, J., Lazar, A., and Nielsen, T. (2015). NY-ESO-1 (CTAG1B) expression in mesenchymal tumors. *Modern Pathology* 28, 587–595.
- Enthaler, B., Bussmann, T., Pruns, J.K., Rapp, C., Fischer, M., and Vietzke, J.-P. (2013a). Influence of various on-tissue washing procedures on the entire protein quantity and the quality of matrix-assisted laser desorption/ionization spectra. *Rapid Commun Mass Spectrom* 27, 878–884.
- Enthaler, B., Trusch, M., Fischer, M., Rapp, C., Pruns, J.K., and Vietzke, J.-P. (2013b). MALDI imaging in human skin tissue sections: focus on various matrices and enzymes. *Anal Bioanal Chem* 405, 1159–1170.
- Esteve, C., Marina, M.L., and García, M.C. (2015). Novel strategy for the revalorization of olive (*Olea europaea*) residues based on the extraction of bioactive peptides. *Food Chem* 167, 272–280.
- Esteve, C., Tolner, E.A., Shyti, R., van den Maagdenberg, A.M.J.M., and McDonnell, L.A. (2016). Mass spectrometry imaging of amino neurotransmitters: a comparison of derivatization methods and application in mouse brain tissue. *Metabolomics* 12, 30.
- Fenn, J.B., Mann, M., Meng, C.K., Wong, S.F., and Whitehouse, C.M. (1989). Electrospray ionization for mass spectrometry of large biomolecules. *Science* 246, 64–71.
- Fenn, J.B., Mann, M., Meng, C.K., Wong, S.F., and Whitehouse, C.M. (1990). Electrospray ionization—principles and practice. *Mass Spectrom Rev* 9, 37–70.
- Fernandes, B., Sagman, U., Auger, M., Demetrio, M., and Dennis, J.W. (1991).  $\beta$ 1–6 branched oligosaccharides as a marker of tumor progression in human breast and colon neoplasia. *Cancer Res* 51, 718–723.
- Fischer, W.H., Rivier, J.E., and Craig, A.G. (1993). In situ reduction suitable for matrix-assisted laser desorption/ionization and liquid secondary ionization using tris(2-carboxyethyl)phosphine. *Rapid Commun Mass Spectrom* 7, 225–228.
- Fletcher, C.D.M., Bridge, J.A., Hogendoorn, P.C.W., and Mertens, F. (2013). World Health Organization classification of tumours. Pathology and genetics of tumours of soft tissue and bone. 4th ed. Lyon: IARC Press.
- Fletcher, C.D.M. (2014). The evolving classification of soft tissue tumours - an update based on the new 2013 WHO classification. *Histopathology* 64, 2–11.
- Franck, J., El Ayed, M., Wisztorski, M., Salzet, M., and Fournier, I. (2009). On-tissue N-terminal peptide derivatizations for enhancing protein identification in MALDI mass spectrometric imaging strategies. *Anal Chem* 81, 8305–8317.
- Francl, T.J., Sherman, M.G., Hunter, R.L., Locke, M.J., Bowers, W.D., and McIver, R.T. (1983). Experimental determination of the effects of space charge on ion cyclotron resonance frequencies. *Int J Mass Spectrom Ion Process* 54, 189–199.
- Frankevich, V.E., Zhang, J., Friess, S.D., Dashtiev, M., and Zenobi, R. (2003). Role of electrons in laser desorption/ionization mass spectrometry. *Anal Chem* 75, 6063–6067.
- Freeze, H.H. (2006). Genetic defects in the human glycome. *Nat Rev Genet* 7, 537–551.
- Frese, C.K., Altaalar, A.F.M., Hennrich, M.L., Nolting, D., Zeller, M., Griep-Raming, J., Heck, A.J.R., and Mohammed, S. (2011). Improved peptide identification by targeted fragmentation using CID, HCD and ETD on an LTQ-Orbitrap Velos. *J Proteome Res* 10, 2377–2388.
- Frese, C.K., Mikhaylova, M., Stucchi, R., Gautier, V., Liu, Q., Mohammed, S., Heck, A.J.R., Altaalar, A.F.M., and Hoogenraad, C.C. (2017). Quantitative map of proteome dynamics during neuronal differentiation. *Cell Rep* 18, 1527–1542.

- Fritchie, K.J., Goldblum, J.R., Tubbs, R.R., Sun, Y., Carver, P., Billings, S.D., and Rubin, B.P. (2012). The expanded histologic spectrum of myxoid liposarcoma with an emphasis on newly described patterns: implications for diagnosis on small biopsy specimens. *Am J Clin Pathol* 137, 229–239.
- Ganisl, B., Valovka, T., Hartl, M., Taucher, M., Bister, K., and Breuker, K. (2011). Electron detachment dissociation for top-down mass spectrometry of acidic proteins. *Chem Eur J* 17, 4460–4469.
- Gatlin, C.L., Eng, J.K., Cross, S.T., Detter, J.C., and Yates, J.R. (2000). Automated identification of amino acid sequence variations in proteins by HPLC/microspray tandem mass spectrometry. *Anal Chem* 72, 757–763.
- Gerlinger, M., Rowan, A., Horswell, S., Larkin, J., Endesfelder, D., Gronroos, E., Martinez, P., Matthews, N., Stewart, A., Tarpey, P., et al. (2012). Intratumor Heterogeneity and Branched Evolution Revealed by Multiregion Sequencing. *N Engl J Med* 366, 883–892.
- Glish, G.L., and Vachet, R.W. (2003). The basics of mass spectrometry in the twenty-first century. *Nat Rev Drug Discov* 2, 140–150.
- Goodwin, R.J. (2012). Sample preparation for mass spectrometry imaging: small mistakes can lead to big consequences. *J Proteomics* 75, 4893–4911.
- Graadt van Roggen, J.F., Hogendoorn, P.C., and Fletcher, C.D. (1999). Myxoid tumours of soft tissue. *Histopathology* 35, 291–312.
- Granovsky, M., Fata, J., Pawling, J., Muller, W.J., Khokha, R., and Dennis, J.W. (2000). Suppression of tumor growth and metastasis in Mgat5-deficient mice. *Nat Med* 6, 306–312.
- Grassl, J., Taylor, N.L., and Millar, A.H. (2011). Matrix-assisted laser desorption/ionisation mass spectrometry imaging and its development for plant protein imaging. *Plant Methods* 7, 21.
- Greaves, and Maley (2012). Clonal evolution in cancer. *Nature* 481, 306–313.
- Green-Mitchell, S.M., Cazares, L.H., Semmes, O.J., Nadler, J.L., and Nyalwidhe, J.O. (2011). On-tissue identification of insulin: in situ reduction coupled with mass spectrometry imaging. *Proteomics Clin Appl* 5, 448–453.
- Grey, A.C., Chaurand, P., Caprioli, R.M., and Schey, K.L. (2009). MALDI imaging mass spectrometry of integral membrane proteins from ocular lens and retinal tissue. *J Proteome Res* 8, 3278–3283.
- Groeneveld, G., de Puit, M., Bleay, S., Bradshaw, R., and Francese, S. (2015). Detection and mapping of illicit drugs and their metabolites in fingerprints by MALDI MS and compatibility with forensic techniques. *Sci Rep* 5, 11716.
- Groseclose, M.R., and Castellino, S. (2013). A mimetic tissue model for the quantification of drug distributions by MALDI imaging mass spectrometry. *Anal Chem* 85, 10099–10106.
- Groseclose, M.R., Andersson, M., Hardesty, W.M., and Caprioli, R.M. (2007). Identification of proteins directly from tissue: in situ tryptic digestions coupled with imaging mass spectrometry. *J Mass Spectrom* 42, 254–262.
- Groseclose, M.R., Massion, P.P., Chaurand, P., and Caprioli, R.M. (2008). High-throughput proteomic analysis of formalin-fixed paraffin-embedded tissue microarrays using MALDI imaging mass spectrometry. *Proteomics* 8, 3715–3724.
- Guilhaus, M., Mlynski, V., and Selby, D. (1997). Perfect timing: time-of-flight mass spectrometry. *Rapid Commun Mass Spectrom* 11, 951–962.
- Gustafsson, O.J.R., Oehler, M.K., Ruszkiewicz, A., McColl, S.R., and Hoffmann, P. (2011). MALDI Imaging Mass Spectrometry (MALDI-IMS) - application of spatial proteomics for ovarian cancer classification and diagnosis. *Int J Molecular Sci* 12, 773–794.
- Gustafsson, O.J.R., Eddes, J.S., Meding, S., McColl, S.R., Oehler, M.K., and Hoffmann, P. (2013). Matrix-assisted laser desorption/ionization imaging protocol for in situ characterization of tryptic peptide identity and distribution in formalin-fixed tissue. *Rapid Commun Mass Spectrom* 27, 655–670.
- Gustafsson, O.J.R., Briggs, M.T., Condina, M.R., Winderbaum, L.J., Pelzing, M., McColl, S.R., Everest-Dass, A.V., Packer, N.H., and Hoffmann, P. (2015). MALDI imaging mass spectrometry of N-linked glycans on formalin-fixed paraffin-embedded murine kidney. *Anal Bioanal Chem* 407, 2127–2139.
- Hamm, G., Bonnel, D., Legouffe, R., Pamelard, F., Delbos, J.-M., Bouzom, F., and Stauber, J. (2012). Quantitative mass spectrometry imaging of propranolol and olanzapine using tissue extinction calculation as normalization factor. *J Proteomics* 75, 4952–4961.
- Han, H., Pappin, D., Ross, P., and McLuckey, S. (2008). Electron transfer dissociation of iTRAQ labeled peptide ions. *J Proteome Res* 7, 3643–3648.
- Hankin, J.A., Barkley, R.M., and Murphy, R.C. (2007). Sublimation as a method of matrix application for mass spectrometric imaging. *J Am Soc Mass Spectrom* 18, 1646–1652.
- Hanton, S.D., Cornelio Clark, P.A., and Owens, K.G. (1999). Investigations of matrix-assisted laser desorption/ionization sample preparation by time-of-flight secondary ion mass spectrometry. *J Am Soc Mass Spectrom* 10, 104–111.
- Hattori, K., Kajimura, M., Hishiki, T., Nakanishi, T., Kubo, A., Nagahata, Y., Ohmura, M., Yachie-Kinoshita, A., Matsuura, T., Morikawa, T., et al. (2010). Paradoxical ATP elevation in ischemic penumbra revealed by quantitative imaging mass spectrometry. *Antioxid Redox Signal* 13, 1157–1167.
- Heijs, B., Carreira, R.J., Tolner, E.A., de Ru, A.H., Maagdenberg, A.M., van Veelen, P.A., and McDonnell, L.A. (2015). Comprehensive analysis of the mouse brain proteome sampled in mass spectrometry imaging. *Anal Chem* 87, 1867–1875.
- Heijs, B., Holst, S., Briaire-de Bruijn, I.H., Pelt, G., de Ru, A.H., van Veelen, P.A., Drake, R.R., Mehta, A.S., Mesker, W.E., Tollenaar, R.A., et al. (2016). Multimodal mass spectrometry imaging of N-glycans and proteins from the same tissue section. *Anal Chem* 88, 7745–7753.
- Himmelsbach, M. (2012). 10 years of MS instrumental developments – impact on LC-MS/MS in clinical chemistry. *J Chromatogr B Analyt Technol Biomed Life Sci* 883–884, 3–17.



- Hoffman, A., Ghadimi, M.P.H., Demicco, E.G., Creighton, C.J., Torres, K., Colombo, C., Peng, T., Lusby, K., Ingram, D., Hornick, J.L., et al. (2013). Localized and metastatic myxoid/round cell liposarcoma: clinical and molecular observations. *Cancer* 119, 1868-1877.
- Hohmann, L., Sherwood, C., Eastham, A., Peterson, A., Eng, J.K., Eddes, J.S., Shteynberg, D., and Martin, D.B. (2009). Proteomic analyses using *Grifola frondosa* metalloendoprotease Lys-N. *J Proteome Res* 8, 1415-1422.
- Holle, A., Haase, A., Kayser, M., and Höhdorf, J. (2006). Optimizing UV laser focus profiles for improved MALDI performance. *J Mass Spectrom* 41, 705-716.
- Holst, S., Wuhrer, M., and Rombouts, Y. (2015). *Advances in Cancer Research*.
- Holst, S., Heijs, B., de Haan, N., van Zeijl, R.J.M., Briaire-de Bruijn, I.H., van Pelt, G.W., Mehta, A.S., Angel, P.M., Mesker, W.E., Tollenaar, R.A., et al. (2016). Linkage-specific in situ sialic acid derivatization for N-glycan mass spectrometry imaging of formalin-fixed paraffin-embedded tissues. *Anal Chem* 88, 5904-5913.
- Houel, S., Abernathy, R., Renganathan, K., Meyer-Arendt, K., Ahn, N.G., and Old, W.M. (2010). Quantifying the impact of chimera MS/MS spectra on peptide identification in large-scale proteomics studies. *J Proteome Res* 9, 4152-4160.
- Hurvitz, S.A., Hu, Y., O'Brien, N., and Finn, R.S. (2013). Current approaches and future directions in the treatment of HER2-positive breast cancer. *Cancer Treat Rev* 39, 219-229.
- Ibáñez, A.J., Muck, A., and Svatoš, A. (2007). Dissipation of charge on MALDI-TOF polymeric chips using an electron-acceptor: analysis of proteins. *J Mass Spectrom* 42, 634-640.
- Itkonen, H., and Mills, I. (2015). *Receptor Tyrosine Kinases* (Springer).
- Jansen, B.C., Reiding, K.R., Bondt, A., Ederveen, A.L., Palmblad, M., Falck, D., and Wuhrer, M. (2015). MassyTools: a high-throughput targeted data processing tool for relative quantitation and quality control developed for glycomic and glycoproteomic MALDI-MS. *J Proteome Res* 14, 5088-5098.
- Jennings, K.R. (1968). Collision-induced decompositions of aromatic molecular ions. *Int J Mass Spectrom Ion Phys* 1, 227-235.
- Jensen, L.J., Kuhn, M., Stark, M., Chaffron, S., Creevey, C., Muller, J., Doerks, T., Julien, P., Roth, A., Simonovic, M., et al. (2009). STRING 8 - a global view on proteins and their functional interactions in 630 organisms. *Nucleic Acids Res* 37, D412-D416.
- Johnson, R.S., Martin, S.A., Biemann, K., Stults, J.T., Watson, J.T. (1987). Novel fragmentation process of peptides by collision-induced decomposition in a tandem mass spectrometer: differentiation of leucine and isoleucine. *Anal Chem* 59, 2621-2625.
- Jones, E.A., van Remoortere, A., van Zeijl, R.J.M., Hogendoorn, P.C., Bovée, J.V., Deelder, A.M., and McDonnell, L.A. (2011). Multiple statistical analysis techniques corroborate intratumor heterogeneity in imaging mass spectrometry datasets of myxofibrosarcoma. *PLoS ONE* 6, e24913.
- Jones, E.A., Schmitz, N., Waaijer, C.J., Frese, C.K., van Remoortere, A., van Zeijl, R.J.J., Heck, A.J., Hogendoorn, P.C., Deelder, A.M.M., Altelaar, A.F., et al. (2013). Imaging mass spectrometry-based molecular histology differentiates microscopically identical and heterogeneous tumors. *J. Proteome Res.* 12, 1847-1855.
- Kaftan, F., Vrkoslav, V., Kynast, P., Kulkarni, P., Böcker, S., Cvačka, J., Knaden, M., and Svatoš, A. (2014). Mass spectrometry imaging of surface lipids on intact *Drosophila melanogaster* flies. *J Mass Spectrom* 49, 223-232.
- Källback, P., Shariatgorji, M., Nilsson, A., and Andrén, P.E. (2012). Novel mass spectrometry imaging software assisting labeled normalization and quantitation of drugs and neuropeptides directly in tissue sections. *J Proteomics* 75, 4941-4951.
- Kaprio, T., Satomaa, T., Heiskanen, A., Hokke, C.H., Deelder, A.M., Mustonen, H., Hagström, J., Carpen, O., Saarinen, J., and Haglund, C. (2015). N-glycomic profiling as a tool to separate rectal adenomas from carcinomas. *Mol Cell Proteomics* 14, 277-288.
- Karas, M., and Hillenkamp, F. (1988). Laser desorption ionization of proteins with molecular masses exceeding 10,000 daltons. *Anal Chem* 60, 2299-2301.
- Karas, M., Bachmann, D., Bahr, U., and Hillenkamp, F. (1987). Matrix-assisted ultraviolet laser desorption of non-volatile compounds. *Int J Mass Spectrom Ion Proc* 78, 53-68.
- Kaspar, S., Peukert, M., Svatos, A., Matros, A., and Mock, H.P. (2011). MALDI-imaging mass spectrometry - an emerging technique in plant biology. *Proteomics* 11, 1840-1850.
- Kaufman, M., and Bard, J. (1999). *The anatomical basis of mouse development*. 1st ed. San Diego: Academic Press.
- Kawamoto, T. (2003). Use of a new adhesive film for the preparation of multi-purpose fresh-frozen sections from hard tissues, whole-animals, insects and plants. *Arch Histol Cytol* 66, 123-143.
- Kero, F.A., Pedder, R.E., and Yost, R.A. (2005). Quadrupole mass analyzers: theoretical and practical considerations. *Encyclopedia of Genetics, Genomics, Proteomics and Bioinformatics*. 3:3.1:8.
- Kertesz, V., and Berkel, G.J. (2010). Fully automated liquid extraction-based surface sampling and ionization using a chip-based robotic nanoelectrospray platform. *J Mass Spectrom* 45, 252-260.
- Keuschnigg, J., Henttinen, T., Auvinen, K., Karikoski, M., Salmi, M., and Jalkanen, S. (2009). The prototype endothelial marker PAL-E is a leukocyte trafficking molecule. *Blood* 114, 478-484.
- Khalil, S.M., Römpf, A., Pretzel, J., Becker, K., and Spengler, B. (2015). Phospholipid topography of whole-body sections of the *Anopheles stephensi* mosquito, characterized by high-resolution atmospheric-pressure scanning microprobe matrix-assisted laser desorption/ionization mass spectrometry imaging. *Anal Chem* 87, 11309-11316.
- Klein, S., Staring, M., Murphy, K., Viergever, M.A., and Pluim, J.P. (2010). Elastix: a toolbox for intensity-based medical image registration. *IEEE Trans Med Imaging* 29, 196-205.
- Klein, S., Staring, M., Andersson, P., and Pluim, J.P. (2011). Preconditioned stochastic gradient descent optimisation for monomodal image registration. *Med Image Comput Assist Interv* 14, 549-556.

- Knochenmuss, R. (2004). Photoionization pathways and free electrons in UV-MALDI. *Anal Chem* 76, 3179–3184.
- Krause, E., Wenschuh, H., and Jungblut P.R. (1999). The dominance of arginine-containing peptides in MALDI-derived tryptic mass fingerprints of proteins. *Anal Chem* 71, 4160–4165.
- Kriegsmann, M., Casadonte, R., Kriegsmann, J., Dienemann, H., Schirmacher, P., Hendrik Kobarg, J., Schwamborn, K., Stenzinger, A., Warth, A., and Weichert, W. (2016). Reliable entity subtyping in non-small cell lung cancer by matrix-assisted laser desorption/ionization imaging mass spectrometry on formalin-fixed paraffin-embedded tissue specimens. *Mol Cell Proteomics* 15, 3081–3089.
- Krusemark, C.J., Frey, B.L., Belshaw, P.J., and Smith, L.M. (2009). Modifying the charge state distribution of proteins in electrospray ionization mass spectrometry by chemical derivatization. *J Am Soc Mass Spectrom* 20, 1617–1625.
- Kulak, N.A., Pichler, G., Paron, I., Nagaraj, N., and Mann, M. (2014). Minimal, encapsulated proteomic-sample processing applied to copy-number estimation in eukaryotic cells. *Nat Methods* 11, 319–324.
- Lanekoff, I., Burnum-Johnson K., Thomas, M., Short, J., Carson, J.P., Cha, J., Dey, S.K., Yang, P., Prieto Conaway, M.C., Laskin, J. (2013). High-speed tandem mass spectrometric in situ imaging by nanospray desorption electrospray ionization mass spectrometry. *Anal Chem* 85, 9596–9603.
- Ledford, E.B. Jr, Rempel, D.L., and Gross M.L. (1984). Space charge effects in Fourier transform mass spectrometry. Mass calibration. *Anal Chem* 56, 2744–2748.
- Lee, J.Y., Kim, J.Y., Park, G.W., Cheon, M.H., Kwon, K.-H., Ahn, Y.H., Moon, M.H., Lee, H.J., Paik, Y.K., and Yoo, J.S. (2011). Targeted mass spectrometric approach for biomarker discovery and validation with nonglycosylated tryptic peptides from N-linked glycoproteins in human plasma. *Mol Cell Proteomics* 10, M111.009290.
- Lemaire, R., Wisztorski, M., Desmons, A., Tabet, J.C., Day, R., Salzert, M., and Fournier, I. (2006). MALDI-MS direct tissue analysis of proteins: improving signal sensitivity using organic treatments. *Anal Chem* 78, 7145–7153.
- Lemaire, R., Desmons, A., Tabet, J.C., Day, R., Salzert, M., and Fournier, I. (2007). Direct analysis and MALDI imaging of formalin-fixed, paraffin-embedded tissue sections. *J Proteome Res* 6, 1295–1305.
- Lemeur, M., Mattei, J.-C., Souteyrand, P., Chagnaud, C., Curvale, G., and Rochwerger, A. (2015). Prognostic factors for the recurrence of myxoid liposarcoma: 20 cases with up to 8 years follow-up. *Orthop Traumatol Surg Res* 101, 103–107.
- Lin, T.-W., Chang, H.-T., Chen, C.-H., Chen, C.-H., Lin, S.-W., Hsu, T.-L., and Wong, C.-H. (2015). Galectin-3 binding protein and galectin-1 interaction in breast cancer cell aggregation and metastasis. *J Am Chem Soc* 137, 9685–9693.
- Liu, D.Q., and Hop, C.E. (2005). Strategies for characterization of drug metabolites using liquid chromatography-tandem mass spectrometry in conjunction with chemical derivatization and on-line H/D exchange approaches. *J Pharm Biomed Anal* 37, 1–18.
- Liu, X., Ide, J.L., Norton, I., Marchionni, M.A., Ebling, M.C., Wang, L.Y., Davis, E., Sauvageot, C.M., Kesari, S., Kellersberger, K.A., et al. (2013a). Molecular imaging of drug transit through the blood-brain barrier with MALDI mass spectrometry imaging. *Sci Rep* 3, 2859.
- Liu, X., Nie, H., Zhang, Y., Yao, Y., Maitikabili, A., Qu, Y., and Shi, S (2013b). Cell surface-specific N-glycan profiling in breast cancer. *PLoS One* 8, e72704.
- Lou, S., Balluff, B., de Graaff, M.A., Cleven, A.H., Briaire-de Bruijn, I., Bovée, J.V., and McDonnell, L.A. (2016a). High-grade sarcoma diagnosis and prognosis: biomarker discovery by mass spectrometry imaging. *Proteomics* 16, 1802–1813.
- Lou, S., Balluff, B., Cleven, A.H., Bovée, J.V., and McDonnell, L.A. (2016b). An experimental guideline for the analysis of histologically heterogeneous tumors by MALDI-TOF mass spectrometry imaging. *Biochim Biophys Acta* S1570-9639, 30205–30209.
- Lou, S., Balluff, B., Cleven, A.H., Bovée, J.V., and McDonnell, L.A. (2017). Prognostic Metabolite Biomarkers for Soft Tissue Sarcomas Discovered by Mass Spectrometry Imaging. *J. Am. Soc. Mass Spectrom.* 28, 376–383.
- Maes, F., Collignon, A., Vandermeulen, D., Marchal, G., and Suetens, P. (1997). Multimodality image registration by maximization of mutual information. *IEEE Trans Med Imaging* 16, 187–198.
- Maier, S.K., Hahne, H., Gholami, A.M., Balluff, B., Meding, S., Schoene, C., Walch, A.K., and Kuster, B. (2013). Comprehensive identification of proteins from MALDI imaging. *Mol Cell Proteomics* 12, 2901–2910.
- Makarov, A. (2000). Electrostatic axially harmonic orbital trapping: a high-performance technique of mass analysis. *Anal Chem* 72, 1156–1162.
- Maleki, H., Kondalaji, S.G., Khakinejad, M., and Valentine, S.J. (2016). Structural assignments of sulfur-containing compounds in crude oil using ion mobility spectrometry-mass spectrometry (IMS-MS). *Energy Fuels* 30, 9150–9161.
- Mamyrin, B.A., Karataev, V.I., Shmikk, D.V., and Zagulin, V.A. (1973). The mass-reflectron, a new nonmagnetic time-of-flight mass spectrometer with high resolution. *Zh Eksp Teor Fiz* 64, 82–89.
- Markesbery, W.R. (1997). Oxidative stress hypothesis in Alzheimer's disease. *Free Radic Biol Med* 23, 134–147.
- Marshall, A.G., Hendrickson, C.L., and Jackson, G.S. (1998). Fourier transform ion cyclotron resonance mass spectrometry: A primer. *Mass Spectrom Rev* 17, 1–35.
- Marshall, A.G. (1998). Fourier transform ion cyclotron resonance mass spectrometry. *AIP Conf Proc* 430, 3.
- Martin-Lorenzo, M., Alvarez-Llamas, G., McDonnell, L.A., and Vivanco, F. (2015). Molecular histology of arteries: mass spectrometry imaging as a novel ex vivo tool to investigate atherosclerosis. *Expert Rev Proteomics* 13, 69–81.
- McDonnell, L.A., and Heeren, R.M. (2007). Imaging mass spectrometry. *Mass Spectrom Rev* 26, 606–643.
- McDonnell, L.A., Walch, A.K., Stoekli, M., and Corthals, G.L. (2014). MSiMass list: a public database of identifications for protein MALDI MS imaging. *J Proteome Res* 13, 1138–1142.

- McLafferty, F.W., Bente, P.F., Kornfeld, R., Tsai, S.-C., and Howe, I. (1973). Metastable ion characteristics. XXII. Collisional activation spectra of organic ions. *J Am Chem Soc* 95, 2120–2129.
- McLean, J.A., Ridenour, W.B., and Caprioli, R.M. (2007). Profiling and imaging of tissues by imaging ion mobility-mass spectrometry. *J Mass Spectrom* 42, 1099–1105.
- Meding, S., Nitsche, U., Balluff, B., Elsner, M., Rauser, S., Schöne, C., Nipp, M., Maak, M., Feith, M., Ebert, M., et al. (2012). Tumor classification of six common cancer types based on proteomic profiling by MALDI imaging. *J Proteome Res* 11, 1996–2003.
- Meding, S., Martin, K., Gustafsson, O.J.R., Eddes, J.S., Hack, S., Oehler, M.K., and Hoffmann, P. (2013). Tryptic peptide reference data sets for MALDI imaging mass spectrometry on formalin-fixed ovarian cancer tissues. *J Proteome Res* 12, 308–315.
- Melikian, A.A., O'Connor, R., Prahald, A.K., Hu, P., Li, H., Kagan, M., and Thompson, S. (1999). Determination of the urinary benzene metabolites S-phenylmercapturic acid and trans,trans-muconic acid by liquid chromatography-tandem mass spectrometry. *Carcinogenesis* 20, 719–726.
- Min, Y., Kristiansen, K., and Boggs, J.M., Husted, C., Zasadzinski, J.A., Israelachvili, J. (2009). Interaction forces and adhesion of supported myelin lipid bilayers modulated by myelin basic protein. *Proc Natl Acad Sci USA* 106, 3154–3159.
- Miyoshi, E., and Nakano, M. (2008). Fucosylated haptoglobin is a novel marker for pancreatic cancer: detailed analyses of oligosaccharide structures. *Proteomics* 8, 3257–3262.
- Morth, J.P., Poulsen, H., Toustrup-Jensen, M.S., Schack, V.R., Egebjerg, J., Andersen, J.P., Vilsen, B., and Nissen, P. (2009). The structure of the Na<sup>+</sup>,K<sup>+</sup>-ATPase and mapping of isoform differences and disease-related mutations. *Philos Trans R Soc Lond B Biol Sci* 364, 217–227.
- Mótyán, J.A., Tóth, F., and Tőzser, J. (2013). Research applications of proteolytic enzymes in molecular biology. *Biomolecules* 3, 923–942.
- Muinelo-Romay, L., Vázquez-Martín, C., Villar-Portela, S., Cuevas, E., Gil-Martín, E., and Fernández-Briera, A. (2008). Expression and enzyme activity of alpha(1,6)fucosyltransferase in human colorectal cancer. *Int J Cancer* 123, 641–646.
- Mulder, I.A., Esteve, C., Wermer, M.J., Hoehn, M., Tolner, E.A., van den Maagdenberg, A.M.J.M., and McDonnell, L.A. (2016). Funnel-freezing versus heat-stabilization for the visualization of metabolites by mass spectrometry imaging in a mouse stroke model. *Proteomics* 16, 1652–1659.
- Muller, L., Kailas, A., Jackson, S.N., Roux, A., Barbacci, D.C., Schultz, J.A., Balaban, C.D., and Woods, A.S. (2015). Lipid imaging within the normal rat kidney using silver nanoparticles by matrix-assisted laser desorption/ionization mass spectrometry. *Kidney Int* 88, 186–192.
- Negri, T., Viridis, E., Brich, S., Bozzi, F., Tamborini, E., Tarantino, E., Jocolè, G., Cassinelli, G., Grosso, F., Sanfilippo, R., et al. (2010). Functional mapping of receptor tyrosine kinases in myxoid liposarcoma. *Clin Cancer Res* 16, 3581–3593.
- Nemes, P., and Vertes, A. (2007). Laser ablation electrospray ionization for atmospheric pressure, in vivo, and imaging mass spectrometry. *Anal Chem* 79, 8098–8106.
- Nezu, Y., Hagiwara, K., Yamamoto, Y., Fujiwara, T., Matsuo, K., Yoshida, A., Kawai, A., Saito, T., and Ochiya, T. (2016). miR-135b, a key regulator of malignancy, is linked to poor prognosis in human myxoid liposarcoma. *Oncogene* 35, 6177–6188.
- Nicklay, J.J., Harris, G.A., Schey, K.L., and Caprioli, R.M. (2013). MALDI imaging and in situ identification of integral membrane proteins from rat brain tissue sections. *Anal Chem* 85, 7191–7196.
- Nikolaev, E.N., Kostyukovich, Y.I., and Vladimirov, G.N. (2016). Fourier transform ion cyclotron resonance (FT ICR) mass spectrometry: theory and simulations. *Mass Spectrom Rev* 35, 219–258.
- Nishida, Y., Tsukushi, S., Nakashima, H., and Ishiguro, N. (2010). Clinicopathologic prognostic factors of pure myxoid liposarcoma of the extremities and trunk wall. *Clin Orthop Relat Res* 468, 3041–3046.
- Nonami, H., Fukui, S., and Erra-Balsells, R. (1997).  $\beta$ -carboline alkaloids as matrices for matrix-assisted ultraviolet laser desorption time-of-flight mass spectrometry of proteins and sulfated oligosaccharides: a comparative study using phenylcarbonyl compounds, carbazoles and classical matrices. *J Mass Spectrom* 32, 287–296.
- Nordström, A., Want, E., Northen, T., Lehtiö, J., and Siuzdak, S. (2008). Multiple ionization mass spectrometry strategy used to reveal the complexity of metabolomics. *Anal Chem* 80, 421–429.
- Oviaño, M., Sparbier, K., Barba, M.J., Kostrzewa, M., and Bou, G. (2016). Universal protocol for the rapid automated detection of carbapenem-resistant Gram-negative bacilli directly from blood cultures by matrix-assisted laser desorption/ionisation time-of-flight mass spectrometry (MALDI-TOF/MS). *Int J of Antimicrob Agents* 48, 655–660.
- Park, S.-Y., Lee, S.-H., Kawasaki, N., Itoh, S., Kang, K., Hee Ryu, S., Hashii, N., Kim, J.-M., Kim, J.-Y., and Hoe Kim, J. (2011).  $\alpha$ 1-3/4 fucosylation at Asn 241 of  $\beta$ -haptoglobin is a novel marker for colon cancer: a combinatorial approach for development of glycan biomarkers. *Int J Cancer* 130, 2366–2376.
- Pecoraro, V., Roli, L., Plebani, M., and Trenti, T. (2016). Clinical utility of the (-2) proPSA and evaluation of the evidence: a systematic review. *Clin Chem Lab Med* 54, 1123–1132.
- Peukert, M., Matros, A., Lattanzio, G., Kaspar, S., Abadía, J., and Mock, H.P. (2012). Spatially resolved analysis of small molecules by matrix-assisted laser desorption/ionization mass spectrometric imaging (MALDI-MSI). *New Phytol* 193, 806–815.
- Pinho, S.S., and Reis, C.A. (2015). Glycosylation in cancer: mechanisms and clinical implications. *Nat Rev Cancer* 15, 540–555.
- Plum, J.P., Maintz, J.B., and Viergever, M.A. (2003). Mutual-information-based registration of medical images: a survey. *IEEE Trans Med Imaging* 22, 986–1004.

- Porta, T., Lesur, A., Varesio, E., and Hopfgartner, G. (2015). Quantification in MALDI-MS imaging: what can we learn from MALDI-selected reaction monitoring and what can we expect for imaging? *Anal Bioanal Chem* 407, 2177–2187.
- Porter, A., Irwin, R., Miller, J., Horan, D.J., Robling, A.G., and McCabe, L.R. (2017). Quick and inexpensive paraffin-embedding method for dynamic bone formation analyses. *Sci Rep* 7, 42505.
- Poté, N., Alexandrov, T., Faouder, J., Laouirem, S., Léger, T., Mebarki, M., Belghiti, J., Camadro, J.-M., Bedossa, P., and Paradis, V. (2013). Imaging mass spectrometry reveals modified forms of histone H4 as new biomarkers of microvascular invasion in hepatocellular carcinomas. *Hepatology* 58, 983–994.
- Poulsen, H., Khandelia, H., Morth, J.P., Bublitz, M., Mouritsen, O.G., Egebjerg, J., and Nissen, P. (2010). Neurological disease mutations compromise a C-terminal ion pathway in the Na(+)/K(+)-ATPase. *Nature* 467, 99–102.
- Powers, M.P., Wang, W.-L.L., Hernandez, V.S., Patel, K.S., Lev, D.C., Lazar, A.J., and López-Terrada, D.H. (2010). Detection of myxoid liposarcoma-associated FUS-DDIT3 rearrangement variants including a newly identified breakpoint using an optimized RT-PCR assay. *Mod Pathol* 23, 1307–1315.
- Powers, T.W., Jones, E.E., Betesh, L.R., Romano, P.R., Gao, P., Copland, J.A., Mehta, A.S., and Drake, R.R. (2013). Matrix assisted laser desorption ionization imaging mass spectrometry workflow for spatial profiling analysis of N-linked glycan expression in tissues. *Anal Chem* 85, 9799–9806.
- Powers, T.W., Neely, B.A., Shao, Y., Tang, H., Troyer, D.A., Mehta, A.S., Haab, B.B., and Drake, R.R. (2014). MALDI imaging mass spectrometry profiling of N-glycans in formalin-fixed paraffin embedded clinical tissue blocks and tissue microarrays. *PLoS ONE* 9, e106255.
- Powers, T.W., Holst, S., Wuhrer, M., Mehta, A.S., and Drake, R.R. (2015). Two-dimensional N-glycan distribution mapping of hepatocellular carcinoma tissues by MALDI-imaging mass spectrometry. *Biomolecules* 5, 2554–2572.
- Prideaux, B., and Stoekli, M. (2012). Mass spectrometry imaging for drug distribution studies. *J Proteomics* 75, 4999–5013.
- Proskuryakov, S.Y., Konoplyannikov, A.G., and Gabai, V.L. (2003). Necrosis: a specific form of programmed cell death? *Exp Cell Res* 283, 1–16.
- Puolitaival, S.M., Burnum, K.E., Cornett, D.S., and Caprioli, R.M. (2008). Solvent-free matrix dry-coating for MALDI imaging of phospholipids. *J Am Soc Mass Spectrom* 19, 882–886.
- Qi, Y., and Volmer, D.A. (2017). Electron-based fragmentation methods in mass spectrometry: an overview. *Mass Spectrom Rev* 36, 4–15.
- Qiao, H., Spicer, V., and Ens, W. (2008). The effect of laser profile, fluence, and spot size on sensitivity in orthogonal-injection matrix-assisted laser desorption/ionization time-of-flight mass spectrometry. *Rapid Commun Mass Spectrom* 22, 2779–2790.
- Radionova, A., Filippov, I., and Derrick, P.J. (2016). In pursuit of resolution in time-of-flight mass spectrometry: a historical perspective. *Mass Spectrom Rev* 35, 738–757.
- Rao, W., Celiz, A.D., Scurr, D.J., Alexander, M.R., and Barrett, D.A. (2013). Ambient DESI and LESA-MS analysis of proteins adsorbed to a biomaterial surface using in-situ surface tryptic digestion. *J Am Soc Mass Spectrom* 24, 1927–1936.
- Reilly, J.P. (2009). Ultraviolet photofragmentation of biomolecular ions. *Mass Spectrom Rev* 28, 425–447.
- Reyzer, M.L., Hsieh, Y., Ng, K., Korfmacher, W.A., and Caprioli, R.M. (2003). Direct analysis of drug candidates in tissue by matrix-assisted laser desorption/ionization mass spectrometry. *J Mass Spectrom* 38, 1081–1092.
- Rietschel, B., Arrey, T.N., Meyer, B., Bornemann, S., Schuerken, M., Karas, M., and Poetsch, A. (2008). Elastase digests: new ammunition for shotgun membrane proteomics. *Mol Cell Proteomics* 8, 1029–1043.
- Riley, N.M., Rush, M.J., Rose, C.M., Richards, A.L., Kwicien, N.W., Bailey, D.J., Hebert, A.S., Westphall, M.S., and Coon, J.J. (2015). The negative mode proteome with activated ion negative electron transfer dissociation (AI-NETD). *Mol Cell Proteome* 14, 2644–2660.
- Roepstorff, P., Fohlman, J. (1984). Proposal for a common nomenclature for sequence ions in mass spectra of peptides. *Biomed Mass Spectrom* 11, 601.
- Ronci, M., Bonanno, E., Colantoni, A., Pieroni, L., Ilio, C., Spagnoli, L.G., Federici, G., and Urbani, A. (2008). Protein unlocking procedures of formalin-fixed paraffin-embedded tissues: application to MALDI-TOF imaging MS investigations. *Proteomics* 8, 3702–3714.
- Schober, Y., Schramm, T., Spengler, B., and Römpf, A. (2011). Protein identification by accurate mass matrix-assisted laser desorption/ionization imaging of tryptic peptides. *Rapid Commun Mass Spectrom* 25, 2475–2483.
- Schober, Y., Guenther, S., Spengler, B., and Römpf, A. (2012). High-resolution matrix-assisted laser desorption/ionization imaging of tryptic peptides from tissue. *Rapid Commun Mass Spectrom* 26, 1141–1146.
- Schwartz, S.A., Reyzer, M.L., and Caprioli, R.M. (2003). Direct tissue analysis using matrix-assisted laser desorption/ionization mass spectrometry: practical aspects of sample preparation. *J Mass Spectrom* 38, 699–708.
- Scigelova, M., Hornshaw, M., Giannakopoulos, A., and Makarov, A. (2011). Fourier transform mass spectrometry. *Mol Cell Proteomics* 10, M111.009431.
- Selman, M.H., Hemayatkar, M., Deelder, A.M., and Wuhrer, M. (2011). Cotton HILIC SPE microtips for microscale purification and enrichment of glycans and glycopeptides. *Anal Chem* 83, 2492–2499.
- Shariatgorji, M., Källback, P., Gustavsson, L., Schintu, N., Svenningsson, P., Goodwin, R.J., and Andren, P.E. (2012). Controlled-pH tissue cleanup protocol for signal enhancement of small molecule drugs analyzed by MALDI-MS imaging. *Anal Chem* 84, 4603–4607.
- Shariatgorji, M., Nilsson, A., Goodwin, R.J., Källback, P., Schintu, N., Zhang, X., Crossman, A.R., Bezdard, E., Svenningsson, P., Andren, P.E. (2014). Direct targeted quantitative molecular imaging of neurotransmitters in brain tissue sections. *Neuron* 84, 697–707.

- Shi, S.R., Taylor, C.R., Fowler, C.B., and Mason, J.T. (2013). Complete solubilization of formalin-fixed, paraffin-embedded tissue may improve proteomic studies. *Proteomics Clin Appl* 7, 264–272.
- Shi, S.R., Key, M.E., and Kalra, K.L. (1991). Antigen retrieval in formalin-fixed, paraffin-embedded tissues: an enhancement method for immunohistochemical staining based on microwave oven heating of tissue sections. *J Histochem Cytochem* 39, 741–748.
- Shimma, S., Furuta, M., Ichimura, K., Yoshida, Y., and Setou, M. (2006). Direct MS/MS analysis in mammalian tissue sections using MALDI-QIT-TOFMS and chemical inkjet technology. *Surf Interface Anal* 38, 1712–1714.
- Shimma, S., Sugiura, Y., Hayasaka, T., Zaima, N., Matsumoto, M., Setou, M. (2008). Mass imaging and identification of biomolecules with MALDI-QIT-TOF-based system. *Anal Chem* 80, 878–885.
- Shroff, R., and Svatoš, A. (2009). Proton sponge: a novel and versatile MALDI matrix for the analysis of metabolites using mass spectrometry. *Anal Chem* 81, 7954–7959.
- Siegel, G.J., Agranoff, B.W., Albers, R.W., Fisher, S.K., and Uhler, M.D. (1999). *Basic neurochemistry*. Philadelphia: Lippincott-Raven.
- Signor, L., and Boeri Erba, E. (2013). Matrix-assisted laser desorption/ionization time of flight (MALDI-TOF) mass spectrometric analysis of intact proteins larger than 100 kDa. *J Vis Exp* 79.
- Singh, R., Harshman, S., Ruppert, A.S., Mortazavi, A., Lucas, D.M., Thomas-Ahner, J.M., Clinton, S.K., Byrd, J.C., Freitas, M.A., and Parthun, M.R. (2015). Proteomic profiling identifies specific histone species associated with leukemic and cancer cells. *Clin Proteomics* 12, 22.
- De Sio, G., Smith, A.J., Galli, M., Garancini, M., Chinello, C., Bono, F., Pagni, F., and Magni, F. (2015). A MALDI-mass spectrometry imaging method applicable to different formalin-fixed paraffin-embedded human tissues. *Mol Biosyst* 11, 1507–1514.
- Slodzian, G., Daigne, B., Girard, F., Boust, F., and Hillion, F. (1992). Scanning secondary ion analytical microscopy with parallel detection. *Biol Cell* 74, 43–50.
- Smargiasso, N., Quinton, L., and De Pauw, E. (2012). 2-Aminobenzamide and 2-aminobenzoic acid as new MALDI matrices inducing radical mediated in-source decay of peptides and proteins. *J Am Soc Mass Spectrom* 23, 469–474.
- Smith, D.F., Klein, G.C., Yen, A.T., Squicciarini, M.P., Rodgers, R.P., and Marshall, A.G. (2008). Crude oil polar chemical composition derived from FT-ICR mass spectrometry accounts for asphaltene inhibitor specificity. *Energy Fuels* 22, 3112–3117.
- Spraggins, J.M., Rizzo, D.G., Moore, J.L., Rose, K.L., Hammer, N.D., Skaar, E.P., and Caprioli, R.M. (2015). MALDI FTICR IMS of intact proteins: using mass accuracy to link protein images with proteomics data. *J Am Soc Mass Spectrom* 26, 974–985.
- Stauber, J., MacAleese, L., Franck, J., Claude, E., Snel, M., Kaletas, B.K., Wiel, I.M., Wisztorski, M., Fournier, I., and Heeren, R.M. (2010). On-tissue protein identification and imaging by MALDI-ion mobility mass spectrometry. *J Am Soc Mass Spectrom* 21, 338–347.
- Steven, R.T., and Bunch, J. (2013). Repeat MALDI MS imaging of a single tissue section using multiple matrices and tissue washes. *Anal Bioanal Chem* 405, 4719–4728.
- Stoeckli, M., and Staab, D. (2015). Reproducible matrix deposition for MALDI MSI based on open-source software and hardware. *J Am Soc Mass Spectrom* 26, 911–914.
- Stoeckli, M., Farmer, T.B., Caprioli, R.M. (1999). Automated mass spectrometry imaging with a matrix-assisted laser desorption ionization time-of-flight instrument. *J Am Soc Mass Spectrom* 10, 67–71.
- Stoeckli, M., Chaurand, P., Hallahan, D.E., Caprioli, R.M. (2001). Imaging mass spectrometry: A new technology for the analysis of protein expression in mammalian tissues. *Nat Med* 7, 493–496.
- Stoeckli, M., Staab, D., and Schweitzer, A. (2007). Compound and metabolite distribution measured by MALDI mass spectrometric imaging in whole-body tissue sections. *Int J Mass Spectrom* 260, 195–202.
- Strohalm, M., Hassman, M., Kosata, B., and Kodíček, M. (2008). mMass data miner: an open source alternative for mass spectrometric data analysis. *Rapid Commun Mass Spectrom* 22, 905–908.
- Strohalm, M., Strohalm, J., Kaftan, F., Krásný, L., Volný, M., Novák, P., Ulbrich, K., and Havlíček, V. (2011). Poly[N-(2-hydroxypropyl)methacrylamide]-based tissue-embedding medium compatible with MALDI mass spectrometry imaging experiments. *Anal Chem* 83, 5458–5462.
- Sturm, R.M., Greer, T., Woodards, N., Gemperline, E., and Li, L. (2013). Mass spectrometric evaluation of neuropeptidomic profiles upon heat stabilization treatment of neuroendocrine tissues in crustaceans. *J Proteome Res* 12, 743–752.
- Sturtevant, D., Lee, Y.J., and Chapman, K.D. (2016). Matrix assisted laser desorption/ionization-mass spectrometry imaging (MALDI-MSI) for direct visualization of plant metabolites in situ. *Curr Opin Biotechnol* 37, 53–60.
- Sugiura, Y., Honda, K., Kajimura, M., and Suematsu, M. (2014). Visualization and quantification of cerebral metabolic fluxes of glucose in awake mice. *Proteomics* 14, 829–838.
- Svensson, M., Boren, M., Sköld, K., Fälth, M., Sjögren, B., Andersson, M., Svenningsson, P., and Andren, P.E. (2009). Heat stabilization of the tissue proteome: a new technology for improved proteomics. *J Proteome Res* 8, 974–981.
- Takáts, Z., Wiseman, J.M., Gologan, B., and Cooks, R.G. (2004). Mass spectrometry sampling under ambient conditions with desorption electrospray ionization. *Science* 306, 471–473.
- Takáts, Z., Wiseman, J.M., and Cooks, R.G. (2005). Ambient mass spectrometry using desorption electrospray ionization (DESI): instrumentation, mechanisms and applications in forensics, chemistry, and biology. *J Mass Spectrom* 40, 1261–1275.
- Tanca, A., Pagnozzi, D., and Addis, M.F. (2012). Setting proteins free: progresses and achievements in proteomics of formalin-fixed, paraffin-embedded tissues. *Proteomics Clin Appl* 6, 7–21.

- Taylor, B.S., Barretina, J., Maki, R.G., Antonescu, C.R., Singer, S., and Ladanyi, M. (2011). Advances in sarcoma genomics and new therapeutic targets. *Nat Rev Cancer* 11, 541–557.
- te Brake, L., Dian, S., Ganiem, A.R., Ruesen, C., Burger, D., Donders, R., Ruslami, R., van Crevel, R., and Aarnoutse, R. (2015). Pharmacokinetic/pharmacodynamic analysis of an intensified regimen containing rifampicin and moxifloxacin for tuberculous meningitis. *Int J Antimicrob Agents* 45, 496–503.
- Thavarajah, R., Mudimbaimannar, V., Elizabeth, J., Rao, U.K., and Ranganathan, K. (2012). Chemical and physical basics of routine formaldehyde fixation. *J Oral Maxillofac Pathol* 16, 400–405.
- Thirunavukarasu, P., Sukumar, S., Sathaiah, M., Mahan, M., Pragatheeshwar, K.D., Pingpank, J.F., Zeh, H., Bartels, C.J., Lee, K.K., and Bartlett, D.L. (2011). C-stage in colon cancer: implications of carcinoembryonic antigen biomarker in staging, prognosis, and management. *J Nat Cancer Inst* 103, 689–697.
- Thomas, A., and Chaurand, P. (2014). Advances in tissue section preparation for MALDI imaging MS. *Bioanalysis* 6, 967–982.
- Thomas, A., Patterson, N.H., Laveaux Charbonneau, J., and Chaurand, P. (2013). Orthogonal organic and aqueous-based washes of tissue sections to enhance protein sensitivity by MALDI imaging mass spectrometry. *J Mass Spectrom* 48, 42–48.
- Thomson, J.J. (1912). Further experiments on positive rays. *Philos Mag (series 6)* 24, 209–253.
- Touboul, D., Halgand, F., Brunelle, A., Kersting, R., Tallarek, E., Hagenhoff, B., and Laprèvote, O. (2004). Tissue molecular ion imaging by gold cluster ion bombardment. *Anal Chem*, 76, 1550–1559.
- Toue, S., Sugiura, Y., Kubo, A., Ohmura, M., Karakawa, S., Mizukoshi, T., Yoneda, J., Miyano, H., Noguchi, Y., Kobayashi, T., et al. (2014). Microscopic imaging mass spectrometry assisted by on-tissue chemical derivatization for visualizing multiple amino acids in human colon cancer xenografts. *Proteomics* 14, 810–819.
- Trim, P.J., Henson, C.M., Avery, J.L., McEwen, A., Snel, M.F., Claude, E., Marshall, P.S., West, A., Princivalle, A.P., and Clench, M.R. (2008). Matrix-assisted laser desorption/ionization-ion mobility separation-mass spectrometry imaging of vinblastine in whole body tissue sections. *Anal Chem* 80, 8628–8634.
- Unser, M., Aldroubi, A., and Gerfen, C. (1993). A multiresolution image registration procedure using spline pyramids. *Proc SPIE* 2034, 160–170.
- Valentine, S.J., Anderson, J.G., Ellington, A.D., and Clemmer, D.E. (1997). Disulfide-intact and -reduced lysozyme in the gas phase: conformations and pathways of folding and unfolding. *J Phys Chem B* 101, 3891–3900.
- Van Berkel, G.J., Sanchez, A.D., and Quirke, J.M. (2002). Thin-layer chromatography and electrospray mass spectrometry coupled using a surface sampling probe. *Anal Chem* 74, 6216–6223.
- Van Berkel, G.J., Kertesz, V., Koeplinger, K.A., Vavrek, M., and Kong, A.N. (2008). Liquid microjunction surface sampling probe electrospray mass spectrometry for detection of drugs and metabolites in thin tissue sections. *J Mass Spectrom* 43, 500–508.
- Vandermarliere, E., Mueller, M., and Martens, L. (2013). Getting intimate with trypsin, the leading protease in proteomics. *Mass Spectrom Rev* 32, 453–465.
- Varki, A., Cummings, R.D., Aebi, M., Packer, N.H., Seeberger, P.H., Esko, J.D., Stanley, P., Hart, G., Darvill, A., Kinoshita, T., et al. (2015). Symbol nomenclature for graphical representations of glycans. *Glycobiology* 25, 1323–1324.
- Vasicek, L.A., Ledvina, A.R., Shaw, J., Griep-Raming, J., Westphall, M.S., Coon, J.J., and Brodbelt, J.S. (2011). Implementing photodissociation in an Orbitrap mass spectrometer. *J Am Soc Mass Spectrom* 22, 1105–1108.
- Végyvári, Á., Fehninger, T.E., Gustavsson, L., Nilsson, A., André, P.E., Kenne, K., Nilsson, J., Laurell, T., Marko-Varga, G. (2010). Essential tactics of tissue preparation and matrix nano-spotting for successful compound imaging mass spectrometry. *J Proteomics* 73, 1270–1278.
- Venter, A., Sojka, P.E., and Cooks, R.G. (2006). Droplet dynamics and ionization mechanisms in desorption electrospray ionization mass spectrometry. *Anal Chem* 78, 5849–5855.
- Vestal, M., and Juhasz, P. (1998). Resolution and mass accuracy in matrix-assisted laser desorption ionization-time-of-flight. *J Am Soc Mass Spectrom* 9, 892–911.
- Wa, C., Cerny, R., and Hage, D.S. (2006). Obtaining high sequence coverage in matrix-assisted laser desorption time-of-flight mass spectrometry for studies of protein modification: analysis of human serum albumin as a model. *Anal Biochem* 349, 229–241.
- Wang, Z., Udeshi, N.D., Slawson, C., Compton, P.D., Sakabe, K., Cheung, W.D., Shabanowitz, J., Hunt, D.F., and Hart, G.W. (2010). Extensive crosstalk between O-GlcNAcylation and phosphorylation regulates cytokinesis. *Sci Signal* 3, ra2.
- Wang, T., Goodman, M.A., McGough, R.L., Weiss, K.R., and Rao, U.N. (2014). Immunohistochemical analysis of expressions of RB1, CDK4, HSP90, cPLA2G4A, and CHMP2B is helpful in distinction between myxofibrosarcoma and myxoid liposarcoma. *Int J Sur Pathol* 22, 589–599.
- Wang, T.Y., Jia, Y.L., Zhang, X., Sun, Q.L., Li, Y.-C., Zhang, J.H., Zhao, C.P., Wang, X.Y., and Wang, L. (2015a). Treating colon cancer cells with FK228 reveals a link between histone lysine acetylation and extensive changes in the cellular proteome. *Sci Rep* 5, 18443.
- Wang, S., Xiao, Z., Xiao, C., Wang, H., Wang, B., Li, Y., Chen, X., and Guo, X. (2015b). (E)-Propyl  $\alpha$ -Cyano-4-Hydroxyl Cinnamate: A High Sensitive and Salt Tolerant Matrix for Intact Protein Profiling by MALDI Mass Spectrometry. *J Am Soc Mass Spectrom* 27, 709–718.
- Watson, G., Paxinos, G., and Puelles, L. (2012). The mouse nervous system. London: Academic.
- Wells, J.M., and McLuckey, S.A. (2005). Collision-induced dissociation (CID) of peptides and proteins. *Methods Enzymol* 402, 148–185.

- Wiley, W.C., and McLaren, I.H. (1955). Time-of-flight mass spectrometer with improved resolution. *Rev Sci Instrum* 26, 1150–1157.
- Willems, S.M., van Remoortere, A., van Zeijl, R.J.M., Deelder, A.M., McDonnell, L.A., and Hogendoorn, P.C.W. (2010a). Imaging mass spectrometry of myxoid sarcomas identifies proteins and lipids specific to tumour type and grade, and reveals biochemical intratumour heterogeneity. *J Pathol* 222, 400–409.
- Willems, S.M., Wivewer, M., Graadt van Roggen, J.F., Hogendoorn, P.C.W. (2010b). Running GAGs: myxoid matrix in tumor pathology revisited. *Virchows Arch* 456, 181–192.
- Wilm, M. (2011). Principles of electrospray ionization. *Mol Cell Proteomics* 10, M111.009407.
- Wolstenholme, R., Bradshaw, R., Clench, M.R., and Francese, S. (2009). Study of latent fingerprints by matrix-assisted laser desorption/ionisation mass spectrometry imaging of endogenous lipids. *Rapid Commun Mass Spectrom* 23, 3031–3039.
- Wu, J.M., Halushka, M.K., Argani, P. (2010) Intratumoral heterogeneity of HER-2 gene amplification and protein overexpression in breast cancer. *Hum Pathol* 41, 914–917.
- Wu, C., Dill, A., Eberlin, L.S., Cooks, R.G., and Ifa, D.R. (2013). Mass spectrometry imaging under ambient conditions. *Mass Spectrom Rev* 32, 218–243.
- Wysocki, V.H., Resing, K.A., Zhang, Q., and Cheng, G. (2005). Mass spectrometry of peptides and proteins. *Methods* 35, 211–222.
- Yamashita, M., and Fenn, J.B. (1984). Electrospray ion source. Another variation on the free-jet theme. *J Phys Chem* 88, 4451–4459.
- Yang, J., and Caprioli, R.M. (2011). Matrix sublimation/recrystallization for imaging proteins by mass spectrometry at high spatial resolution. *Anal Chem* 83, 5728–5734.
- Zagon, I.S., Higbee, R., Riederer, B.M., and Goodman, S.R. (1986). Spectrin subtypes in mammalian brain: an immunoelectron microscopic study. *J Neurosci* 6, 2977–2986.
- Zavalin, A., Todd, E.M., Rawhouser, P.D., Yang, J., Norris, J.L., and Caprioli, R.M. (2012). Direct imaging of single cells and tissue at sub-cellular spatial resolution using transmission geometry MALDI MS. *J Mass Spectrom* 47, 1.
- Zenobi, R., and Knochenmuss, R. (1998). Ion formation in MALDI mass spectrometry. *Mass Spectrom Rev* 17, 337–366.
- Zhang, S.-Y., Lin, M., and Zhang, H.-B. (2015). Diagnostic value of carcinoembryonic antigen and carcinoma antigen 19-9 for colorectal carcinoma. *Int J Clin Exp Pathol* 8, 9404–9409.
- Zhao, Y., Takahashi, M., Gu, J., Miyoshi, E., Matsumoto, A., Kitazume, S., and Taniguchi, N. (2008). Functional roles of N-glycans in cell signaling and cell adhesion in cancer. *Cancer Science* 99, 1304–1310.
- Zlokovic, B.V. (2011). Neurovascular pathways to neurodegeneration in Alzheimer’s disease and other disorders. *Nat Rev Neurosci* 12, 723–738.







# APPENDIX

# List of abbreviations

9-AA	9-aminoacridine		
ACN	Acetonitrile	LAESI	Laser ablation electrospray ionization
ADC	Adenocarcinoma		
APCI	Atmospheric pressure chemical ionization	LC	Liquid chromatography
CE	Capillary electrophoresis	LESA	Liquid extraction surface analysis
CEA	Carcinoembryonic antigen	LLO	Lipid-linked oligosaccharide
CHCA	$\alpha$ -cyano-4-hydroxycinnamic acid	LMJ-SSP	Liquid microjunction surface sampling
CID	Collision-induced dissociation	LMS	Leiomyosarcoma
CMC	Carboxymethyl cellulose	LPS	Liposarcoma
COX7A	Cytochrome C oxidase 7A2	MALDI	Matrix-assisted laser desorption/ionization
CRC	Colorectal carcinoma		
CSV	Comma-separated values	MAP6	Microtubule associated protein 6
Da	Dalton		
DC	Direct current	MBP	Myelin basic protein
DESI	Desorption electrospray ionization	MFS	Myxofibrosarcoma
DHB	2,5-dihydroxybenzoic acid	MLS	Myxoid liposarcoma
DSC	Dice similarity coefficient	MMP2	Matrix metalloproteinase 2
DTT	Dithiothreitol	mmu	Millimass units
ECM	Extracellular matrix	MRM	Multi reaction monitoring
EDD	Electron-detachment dissociation	MS	Mass spectrometry
EDTA	Ethylenediaminetetraacetic acid	MSI	Mass spectrometry imaging
ER	Endoplasmic reticulum	MS/MS	Tandem mass spectrometry
ESI	Electrospray ionization	MWCO	Molecular weight cut off
ETD	Electron-transfer dissociation	MYX	Myxoid MLS
FA	Formic acid	$m/z$	mass-to-charge ratio
FDR	False discovery rate	NETD	Negative electron transfer dissociation
FFPE	Formalin-fixed paraffin embedded	NSCLC	Non-small cell lung cancer
FID	Free-induction-decay	OCT	Optimal cutting temperature
FT	Fourier transform	OS	Osteosarcoma
FTICR	Fourier transform ion cyclotron resonance	PC	Phosphatidylcholines
FTMS	Fourier transform mass spectrometry	PEG	Polyethylene glycol
GnT-V	<i>N</i> -acetylglucosaminyl-transferase V	PEV	Polyethylene vinyl
HCD	Higher-energy collisional dissociation	pHPMA	Poly[ <i>N</i> -(2-hydroxy-propyl)-methacryl-amide]
H&E	Haematoxylin & eosin staining	PIK3CA	Phosphatidylinositol 4,5-bisphosphate 3-kinase catalytic subunit alpha isoform
HEPES	4-(2-hydroxyethyl)-1-piperazineethanesulfonic acid	PNGase F	Peptide <i>N</i> -glycosidase F
HG-MSI	Histology-guided mass spectrometry imaging	ppm	Parts-per-million
HIAR	Heat-induced antigen retrieval	PTEN	Phosphatase and tensin homolog
HILIC	Hydrophilic interaction liquid chromatography	qTOF	Quadrupole-time-of-flight
HRAM	High-resolution, accurate mass	RC	Round cell MLS
ICR	Ion cyclotron resonance	RF	Radio frequency
IGF1R	Insulin-like growth factor 1 receptor	ROI	Region of interest
IHC	Immunohistochemistry	SA	Sinaptic acid
ILRS	Isotopically-labeled reference standard	SIMS	Secondary ion mass spectrometry
IMS	Ion mobility separation	S/N	Signal-to-noise
INT	Intermediate grade MLS	SPE	Solid phase extraction
IRMPD	Infrared multi-photon dissociation	SPTN1	Spectrin-1
ITO	Indium-tin-oxide	SqCC	Squamous cell carcinoma
		STS	Soft tissue sarcoma
		TCEP	Tris(2-carboxyethyl)phosphine
		TFA	Trifluoroacetic acid
		TG	Triglyceride lipids
		TMA	Tissue microarray
		TOF	Time-of-flight
		TSP2	Thrombospondin-2
		UPS	Undifferentiated pleomorphic sarcoma

# Nederlandse samenvatting

*In dit proefschrift staat een aantal verbeteringen en toepassingen van in-situ chemie beschreven. In-situ chemie wordt gebruikt als monster voorbereidingsmethode voor de biomoleculaire analyse met behulp van "matrix-assisted laser desorption/ionisation" (MALDI) "mass spectrometry imaging" (MSI). In de beschreven methoden worden enzymatische reacties direct toegepast op weefselcoupes om de moleculaire informatie, verkregen via de MALDI-MSI-analyse, te verrijken. Ook staat een geautomatiseerd histologie-gedreven MSI-platform beschreven dat gebruik maakt van moderne beeld bewerkingsalgoritmen. Dit nieuwe platform maakt het mogelijk MSI met hoge beeld- en massaresolutie toe te passen met behoud van werkbare data acquisitie tijden en data grootte. Tenslotte hebben we het belang van deze methoden aangetoond in een klinische studie naar de tumor progressie van myxoid liposarcoom. Hieronder volgen een samenvatting en een discussie van de gepresenteerde resultaten, alsmede een uiteenzetting van de toekomstperspectieven van het in dit proefschrift beschreven werk.*

## Technologische ontwikkelingen

### De verbetering en innovatie van *in-situ* chemie voor MALDI-MSI-analyse van eiwitten en post-translationele eiwitmodificaties

In 2006 werd de *in-situ* enzymatische digestie met trypsine door Shimma *et al.* (Shimma *et al.*, 2006) geïntroduceerd. Na haar introductie is de techniek snel populair geworden onder de gebruikers van MSI. De *in-situ* enzymatische digestie maakt het mogelijk om een groter deel van het proteoom te analyseren met MSI, helpt bij de identificatie van eiwitten/peptiden, en maakt de eiwitanalyse van formaline gefixeerd en daarna in paraffine ingebed (FFPE) weefsel mogelijk. Dit laatste zorgt ervoor dat er veel meer patiëntmateriaal beschikbaar komt voor klinische MSI-studies.

Het gebruik van proteolytische enzymen in oplossing, de herhaalbaarheid van de enzymatische digestie en de effecten van de enzymatische digestie op kwantitatieve, "bottom-up" eiwitanalyse is veelvuldig bestudeerd (Brownridge en Beynon, 2011). Tijdens een bijeenkomst van een werkgroep georganiseerd door het Europese MSI-netwerk COST Actie BM1104, gericht op de vergelijking van MSI resultaten verkregen na *in-situ* eiwit digestie, werd maar weinig overeenstemming gevonden in de behaalde resultaten verkregen met verschillende *in-situ* enzymatische digestie methoden ontwikkeld in verschillende laboratoria. Desondanks is er maar een klein aantal studies uitgevoerd naar de fundamentele en de herhaalbaarheid van de enzymatische digestie op weefselcoupes. Diehl *et al.*, beschrijven bijvoorbeeld het effect van verschillende experimentele parameters op de *in-situ* enzymatische digestie, waaronder de keuze van het proteolytisch enzym, de incubatietijd en de MALDI-matrix. Deze studie was met name gericht op het verbeteren van de beeldresolutie en de kwaliteit en reproduceerbaarheid van de door MSI geproduceerde visualisaties van moleculaire distributies (Diehl *et al.*, 2015). In twee recentere studies door Erich *et al.* en De Sio *et al.* werden reeds gepubliceerde *in-situ* enzymatische digestie methoden vergeleken en

de herhaalbaarheid van deze methoden getest (Erich et al., 2016; Sio et al., 2015). Erich *et al.* omschreven ook een geautomatiseerd en gebruikersonafhankelijk algoritme om een objectievere beoordeling van de herhaalbaarheid van een MALDI-MSI-experiment te geven (Erich et al., 2016). In **Hoofdstuk 2** hebben wij de dynamiek van de *in-situ* enzymatische digestie in zowel plaats als tijd onderzocht. Deze studie was gebaseerd op de MSI-analyse van drie groepen monsters na enzymatische digestie met variërende trypsine incubatietijden (1.5 uur, 3 uur, en 18 uur). Deze analyses leidden tot de bevinding dat langere incubatietijden resulteerden in een betere herhaalbaarheid van de *in-situ* enzymatische digestie. Ook werd geconcludeerd dat het gevarieerde chemische "landschap" van verschillende morfologische gebieden in het muis brein, de witte en grijze stof bijvoorbeeld, effect had op de digestie efficiëntie. Deze artefacten van de monster voorbereiding verdwenen wanneer langere incubatietijden werden gebruikt. Hiermee werd de hypothese bevestigd dat langere incubatietijden de herhaalbaarheid van de *in-situ* enzymatische digestie bevorderen. Deze verbeterde herhaalbaarheid komt voort uit een completere eiwitdigestie in alle morfologische gebieden.

Tijdens de studie naar de dynamiek van de *in-situ* enzymatische digestie werd gekeken naar de globale verschillen in de massaspectra na het toepassen van de drie incubatietijden. Deze verschillen werden bepaald door het vergelijken van het totaal aantal pieken in de gemiddelde spectra. Ook werd de digestiedynamiek bestudeerd door het volgen van de digestie van het eiwit Myelin Basic Protein (MBP, MBP\_MOUSE) gedurende de volledige lengte van de incubatietijd door het hele weefsel. Om ionisatie effecten te reduceren en de verschillende datasets ( $n = 27$ , negen replicaties per incubatietijd) meer vergelijkbaar te maken werden drie proteolytische fragmenten van MBP geselecteerd en gesynthetiseerd als isotoop-gelabelde referentie standaard (ILRS) peptiden. Deze ILRS-peptiden werden vervolgens homogeen op de weefsels aangebracht als interne standaard. Onder de gekozen MBP-fragmenten waren twee zogenaamde 'limiet peptiden' (eindproducten van de proteolytische digestie), en één 'intermediair peptide' (partieel geknipt digestie product). De fragmenten waren zodanig gekozen dat de volledige digestie van het intermediair peptide resulteerde in een van de geselecteerde limiet peptiden. Op deze manier kon de digestie efficiëntie bepaald worden door middel van de verschillen in relatieve intensiteit tussen de limiet en intermediair peptiden. De berekende digestie efficiëntie is mogelijk anders voor andere eiwitten, en ook het gebruik van andere weefseltypen kan de digestie dynamiek beïnvloeden. De hier gepresenteerde resultaten volgden uit de analyse van diepgevroren weefsel. Het gebruik van FFPE-weefsel kan de dynamiek van de *in-situ* digestie mogelijk veranderen. Deze studie geeft een nuttig inzicht in de dynamiek van de *in-situ* enzymatische digestie, maar om een volledig beeld te krijgen van alle factoren die de dynamiek van eiwitdigestie op een weefselcoupe beïnvloeden zal een grootschalige studie met meer verschillende weefseltypen en meer eiwitten moeten worden uitgevoerd. Desalniettemin kan de methodiek die in **Hoofdstuk 2** beschreven

wordt, namelijk het verkrijgen van kwantitatieve data over de enzymatische digestiesnelheid (voor één knip locatie) in verschillende morfologische gebieden in het weefsel, voor de gehele studie naar andere weefsels en eiwitten toegepast worden.

De grote hoeveelheid onderzoek die de afgelopen twee decennia in het *proteomics*-veld is gedaan heeft geresulteerd in een onuitputtelijke bron van informatie die kan worden gebruikt voor het aanpassen, verbeteren en ontwikkelen van MALDI-MSI-methoden. Zoals eerder beschreven heeft de aanpassing van de *bottom-up proteomics* aanpak geleid tot de introductie van de *in-situ* enzymatische digestie als monsteropwerking voor MALDI-MSI-analyse. Net zoals in eiwitstudies op basis van digestie in vloeistof wordt de *in-situ* digestie voornamelijk met trypsine uitgevoerd. De reden hiervoor is de restrictiespecificiteit van het enzym: trypsine knipt eiwitten aan de C-terminale zijde van de basische aminozuren arginine en lysine. Hierdoor produceert trypsine proteolytische fragmenten met een intrinsiek positief geladen C-terminus. Dit zorgt voor een hogere detectiegevoeligheid in de massaspectrometrie analyse in positieve ion modus (Brownridge en Beynon, 2011; Vandermarliere et al., 2013). Onderzoek in het *proteomics*-veld heeft ook uitgewezen dat het gebruik van meerdere proteolytische enzymen (zelfs met gedeelde specificiteit voor dezelfde aminozuren) kan leiden tot een diepere analyse van het proteoom (Choudhary et al., 2003; Hohmann et al., 2009). In **Hoofdstuk 3** en **Hoofdstuk 5** worden twee verschillende methodieken beschreven waarbij meerdere enzymen *in-situ* worden gebruikt; **Hoofdstuk 3** beschrijft de combinatie van verschillende proteolytische enzymen met een specificiteit voor arginine en lysine en hoe het gebruik van deze enzymen zowel de totale hoeveelheid geanalyseerde eiwitten alsmede de eiwit-aminozuursequentiedekking beïnvloedt; **Hoofdstuk 5** beschrijft een multimodale MSI methode waarin twee opvolgende *in-situ* enzymatische digesties worden uitgevoerd. De eerste digestie wordt gedaan met de glycosidase PNGase F en de tweede digestie met de protease trypsine. Deze sequentiële digestie maakt het mogelijk om achtereenvolgens *N*-glycanen en proteolytische peptiden te analyseren vanaf hetzelfde weefsel. De methode beschreven in **Hoofdstuk 3** is afhankelijk van de analyse van meerdere weefselcoupes, terwijl voor de methode beschreven in **Hoofdstuk 5** maar een enkele weefselcoupe nodig is voor de analyse van de twee datasets. Het voordeel van het de methode beschreven in **Hoofdstuk 5** is dat de moleculaire informatie die verkregen wordt in beide datasets zijn origine vindt in exact dezelfde morfologische gebieden van het weefsel. Hierdoor beschrijven de twee datasets de moleculaire informatie van dezelfde histopathologische karakteristieken van deze weefsels. Hierbij moet wel vermeld worden dat de MALDI-MS-analyse van *N*-glycanen verbeterd kan worden door middel van een bindings-specifieke derivatisering van de siaalzuren. Deze procedure stabiliseert de normaliter labiele siaalzuren, zorgt ervoor dat de isobare  $\alpha$ 2,3- en  $\alpha$ 2,6-gebonden siaalzuren van elkaar onderscheiden kunnen worden en reduceert de negatieve effecten die het negatief geladen siaalzuur heeft op de ionisatie van positieve ionen (Holst et al., 2016). De chemische dimethylamidatie-reactie, die voor de derivatisatie wordt uitgevoerd,



reageert met alle vrije carboxylgroepen (COOH) en heeft als bijkomend effect dat ook de C-termini van eiwitten en de zijgroepen van zure aminozuren worden gemodificeerd. De exacte modificaties van de eiwitten ten gevolge van de derivatisatie zijn niet in detail gekarakteriseerd en zullen ervoor zorgen dat de *in-situ* identificatie van de proteolytische fragmenten van hetzelfde FFPE-weefsel moeilijker wordt. Desalniettemin is in **Hoofdstuk 5** aangetoond dat de sequentiële *in-situ* digestie een bruikbare en waardevolle techniek is voor de analyse van *N*-glycanen.

### Histologie-gedreven MALDI-MSI

Recente technologische ontwikkelingen, met name de ontwikkeling van een ultrasnel MALDI-TOF-MS-platform, en de verbeterde resolutie van MALDI-FTICR-MS-analyse, hebben ervoor gezorgd dat MSI met hoge beeld- en massaresolutie beschikbaar kwam. De toename in cellulaire en chemische specificiteit, als resultaat van de hoge beeld en massaresolutie, gaat ten koste van de data acquisitie tijd en data grootte. Vooral in het klinisch MSI-onderzoek levert dit uitdagingen op voor de MSI-infrastructuur en data managementsystemen door de grote weefselreeksen van patiëntmateriaal die gemeten worden. Om de data-acquisitietijd en -grootte binnen de perken te houden hebben we in **Hoofdstuk 4** een histologie-gedreven MSI (HG-MSI) platform ontwikkeld gebaseerd op een serie geautomatiseerde beeldregistratie algoritmen. Tijdens de beeldregistratie wordt een geannoteerd histologisch beeld van een weefselcoupe, opgenomen met een hoge beeldresolutie, ge-co-registreerd aan een ander beeld van een opeenvolgende coupe, opgenomen met een lagere beeldresolutie. Deze tweede weefselcoupe is opgewerkt voor MALDI-MSI-analyse. Na deze beeldregistratie worden de contouren van de annotaties gereproduceerd op het lage-resolutie beeld van de MSI-weefselcoupe. Dit geeft de mogelijkheid om exclusief de *a priori* geselecteerde regionen van interesse (ROIs) met MSI te analyseren en daarmee de data acquisitie tijd en grootte te verminderen. Het succes van het platform werd aangetoond door de analyse van een kleine weefselreeks met behulp van het HG-MSI-platform. Deze analyse resulteerde in een reductie van de data grootte en acquisitietijd van ongeveer 80% in vergelijking met de analyse van de volledige weefselcoupes. Met het gebruik van het HG-MSI-platform is de toepassing en het routinematig gebruik van MSI met hoge beeld- en massaresolutie in klinisch onderzoek een stap dichterbij gekomen.

De strategie toegepast in de HG-MSI-methode, waarbij de histopathologische specificatie van het weefsel is gedaan voorafgaand aan de MSI-analyse, is zeer geschikt voor toepassingen waar de *a priori* histologische specificatie mogelijk, betekenisvol, en/of nodig is. Een voorbeeld hiervan is de analyse van tumor progressie, gebaseerd op cellulaire differentiatie of andere specifieke morfologische karakteristieken. Een ander voorbeeld is de toepassing van MSI waar hoge beeldresolutie of hoge massaresolutie nodig is, maar onpraktisch is door een te groot aantal te analyseren pixels, of een langzame data acquisitie. **Hoofdstuk 4** beschrijft de toepassing van het HG-MSI-platform voor de analyse van proteolytische peptiden van FFPE-weefsels, gebruik makende van een Bruker Daltonics MALDI-FTICR-MS-

instrument dat met ultrahoge massa-resolutie meet. Om ervoor te zorgen dat het HG-MSI platform bruikbaar en waardevol zou zijn voor de hele MSI-gemeenschap is ervoor gezorgd dat het gebruikt kan worden met massaspectrometers van alle producenten, met alle MSI-modaliteiten (SIMS, DESI, LESA, etc.), en dat het gratis/vrij beschikbaar is op het internet.

De analyse van *tissue microarrays* (TMAs), zoals beschreven in **Hoofdstuk 6**, is een andere oplossing voor het analyseren van grote reeksen patiëntweefsels. Een TMA is een verzameling van "punches" (diameter 0.5 – 2 mm), genomen uit specifieke gebieden van weefselblokken na histopathologische analyse van de weefsels. De voordelen van de analyse van een TMA zijn dat je de weefsels van een groot aantal patiënten in een kort tijdsbestek kunt vergelijken en dat de experimentele variantie aanzienlijk wordt verminderd, omdat de weefsels afkomstig van verschillende patiënten op hetzelfde moment dezelfde monsteropwerking ondergaan en samen worden geanalyseerd.

## Klinische applicatie

### De moleculaire achtergrond van tumor progressie in myxoid liposaroom

De methoden beschreven in dit proefschrift, met name deze in **Hoofdstukken 4 en 5**, werden ontwikkeld voor toepassing in klinisch onderzoek. **Hoofdstuk 6** beschrijft de toepassing van de multimodale MSI-methode omschreven in **Hoofdstuk 5** in een studie waarin de moleculaire achtergrond van tumor progressie in myxoid liposaroom (MLS) werd onderzocht. In deze studie werd aangetoond dat er een associatie bestaat tussen de progressie van MLS en een hogere aanwezigheid van het type mannose-rijke glycanen en het type complexe glycanen met een verhoogd aantal antennes. Deze moleculaire veranderingen werden niet eerder beschreven voor MLS of andere mesenchymale tumoren, maar wel voor colorectaal-, borst-, en eierstoktumoren. Mannose-rijke glycanen worden zowel intra- als extracellulair aangetroffen. De MALDI-MSI-analyse in **Hoofdstuk 6** werd echter uitgevoerd met een beeldresolutie die het niet mogelijk maakt om het verschil te kunnen zien tussen intra- en extracellulaire moleculen. Om de gevonden resultaten te valideren en verdere informatie te verzamelen over de precieze locatie van de glycanen in het cellulaire milieu zullen experimenten met complementaire technieken, zoals immunohistochemie, moeten worden uitgevoerd. Verdere inzichten in de moleculaire achtergrond van MLS-tumorprogressie zouden ook gehaald kunnen worden uit extra MSI-analyses van lipiden en eiwitten. Ook een diepgaande analyse van het proteoom zou van toegevoegde waarde kunnen zijn en inzicht kunnen geven over de moleculaire veranderingen die ten grondslag liggen aan de progressie van MLS.

## Toekomstperspectief

In dit proefschrift wordt de optimalisatie en toepassing van *in-situ* enzymatische digestie in combinatie met MALDI-MSI beschreven om de toepassing hiervan in klinisch onderzoek te bevorderen. Sinds de introductie van MSI is het koppelen van een moleculaire identiteit aan een gedetecteerde  $m/z$  waarde een van de grootste uitdagingen. Voor klinische studies en studies waarin men tracht biomarkers te vinden is de identiteit van de gedetecteerde moleculen van essentieel belang om de biologische achtergrond van de biomarker te doorgronden. Eén van de voordelen van het toepassen van de *in-situ* enzymatische eiwit digestie vóór de analyse met MALDI-MSI, is dat het de identificatie van de eiwitten achteraf bevordert. Het werk beschreven in dit proefschrift laat zien dat het aantal verschillende geïdentificeerde eiwitten, toegekend aan pieken in het MSI-massaspectrum, aanzienlijk toeneemt wanneer de MSI-analyse met hoge massa-resolutie wordt uitgevoerd. Hier moet echter wel bij vermeld worden dat slechts 10-15% van het totale aantal pieken in het MSI-massaspectrum geïdentificeerd kon worden. Ook bleven de pieken met de hoogste intensiteit vaak ongeïdentificeerd. Door de complexiteit van het probleem, heeft de oplossing die resulteert in een hoger aantal peptide identificaties verschillende facetten.

In FFPE-weefsel wordt formaldehyde gebruikt om eiwitten aan elkaar te koppelen. Deze koppeling vindt plaats door de verbinding van de basische aminozuren lysine, arginine en histidine. Om het mogelijk te maken eiwitten in FFPE-weefsels te analyseren moeten deze verbindingen verbroken worden tijdens een antigeenherwinning. Het proces van de formaline fixatie is echter niet volledig reversibel, en de eiwitten blijven vaak achter met onregelmatige, en veelal niet gekarakteriseerde moleculaire modificaties. Deze modificaties resulteren in een groot aantal niet-geïnterpreteerde MS/MS-spectra na de LC-MS/MS-analyse, wat een groot aantal ongeïdentificeerde pieken in het MSI-massaspectrum ten gevolge heeft. Om het volledige potentieel van eiwit MSI van FFPE-weefsels te benutten zouden de formaline-geïnduceerde modificaties grondig gekarakteriseerd moeten worden. Eerdere pogingen, en het feit dat de meerderheid van het *bottom-up proteomics* veld ver weg blijft van FFPE-weefsels, geven aan dat dit een enorme uitdaging behelst. Een alternatief om de hoeveelheid identificaties te vergroten zou zijn om doelmatige LC-MS/MS-analyses te doen, gebaseerd op de pieklijsten verkregen uit de MSI-analyse.

Verder is het enzymatisch gedigesteerde proteoom een zeer complex geheel en resulteert, mede door het grote aantal isobare proteolytische peptiden, in een uitermate complex massaspectrum met veel overlappende isotoop patronen. De massaspectra worden nog complexer gemaakt door de aanwezigheid van zoutcomplexen. Weefsels hebben een zoutrijk milieu, en zoals beschreven in **Hoofdstuk 5** wordt een variëteit aan peptide-zoutcomplexen, zoals  $\text{Na}^+$ ,  $2\text{Na-H}^+$ ,  $\text{K}^+$ ,  $2\text{K-H}^+$  waargenomen. Dit terwijl er vóór de eiwitanalyse een aantal spoel stappen in de monstervoorbewerking zijn opgenomen om zouten en lipiden uit het weefsel te

verwijderen. Na de MSI-analyse zou het identificeren en verwijderen van de zoutcomplex-pieken uit het massaspectrum een oplossing kunnen bieden om het massaspectrum minder complex te maken. Het zou echter beter zijn om de daadwerkelijke formatie van de zoutcomplexen te voorkomen. Dit zou bereikt kunnen worden door het toepassen van additionele weefsel spoel stappen, of door het toepassen van een meer zout resistente MALDI-matrix die de vorming van zoutadducten tegengaat. Wang *et al.* hebben recentelijk gepubliceerd over de matrix (*E*)-propyl *α*-cyano-4-hydroxycinnamylaat, gevormd door de reactie van de reguliere MALDI-matrix *α*-cyano-4-hydroxycinnamic acid met een propyl-alcohol, welke een hoge zouttolerantie heeft voor de analyse van intacte eiwitten (Wang et al., 2015b). Nadat we deze MALDI-matrix gesynthetiseerd hadden en hier proteolytische peptiden mee hebben geanalyseerd, toonden de preliminaire resultaten een verhoogd aantal zoutcomplexen.

De toegekende peptide identiteiten, beschreven in **Hoofdstuk 3** en **Hoofdstuk 5** van dit proefschrift werden allen gedaan op basis van de accurate massa van de moleculen. Hoewel de beschreven methode waardevolle informatie geeft over de potentiële identiteit van de gedetecteerde moleculen, heeft *in-situ* fragmentatie en directe tandem MS-analyse vanaf het weefsel de voorkeur. Deze aanpak is veelvuldig beschreven in de literatuur met gebruik van massaspectrometers met lage massa resolutie (zoals MALDI-TOF-MS-platformen), maar de beschikbaarheid van deze techniek voor instrumenten met hoge massa-resolutie is erg beperkt. Om de definitieve identificatie van peptiden te doen met behulp van MSI zullen massaspectrometers moeten worden uitgerust met verbeterde *quadrupole* technologie, zodat een specifiekere selectie van ionen kan plaatsvinden, wat uiteindelijk zal leiden tot een meer accurate peptide identificatie direct vanaf het weefsel.

Het additionele werk wat hierboven beschreven is zal ons inzicht in de moleculaire histologie van de weefsels waarmee we werken drastisch vergroten, wat uiteindelijk zal resulteren in meer specifieke en efficiënte methoden die nog beter geschikt zijn voor de MSI-analyse van FFPE-weefsel. Ondanks de huidige tekortkomingen van de techniek is de impact van MSI op klinisch onderzoek de laatste jaren enorm toegenomen. Verbeterde methoden en meer geavanceerde technologie zullen deze impact met zekerheid gaan vergroten wat de implementatie van MSI in klinisch onderzoek zal versterken en mogelijk de implementatie van MSI in de moleculaire diagnostiek zal bewerkstelligen.

# List of publications

- (i) Isabella Piga, **Bram Heijs**, Simone Nicolardi, Laura Giusti, Lorella Marselli, Piero Marchetti, Maria Rosa Mazzoni, Antonio Lucacchini, Liam A. McDonnell. "Ultra-high resolution MALDI-FTICR-MSI analysis of intact proteins in mouse and human pancreas tissue," *In press*, International Journal of Mass Spectrometry, 2017.
- (ii) **Bram Heijs\***, Stephanie Holst\*, Inge H. Briaire-de Bruijn, Gabi W. van Pelt, Arnoud H. de Ru, Peter A. van Veelen, Richard R. Drake, Anand S. Mehta, Wilma E. Mesker, Rob A. Tollenaar, Judith V.M.G. Bovée, Manfred Wuhrer, Liam A. McDonnell. "Multimodal Mass Spectrometry Imaging of N-Glycans and Proteins from the Same Tissue Section," *Analytical Chemistry*, vol. 88, no. 15, pp. 7745–7753, 2016.
- (iii) Stephanie Holst\*, **Bram Heijs\***, Noortje de Haan, René J.M. van Zeijl, Inge H. Briaire-de Bruijn, Gabi W. van Pelt, Anand S. Mehta, Peggi M. Angel, Wilma E. Mesker, Rob A. Tollenaar, Richard R. Drake, Judith V.M.G. Bovée, Liam A. McDonnell, Manfred Wuhrer, "Linkage-Specific in Situ Sialic Acid Derivatization for N-Glycan Mass Spectrometry Imaging of Formalin-Fixed Paraffin-Embedded Tissues," *Analytical Chemistry*, vol. 88, no. 11, pp. 5904–5913, 2016.
- (iv) **Bram Heijs\***, W.M. Abdelmoula\*, Sha Lou, Inge H. Briaire-de Bruijn, Jouke Dijkstra, Judith V.M. G. Bovée, and Liam A. McDonnell, "Histology-Guided High-Resolution Matrix-Assisted Laser Desorption Ionization Mass Spectrometry Imaging," *Analytical Chemistry*, vol. 87, no. 24, pp. 11978–11983, 2015.
- (v) **Bram Heijs**, Else A. Tolner, Judith V.M.G. Bovée, Arn M.J.M. van den Maagdenberg, Liam A. McDonnell, "Brain Region-Specific Dynamics of On-Tissue Protein Digestion Using MALDI-MSI," *Journal of Proteome Research*, vol. 14, no. 12, pp. 5348–5354, 2015.
- (vi) **Bram Heijs**, Ricardo J. Carreira, Else A. Tolner, Arnoud H. de Ru, Arn M.J.M. van den Maagdenberg, Peter A. van Veelen, Liam A. McDonnell, "Comprehensive Analysis of the Mouse Brain Proteome Sampled in Mass Spectrometry Imaging," *Analytical Chemistry*, vol. 87, no. 3, pp. 1867–1875, 2015.

# Curriculum Vitæ

Bram Petrus Antonius Maria Heijs was born on November 7th, 1986 in Tilburg, the Netherlands. In 2005 he graduated from Theresia Lyceum in Tilburg, and started his studies in Life Science & Technology at Leiden University and Delft University of Technology. Following the bachelor's degree in Life Science & Technology, he started his masters in Life Science & Technology at Leiden University in 2010. The master program focused on molecular biology and biochemistry and included two internships; the first being at the Leiden Institute of Chemistry (LIC) at Leiden University, under the supervision of dr. Claude Backendorf and prof. dr. Mathieu Noteborn, focusing on the purification of the PTD4-apoptin protein. The second internship was performed under the supervision of prof. dr. Per Andrén of the Medical Mass Spectrometry group at the Center for Biomedicine at Uppsala University in Uppsala, Sweden. The aim was to optimize methods to study the molecular alterations in human cerebrospinal fluid and mouse brain tissue caused by Parkinson's disease. After obtaining the title of Master of Science in Life Science & Technology in 2013, he started as a PhD candidate at the Mass Spectrometry Imaging group of the Center for Proteomics & Metabolomics (CPM) at the Leiden University Medical Center (LUMC). The project, under supervision of dr. Liam McDonnell, was in close collaboration with prof. dr. Judith Bovée at the Department of Pathology of the LUMC. His work at CPM, largely described in this thesis, focused on the development and improvement of *in-situ* (enzymatic) chemistry methods for improved mass spectrometry imaging and application of these methods in a clinical study on myxoid liposarcoma. Parts of this work were presented at a number of (inter)national conferences by the Dutch Society for Mass Spectrometry (NVMS, 2014, 2016), the American Society for Mass Spectrometry (ASMS, 2014), the European OurCon Mass Spectrometry Imaging Society (2014, 2015, 2016, 2017) and the International Mass Spectrometry Society (2016). In September 2017 during the OurCon conference, Bram was awarded with the ImaBiotech Mass Spectrometry Imaging Award for young and innovative scientists in the field of mass spectrometry imaging. Besides research activities, he also is involved in the CPM quality management team and the design committee for the new laboratories CPM will occupy in 2019. Since April 2017, Bram is working as a researcher at the CPM where he will continue the clinical study on the molecular alterations underlying the tumor progression of myxoid liposarcoma. After obtaining his PhD degree, he will continue his career at the CPM as group leader of the Mass Spectrometry Imaging group.



# Acknowledgements

Much like a summer vacation being reduced to a single photo album, my PhD journey was an incredible experience that has been reduced to the work presented in this thesis. Like a photo album, this thesis contains countless unwritten memories, shared and made possible by a large number of people who I am forever thankful! On this final page of my thesis I would like to acknowledge all of you who have, in any way, shape, or form, contributed to establishing this thesis!

First, I would like to express my sincerest gratitude to my promotor, professor Judith Bovée, and my co-promotor and supervisor, dr. Liam McDonnell, for giving me the opportunity to be a PhD candidate in the Mass Spectrometry Imaging group. Thank you for your support, guidance, and for being incredibly inspiring mentors!

Without a doubt science is a team effort, so I would also like to thank all current and past members of the Mass Spectrometry Imaging group. Benjamin, Clara, Fanny, Hans, Isabella, René, Ricardo, Ruben, Sha, Stephi, and Walid, without your help and support I couldn't have done this.

In this light I would also like to express my gratitude to all colleagues at the Center for Proteomics & Metabolomics, the Department of Pathology, and all the people I have collaborated with throughout the LUMC. I would like to give special thanks to: Prof. Manfred Wuhrer, thank you for your guidance and support and for the trust you put in me for the future; Sarantos, thank you for our nice discussions about science, music, and life in general; Hulda, Aswin, Gerda, and Tiziana, without you R6-26 wouldn't have been the great office that it was; Inge and Marieke, thank you for always taking the time to help me with sampling and clinical information, and having a nice chat; Anton, Bart, Dana, Dick-Paul, Frank, Guinevere, Isabelle, Linda, Peter, Robert, Simone, Tugçe, a wholehearted thank you for being great colleagues and friends.

Ik wil mijn bandmaatjes in Transient State, Hologram Earth en Mudguard, mijn LST-buddies, en Michiel bedanken voor hun oneindige support! Ik wil mijn familie en schoonfamilie bedanken omdat ze er altijd voor me zijn; pap en mam, Janne en Pieter, Jennie en Willem, zonder jullie steun en begrip was me dit niet gelukt! Ingeborg, mijn steun en toeverlaat, jouw relativerend vermogen brengt de dalen dicht bij de toppen! Dank je dat je altijd voor me klaar staat!

